The Automatic Tracking Of *Caenorhabditis elegans* And Its Use In Determining Genetic Function

Thesis

Contents

i Publications

Automated and controlled mechanical stimulation and functional imaging: *In vivo C. elegans.*
Cho Y, Porto D, Hwang H, Grundy L, Schafer W, Lu H. Lab on a chip. 2017 vol,17 (15)

PARCG, a protein linked to ciliary motility, mediates cellular signalling.
Loukes C, Bialas N, Dekkers M, Walker D, Grundy L, Li C, Inglis P, Kida K, Schafer W, Blaque O, Jansen G, Leroux M. Molecular Biology of the Cell. 2016, vol. 27 (13)

The bright fluorescence protein mNeonGreen facilitates protein expression analysis *in vivo.*
Hostettler L, Grundy L, Kaser-Pebernard S, Wicky C, Schafer W, Glauser D.

Spatial asymmetry in the mechanosensory phenotypes of the *C. elegans* DEG/ENaC gene *mec-10.*
Chatzigeorgiou M, Grundy L, Kindt K, Lee W, Driscoll M, Schafer W.
Journal of Neurophysiology. 2010. Vol 104 (6)

A database of Caenorhabditis elegans behavioural phenotypes.
Yemini E, Jucikas T, Grundy L, Brown A, Schafer W.
Nature Methods. 2013 vol. 10 (9)

Changes in postural syntax characterise sensory modulation and natural variation of *C. elegans* locomotion.
Schwartz R, Branicky R, Grundy L, Schafer W, Brown A.
PLoS Computational Biology. 2015 vol. 11 (8)

A dictionary of behavioural motifs reveals clusters of genes affecting Caenorhabditis elegans locomotion.
Brown A, Yemini E, Grundy L, Jucikas T, Schafer W.
Proceedings of the National Academy of Sciences of the United States of America. 2013, vol. 110 (2)

ii Acknowledgements

I would like to thank my supervisor, Bill Schafer, whose support and guidance was gratefully received and without which this thesis would not have been possible. He has allowed me to pursue my own scientific ideas and I have grown as a scientist during my time in his lab.

I would also like to thank my second supervisor, Mario DeBono for useful advice and contributions during the many meetings we have had over the course of my PhD.

I thank the Medical Research Council for funding my research studentship and for catering to my personal needs in providing me with the option to study for a PhD part-time. I would also like to thank all the staff in the student support office at the Laboratory of Molecular Biology who had to make special arrangements for my less than usual study arrangement.

The LMB I thank for providing all facilities and materials for me during my time as a student there.

I would like to thank Denise Walker for her endless advice and for suffering all of my angst throughout my PhD, and also for reviewing the majority of my thesis. I also thank Kristin Webster and Yee Lian Chew for reviewing a chapter each of my thesis. I thank all the members of the Schafer lab for their help and companionship over the last six years, as well as the members of the DeBono and Taylor labs.

Finally I would like to thank my family for their support throughout my PhD and for believing in me even when I did not, particularly Mark and Peggy, the sources of my sanity and my dad for his help with statistical analysis.

iii Abbreviations

Worm genes unc-, itr-, dop described in abstract

AT2	Analysis Toolbox 2
CaM	Calmodulin
cDNA	Coding Deoxyribonucleic Acid
C.elegans	Caenorhabditis Elegans
CGC	Caenorhabditis Genetics Centre
Chrd2	Channel Rhodopsin 2
CTX	Chemotaxis
DEG/ENaC	Degenerin/Epithelium Sodium Channel
DNA	Deoxyribonucleic Acid
E.coli	Escherisha Coli
EEO	Electroendosmosis
EGTA	Ethylene glycol-bis(β-aminoethyl ether)-N,N,N',N'-tetraacetic acid
ER	Endoplasmic Reticulum
FRET	Fluorescence Resonance Energy Transfer
GABA	*Gamma-Amino Butyric Acid*
gDNA	Genomic Deoxyribonucleic Acid
GECI	Genetically Encoded Calcium Indicator
GFP	Green Fluorescence Protein
LED	Light-Emitting Diode
NEB	New England Biolabs
NGM	Nematode Growth Medium
PCR	Polymerase Chain Reaction
RFP	Red Fluorescence Protein
RNAi	Ribonucleic Acid Interference
RT-PCR	Revserse Trancsciption-Polymerase Chain Reaction
SEM	Standard Error of the Mean
TYE	Tryptone Yeast Extract
WT1	Worm Tracker 1
WT2	Worm Tracker 2

iv Figure List

Chapter 1

Chapter 2

Chapter 3

Chapter 4

v Abstract

Even with its simple nervous system, the nematode worm *Caenorhabditis elegans* can display a range of complex behaviours. Movement can be viewed as the main output of the *C. elegans* nervous system, and aberrations in the worm's locomotion can be used as an indicator for genetic function in mutant strains of *C. elegans*. Automated tracking of *C. elegans* locomotion has been used to determine phenotypic fingerprints for ~300 mutant *C. elegans* strains. Two methods of creating phenotypic fingerprints were used. The first based on pre-determined micro-behaviours previously described in worms, but never before analysed using automated tracking. The second used the tracking data itself to determine micro-motifs, repeated sets of behaviours observed at least twice in at least two mutant or wild-type strains.

Both methods of clustering successfully grouped together strains with mutations in genes known to interact together, verifying that the technique is able to detect meaningful connections between mutant strains. The following step was to determine whether the technique can be used to establish connections between genes on unknown function. A pair of strains with mutations in DEG/ENaC subunit encoding genes clustered strongly together using the micro-motif method, due to similar defects in their behaviours upon turning. The function of these genes, *asic-2* and *acd-5*, was unknown. Upon further investigation it was found that the two genes are expressed in different classes of neurons, the IL2s in the case of *asic-2* and the ASIs in the case of *acd-5*. Following investigation into behaviours known to be modulated by these two neuron classes it was found that the mutant strains displayed mutant phenotypes in similar behaviours, but that their mutant phenotypes are opposing. Mutations in *asic-2* cause increased lifespan and healthspan and a reduction in dauer entry in response to exogenous, purified ascarosides. Mutations in *acd-5* cause decreased lifespan and healthspan and a reduction in dauer entry in response to crude dauer pheromone. This suggested that the two genes were unlikely to be working in the same pathway, but do function in similar pathways.

Calcium imaging is a technique used in *C. elegans* to measure responses in excitable cells, in this case in neurons. Many calcium indicators are available for use in this technique, one in particular is GCaMP. GCaMP has undergone many rounds of targeted mutations with the aim to increase the molecule's dynamic range and dissociation constant. At the time of commencing this project, new variants of GCaMP, known as GCaMP6s, became available, and had yet to be tested in *C. elegans* neurons. The effectiveness of a total of 6 new variants was tested in the gentle touch neurons of *C. elegans*. It was found that the alterations made to GCaMP5G in order to make the GCaMP6 variants did not result in improved dynamic range or dissociation constant in the PLM of *C. elegans*.

Chapter 1

1.1 Introduction

1.1.1 *Caenorhabditis elegans*

An interesting question in biological research, and one for which sufficient answers still evade scientists, is how gene products interact to create coordinated and complex behaviours.

As humans our thought processes and resultant actions are so complex that an explanation for this question seems beyond the realms of possibility. Even those processes for which no conscious thought is necessary are complex and multifaceted, with many genes interacting to perform some of the smallest of actions. Due to these factors human experimentation would be time-consuming and costly, not to mention unethical. For this reason researchers have, for many years, attempted to identify human homologies in the genetics of simpler organisms that are more genetically tractable.

Several organisms have been found to be ideal for just this, *Caenorhabditis elegans* (*C. elegans)* is one such organism. This soil dwelling nematode has become a favourite model species. Initially the appeal of the worm lay in its basic anatomy. Its small size (approx 1mm) and large brood size means it is easy to grow in large numbers in a relatively small amount of space. The worm is transparent and can be imaged under a light microscope, allowing for live observations.

The worm has simple nutritional needs, an agar plate seeded with bacteria is sufficient to keep dozens of individuals fed for several days (Brenner 1974). In this feeding environment, at 22°C, a single worm will develop, in 72 hours, from egg to adult (Maniatis et al. 1982). During this development the worm passes through 4 typical larval stages, L1 - L4 (Fig.1.1A) (Cassada & Russell 1975). *C. elegans* are easily staged by picking L4 larvae, noticeable due to their characteristic ‘saddle’, a clear semicircle on one side of the body formed by the invagination of the developing vulva (Fig.1.1B). One mature individual can lay approximately 300 viable eggs in a lifetime (LeDoux 2005). Since the worm is mainly hermaphroditic, with a low incidence of male births (approximately 0.2%) (Chaffey 2003), potentially huge numbers of identical, genetically stable worms can be grown in just two generations. Consequently, a large population of clones can be reached very quickly. When starved, *C. elegans* larvae will enter an alternate developmental pathway, forming what is known as a dauer larva. Dauers can survive for at least 6 months in starvation and will re-enter the normal path of development when reintroduced to food (Cassada & Russell 1975).

It was for these reasons that *C. elegans* was originally picked by Sydney Brenner as a candidate for research into developmental biology and neurology (Brenner 1974). Initial work on the worm involved the introduction of mutations into the worm’s genome using EMS (Ethyl Methane Sulphonate). Any worms that were exhibiting an obvious locomotory or morphological phenotypes were cultivated to produce colonies of mutants. Examples are dumpy, long and small for morphology (Fig.1.1C) and uncoordinated for locomotion. Using a

series of elegant genetic experiments a rudimentary genetic map of the mutated genes was made (Brenner 1974; Coulson et al. 1986), leading to a basic understanding of *C. elegans* genetics, and allowing the mutations responsible for these phenotypes to be mapped.

Following on from Brenner's work with *C. elegans*, many important discoveries have been made during experimentation with the worm, which have greatly impacted research in the wider research community. Most notable are those for which Nobel prizes have been won.

The first of these came in 2002 for the work carried out by Brenner, Sulston and Horvitz on the basics of organ development and programmed cell death. Sulston and co-workers discovered that during *C. elegans* development many cells undergo apoptosis in a predictable, identical pattern (Sulston and Horvitz 1976). This lead to the understanding that some cancers are caused by a fault in the cell's usual pathway: programmed cell death. Horvitz was able to decipher which genes within the worm were responsible for modulating apoptosis. He found that functioning *ced-3* and *ced-4* genes are required by all cells in *C. elegans* to properly undergo apoptosis (Ellis & Horvitz 1986). He was also able to determine that there is a *ced-3* like gene in the human genome, indicating that humans also have a particular gene required for proper cell death to take place (Yuan et al. 1993).

The second Nobel Prize for work with *C. elegans* was for the discovery of the technique RNAi (RNA interference) by Mello and Fire. This is an easy to use and effective method for silencing targeted genes by introducing double stranded RNA (dsRNA), either directly (e.g. by feeding) or by transgenic expression (Mello and Fire 1998). Since dsRNA usually hails from a viral source, the cell will recognise the RNA as pathogenic and destroy it. The mRNA from the targeted gene is blocked from ever becoming translated, hence it is silenced. Using cell specific promoters, the RNAi can be introduced into targeted cells, where it can silence a gene within this cell only. This technique has since been effectively used for gene silencing in a wide variety of organisms. Clinically, RNAi has been effectively used in treatment of Macular Degeneration (Kaiser et al. 2010) and human respiratory syncitial virus (Alvarez et al. 2009).

Third and finally, a Nobel Prize was won in 2008 by Chalfie, Shimomura and Tsien for the discovery and development GFP (Green Fluorescence Protein) (Chalfie et al 1994, Shimomura 1979; Heim et al. 1994). Chalfie and co-workers were responsible for developing GFP for use in *C. elegans*. Promoter-GFP fusions are incredibly useful in *C. elegans* research as they offer a quick and relatively reliable method of determining the expression pattern of specific genes. One merely has to identify a promoter region for the gene of interest, fuse it to a green fluorescent protein and express it in the worm (Chalfie et al 1994).

The GFP molecule has since been manipulated in many ways to offer a variety of colours of fluorescent protein and has been combined with various protein functional domains to give rise to fluorescent indicators. Indicators exist for a number of different ions; Outside of *C. elegans* research fluorescent indicators are used for a wide variety of applications. Detection of low levels of heavy metals in solutions and environmental samples can be achieved using indicators that bind the target metal (Prestel et al. 2000). In neuronal research the most common indicators used detect changes in sodium or calcium ion concentration. In mammalian research sodium indicators have many uses (Rose & Konnerth 2001; Moore & Fay 1993), but they are of limited use in research with the worm, as *C. elegans* does not have recognised sodium

transients. In *C. elegans* the most commonly used indicators are the calcium indicators: Cameleon, GCaMP and G-GECO, used for measuring calcium transients in excitable cells. In recent years a wider variety of colours of fluorescent indicators has become available, the red-shifted RCaMP and R-GECO and blue-shifted B-GECO (Akerboom et al. 2013; Zhao et al. 2011).

In recent years more elaborate techniques for researching with *C. elegans* have been developed. It is possible to stimulate specific neurons with blue light, using cell specific expression of channelrhodopsin (ChR), a functional ion channel activated by UV light (Nagel 2002). Emissions from red-shifted calcium indicators, expressed in cells postulated to be downstream of ChR containing cells, can then be tracked to elucidate neuron circuitry (Akerboom et al. 2013). We can accurately measure electrical gradients across a cell membrane (Goodman et al. 2012); and, most importantly for the work I have been conducting, we can measure the calcium transients within specific neurons in response to a variety of stimuli (Suzuki et al. 2003; Hilliard et al. 2005; Kimura et al. 2004).

During my study I have been exploiting a number of the techniques known to *C. elegans* researchers, both old and new, to determine the function of unknown genes.

1.1.2. *C. elegans* anatomy

The *C. elegans* hermaphrodite has an un-segmented cylindrical body with a recognisable head and tail at either end. The body is formed of an outer and inner tube held apart by internal hydrostatic pressure. The outer tube consists of the cuticle, hypodermis, excretory system, neurons and muscles (Fig 1.2A). The inner tube is made up of pharynx, intestine and gonad, which produces both egg and sperm (Brenner 1988) (Fig 1.2B and 2D).

The male anatomy is similar, but the male is smaller in comparison to age-matched hermaphrodites and can be identified by their characteristic fanned tail (Fig.1.2C). The male has no ovaries and instead has a single j shaped arm that produces sperm only. Males and hermaphrodites can mate to generate cross-progeny of around 50% of each sex (Ward & Carrel 1979). The *C. elegans* male has 385 neurons in comparison to the 302 in hermaphrodites. 91 of the male neurons are sex specific, while hermaphrodites have only 8 sex specific neurons. The majority of male sex specific neurons are found in the tail and many have specific roles in male mating behaviour. Sex specific neurons in the head are involved in pheromone sensation and mate detection (Sulston and Horvitz 1997).

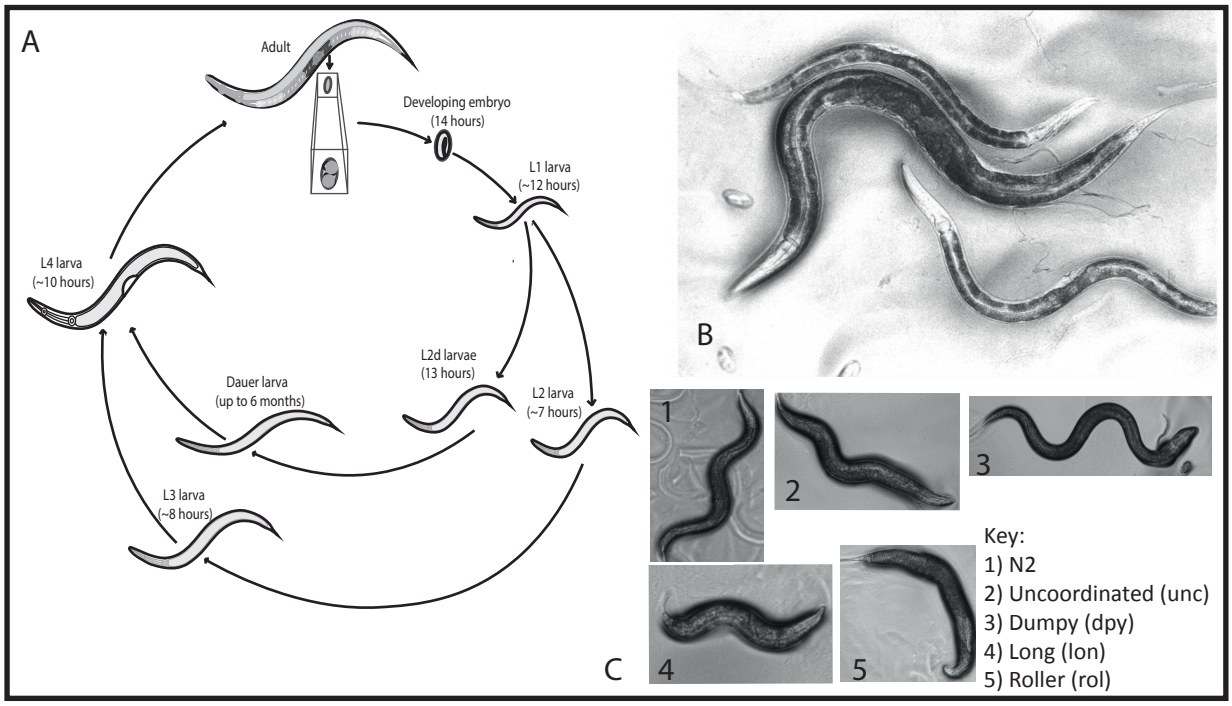

Fig.1.1: The Lifecycle and Anatomy Of *C. elegans.* A: The life-cycle of *C. elegans*, eggs are released from gravid adults, eggs hatch after ~26 hours as L1 larvae, in favourable conditions the worm progresses through larval stage 2 and 3, then become L4 larvae. In low or poor food conditions the worm enters the dauer pathway. B: A larger, adult individual flanked by two L4 larvae. The larvae display the characteristic semicircular arc midway down the body (Genome research limited). C: 1, shows an N2 adult, 2, an uncoordinated adult, 3, a long adult and 4 a dumpy adult and 5, a roller.

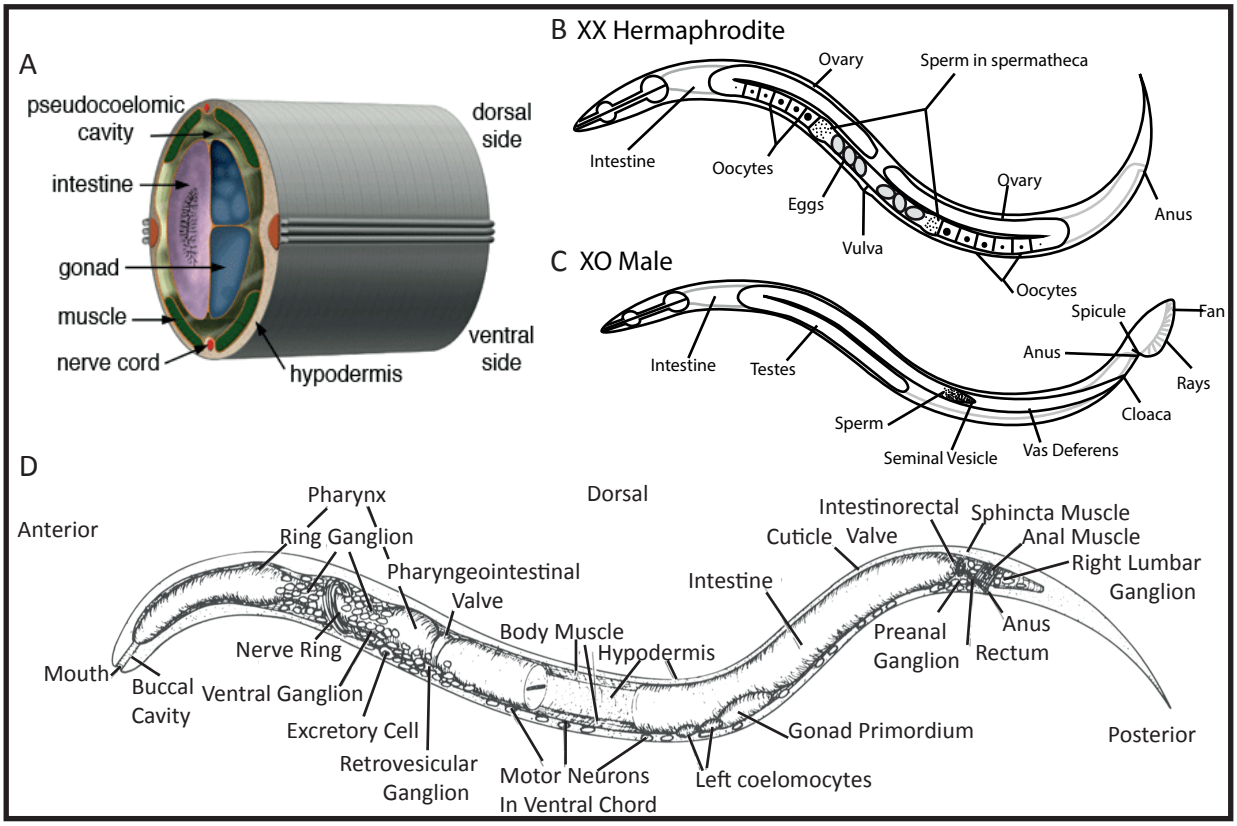

Fig.1.2. The internal anatomy of *C. elegans*. A: A cross section of the *C. elegans* body (Altun and Hall wormatlas). B: The basic bodily structure of the *C. elegans* hermaphrodite (Wormatlas) C: The basic bodily structure of the *C. elegans* male D: A detailed schematic of the *C. elegans* hermaphrodite physiology (Sulston et al. 1983).

1.1.3 *C. elegans* Genetics

Although *C. elegans* has long been a popular organism for genetic research, its appeal increased in 1998 when it became the first multi-cellular organism to have its full genome sequenced (*C. elegans* Sequencing Consortium 1998). Consequently knowledge of the worm's 100MB genome has had somewhat of a head start over other popular model species.

The worm's genome contains around 20,470 protein coding genes (WS277 release letter WormBase). It is thought that there are around 1,200 gene families containing two or more paralogues in *C. elegans* (Cavalcanti et al. 2003; Gu et al. 2002) accounting for 32% of their genes.

A number of genes in the worm are highly conserved with lower complexity organisms; these tend to be encoding essential proteins or are genes that function in processes that are evolutionarily, strongly conserved. Around 300 of the worm's genes are essential to its survival (Kamath et al. 2003). These essential and conserved genes tend to cluster to the centre of the autosomes, while the arms contain fewer, sparser and less vital genes (*C. elegans* Sequencing Consortium 1998; Hutter et al. 2000). At least some of these clusters are thought to act as operons (Blumenthal et al. 2002).

Around 35% of *C. elegans* genes have human orthologs (Shaye et al. 2011), which is incredibly useful for researchers. Particular human disease genes have already come to be much better understood by studying their homologous gene in the worm. An example of this is in the study of the inherited skin fragility disease Kindler syndrome, caused by a mutation in KIND1. KIND1 has a *C. elegans* ortholog, *unc-112*. Since *unc-112* is implicated in linking the actin cytoskeleton to the extracellular matrix (ECM) in worms, it was theorised that kindler syndrome was the result of an actin-ECM defect, rather than the more common keratin-ECM defect. Further investigation in the direction of this theory proved it to be correct (Siegel et al. 2003). Many mammalian orthologues can rescue mutations in their worm counterparts. For example the *C. elegans* mutant, *nlg-1*, an ortholog of the human synaptic cell adhesion protein neuroligin, have their atypical gentle touch and osmotic responses rescued by expression of human NLGN1 or rat *Nlgn1* (Calahorro et al. 2012) suggesting functional conservation of human orthologues.

The worm has 6 chromosome pairs I, II, III, IV, V and X, the final being the sex chromosome. A configuration of XX will cause the individual to be hermaphrodite, and XO will create a male (Riddle 1997). When males are lacking in a population the hermaphrodites will self fertilise and create a colony of clones, which is useful when propagating mutant recessive lines. Crossing with males allows for the introduction of extrachromosomal arrays or integrated genes into the hermaphrodite genome.

1.1.3.1 Introducing mutations and genetic screening

Genetic mutations can be introduced into the worms' genome in a number of ways, for a number of screening techniques. The method by which a gene is mutated largely depends on the experimental requirements of the researcher, and which type of screen is to be done.

Forward genetic screening is a method used to attribute a randomly mutated gene to a specific, observed phenotype, while a reverse genetic screen involves specifically mutating a gene, or genes of interest, and observing the resultant phenotype. Thus, forward genetic screening allows for wide-scale mutagenesis, while reverse screening requires a more specific, targeted method of mutagenising.

Chemical mutagenesis with EMS, Formaldehyde, DES (Diethylsulfate) and DEB (Dipoxybutane) can be used for forward genetic screens. Short wave UV, IR and 32P decay are other useful techniques for creating genome wide mutations.

In reverse genetics both MosTIC (Robert 2012) (see 4.1.9) and CRISPR (Friedland et al. 2013) (see 3.3.3) have proved to be incredibly useful methods for targeting mutations to specific parts of the genome.

1.1.4 *C. elegans* Neurobiology

An adult hermaphrodite has 302 neurons that form two distinctly different systems; the significantly larger of the two is the somatic system which consists of 282 neurons, only the somatic neuronal system contains support cells, of which there are 56. The other, smaller group of 20 neurons comprises the pharyngeal system. The two are connected by just two inter-neurons, the RIP pair (White et al. 1986). During my research with *C. elegans* I have concentrated only on the neurons forming parts of the somatic system.

The worm has two clusters of ganglia and cell bodies; one is located in the head and known as the nerve ring, the other, less populated cluster can be found in the tail. A full map of the connections between all the neurons, labelled the connectome, has been produced (White et al. 1986; Chen et al. 2006; Varshney et al. 2011). Neurons in *C. elegans* can confer responses via both chemical and electrical connections (white et al 1986). In the worm, gap junctions are formed by innexins, for which there are 25 different genes. Innexins encoded by different genes appear to be able to form functional channels with each other, and each forms a distinctive expression pattern (Altun et al. 2009). *C. elegans* chemical synapses release numerous neurotransmitters, depending on the function of the neuron; Table 1.1 shows the neurotransmitters and the neurons from which they are released. When acting upon muscle cells acetylcholine causes excitation, leading to contraction while GABA acts to relax muscle.

Table 1.1 The Neurotransmitters Released by *C. elegans* Neurons.

Neurotransmitter	Neurons
Acetylcholine	ADF, AIA, AIM, AIN, AIY, AS1, ASJ, AVA, AVB, AVD, AVE, AVG, AWB, CEM, DA1, DB1-2, IL2, RIB, RIF, RIH, RIR, RIV, RMD, RMF, RMH, SAA, SAB, SIA, SIB, SMB, SMD, URA, URB, URX, VA1, VB1-2, I1, I3, M1, M2, M4, M5, MC, AS2-10, DA2-7, DB3-7, HSN, VA2-11, VB3-11, VCn, ALN, AS11, DA8-9, DVA, DVE, DVF, HOB, PCB, PCC, PDA, PDB, PDC, PGA, PLN, PVN, PVP, PVV, PVX, PVY, PVZ, R1A, R2A, R3A, R4A, R6A, SPC, SPV, VA12
Dopamine	ADE, CEP, PDE, Male only: R5A, R7A, R9A, SPSo
Octopamine	RIC
Tyramine	RIM
Serotonin (5HT)	ADF, AIM, RIH, NSM, HSN, VC4-5, CP1-6, R1B, R3B, R9B
GABA	AVL, DDL, RIS, RME, VD1-2, DD2-5, VD3-11, DD6, DVB, VD12-13
Glutamate	ADA, ADL ,AFD, AIB, AIM, AIZ, ASE, ASG, ASH, ASK, AQR, AUA, AWC, BAG, FLP, OLL, OLQ, RIA, RIG, RIM, URY, M3, MI, I2, I5, ALM, AVM, DVA, LUA, PHA, PHB, PHC, PLM, PVD, PVQ, PQR, PVR, PVV, R6A

C. elegans do not have recognised sodium action potentials, as observed in mammals, but instead rely solely on opposing calcium and potassium currents across the cell membrane (Lockery & Goodman 2009). It is for this reason that calcium indicators are the only form of fluorescent indicator

used in detecting *C. elegans* neuronal responses. Research is still ongoing to confirm whether *C. elegans* actually produces action potentials at all in its neurons. It has been shown that *C. elegans* pharyngeal muscles fire spontaneous, cardiac-like action potentials that require Na+ and Ca+ (Gao et al. 2011). Electrophysiologists have determined that the 'all-or-nothing' excitation characteristic of an action potential is absent from a number of the worm's neurons. Several neurons that have been tested show a graded response to stimulus, where the calcium transient is higher with a greater stimulus, and vice-versa (Lockery & Goodman 2009). Also, some *C. elegans* neurons appear to follow the plateau pattern of activation and suppression, specifically RMD (Mellem et al. 2008). More recently evidence has emerged that indicates that *C. elegans* body-wall muscles fire all-or-nothing calcium dependent action potentials (Gao & Zhen 2011), suggesting that the method of depolarisation of excitatory cells in *C. elegans* may be different in different tissues.

The worm's genome contains around 70 genes that encode potassium channels, all of which fall into 8 conserved families (Bargmann 1998; Wei et al. 1996). Many of the genes encoding these channels are conserved in mammals, and their functions in neuronal cells remain similar.

There are many classes of neurons within the worm, each with a defining topology and synaptic function (White et al. 1986). Despite having a relatively compact nervous system, various networks of these different classes of neurons can work together to provide the worm with a wide range of complex behaviours. Sensory neurons, with cilia exposed to the outside environment, are found in the head and tail (Ward et al. 1975). These sense both attractive and repellent stimuli in many forms, including high/low osmolarity, high/low temperature, nematode pheromones, oxygen concentration, and food cues, such as salt and benzaldehyde (Dusenbery 1980; Thomas 1993; Cornelia I. Bargmann et al. 1993; Dusenbery 1974). A specific network of command inter-neurons and motor neurons, appropriate to the stimulus, is activated by the sensory neurons and a behavioural response, whether escape or attraction ensues. These responses are relatively plastic and can be modulated by important factors for the worms' survival. For instance, in a wild type worm, the egg laying pathway is inhibited by a lack of food, while the presence of high quality food causes a reduction in worm movement and speed, ensuring the worm remains in a good environment for survival (Trent et al. 1983). Each of these responses is subject to learning by the worm, individuals learn to relate food cues with a good food source, and can be conditioned to relate other stimuli, such as temperature, with food if continually presented in unison (Hedgecock & Russell 1975).

1.1.5 Thesis Aims

The initial chapter of my thesis concerns the high-throughput tracking project, a large screen of *C. elegans* micro-behaviours using automated recording and analysis. Clustering of mutants was performed using the behavioural data in order to highlight possible functional connections between genes of known and unknown function. The final aim of the project was to compile an open-access database of subtle behavioural phenotypes of all tracked strains. The information on all tracked strains will then be accessible by any interested party, for use in their own research.

This was a collaborative project between Eviatar Yemini, Tadas Jucikas, Andre Brown, Victoria Butler and me. I was responsible for the collection of all primary data; this included all ordering, maintenance and tracking of strains. Eviatar Yemini, Tadas Jucikas and Andre Brown were responsible for writing all computer programs and matlab scripts. Victoria Butler helped to develop the tracker hardware and was involved in method development.

The following chapter looks in more depth at a pair of genes that clustered strongly together in the tracking project. *asic-2* and *acd-5* encode members of the DEG/ENaC channel family and mutations in these genes resulted in similar phenotypes. The function of these genes was unknown, but close clustering may indicate that they work in the same pathway. Using various techniques I endeavour to discover the function of the genes and determine whether the pair are functioning in a similar pathway and therefore whether the tracking system is an effective tool for finding genes with a related function.

The final chapter looks at the novel calcium indicator, GCaMP6, a modification of GCaMP5. Several different variants of GCaMP6 were produced via different point mutations. Each of these variants has been shown to work successfully different organisms, but had yet to be used in *C. elegans*. As the neurobiology of *C. elegans* differs from other organisms, and varies between its own neurons, the variants were tested in different neuronal classes within the worm to determine which variant displays the highest dynamic range and peak fluorescence.

1.2 References

Akerboom, J. et al., 2013. Genetically encoded calcium indicators for multi-color neural activity imaging and combination with optogenetics. *Frontiers in molecular neuroscience*, 6, p.2. Available at: http://www.ncbi.nlm.nih.gov/pubmed/23459413 [Accessed September 6, 2017].

Akerboom, J. et al., 2012. Optimization of a GCaMP Calcium Indicator for Neural Activity Imaging. *Journal of Neuroscience*, 32(40), pp.13819–13840.

Altun, Z.F. et al., 2009. High resolution map of *Caenorhabditis elegans* gap junction proteins. *Developmental dynamics : an official publication of the American Association of Anatomists*, 238(8), pp.1936–50. Available at: http://www.ncbi.nlm.nih.gov/pubmed/19621339 [Accessed September 18, 2017].

Alvarez, R. et al., 2009. RNA interference-mediated silencing of the respiratory syncytial virus nucleocapsid defines a potent antiviral strategy. *Antimicrobial agents and chemotherapy*, 53(9), pp.3952–62. Available at: http://aac.asm.org/content/53/9/3952.full [Accessed March 4, 2016].

Bargmann, C.I., 1998. Neurobiology of the *Caenorhabditis elegans* genome. *Science*, 282(5396), pp.2028–2033.

Blumenthal, T. et al., 2002. A global analysis of *Caenorhabditis elegans* operons. *Nature*, 417(6891), pp.851–854. Available at: http://www.nature.com/doifinder/10.1038/nature00831 [Accessed September 14, 2017].

Brenner, S., 1974. The genetics of Caenorhabditis elegans. *Genetics*, 77(1), pp.71–94. Available at: http://www.ncbi.nlm.nih.gov/pubmed/4366476 [Accessed September 11, 2017].

C. elegans Sequencing Consortium, 1998. Genome sequence of the nematode *C. elegans*: a platform for investigating biology. *Science (New York, N.Y.)*, 282(5396), pp.2012–8. Available at: http://www.ncbi.nlm.nih.gov/pubmed/9851916 [Accessed September 14, 2017].

Calahorro, F. et al., 2012. Functional phenotypic rescue of *Caenorhabditis elegans* neuroligin-deficient mutants by the human and rat NLGN1 genes. D. Dupuy, ed. *PLoS ONE*, 7(6), p.e39277. Available at: http://dx.plos.org/10.1371/journal.pone.0039277 [Accessed July 24, 2017].

Cassada, R.C. & Russell, R.L., 1975. The dauer larva, a post-embryonic developmental variant of the nematode *Caenorhabditis elegans*. *DEVELOPMENTAL BIOLOGY*, 46, pp.326–342. Available at: http://ac.els-cdn.com/0012160675901098/1-s2.0-0012160675901098-main.pdf?_tid=da4af008-8ca3-11e7-b1ca-00000aacb35e&acdnat=1504002283_0a98d9cb69a872239e3b2a17613c3e15 [Accessed August 29, 2017].

Cavalcanti, A.R.O. et al., 2003. Patterns of gene duplication in *Saccharomyces cerevisiae* and *Caenorhabditis elegans*. *Journal of Molecular Evolution*, 56(1), pp.28–37. Available at: http://link.springer.com/10.1007/s00239-002-2377-2 [Accessed September 14, 2017].

CHAFFEY, N., 2003. Alberts, B., Johnson, A., Lewis, J., Raff, M., Roberts, K. and Walter, P. Molecular biology of the cell. 4th edn. *Annals of Botany*, 91(3), pp.401–401. Available at: https://academic.oup.com/aob/article-lookup/doi/10.1093/aob/mcg023 [Accessed August 29, 2017].

Chalfie, M., Tu, Y., Euskirchen, G., Ward, W.W., Prasher, D.C. 1994. Green fluorescent protein as a marker for gene expression. *Science,* 263(5248), pp.802-805.

Chen, B.L., Hall, D.H. & Chklovskii, D.B., 2006. Wiring optimization can relate neuronal structure and function. *Proceedings of the National Academy of Sciences of the United States of America*, 103(12), pp.4723–8. Available at: http://www.ncbi.nlm.nih.gov/pubmed/16537428 [Accessed September 18, 2017].

Coulson, A. et al., 1986. Toward a physical map of the genome of the nematode *Caenorhabditis elegans* (ordered clone bank/genomic data base/clone matching). *Genetics*, 83, pp.7821–7825. Available at: https://www.ncbi.nlm.nih.gov/pmc/articles/PMC386814/pdf/pnas00324-0265.pdf [Accessed September 6, 2017].

Dusenbery, D.B., 1974. Analysis of chemotaxis in the nematode *Caenorhabditis elegans* by countercurrent separation. *Journal of Experimental Zoology Part A: Ecological Genetics and Physiology*, 188(1), pp.41–47. Available at: http://onlinelibrary.wiley.com/doi/10.1002/jez.1401880105/abstract [Accessed September 18, 2017].

Dusenbery, D.B., 1980. Journal of Comparative Physiology. A Appetitive Response of the Nematode *Caenorhabditis elegans* to Oxygen. *Physiol*, 136, pp.333–336.

Ellis, H.M. & Horvitz, H.R., 1986. Genetic control of programmed cell death in the nematode *C. elegans. Cell*, 44(6), pp.817–29. Available at: http://www.ncbi.nlm.nih.gov/pubmed/3955651 [Accessed December 15, 2016].

Fire, A., Xu, S., Montgomery, M.K., Kostas, S.A., Driver, S.A., & Mello, C.C. 1998. Potent and Specific Genetic Interference by Double Stranded RNAi in *Caenorhabditis elegans*. *Nature.*391 pp. 806-811

Friedland, A.E. et al., 2013. Heritable genome editing in *C. elegans* via a CRISPR-Cas9 system. *Nature Methods*, 10(8), pp.741–743. Available at: http://www.nature.com/doifinder/10.1038/nmeth.2532 [Accessed December 15, 2016].

Gao, S. & Zhen, M., 2011. Action potentials drive body wall muscle contractions in *Caenorhabditis elegans*. *Proceedings of the National Academy of Sciences of the United States of America*, 108(6), pp.2557–62. Available at: http://www.ncbi.nlm.nih.gov/pubmed/21248227 [Accessed September 18, 2017].

Goodman, M.B., Lindsay, T.H., Lockery, S.R., Richmond, J.E. 2012. Electrophysiological methods for *C. elegans* neurobiology. *Methods Cell Biology*. 107. pp. 409-436.

Gu, Z. et al., 2002. Extent of gene duplication in the genomes of *Drosophila*, nematode, and yeast. *Molecular biology and evolution*, 19(3), pp.256–62. Available at: http://www.ncbi.nlm.nih.gov/pubmed/11861885 [Accessed September 14, 2017].

Hedgecock, E.M. & Russell, R.L., 1975. Normal and mutant thermotaxis in the nematode *Caenorhabditis elegans*. *Genetics*, 72(10), pp.4061–4065. Available at: http://www.pnas.org/content/72/10/4061.full.pdf [Accessed September 1, 2017].

Heim, R. et al., 1994. Wavelength mutations and posttranslational autoxidation of green fluorescent protein (*Aequorea victoria*/blue fluorescent protein/*Escherichia coli*/imidazolidinone). *Biochemistry*, 91, pp.12501–12504.

Hilliard, M.A. et al., 2005. In vivo imaging of C. elegans ASH neurons: cellular response and adaptation to chemical repellents. *The EMBO journal*, 24(1), pp.63–72. Available at: http://www.ncbi.nlm.nih.gov/pubmed/15577941 [Accessed September 14, 2017].

Hutter, H. et al., 2000. Conservation and novelty in the evolution of cell adhesion and extracellular

matrix genes. *Science (New York, N.Y.)*, 287(5455), pp.989–94. Available at: http://www.ncbi.nlm.nih.gov/pubmed/10669422 [Accessed September 14, 2017].

Kaiser, P.K. et al., 2010. RNAi-based treatment for neovascular age-related macular degeneration by Sirna-027. *American journal of ophthalmology*, 150(1), p.33–39.e2. Available at: http://www.sciencedirect.com/science/article/pii/S000293941000111X [Accessed March 4, 2016].

Kamath, R.S. et al., 2003. Systematic functional analysis of the *Caenorhabditis elegans* genome using RNAi. *Nature*, 421(6920), pp.231–237. Available at: http://www.nature.com/doifinder/10.1038/nature01278 [Accessed July 24, 2017].

Kimura, K.D. et al., 2004. The *C. elegans* thermosensory neuron AFD responds to warming. *Current biology : CB*, 14(14), pp.1291–5. Available at: http://www.ncbi.nlm.nih.gov/pubmed/15268861 [Accessed September 14, 2017].

LeDoux, M., 2005. *Animal models of movement disorders*, Elsevier Academic Press. Available at: https://books.google.co.uk/books?id=Qq0SfGR_R_QC&pg=PA219&lpg=PA219&dq=c+elegans+lay+around+300+eggs&source=bl&ots=HZ1RZ8Qn4R&sig=HQQqbo1504Y5hIFs1dRnt1bOKzA&hl=en&sa=X&ved=0ahUKEwifrf_doPzVAhUoK8AKHebqAWgQ6AEIYDAH#v=onepage&q=300 eggs&f=false [Accessed August 29, 2017].

Lockery, S.R. & Goodman, M.B., 2009. The quest for action potentials in *C. elegans* neurons hits a plateau. *Nature Neuroscience*, 12(4), pp.377–378. Available at: http://www.ncbi.nlm.nih.gov/pubmed/19322241 [Accessed October 10, 2017].

Maniatis, T., Fritsch, E.F., Sambrook, J. 1982. Molecular Cloning; A Lab Manual. *Cold Spring Harbour Press.*

Mellem, J.E. et al., 2008. Action potentials contribute to neuronal signaling in *C. elegans*. *Nature neuroscience*, 11(8), pp.865–867.

Moore, E.D.W. & Fay, F.S., 1993. Isoproterenol stimulates rapid extrusion of sodium from isolated smooth muscle cells (Na+,K+-ATPase/fluorescent digital imaging microscopy/ljadrenergic receptors/cyclic AMP). *Physiology*, 90, pp.8058–8062. Available at: http://www.pnas.org/content/90/17/8058.full.pdf [Accessed September 14, 2017].

Nagel, G., 2002. Channelrhodopsin-1: A Light-Gated Proton Channel in Green Algae. *Science*.

Prestel, H., Gahr, A., Niessner, R. 2000. Detection of Heavy Metals In Water by Fluorescence Spectroscopy: On The Way To A Suitable Sensor System. *Anal Chem.* 368. pp. 182-191

Riddle, D.L., 1997. *C. elegans II*, Cold Spring Harbor Laboratory Press.

Robert, V.J.P., 2012. Engineering the *Caenorhabditis elegans* Genome by Mos1-Induced Transgene-Instructed Gene Conversion. , pp.189–201. Available at: https://link.springer.com/protocol/10.1007%2F978-1-61779-603-6_11 [Accessed September 18, 2017].

Rose, C.R. and Konnerth, A. 2001 NMDA Receptor-Mediated Na+ Signals in Spines and Dendrites. *Journal of Neuroscience*. 21 (12) pp. 4207-4214.

Shaye, D.D. et al., 2011. OrthoList: A Compendium of *C. elegans* Genes with Human Orthologs K. M. Iijima, ed. *PLoS ONE*, 6(5), p.e20085. Available at: http://dx.plos.org/10.1371/journal.pone.0020085 [Accessed December 15, 2016].

Shimomura, 0, STRUCTURE OF THE CHROMOPHORE OF AEQUOREA GREEN FLUORESCENT PROTEIN.

Siegel, D.H. et al., 2003. Loss of kindlin-1, a human homolog of the *Caenorhabditis elegans* actin-extracellular-matrix linker protein UNC-112, causes Kindler syndrome. *American journal of human genetics*, 73(1), pp.174–87. Available at: http://www.ncbi.nlm.nih.gov/pubmed/12789646 [Accessed July 24, 2017].

http://doi.wiley.com/10.1002/cne.901630207 [Accessed October 10, 2017].

Sulston, J.E. & Horvitz, H.R., 1977. Post-embryonic cell lineages of the nematode, *Caenorhabditis elegans*. *Developmental biology*, 56(1), pp.110–56. Available at: http://www.ncbi.nlm.nih.gov/pubmed/838129 [Accessed September 18, 2017].

Suzuki, H. et al., 2003. *In Vivo* Imaging of *C. elegans* Mechanosensory Neurons Demonstrates a Specific Role for the MEC-4 Channel in the Process of Gentle Touch Sensation. *Neuron*, 39(6), pp.1005–1017. Available at: http://www.sciencedirect.com/science/article/pii/S0896627303005397 [Accessed September 14, 2017].

Thomas, J.H., 1993. Chemosensory regulation of development in *C. elegans. BioEssays*.

Trent, C., Tsuing, N., Horvitz, H.R. 1983. Egg-Laying Defective Mutants of the Nematode *C. elegans. Genetics.* 104 (4) pp. 619-647.

Varshney, L.R. et al., 2011. Structural Properties of the *Caenorhabditis elegans* Neuronal Network O. Sporns, ed. *PLoS Computational Biology*, 7(2), p.e1001066. Available at: http://dx.plos.org/10.1371/journal.pcbi.1001066 [Accessed September 1, 2017].

Ward, S. et al., 1975. Electron microscopical reconstruction of the anterior sensory anatomy of the nematode *Caenorhabditis elegans*. *Journal of Comparative Neurology*.

Ward, S. & Carrel, J.S., 1979. Fertilization and sperm competition in the nematode *Caenorhabditis elegans. Developmental Biology*, 73(2), pp.304–321. Available at: http://linkinghub.elsevier.com/retrieve/pii/0012160679900691 [Accessed July 24, 2017].

Wei, A., Jegla, T. & Salkoff, L., 1996. Eight potassium channel families revealed by the *C. elegans* genome project. *Neuropharmacology*, 35(7), pp.805–29. Available at: http://www.ncbi.nlm.nih.gov/pubmed/8938713 [Accessed September 18, 2017].

White, J.G. et al., 1986. The structure of the nervous system of the nematode *Caenorhabditis elegans*. *Philosophical transactions of the Royal Society of London. Series B, Biological sciences*, 314(1165), pp.1–340. Available at: http://www.ncbi.nlm.nih.gov/pubmed/22462104 [Accessed September 18, 2017].

Yuan, J. et al., 1993. The *C. elegans* cell death gene *ced-3* encodes a protein similar to mammalian interleukin-1 beta-converting enzyme. *Cell*, 75(4), pp.641–52. Available at: http://www.ncbi.nlm.nih.gov/pubmed/8242740 [Accessed December 15, 2016].

Zhao, Y. et al., 2011. An expanded palette of genetically encoded Ca^{2+} indicators. *Science (New York, N.Y.)*, 333(6051), pp.1888–91. Available at: http://www.ncbi.nlm.nih.gov/pubmed/21903779 [Accessed September 6, 2017].

Chapter 2: The Automatic Analysis of Subtle Behavioural Phenotypes in *C. elegans*

2.1 Introduction

A useful method of identifying genetic aberrations is to assess the behavioural phenotypes they cause in simple organisms. *C. elegans* behavioural phenotypes are well characterised and can easily be quantified; often noticeable changes in these behaviours are due to perturbations within the organism's genome.

In *C. elegans* an easily characterised and measurable behaviour is locomotion. The detection of several mutant locomotory phenotypes, discussed later in this chapter, have lead to identification of the function of the gene causing them. As *C. elegans* has been very well studied, the most obvious phenotypes have already lead to the identification of the genes responsible. There are, however, a number of subtle phenotypes that are not as easily observed by eye, and may still lead to elucidation of the function of the gene controlling them. It stands to reason, therefore, that a high-throughput screen of subtle phenotypes may be a useful start-point for detecting the functionality of unknown genes, and also unknown functions of previously characterised genes. Elucidating the function of the unknown genes in *C. elegans* can guide researchers working on higher organisms to the function of orthologous genes in mammals.

This chapter will discuss the automatic tracking of approximately 300 *C.elegans* mutants, some of known and some of unknown genetic function. With a total of 20-24 videos of individual worms of each strain, together with wild type controls, over 12,000 recordings make up a database of features freely available online. (wormbehaviour.mrc-lmb.cam.ac.uk)

2.1.1 Locomotion in *C. elegans*

In the laboratory setting *C. elegans* will perform two distinct types of locomotion, crawling and swimming (Gray & Lissmann 1964)(Fig 2.1A). Crawling takes place on a solid surface, or in a high viscosity medium, while swimming occurs in liquids of low viscosity. In a liquid of medium viscosity the worm will switch between distinct periods of swimming and crawling. The widely held belief is that the two forms of movement are distinct gaits, and a swimming/crawling hybrid cannot be observed, suggesting that the two gaits are modulated by different pathways (Vidal-Gadea et al. 2011). There is some contest to this, however, that suggests that intermediate behaviours can be observed when allowing worms to move through increasing concentrations of gelatine (Berri et al. 2009).

The two gaits are characterised by differences in the frequency and amplitude of body bends. During swimming the worm's gait bends at a high frequency and low amplitude, while during crawling the worm exhibits the opposite respectively (Vidal-Gadea et al. 2011; Pierce-Shimomura et al. 2011). During the high-throughput tracking project described in this chapter some attempts were made at recording mutants swimming, but the vast bulk of work concentrated on the crawling motion of *C. elegans*.

Crawling is achieved by means of opposing dorsal and ventral contractions of the longitudinal body wall muscles (Brenner 1974), resulting in a typical sinusoidal movement. There are 95 muscles involved in crawling; these are separated into 4 longitudinal quadrants running the length of the worm, with 2 quadrants each for the dorsal and ventral side (Sulston & Horvitz 1977).

A total of 113 of the 302 C. elegans neurons are motor neurons that fall into 8 distinct classes (AS, VA, VB, VC, VD, DA, DB, DD), which are defined based on morphological and synaptic connection similarities. The VA, VB, VC and VD classes of motor neuron innervate the ventral body wall muscles, whereas the DA, DB, DD and AS classes send commissures across the body to innervate the dorsal body wall muscles (White, Southgate et al. 1976; White, Southgate et al. 1986). The A and B motor neurons are acetylcholinergic and excitatory (Riddle 1997; Duerr, Han et al. 2008). The D motor neurons are GABAergic and inhibitory (Mcintire, Jorgensen et al. 1993; Mcintire, Jorgensen et al. 1993).

The range of shapes which the worm can form is limited by the cuticle flexibility and the manner in which the muscles innervate. It has previously been demonstrated that 95% of the postures formed by *C. elegans* when crawling can be described by 4 typical shapes (Stephens et al. 2008) (Fig 2.1B).

Worms will crawl on either their left or right sides. Switching of sides in normal lab conditions is rarely seen in wild-type and most mutant strains, with the exception of roller mutants, which switch sides almost continuously (Cox et al. 1989).

During crawling the worm exhibits a behaviour known as foraging, a trait absent from swimming worms (Vidal-Gadea et al. 2011). This is seen as a rapid dorsal to ventral movement of the nose and head, and is coupled with rapid pumping of the pharyngeal muscles.

Another measurable behaviour is egg-laying. It has been shown that *C. elegans* exhibit particular locomotion during egg-laying events. The worm is seen to speed up immediately prior to, and during, egg-laying; mean-while reversals are repressed (Hardaker et al. 2001). Defecation rhythms also affect the locomotion of *C. elegans*. Defecation occurs every 50-60 seconds, it is preceded by a short reversal and is followed by forward locomotion. It is thought that this behaviour enables the worm to escape its own excrement (Nagy et al. 2015).

As well as sinusoidal postures, *C. elegans* exhibits various turning movements. The worm will begin these turns in order to escape a noxious stimulus or to return to a good food source (Ward 1973). Omega turning is a behaviour where the worm changes in a near opposite direction and, in doing so, its body forms a shape similar to the Greek letter Ω (Croll, 1975). Pirouettes are more shallow bends, preceded by a short reversal, that result in a less severe change in direction. Pirouettes are more commonly seen when the worm is travelling down a gradient, and are therefore believed to be a method of reorienting individuals towards an attractant (Pierce-Shimomura et al. 1999). A third turning behaviour is coiling. Here the worm forms a tight coil, emerging from it in a different direction to which it was previously travelling. Coiled worms can also be indicative of unfavourable environments. For example, worms tend to coil when the surrounding temperature exceeds ~25°C, or during initial introduction to a liquid medium (Croll, 1975).

Several environmental conditions can modulate *C. elegans* locomotion, one of the greatest factors being food. In the presence of food worms will dwell more, move more slowly and turn less regularly. A well fed worm confronted with a foodless, or low quality food, environment will move faster, dwell less and turn frequently, all in the search for a food source (Croll & Smith 1978). Escape responses from noxious stimuli will cause increased reversals and turning (Ward 1973; Dusenbery 1974), as will moderate vibrations and UV light (Ward et al. 2008; Rankin et al. 1990; Chalfie & Sulston 1981). All these aspects must be taken into consideration when conducting behavioural assays in *C. elegans*, in order to eliminate behaviours resulting from confounding variables.

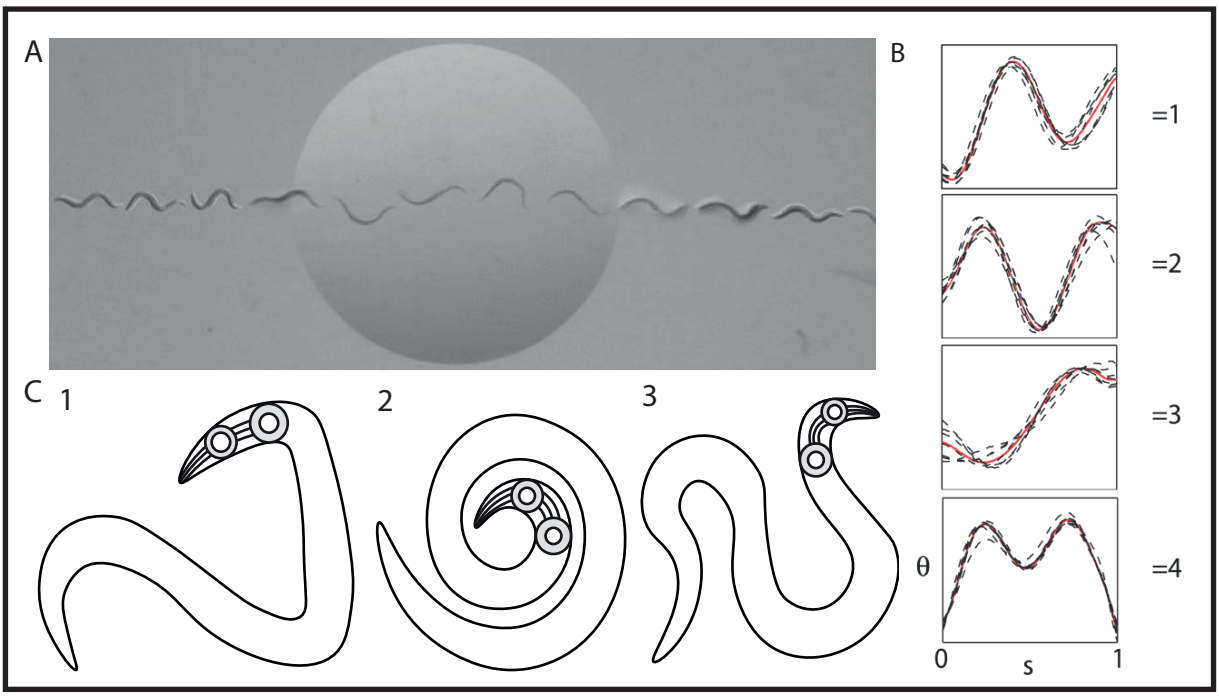

Fig.2.1 *C. elegans* Postures. A: Shows the change in worm posture upon entering and leaving a liquid droplet, prior to entering and following exit the worm is crawling. During the time in the droplet the worm is swimming (Molecular Neuroethology Lab, Illinois State University). B: 1-4 show the 4 eigenworm projections produced by Stephens et al 2008. A combination of these 4 eigenworm shapes is sufficient to describe any 95% of postures created by wild type *C. elegans*. C: 1 a line drawing of the posture of a kinker worm, 2: the posture of a coiler worm 3: The posture of a loopy worm.

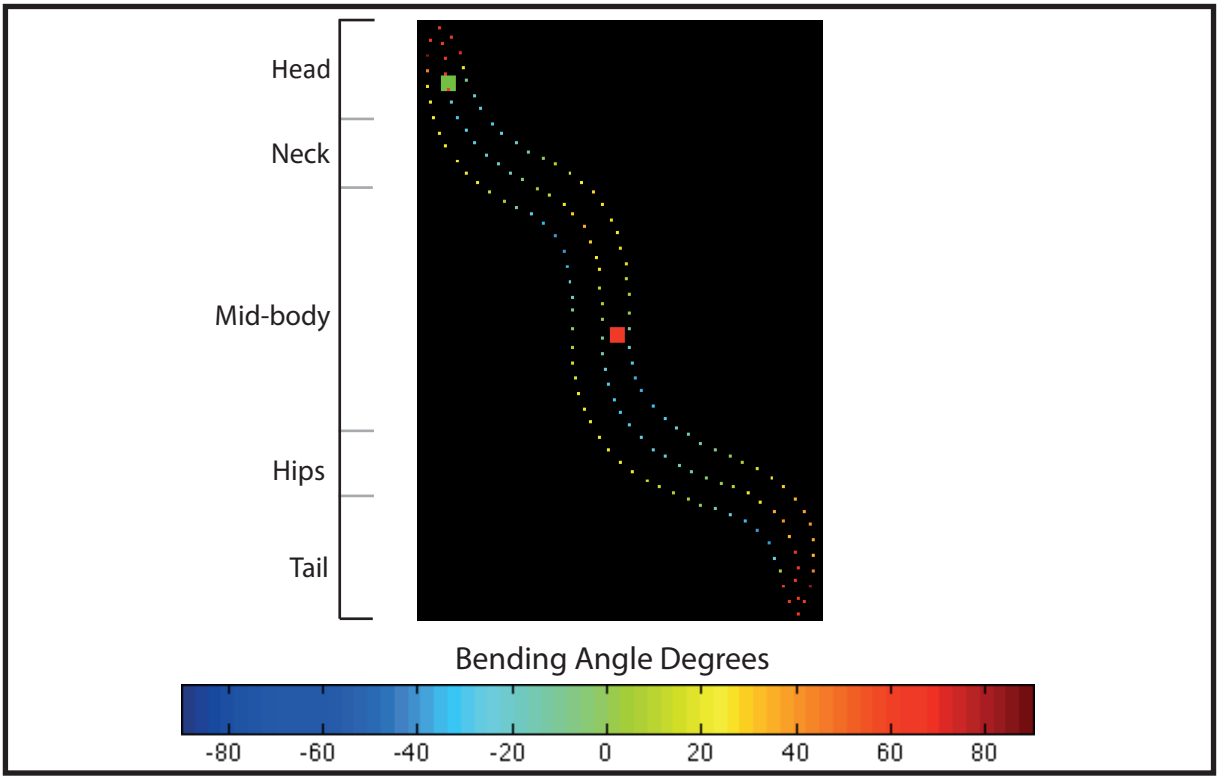

Fig.2.2: *C. elegans* segmentation. An individual worm after segmentation. Dots forming the left, right and midline of the worm are the 49 skeleton points. The colour of the points, blue to red, denote the bending angle in degrees between an individual point and those either side. Dark blue covers the range of -180 to -90 and dark red +90 to +180. The green square annotates the head, and the red square the vulva (Yemini 2011).

2.1.2 Phenotype-guided experimentation

A number of atypical locomotion phenotypes have been observed in *C. elegans*. The first paper to report these mutant phenotypes was the aforementioned study from Brenner in 1974. The EMS induced mutations from this experiment produced mutant strains with two broad groups of locomotion-variable phenotypes, roller and uncoordinated (Brenner 1974). Since this study, finer classification of different *unc* mutants is common. Recognised descriptions include kinker, coiler, loopy (see Fig. 2.1C), sluggish, shrinking and slow. Additional, but coordinated, phenotypes include forward locomotion variants and activity variants (Hart 2006). These worms may move in a coordinated manner, but either move abnormally fast or slow, or spend an abnormal amount of time travelling forwards or backwards. Identification of these phenotypes is important as they can guide experimenters to potential functions for the mutated gene.

Identification of the function of various genes has been possible from the study of locomotion phenotypes. An early example of this is the elucidation of the function of *unc-54*. In his initial study, Brenner identified *unc-54* mutants as paralysed, with a body muscle defect (Brenner 1974). In a following experiment, the musculature of *unc-54* mutants was observed using electron microscopy. The structure of the muscle in the mutant was found to be disorganised in comparison to the of the N2 worms. *unc-54* worms had fewer thick filaments, the myosin containing component of the muscle, than wild-type (Epstein, Waterston, & Brenner, 1974). MacLeod et al. Later proved that *unc-54* does in fact code for the myosin-heavy chain in *C. elegans* (Macleod, Waterstox, Fishpool, & Brenner, 1977).

Once phenotypic data has been established for various genes it is possible to cluster together mutant strains based on their locomotion. In some cases, but not all, mutants displaying similar phenotypes are working within the same pathway, or have similar functions in different pathways. This makes it possible to speculate the function of a particular gene, based on those mutants with common variants.

Examples of this are *unc-54* and *unc-15*; mutations in both of these genes show a paralysed phenotype with abnormal body muscular structure (Brenner 1974). Both are also shown to be involved in myosin filaments, UNC-54 myosin heavy chain and UNC-15 paramyosin (Macleod et al. 1977; Kagawa et al. 1989) .

Brenner's study also identified *unc-14*, *unc-33*, *unc-44*, *unc-60* and *unc-51* mutants as paralysed (Brenner 1974). These mutants are all found to have a role in axon outgrowth or depolarisation, but no role in myosin filaments (Ono et al. 2003; Otsuka et al. 1995; Ogura et al. 1997; Li et al. 1992).

While *unc-14* and *unc-51* are known to work in the same pathway, and mutations in the genes result in similar phenotypes, mutations in the gene encoding the protein UNC-5, which they are involved in localising, have a slightly different phenotype (Ogura et al. 1997; Ogura & Goshima 2006).

This demonstrates how phenotypic comparison can be a useful technique for identifying a gene's function, but it cannot be taken for granted that genes with common phenotypes have similar functionality. Phenotypic analysis, therefore, should be used as a rough guide for the functionality of a gene, but further investigations must be made for full function determination.

2.1.3 Tracking in *C. elegans*

As it would be time consuming to manually observe multiple locomotory phenotypes in *C. elegans,* many laboratories have developed methods of automatic tracking. This simple method provides a

system to make scalable comparisons between mutant behaviours without the issue of experimenter bias.

The first of these developments was the multi-worm tracker created by the Dusenbery lab in 1985. The system was capable of tracking around 25 individuals, and automatically determine the speed of the worms and the number of direction changes they made (Dusenbery 1985). In the experiments that followed the creation of this tracker, the Dusenbery lab was able to show changes in *C. elegans* behaviour upon introduction of differing concentrations of carbon dioxide (Dunsenbery 1985).

The use of multi-worm trackers has been employed in many published works; however, the method does have its drawbacks. Multi-worm trackers have a wide field of vision and low magnification, to allow for worms to be tracked without individuals leaving the area being recorded. When looking at more subtle movements, such as foraging, worm morphology, crawling amplitude and the depth of head/tail bends, the low magnification is not conducive to obtaining accurate results. Measurements of these features require a more magnified view, which necessitates a system that will follow an individual worm as it moves on the agar plate. This stops the worm from crawling out of the field of vision, but also means that only one worm can be assayed at any one time.

Several historic studies have used this method, the first examples involved investigations in egg-laying behaviour. Waggoner at al. successfully used single worm tracking to record egg-laying events over a long period of time. Worm movies generated in this way can be played at fast speed and egg-laying events recorded, saving large amounts of experimenter time (Waggoner et al. 1998). The same method was subsequently used by Kim et al. to observe the role of nicotinic receptors in the egg-laying pathway (Kim et al. 2001). A following paper by Hardaker et al. took single worm tracking further. Here, single worms were tracked over a period of time in order to detect differences in the locomotion of worms in and around egg-laying events. Results showed peaks in worm velocity preceding and following egg-laying events. The tracking system was also used to compare the locomotion during egg-laying of individuals carrying the *egl-1* mutation, a condition that results in the inappropriate cell death of the HSNs. As the typical behaviour of the wild-type worms around egg-laying events was not observed in the mutants, researchers were able to deduce that the HSNs are involved in locomotory regulation during egg-laying. Furthermore, automated tracking of serotonin mutants, *tph-1* and *cat-4*, showed the same atypical locomotory phenotype as *egl-1* mutant worms, consistent with the theory that egg-laying behaviour is modulated by serotonin release by the HSNs (Waggoner et al. 1998; Hardaker et al. 2001). Investigations such as this display how useful automated tracking can be in elucidating connections between locomotor behaviour and cellular signalling.

The tracker used by Hardaker only had the ability to measure worm velocity and directional changes, any other features were annotated manually. This left much scope for improvement on the tracking system. Baek et al. built on the work by Hardaker and produced a tracker that, not only made a video recording of the worm's movements, but also recorded a digitised version of the video file. This digitised file was then analysed for the existing features of velocity and direction change, but also new features. The new tracker was able to detect reversals and body size, shape and posture. Using these parameters experimenters were successful in classifying the locomotory phenotypes of 5 uncoordinated mutants (Baek et al. 2002).

Worm tracking technology developed quickly following the introduction of the new features. Between 2004 and 2007 combined efforts by the Schafer and Sternberg labs resulted in a tracker

that was able to record a high-resolution, digital movie of the worm. The system could automatically assign the head and tail of the worm (Geng et al. 2004), and detect omega bends, egg-laying events and coiled shapes (Geng et al. 2005; Huang et al. 2006). The resultant tracker was subsequently known as Worm Tracker 1 (WT1)(Feng et al. 2004).

2.1.4 Development of WT2

WT1 had some issues; as it was large and expensive it was impractical for high-throughput experiments. The rate of system crashes was high and caused all labs but the initial developer's to abandon the system.

The void left by the decline of WT1 necessitated the development of a system that was both sensitive enough to pick out *C. elegans* micro-behaviours while also being high-throughput.

Worm Tracker 2 (WT2) was developed by the Schafer lab for this role. Comparatively inexpensive, small in size and highly sensitive to minute changes in behaviour, several units can be housed and used simultaneously to produce large amounts of high quality data in a relatively short space of time. The total cost of one WT2 unit was initially ~£3200 (~$5160) a reduction in price from WT1 by approximately 50% (A full list of costs can be found in the appendix). Over the following 8 years there has been a further reduction in price as the USB microscope cameras become available at a cheaper rate. This allows for a single lab to afford several units, and so increase the volume of data that can be produced at any one time. The new tracker system was also able to create digital videos without the need for making any analogue copies, could record at 30 frames a second and produces a high quality 1.3 megapixel image. WT2 also had the advantage of a higher magnification than WT1, with a maximum of 220x. Such a high magnification is useful when it comes to tracking worms in their larval stages. These improvements enable the experimenter to visualise micro-behaviours with relative ease and, hopefully, to identify as yet unnoticed phenotypes (Yemini 2011a). (A full part list and construction method can be found in appendix)

2.1.5 Development of Analysis Toolbox 2

As this is a high-throughput, automated study, there not only needed to be a way of recording worm postures automatically, but also of analysing the resulting large amount of data. It would not be feasible for experimenters to perform any part of the analysis manually when it comes to such a vast data set, necessitating the development of a software package that could pull out all useful data with no user interference. Analysis Toolbox 2 (AT2) is capable of defining 702 features that, when used in conjunction, define detailed information for 22 broader aspects of *C. elegans* locomotion (Yemini et al. 2013)

2.1.6 Genes linked to locomotion and morphology

2.1.6.1 Uncoordinated mutants

To provide an expansive base for comparison of mutant phenotypes, a large number of uncoordinated (*unc*) mutants were tracked. An effort was made to incorporate as much variety in mutant postures, both mild and extreme, in order to better classify all the possible postures that the worm can make. A sample of phenotypes including the well documented uncoordinated groups was used; these consist of coilers, kinkers, paralysed, sluggish and fainters. Table A1 (Appendix) shows the uncoordinated genotypes and their previously assigned phenotypes.

It was hoped that this sample of the *unc* mutants would provide representatives for each of the postures to be characterised. Not only would this help us to cluster unknown mutants with extreme

phenotypes into groups with easily identified characteristics, but also test the tracker software and analysis package in its ability to group known, like mutants together.

Within this group of *unc* mutants were a number of strains where two mutant alleles of the same gene have been tracked, for example *unc-8* and *unc-1* mutants. It is generally the case with most mutant alleles of the same gene that the resulting phenotype are the same, or similar. It is therefore postulated that, should the tracking system function properly that these alleles should cluster strongly together.

Another test for the WT2 system was to determine whether any of the *unc* mutants that were deemed to have similar phenotypes, for example a coiler phenotype, were actually behaving very differently in any other measured variables. In the past, when observing by eye, only the most striking postures were recognised and it may be the case that the more subtle phenotypes have just as great a role in highlighting function as the obvious ones.

2.1.6.2 Other tracked families

A number of other *C. elegans* gene families were chosen for tracking. These were chosen because one or more of their members, when mutated, had already been observed to have some form of locomotory, or measurable behavioural, phenotype.

These families included the G-protein coupled receptor mutants, acetylcholine receptor mutants, dopamine pathway mutants, serotonin pathway mutants, mechanosensory mutants, insulin pathway mutants, egg laying mutants, FMRF-like peptide mutants and morphological mutants.

2.1.7 Project Aims

To track a large number of *C. elegans* mutants of known and unknown function in a precise and replicable manner. To analyse the data computationally and establish possible phenotypic connections between mutants using clustering. Finally, to create an open access database of *C. elegans* mutant behavioural phenotypes for other researchers to access and use the data obtained.

2.2 Materials and Methods

2.2.1 WT2

The worm tracking hardware was developed by Ev Yemini, Tadas Jucikas and Victoria Butler (Yemini et al. 2013; Butler 2012). Each unit comprises of a heavy stainless steel base that functions both as a structural base for the tracking system and as an effective dampener of minor vibrations from the laboratory bench. Onto the base is mounted a 50mm stainless steel Comar cylinder, which itself mounts a plastic bracket with a rack and pinion stage. A clear Perspex square measuring 50x50mm is affixed to this stage and this is where the plate containing a worm is placed during recordings.

Below the rack and pinion, 2 translation stages are mounted to the base, one for backward/forward movement and one for left/right movement. Affixed to each of these is a Zaber automated actuator, these are plugged into the computer where they can be manipulated by the tracker software to move the stages in their assigned direction by a fraction of a millimetre with each click. The resultant range of movement is 50mm x 50mm.

On top of the stage is a wooden base upon which a tripod structure built from 10mm Comar cylinders is mounted. The tripod creates the firm structure required to hold a red LED light, for illumination of the worm, as well as a frosted wide lens and opal diffuser to create even light across the camera field.

Also mounted on the wooden stage is a Dinolite digital USB microscope (AM413T prior to 2016, AM4113T post-2016) connected to the computer. This points directly upward, focusing on the clear Perspex plate mount, with the red light shining directly into the centre of the camera. This alignment is created by removing the diffuser and positioning the LED so that the light is focused onto the centre of the display window in the worm tracking software. The LED lights on the Dinolite microscope are turned off during experimentation.

Distances of 90mm from the camera optic to the light diffuser and 40mm from diffuser to LED light were maintained throughout experiments as this allowed for the best contrast between worm and agar surface. (A full part list and prices and images of the set up can be found in appendix).

2.2.2 WT2 software

The Worm Tracker 2 software and interface were designed by Ev Yemini using MATLAB.

The software allows for calibration of the automated stage, automated tracking of the worm, and selection of desired recording and movement parameters.

Calibration of the automated stage is achieved using an inbuilt function that determines the conversion from onscreen pixels to absolute coordinates. All trackers were calibrated on a weekly basis. In the event of a camera accidentally being moved out of position, this unit would have to be recalibrated in order to maintain accuracy of recordings.

The tracking parameters used for all tracking experiments used in the behavioural database can be found in appendix.

Using the software the automated stage can be manipulated forward/backward, left/right and diagonally by clicking the manual direction keys. In this fashion a worm can be found on the agar surface, and once found a click of the start button will begin the automated tracking of the worm. The dark mass of the worm is identified by the software and ensures that the centre of the mass

never leaves an experimenter defined centroid boundary. A detailed description of the scripts used to automatically track the worm can be found in Ev Yemini's thesis (Eviatar Yemini, 2011a).

2.2.3 Method for high-throughput worm tracking

To ensure standardisation of the conditions in which worms were grown a strict method was devised and followed for the maintenance of all worm strains.

Worms were grown on standard 6cm NGM plates (Appendix, Recipes, NGM) that had been dried for 2 days at 22° C and seeded with 100µl of OP50, then allowed to grow for another 24 hours at 22°C. Six gravid hermaphrodites were picked from a three day old plate onto a fresh plate, and the strains were then picked in this fashion every three days whilst in use.

For experimentation 10 worms of each strain were picked as L4 larvae approximately 18 hours before tracking onto a fresh, OP50-seeded, NGM plate.

Tracking plates were made with low peptone NGM (Appendix, Recipes, Low Peptone NGM) to keep the OP50 lawn thin, and were dried for 48hours before use. On the day of experimentation plates were seeded with 20µl of OP50 in the centre of the plate and allowed to dry for half an hour. The resultant food lawn was approximately 5cm in diameter, situated in the centre of the 3cm plate Once dry a single worm was picked to each of 8 plates and was allowed to acclimatise for 30 minutes prior to recording. At this point the left/right (L/R) orientation of the vulva was noted, this was later included in the video name at the analysis stage. This is important for determining the position of the head and tail and for dorsal/ventral orientation.

5 minutes before recording is set to commence the tracking plate containing a single worm is placed onto the Perspex mounting stage and, using the manual stage manipulation keys, the camera is moved by the operator to find the worm. Upon finding the worm in the recording window the 'start' tracking button is clicked and the automated tracking commences. In the event of a worm crawling too close to the edge of the plate, and not returning before the video is set to start, the recording for this unit is abandoned.

Videos were recorded using the WT2 hardware set up as previously described. All videos were recorded at 30 frames per second for 15 minutes each. Each strain was recorded on each of 8 trackers once on each of 3 days, totalling 24 videos per strain, with the aim of having at least 20 analysable videos per mutant. Strains were rotated around the trackers with an N2 control throughout the day. This allowed for comparison of N2 behaviour throughout the day and over several days to rule out any behavioural differences that may be a result of temperature or daylight fluctuations. All experiments were carried out between 8am and 6pm at 22°C, in artificially lit laboratory space and always out of direct sunlight. Mutant genes of the same family were tracked as a group over a period of around 3 weeks.

2.2.4 Strains

A list of strains, including strain name, gene, allele, chromosome and source can be found in appendix table A2.

2.2.5 Analysis

Analysis of videos was performed using in-house developed MATLAB-based software; Analysis Toolbox 2 (AT2) developed by Eviartar Yemini, Tadas Jucikas and André Brown (André E X Brown et al. 2013; Yemini et al. 2013).

AT2 analyses the video frame by frame, in each instance the worm is segmented from its background. The worm is located by grouping together pixels that are darker than a particular threshold (Otsu threshold). The segmented worm is then skeletonised, reducing the shape to a contour and midline dissecting the length of the worm. The points of highest curvature along the outer line are taken to be the head and tail. The skeleton is then divided into 49 equally spaced sections and the orientation of each segment in comparison to the other is used to determine the posture of the worm (Fig.2.2). Skeleton points 1-8 of the worm are defined as the head, 9-16 as the neck, 17-33 as the mid-body, 34-41 as the hips and 42-49 as the tail. For features detailing the head and tail tips, skeleton points 1-4 and 46-49 respectively were used.

L/R orientation of the vulva was entered manually into the file name of the video and the software package was able to identify this from the file name. The entry of vulva side allowed more accurate automatic detection of head and tail, and allowed for detection of any dorsoventral asymmetry. The velocity of the worm is calculated automatically by logging the number and direction of stage movements. Each stage movement in the X or Y direction is manually set at a specific number of microns, the number of movements can then be used to calculate the distance travelled. The time it took to make the movements is used to calculate speed. The combined distance travelled in the X and Y directions indicates velocity.

The process of automatic analysis takes around 1 hour for each video. A folder of 16 videos can be automatically analysed over night without any user input.

Several features are subdivided into forward, backward and paused locomotory states. Using this method it is possible to measure features such as speed, foraging amplitude, crawling amplitude and many other such traits during the different directional movement. This is particularly important as we know that certain traits, such as foraging, are suppressed during reversals (Alkema & Hunter-Ensor 2005). A mutant that continues to forage on reversing would be interesting to investigate.

Coiling, turning and motion states were measured both in frequency and in total time and distance any one worm spent in said form throughout an experiment.

A detailed description of algorithms and scripts for AT2 can be found in Eviatar Yemini's thesis (Yemini 2011a).

The features file that results from the software can be entered into a MATLAB script, written by Andre Brown, to produce an excel spreadsheet containing numerical scores for all the features for individual videos. To test the differences between mutant strains and wild-type controls the Wilcoxon rank-sum was used and Fisher's exact test was used for measurements found exclusively in the control or experiment group. In order to control for false discovery rates, p values were converted to their q equivalents. Each group was given its minimum q value as a measure of group significance. A q value of ≤0.05 was used to determine significance (Yemini 2011b).

2.2.5.1 General features

1: Morphology features:

Length, width, area, area/length and **mid-body/length**

These highlight large, small, fat or thin worms

2: Posture features:

Bends, results are shown as head, neck, mid-body, hip and tail bend. Positive numbers denote a dorsal bend, while negatives denote ventral bends.

Bend count, the number of bends.

Eccentricity, a measure that is primarily used to calculate other features, amplitude, wavelength and track-length and is not used as an informative result on its own.

Amplitude, the depth of the bends produced during sinusoidal crawling.

Wavelength, the breadth of the bends produced during sinusoidal movement.

Track-length, the range of the skeletons horizontal projection.

Coils, are noted as positive or negative to denote dorsally/ventrally entered coils.

Eigenworms, discussed in more detail later in the chapter, the result for each eigenworm projection, 1-6, denotes the proportion of time each animal spent in this posture.

Orientation, the angular direction from tail to head centroid.

3: Motion features:

Velocity, measures speed and direction at the head, mid-body and tail. A negative number denotes a reversal, while positive is forward motion, the number represents speed in microns/sec. The head and tail of the worm are determined in order to judge the direction of movement of the worm. Firstly the 2 points with the sharpest angle between skeleton points are detected. These represent the head and tail. Secondly, the movement and pixel intensities at the two points are calculated, the darker, more frequently moving end of the worm is labelled as the head. Movements in the direction of the head are considered forward locomotion and those in the direction of the tail are considered reversals.

Motion state, Forward, backward and paused.

Crawling, expressed as both amplitude and frequency at the head, mid-body and tail. Positive crawling amplitudes and frequencies show the time spent with the dorsal side is contained within the concave part of the bend, while negative is ventral.

Foraging, a measure of aperiodic nose movements, shown as amplitude and speed. A higher amplitude indicates greater nose bending and a higher speed faster nose bending.

Turns, Omega and Upsilon turn frequency, time and dorsal/ventral entry is shown.

4: Path Features:

Range, is the distance the worm travels over the experiment.

Dwelling, shown for head, mid-body, tail and whole worm, this features tells how much time the worm spends dwelling.

Curvature, the angle of the worm's path (radians) divided by the distance travelled (microns) as a measure of the general curvature and ventral/dorsal bias of an individual.

For detailed explanations of the mathematics involved in calculating numerical values for each feature see Eviartar Yemini's thesis (Yemini 2011a).

A full list of features can be found in appendix table A3.

2.2.5.2 Eigenworms

As previously discussed, 4 *C. elegans* postures are sufficient to describe 95% wild-type locomotion (Stephens et al. 2008). Using 15 hours of our Bristol N2 tracking footage, six postures, or eigenworms, were found that describe 97% of posture variance.

At least one hour of locomotion data was pooled for each of the strains tracked, and their skeleton angles for each frame were projected onto the previously described wild-type eigenworms. Results are shown as the mean probability that, at any point in the recording, the mutant will fit a particular eigen-projection, in either the dorsal or ventral orientation.

2.2.5.3 Eigenworm motifs

Motifs were determined by finding sequences of behaviours that are repeated at least twice within the 15 minute recording. A total of 2,223 motifs, of varying lengths, were used to produce a behavioural motif dictionary. A quantitative fingerprint of motifs is then produced for each recording, formed by a vector of distances of the mutant behaviour from each of the motifs (A.E.X. Brown et al. 2013). The distance between the fingerprints for each individual of a strain was averaged to create a quantitative measure of their phenotypic dissimilarity.

To compare the motifs for the whole set of data the dictionary was reduced to 700 elements, chosen using the minimum redundancy maximum relevance criterion (Peng et al. 2005). The smaller subset was found to give robust results while reducing computer analysis time.

2.2.6 Clustering

For both clustering protocols, analytical scripts were written in MATLAB in a combined effort by Andre Brown and Eviatar Yemini. Where possible existing MATLAB toolboxes were used: videoIO toolbox by Gerald Dalley, swtest function by Ahmed Ben Saïda, fexact function by Michael Boedigheimer, 191 function by Oliver Woodford, notBoxPlot function by Rob Campbell, and rdir function by Gus Brown.

2.2.6.1 Motifs

In order to cluster mutants into phenotypically similar groups, affinity propagation was used. Affinity propagation is a clustering algorithm used in data mining that does not require the number of clusters to be determined or estimated before analysis (Frey & Dueck 2008). Inverse Mahalanobis distance between strains as the similarity measure. The Mahalanobis distance is a distance metric used to measure the distance between two points in a feature space. Unlike the Euclidean distance, it uses the covariance matrix to "adjust" for covariance among the various features. The Mahalanobis distance formula uses the inverse of the covariance Clustering was repeated 100 times with replacement and the most frequent 10% of connections was used in the phenotypic similarity network (A.E.X. Brown et al. 2013).

2.2.6.2 Feature Clustering

The mean for individual features, for each mutant strain, was calculated and normalised against the corresponding features in N2 worms recorded on the same day. Means were normalised by subtracting the N2 mean from that of the mutant and were scaled by their variance.

2.2.6.3 Internal controls

To determine whether N2 results were consistent across all hours, days and months, all N2 recordings were subject to normalisation against each other. Each wild type recording was grouped into various categories determined by the hour, day or month in which they were recorded. Each of these groups was then normalised against all other recordings in the remaining groups. For example, N2s recorded at 9am were grouped and normalised against all other time points.

Rarely, measures were only found in the mutant strain or its control. In this case it is not possible to normalise the mutant against N2. Instead the z-score was given as double the population maximum if the measure is found in the mutant but not control. If the measure is present in the control but not the mutant, double the population minimum was given as the z-score (Yemini 2011a).

2.3 Results

For analysis of the large amount of data compiled in the high-throughput tracking project two different types of clustering were used; both provided some promising results, with mutants in genes of known function clustering strongly with those known to be working in the same pathway, but the results were slightly different between the two methods.

2.3.1 Features Clustering

The clustering scripts and analysis of the results of this form of clustering were done by Eviatar Yemini. A detailed description of the algorithms used can be found in Eviatar Yemini, 2011a.

2.3.1.1 Reproducibility of Results

Variability in worm behaviour is to be expected within worms of the same genetic stock, these variations can arise from environmental conditions, worm age or feeding state. Although much care was taken to reduce these factors for variability, small differences are expected. A number of analytical tests were performed on the dataset to determine how influential the external factors have been on reproducibility and accuracy.

2.3.1.2 Variability within Single Animals

C. elegans are sensitive to touch and vibrations and become aroused for a short time after the mechanical stimulus is invoked. During arousal worms will move at a higher speed, perform more escape responses and respond to external stimuli in a more pronounced fashion (Chew/Schafer, unpublished). Therefore, when picking a worm to a new plate, that worm is expected to be aroused for some time after the picking event. To determine the time it took for behaviours to stabilise after picking, 2 hour, continuous recordings of 25 day 1 adult N2s were made. The rate in decline of speed, crawling amplitude and crawling frequency was plotted (Fig.2.3.B, C and D) and the length of time for speed and crawling frequency began to plateau at around half an hour. The rate in decline of crawling amplitude was slightly slower, with amplitude plateauing at around 1 hour. It was for these reasons that worms were allowed to acclimatise to the tracking plate for 30 minutes after picking.

The growth rate of N2 worms over this period was also measured in order to determine how much difference there may be between day 1 adults over the time course of 2 hours. There is a small percentage increase in width and length of the worm over the 2 hour recording (~3% for width and 2% for length) (Fig.2.3 A). At this rate of size increase worms tracked at 5pm would be ~12% larger than those tracked at 9am.

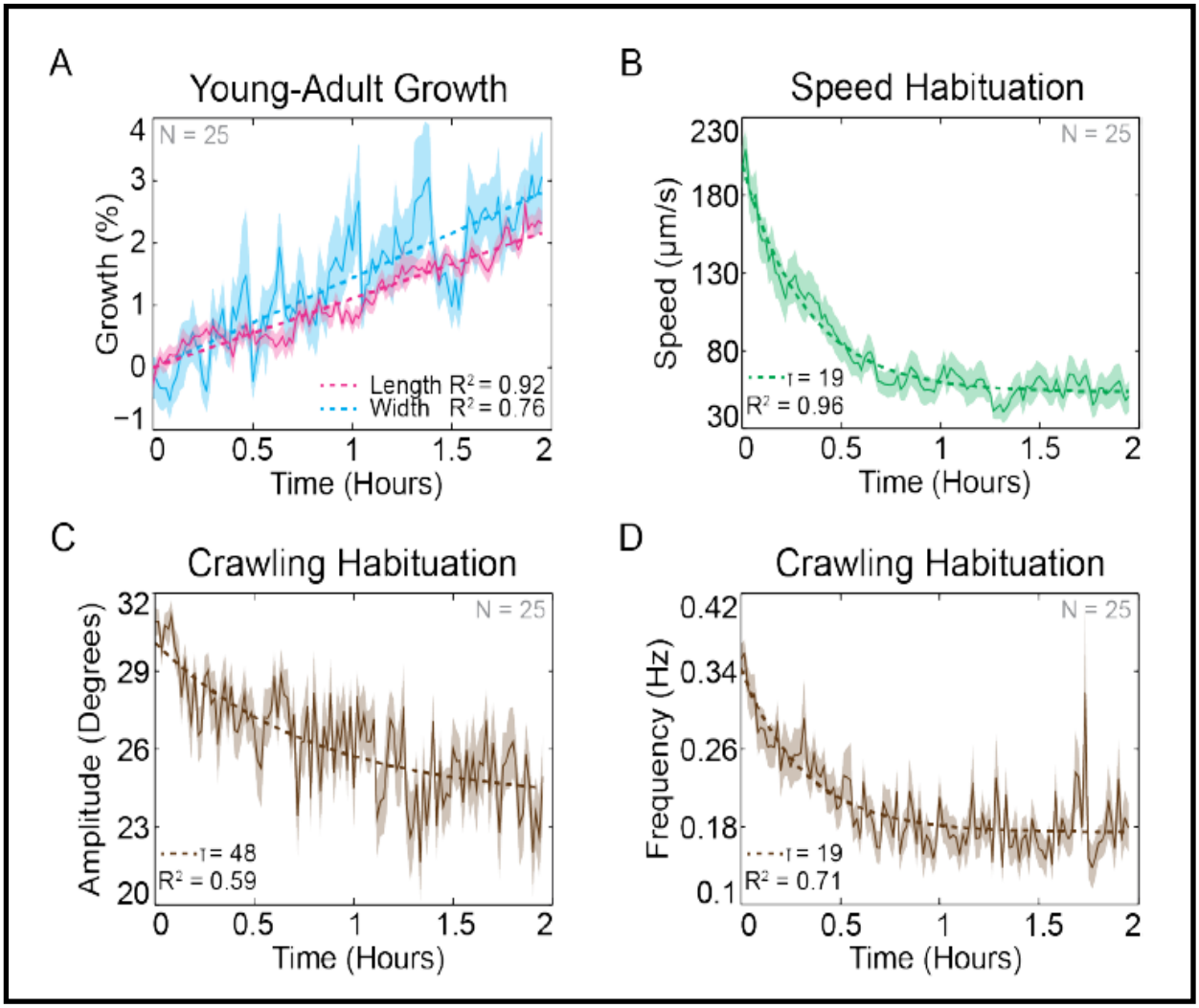

Fig.2.3: The Difference In Size, Speed and Crawling In N2 Worms Over A 2 Hour Period From Picking. A: The average size of 25 N2 young adults from picking, over a 2 hour recording. B: The average speed of 25 N2 young adults from picking over a 2 hour recording. C: The average crawling amplitude of 25 N2 young adults from picking over a 2 hour recording. D: The average crawling frequency of 25 N2 young adults from picking over a 2 hour recording. (Ev Yemini 2011a).

2.3.1.3 Variability between Animals of the Same Genotype

Over the time-course of the high-throughput tracking project, 2011-2013, a total of 1,218 good recordings of day 1 N2 individuals were made. The variability in the results gained from these recordings on the grounds of month of the year, day of the week and hour of the day were assessed by Eviatar Yemini. Six features were chosen for the measurement of variability: Length, positive mid-body speed, absolute foraging amplitude, backward motion frequency, coiling frequency and path range (Fig.2.4. and 2.5). One-way ANOVA tests were performed with Bonferroni correction for 18 tests and checked for significance at $p \leq 0.05$. As expected the length of individuals was greater at 4pm than that at 9am, the mean length of worms later in the day was around 10% higher than in the morning (Fig.2.5.). This is consistent with the length increase seen over the course of the 2 hour recordings. Fluctuations in temperature from month to month were expected to cause some alterations to behaviour, this seems to be the case, with speed and path range becoming more variable in the warmer summer months than in the period from November to March. These differences are not observed in the results from day to day, showing that the perturbations were likely due to variable seasonal temperatures.

All features, apart from coiling frequency, were significantly different from one hour to the next and from one month to the next. In order to combat this N2s and strains were tracked over the whole day, rather than controls tracked at one time on all 8 trackers then strains tracked likewise through the day. In this way an N2 was always being tracked at the same time as mutant strains and strains were tracked from 9am until 5pm. To combat differences in results gained from month to month mutant strains were compared only to N2s tracked on the same day. In this way features that may be influenced by seasonal changes were only significant in the mutant if the N2 was not exhibiting the same seasonal behaviour.

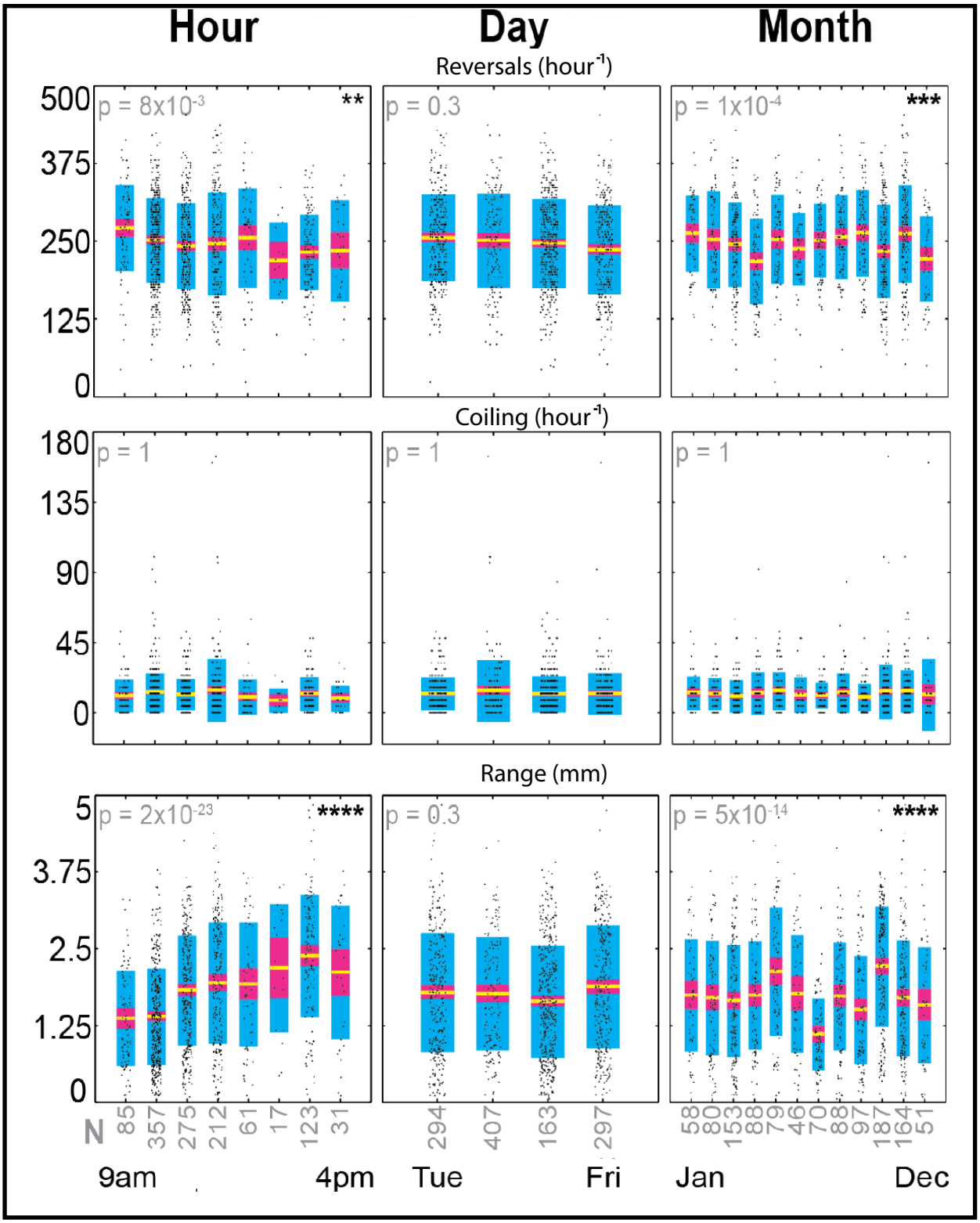

Fig.2.4: The Variation Between Recordings Of N2 Young Adults Over Hours, Days and Months. Black spots represent means for individual recordings, blue boxes show standard deviation from the mean of all recordings on the given hour/day/month, red boxes show the interquartile range and yellow lines indicate the mean of recordings on the given hour/day/month. Significance between results is indicated by asterisks in the top right hand corner of each graph. *= P<0.05, **= P<0.01, *** = P<0.001, ****= P<0.0001. (Ev Yemini 2011a)

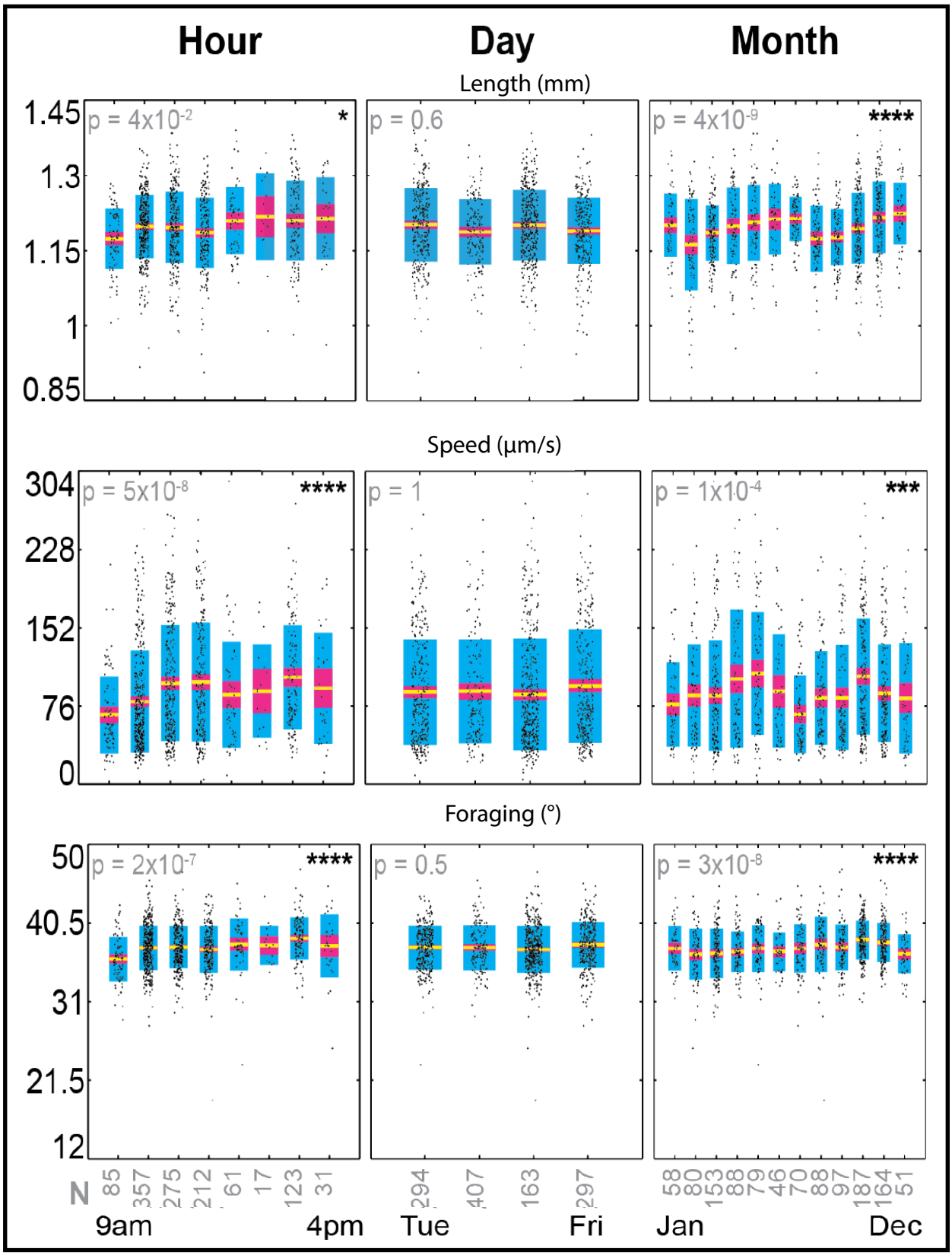

Fig.2.5: The Variation Between Recordings Of N2 Young Adults Over Hours, Days and Months. Black spots represent means for individual recordings, blue boxes show standard deviation from the mean of all recordings on the given hour/day/month, red boxes show the interquartile range and yellow lines indicate the mean of recordings on the given hour/day/month. Significance between results is indicated by asterisks in the top right hand corner of each graph. *= P<0.05, **= P<0.01, *** = P<0.001, ****= P<0.0001. (Ev Yemini 2011a)

2.1.3.4 Clustering Analysis

All clustering analysis was performed by Eviatar Yemini and detailed information on clustering parameters can be found in Eviatar Yemini 2011a. Clustering is a useful method of assessing the similarity between strains in the results from many parameters. It is therefore the best way to assess the similarities between mutant strains tracked in the high-throughput tracking project. Hierarchical clustering was performed using the mean values of 702 features (Table A3, Appendix). Each mutant's measures were normalised to their N2 controls and converted to Z-scores based on the population of 330 mutant strains as a whole, see appendix for full clustering diagram.

As a control for the clustering results, the Schafer lab stock N2s were divided into subsets based on day tracked, time tracked and month tracked, and compared alongside all 330 mutant strains for similarity. Pair-wise correlation values in clustering are from 0 to 1 with 0 being completely un-correlated and 1 being completely correlated. AU (Approximately Unbiased) values are p-values of the cluster from 0-1 and indicate how strongly the cluster is supported by the data, 0 being not at all and 1 being highly supported. The maximum pair-wise correlation (0.95) in the entire dataset was between all lab stock N2 recordings and N2s tracked on Tuesdays. Promisingly, all the subsets of the Schafer lab N2 stocks clustered together apart from the two seasonal extremes, December and August, with a correlation of 0.75 and an AU of 98.56% (Fig.2.6. A). The maximum AU in the dataset is 1 (as is always the case for hierarchical clustering), and the next lowest AU was 99.98% for the two alleles of *unc-108* (Fig.2.6. C). Minimum correlation was 0.34, for comparison of *unc-1 (e1598)* to all other datasets, and 165 of the branches (out of 329) had an AU of 0%.

Several wild-type isolates, other than Bristol N2, were tracked; these isolates sometimes have slight genetic differences that enable them to survive the environment that they naturally inhabit. For example the isolates from Hawaii, Freiburg and the LSJ1 Bristol N2 isolate carry an allele of the gene *npr-1* that enhances social feeding in the worm. The Hawaiian and German isolates clustered strongly together at 0.88 (AU= 97.97%) (Fig.2.6. B). Also closely clustered to this pair are the LSJ1 Bristol isolate (0.8, AU= 96.22%) and an N2 strain carrying a mutation in the *npr-1* gene (0.81, AU= 97.1%). The neuropeptide related gene mutants *npr-3 (tm1583)IV* and *nlp-17 (ok3461)IV* are also clustered fairly strongly to this group, indicating that they may play a role in *npr-1* signalling.

A number of other mutants known to work together in known pathways clustered well together. The genes *eat-16* and *egl-30* clustered exclusively at 0.89 correlation (AU= 99.71%), both are known to modulate locomotion, pharyngeal pumping, egg laying and synaptic transmission and interact in the same pathway. The mutant for *goa-1* is also closely clustered with this pair and is known to interact with *egl-30* and modulate similar behaviours/functions (Fig.2.6. C). Some other examples include:

The mutants for the genes *unc-38* and *unc-63* cluster together at 0.76 (AU =97.3%), both encode for alpha-subunits of the same acetylcholine receptor (Culetto et al. 2004). *unc-79* and *unc-80* cluster at 0.84 (AU= 99.33%) and both encode for subunits of the NALCN sodium channel (Yeh et al. 2008). *unc-37* clustered exclusively with both *unc-4* alleles at 0.68 (AU=99.19%), *unc-37* is required for *unc-4* activity (Winnier et al. 1999). Both alleles of *egl-21* clustered together at 0.62 (AU=99.94%). Mutants in the gene responsible for serotonin synthesis *bas-1* clustered with the serotonin receptor gene mutants *ser-1, ser-4* and *ser-7* and the octopamine receptor *ser-2* (0.74, au= 98.36%). The innexin genes *unc-9* and *unc-7* clustered exclusively at 0.66 (AU= 94.36%) (Fig.2.6. C).

A set of seven acetylcholine receptor mutants clustered together with a correlation of 0.82 and AU of 99.53% (Fig.2.6. D). In this set *acr-2* and *acr-3* are the only genes with a known function, both form functional channels when expressed with *unc-38* and are thought to modulate locomotion.

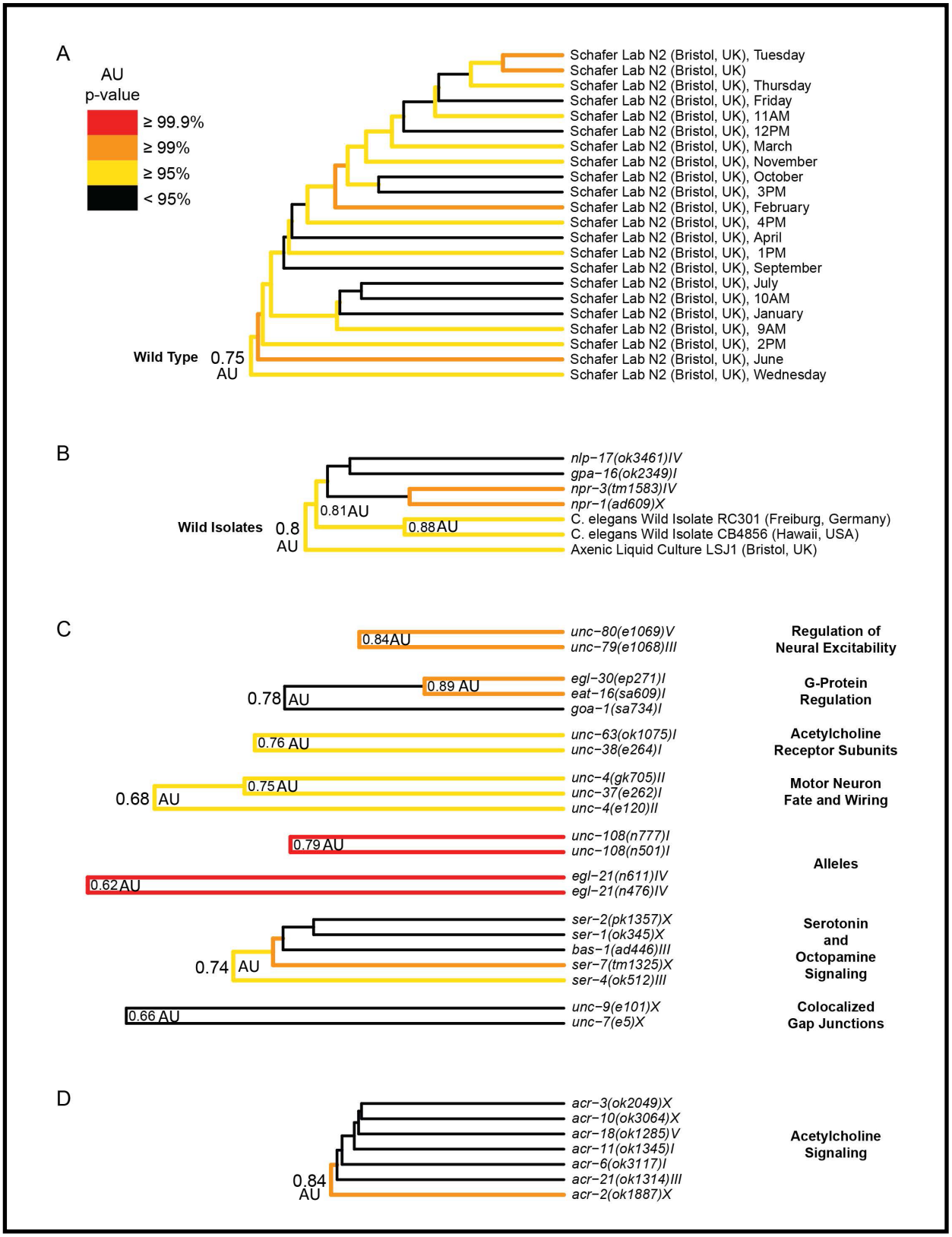

Fig.2.6: Clustering Results For Genes Working In The Same Pathways. A: The comparison between different sub-groups of tracked Bristol N2 wild-type *C. elegans.* B: Clustering results for wild type isolated carrying a variation of the *npr-1* gene and the N2 mutants strain *npr-1 (ad609)X.* C: Clustering results for genes working in like pathways. D: A set of mutant strains of genes with known and unknown function, all postulated to code for proteins in the same family. The horizontal length of each branch is scaled to its correlation value. The horizontal branches are color coded to show the AU of the clusters below them. AU ≥ 99.9% is colored red, AU ≥ 99% orange, AU ≥ 95% yellow, and all else is black. (Ev Yemini 2011a)

2.3.2 Motif clustering

An alternative method of analysing the dataset from the high-throughput tracking project was performed by Andre Brown and Tadas Jucikas. Rather than using all of the 702 features to assess the similarity of each mutant strain, Andre and Tadas used behavioural motifs. As detailed in the introduction, these are sets of concurrent eigenworm shapes that have been observed in several mutant and wild type recordings. The Bristol N2 worms and the various mutant strains were clustered using affinity propagation and inverse Mahalanobis distance between strains was used as a measure of similarity.

This method of clustering produces a spatial 'map' of similarities between the different mutant strains, with the proximity of one node to another displaying their similarity. Nodes that are close together are alike, while those that are farther apart are less similar (Fig.2.7). This method of clustering appears to group together mutant strains of like-proteins, the lower left cluster consists mainly of mono-amine related genes (Fig.2.8), to the top left are mainly uncoordinated mutants (Fig.2.9), to the bottom right are many of the neuropeptide related mutants (Fig.2.10) and to the top right is N2 and mutants with very similar motif fingerprints to N2 (Fig.2.11), although some of these mutants are still significantly different to wild type. Figure 2.6 displays the full diagram without all genes labelled, the node colours show that like-mutants tend to cluster together. Red dashed lines are the connections between mutant alleles of the same gene, these were found to cluster together with an average of 1.6 edges, significantly less than the average network distance of 3.7 ($P = 6 \times 10{-}5$, Wilcoxon rank-sum test). Once again mutant alleles of *unc-108* cluster strongly together (1 edge), using this method of clustering several of the other alleles of the same gene are clustered more strongly than in the features clustering (described above): *egl-21(n476)* and *egl-21(n611)* (one edge); *ocr-4 (tm2173)* and *ocr-4(vs137)* (two edges); *trp-2(sy691)* and *trp-2 (gk298)* (two edges); *unc-10(md1117)* and *unc-10(e102)* (two edges); *unc-89(e1460)* and *unc-89(st85)* (one edge).

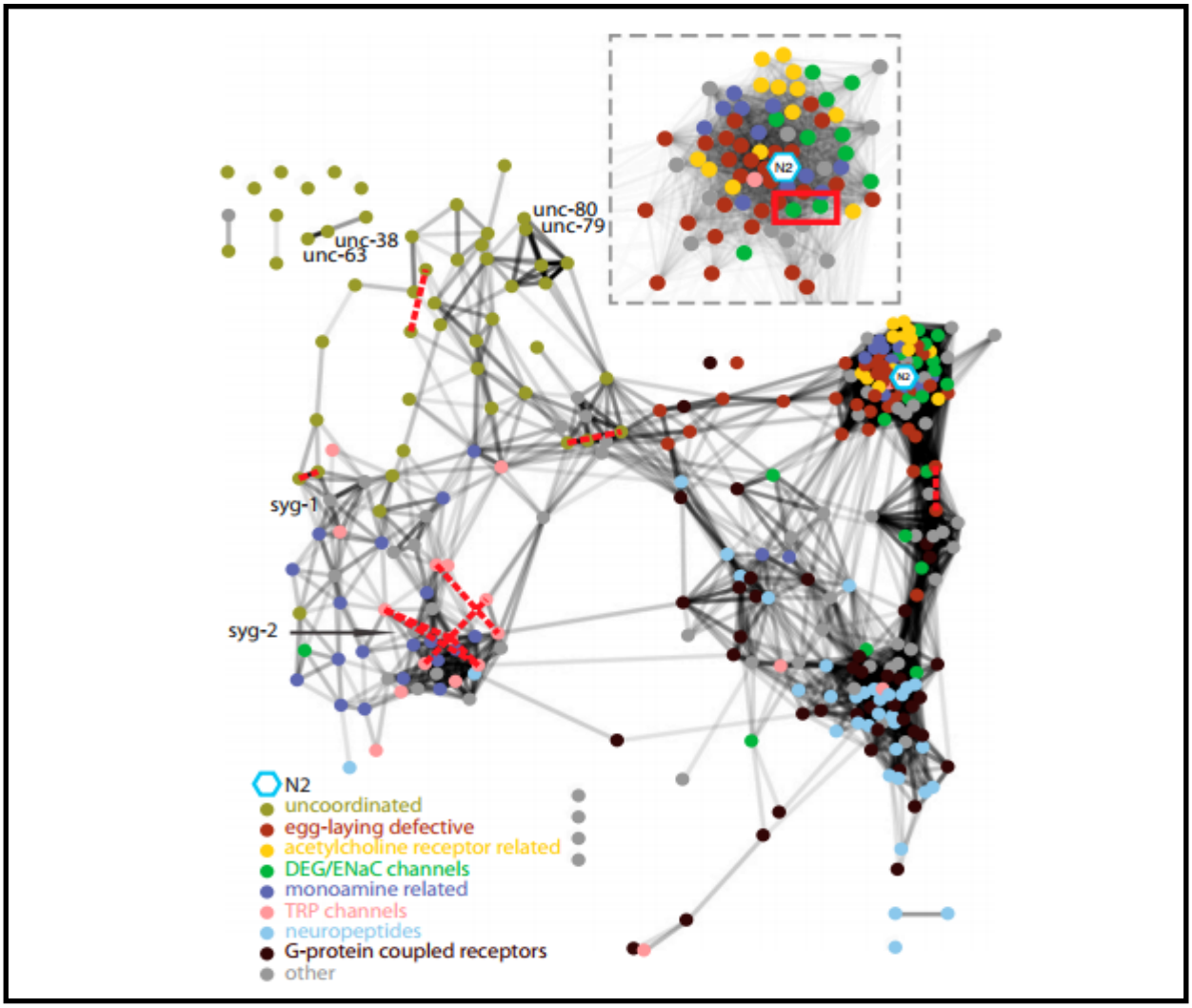

Fig.2.7: A Clustering Network of Tracked C. elegans Mutant Strains Based On Behavioural Motif Fingerprinting. The nodes (coloured circles) are colored by phenotypic or molecular class, as detailed in the key. Edges show the phenotypic connections between nodes. The transparency of edges represents the frequency at which nodes were clustered together after resampling from the data with replacement. Frequently clutstered strains have darker connections. The network layout was determined using spring embedding with edge weights determined by the inverse phenotypic distance. The DEG/ENaC mutants discussed in section 2.3.2. are shown with a red rectangle. (A.E.X Brown et al. 2013)

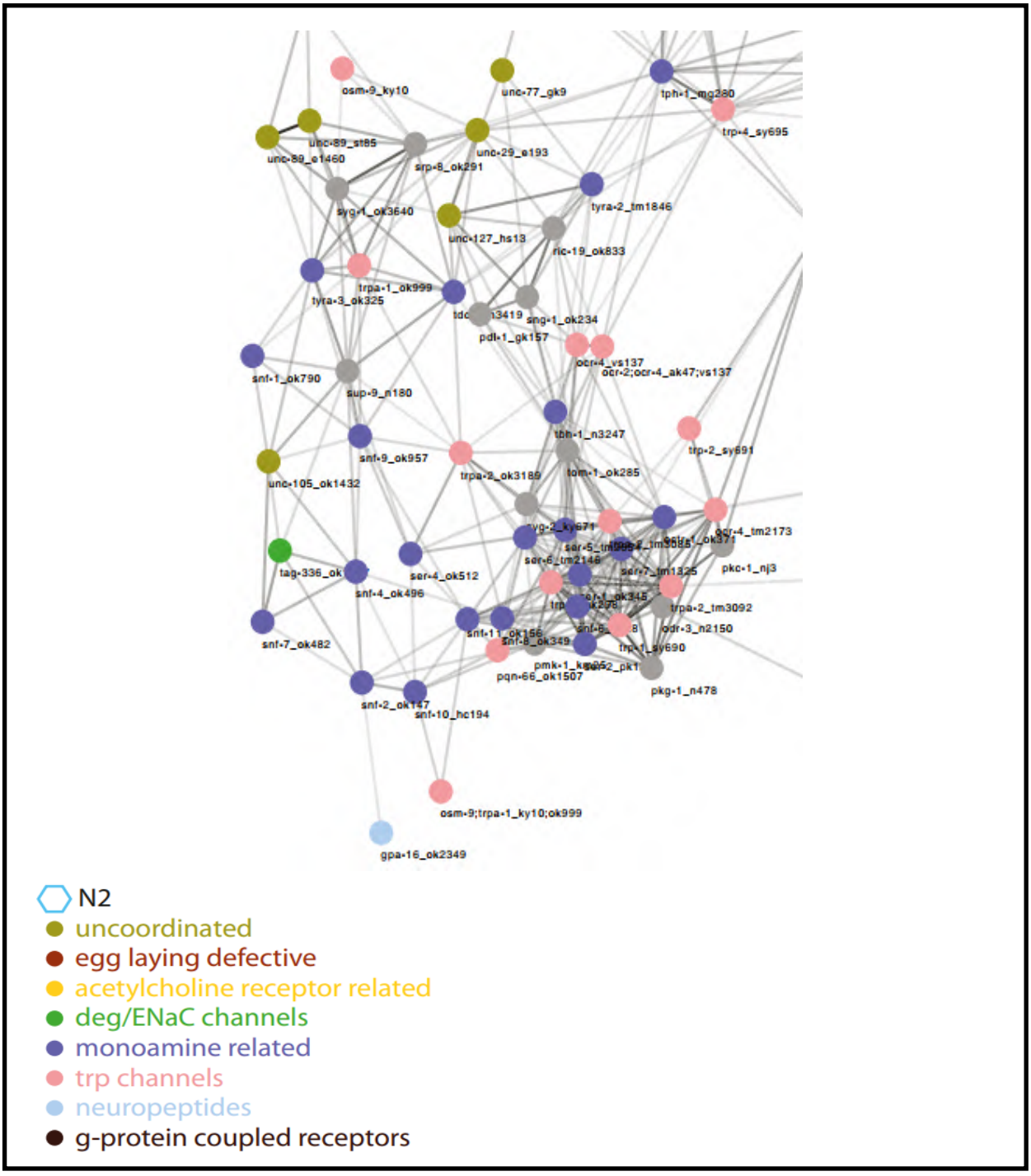

Fig.2.8: A Detailed Image of the 'Mono-amine Cluster'. Nodes are coloured as described in the key, each node represents a mutant strain of each of the families described in the key. The nodes are labelled with the gene in which the mutation is present and the mutant allele in the strain tracked. Grey lines show the phenotypic connections between nodes, line transparency is a measure of the number of times the connected genes were clustered together, darker lines indicate more regular clustering (A.E.X. Brown et al. 2013).

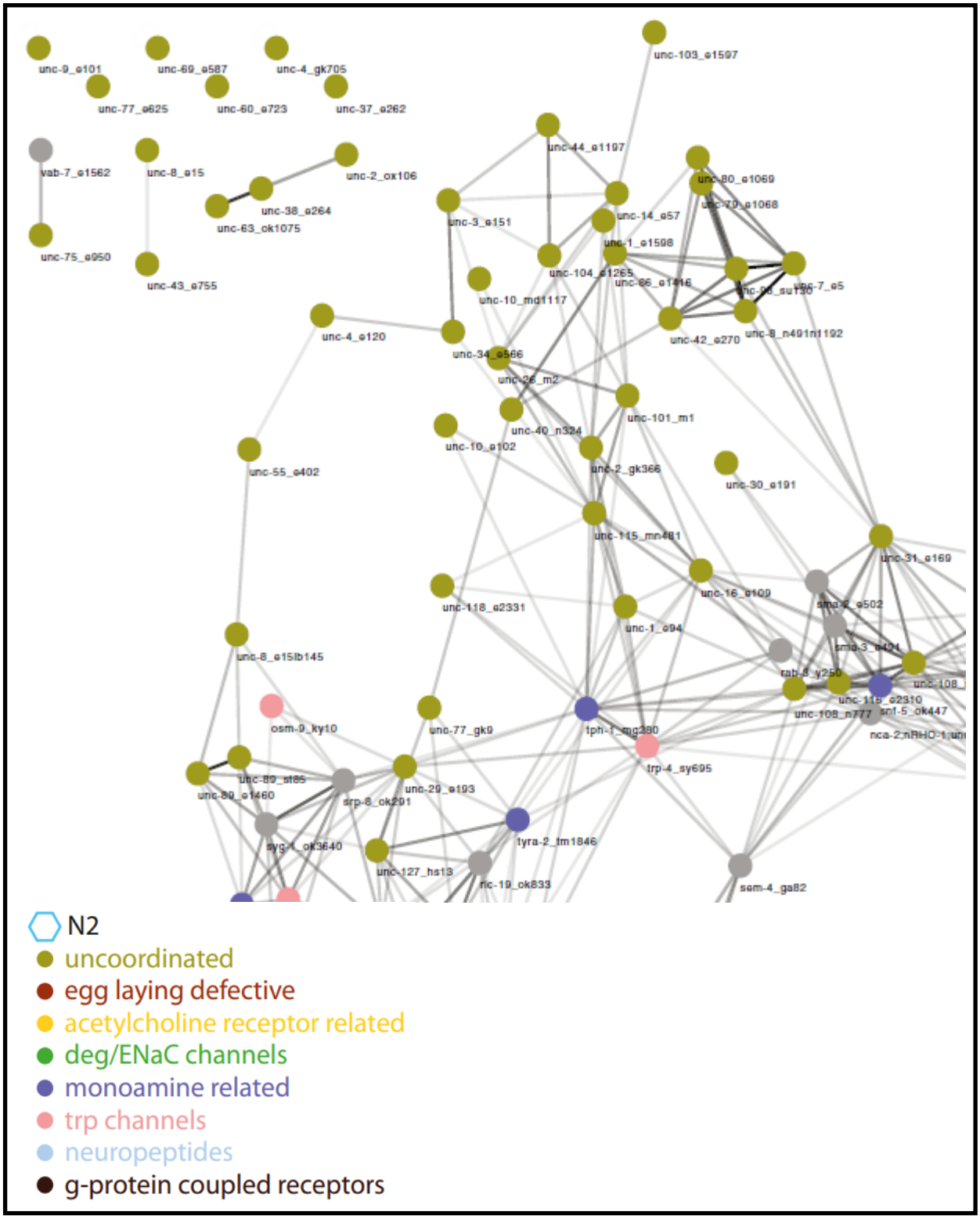

Fig.2.9: A Detailed Image of the 'Uncoordinated Cluster'. Nodes are coloured as described in the key, each node represents a mutant strain of each of the families described in the key. The nodes are labelled with the gene in which the mutation is present and the mutant allele in the strain tracked. Grey lines show the phenotypic connections between nodes, line transparency is a measure of the number of times the connected genes were clustered together, darker lines indicate more regular clustering. (A.E.X. Brown et al. 2013)

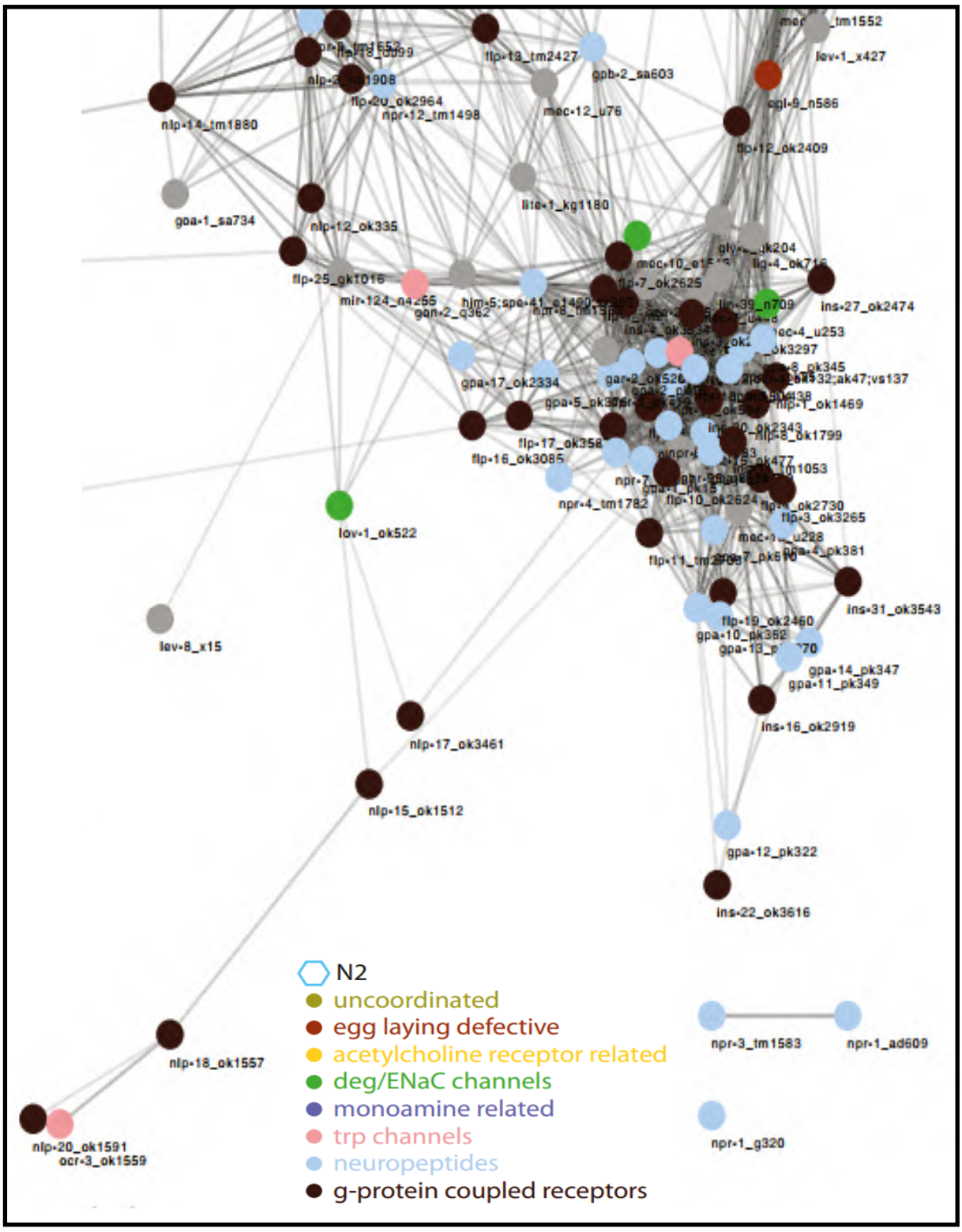

Fig.2.10: A Detailed Image of the 'Neuropeptide Related Cluster'. Nodes are coloured as described in the key, each node represents a mutant strain of each of the families described in the key. The nodes are labelled with the gene in which the mutation is present and the mutant allele in the strain tracked. Grey lines show the phenotypic connections between nodes, line transparency is a measure of the number of times the connected genes were clustered together, darker lines indicate more regular clustering. (A.E.X. Brown et al. 2013)

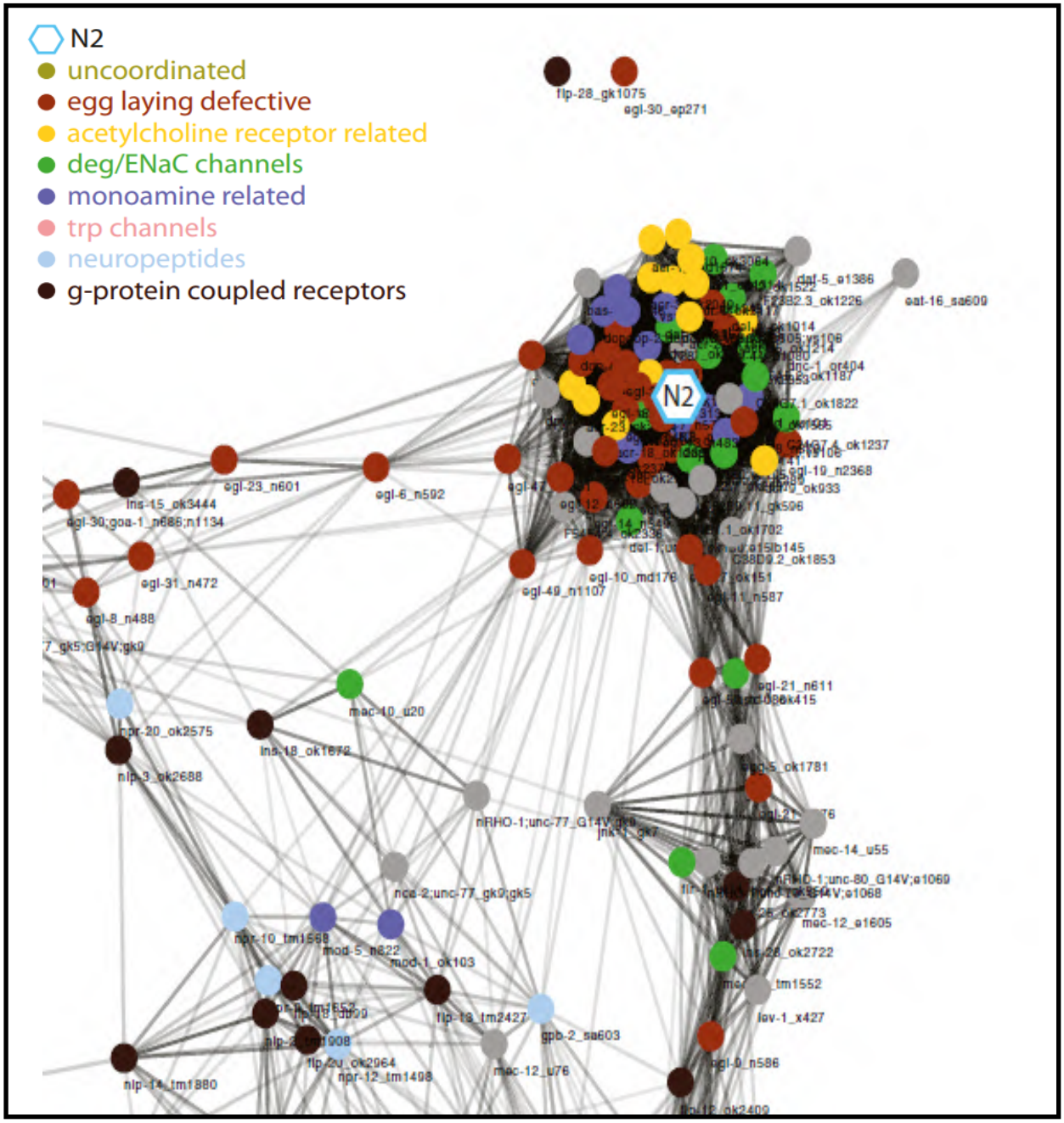

Fig.2.11: A Detailed Image of the 'N2-like Cluster'. Nodes are coloured as described in the key, each node represents a mutant strain of each of the families described in the key. The nodes are labelled with the gene in which the mutation is present and the mutant allele in the strain tracked. Grey lines show the phenotypic connections between nodes, line transparency is a measure of the number of times the connected genes were clustered together, darker lines indicate more regular clustering (A.E.X. Brown et al. 2013).

Some genes that are known to function in the same pathway have clustered significantly closer together than the network average. Once again, *unc-38* and *unc-63* have clustered together as have *unc-79* and *unc-80*. Larger scale comparison of whole families of mutants shows strong correlation between genes encoding proteins in similar pathways. For example, dopamine signalling mutants cluster strongly together with a mean shortest path of 1 edge (Fig. 2.12. A). The majority of serotonin signalling pathway mutants cluster well, with a mean shortest path of 1.8 edges, not including *cat-4* and *bas-1* mutants (Fig.2.12 B). Both of these genes also play a part in dopamine signalling (Loer & Kenyon 1993), and cluster closely with mutants in this pathway. Mutants of the tyramine signalling pathway cluster with a mean shortest path of 2 edges and octopamine signalling pathway mutants cluster with a mean shortest length of 1.5 edges (Fig.2.12 C and D).

As many of the tracked neuropeptides create a cluster with the G-protein coupled receptors (Fig 2.9) it may be possible to use the motif clustering data to determine possible ligand/receptor relationships.

An interesting pair of DEG/ENaC subunit mutants with unknown function, *asic-2* and *acd-5* cluster strongly together within the N2-like group (shown in the red rectangle Fig.2.7). The two most distinguishable behavioural motifs that both mutants share when compared to N2 are a bout of forward locomotion and a pause in a curved shape (*asic-2 (ok289)I* vs. N2, P = 0.0019; *acd-5(ok2657)I* vs. N2, P = 9 × 10−6 based on Hotelling t-test). Using the same statistical analysis the mutants were found to have no significant difference in these motifs when compared to each other (P= 0.796) (Fig.2.13). The same comparison was used for other mutants that cluster together in the N2-like group; the same significance profile when comparing to N2 or to each other was not observed. This suggests that these two DEG/ENaC subunit genes could encode proteins that function in the same pathway (A.E.X. Brown et al. 2013).

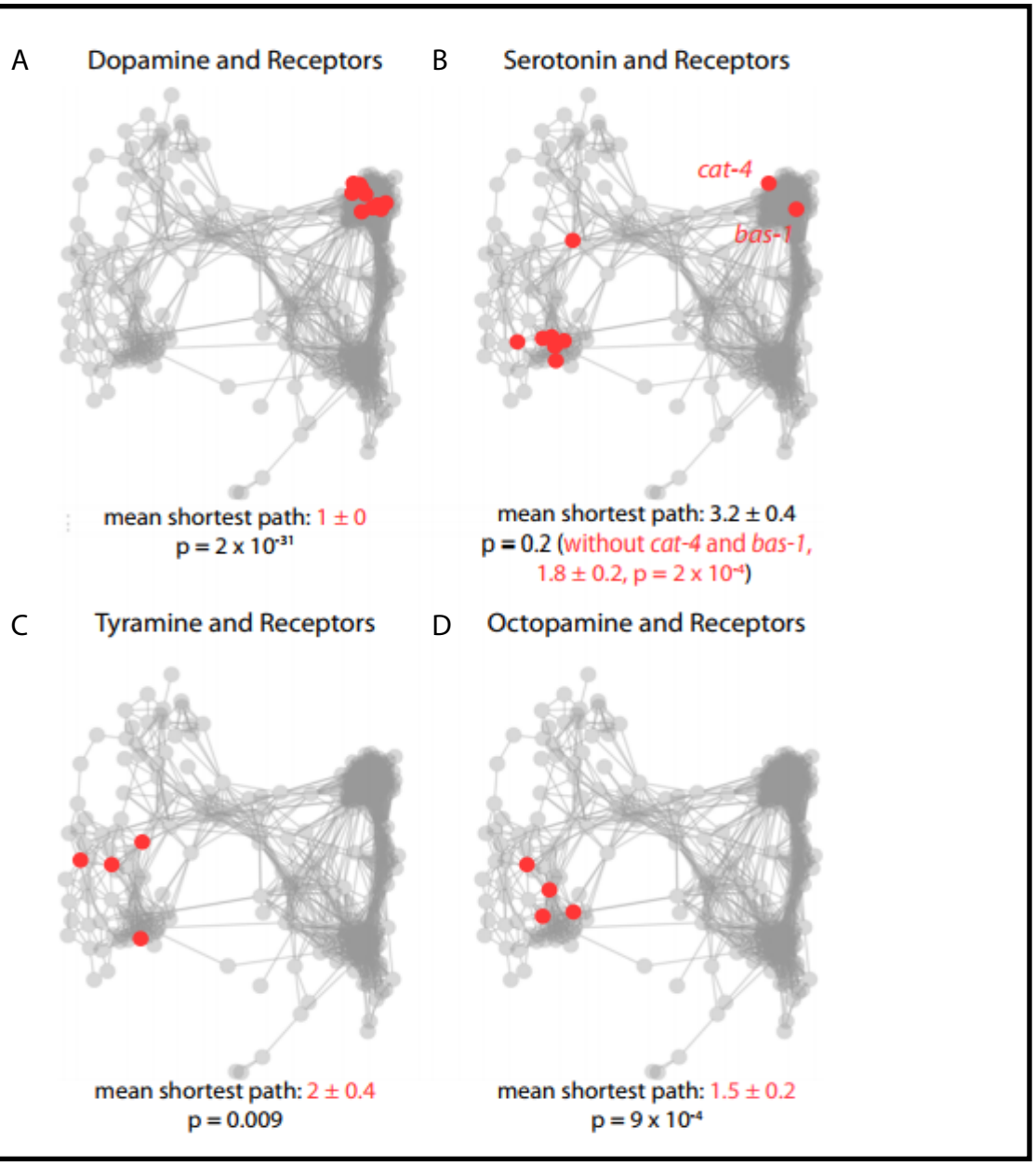

Fig.2.12: Clustering Of Mutant Families Within The Motif Clustering Network. A: Clustering of dopamine signalling mutants within the network. The grey nodes and connections represent the whole network, red nodes show the members of the dopamine signalling pathway family. B: Clustering of serotonin signalling mutants within the network. The grey nodes and connections represent the whole network, red nodes show the members of the serotonin signalling pathway family. C: Clustering of tyramine signalling mutants within the network. The grey nodes and connections represent the whole network, red nodes show the members of the tyramine signalling pathway family. D: Clustering of octopamine signalling mutants within the network. The grey nodes and connections represent the whole network, red nodes show the members of the octopamine signalling pathway family (A.E.X Brown et al. 2013).

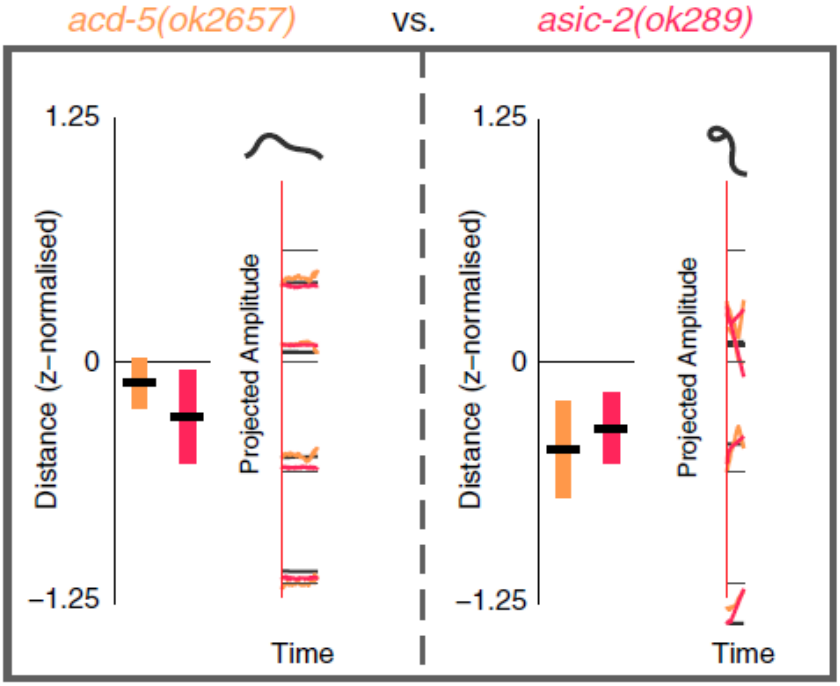

Fig.2.13: Motif Clustering Similarities Between the DEG/ENaC Mutants *asic-2 (ok289)I* and *acd-5 (ok2657)I.* The results for the bout of forward locomotion behavioural motif (left) and paused curve behavioural motif (right). Results for *acd-5 (ok2657)I* are shown in orange and *asic-2 (ok289)I* in red, boxes on the graph represent SEM and black bars on boxes represent the mean. There is no significant difference between the two DEG/ENaC mutants when comparing their results for these motifs (A.E.X. Brown et al. 2013).

2.3.2.1 *acd-5* and *asic-2*

Upon further investigation of this pair of DEG/ENaC subunit-encoding genes it was noted that both animals were significantly different from wild type in their turning activity. Both appeared to have a bias towards entering turns in the dorsal direction, this phenotype was more pronounced in *asic-2 (ok289)I* when entering reorienting turns, e.g. omega bends, upsilon bends (Fig.2.14) and coils (Fig.2.15), and was more pronounced in *acd-5 (ok2657)I* during crawling (Fig.2.16, 2.17, 2.18). There is also a reduction in the number of omega bends in *acd-5 (ok2657)I* and an increase in coiling in comparison to N2. Upsilon bends and omega bends are prolonged in both mutants (Fig.2.14). In addition *acd-5 (ok2657)I* mutants showed a pronounced decrease in the area that worms covered during recording (Fig.2.19 A), a decrease in speed (Fig.2.19 B) and anomalies in foraging amplitude when compared to N2 (Fig.2.20).

This pair of genes did not cluster together when clustering on features instead of motifs. Table 2.1 shows all the features that are significantly different for both *acd-5 (ok2657)I* and *asic-2 (ok289)I.* Many more features were significantly different for each mutant but were not common to each other. A table of these can be found in the appendix (Table A10 and A11)

Table 2.1 Features that are significantly different from N2 for both DEG/ENaC mutants, *acd-5 (ok2657)I* and *asic-2 (ok289)I.*

Features that are significant from N2	*acd-5 (ok2657)I* P value	*asic-2 (ok289)I* P value
'Absolute Backward Head Bend S.D. (+/- = D/V Inside)'	0.021957	0.040658
'Absolute Backward Midbody Bend Mean (+/- = D/V Inside)'	0.038662	0.000664
'Absolute Backward Neck Bend Mean (+/- = D/V Inside)'	0.001138	0.007981
'Absolute Forward Midbody Bend Mean (+/- = D/V Inside)'	0.001731	0.008512
'Absolute Midbody Bend Mean (+/- = D/V Inside)'	0.043267	0.001575
'Absolute Midbody Crawling Frequency (+/- = D/V Inside)'	0.000004	0.031724
'Absolute Paused Midbody Crawling Amplitude (+/- = D/V Inside)'	0.014645	0.027374
'Backward Eccentricity'	0.002508	0.011725
'Backward Eigen Projection 2'	0.022234	0.004414
'Backward Eigen Projection 3'	0.044656	0.005023
'Backward Foraging Amplitude (+/- = Toward D/V)'	0.000487	0.008801
'Backward Head Bend Mean (+/- = D/V Inside)'	0.001909	0.016046
'Backward Max Amplitude'	0.000031	0.001566
'Backward Midbody Bend Mean (+/- = D/V Inside)'	0.021332	0.003127
'Backward Neck Bend Mean (+/- = D/V Inside)'	0.008238	0.015894
'Backward Secondary Wavelength'	0.003536	0.000638
'Backward Track Length'	0.002948	0.000605
'Bend Count'	0.000215	0.002269
'Eccentricity'	0.001416	0.008068
'Eigen Projection 1'	0.000092	0.001182
'Forward Amplitude Ratio'	0.000599	0.006538
'Forward Bend Count'	0.000288	0.004462
'Forward Eccentricity'	0.003621	0.001107
'Forward Eigen Projection 1'	0.000045	0.010582
'Forward Eigen Projection 2'	0.000863	0.003647

'Forward Max Amplitude'	0.002176	0.000488
'Forward Midbody Bend Mean (+/- = D/V Inside)'	0.000768	0.028375
'Forward Track Length'	0.003721	0.000402
'Inter Upsilon Distance (+/- = Previous D/V)'	0.006429	0.021315
'Midbody Bend Mean (+/- = D/V Inside)'	0.024373	0.017041
'Midbody Crawling Frequency (+/- = D/V Inside)'	0.000042	0.029844
'Negative Backward Head Motion Direction (+/- = Toward D/V)'	0.02164	0.022279
'Negative Backward Hips Bend Mean (+/- = D/V Inside)'	0.03871	0.002402
'Negative Backward Hips Bend S.D. (+/- = D/V Inside)'	0.021215	0.015469
'Negative Backward Midbody Bend Mean (+/- = D/V Inside)'	0.00184	0.000137
'Negative Backward Midbody Bend S.D. (+/- = D/V Inside)'	0.001611	0.000227
'Negative Backward Tail Bend S.D. (+/- = D/V Inside)'	0.002094	0.002444
'Negative Forward Hips Bend Mean (+/- = D/V Inside)'	0.002871	0.000987
'Negative Forward Hips Bend S.D. (+/- = D/V Inside)'	0.003331	0.001551
'Negative Paused Head Speed (+/- = Forward/Backward)'	0.000011	0.0279
'Negative Paused Head Tip Speed (+/- = Forward/Backward)'	0.000013	0.01904
'Paused Amplitude Ratio'	0.000213	0.043364
'Paused Bend Count'	0.001156	0.002281
'Paused Eccentricity'	0.004193	0.00167
'Paused Eigen Projection 1'	0.000115	0.001625
'Paused Eigen Projection 2'	0.035201	0.002397
'Paused Max Amplitude'	0.008662	0.022919
'Paused Midbody Bend Mean (+/- = D/V Inside)'	0.03375	0.023642
'Paused Midbody Crawling Amplitude (+/- = D/V Inside)'	0.005562	0.041568
'Paused Track Length'	0.00585	0.001663
'Positive Backward Eigen Projection 4'	0.041253	0.030781
'Positive Backward Hips Bend Mean (+/- = D/V Inside)'	0.001766	0.030698
'Positive Backward Tail Bend Mean (+/- = D/V Inside)'	0.007808	0.009369
'Positive Forward Tail Tip Speed (+/- = Forward/Backward)'	0.000318	0.04124
'Positive Hips Bend Mean (+/- = D/V Inside)'	0.000007	0.041301
'Positive Neck Bend S.D. (+/- = D/V Inside)'	0.015303	0.040078
'Positive Paused Hips Bend Mean (+/- = D/V Inside)'	0.000008	0.035049
'Positive Paused Tail Bend Mean (+/- = D/V Inside)'	0.00549	0.013029
'Positive Tail Bend Mean (+/- = D/V Inside)'	0.001596	0.016292
'Track Length'	0.001264	0.005825

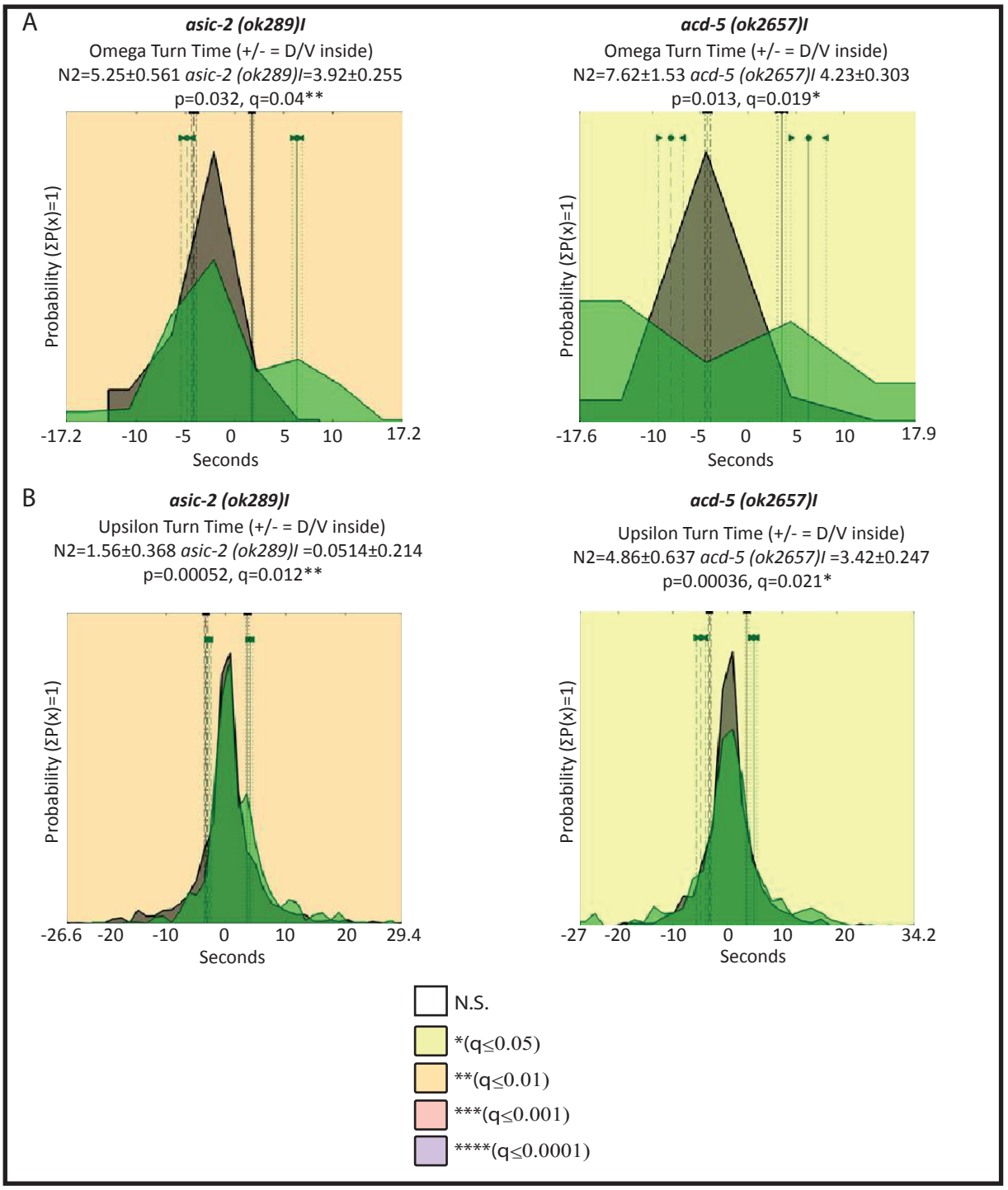

Fig.2.14: The Omega and Upsilon Turn Time of *asic-2 (ok289)I* and *acd-5 (ok2657)I* Mutant Allele Strains.

Graphs show the time mutant worms spent in omega and upsilon bends during recording. Results for 20 individuals of the *asic-2 (ok289)I* mutant and 21 individuals of the *acd-5 (ok2657)I* mutant allele strain are shown. The colour of the graph background represents the significance of the mutant result when compared to N2 individuals tracked on the same day. A white background denotes no siginificance, and shades pale yellow to purple display increasing levels of significance (as shown in the key). The grey shaded area of the graph shows the results for N2. The overlayed, green shaded area shows the result for the mutants. Positive results display the time spent by each strain in turns performed in the dorsal direction, while negative results display the time spent by each strain in turns performed in the ventral direction.

A: The omega turn time of *asic-2 (ok289)I* and *acd-5 (ok2657)I* B: The upsilon turn time of *asic-2 (ok289)I* and *acd-5 (ok2657)I.*

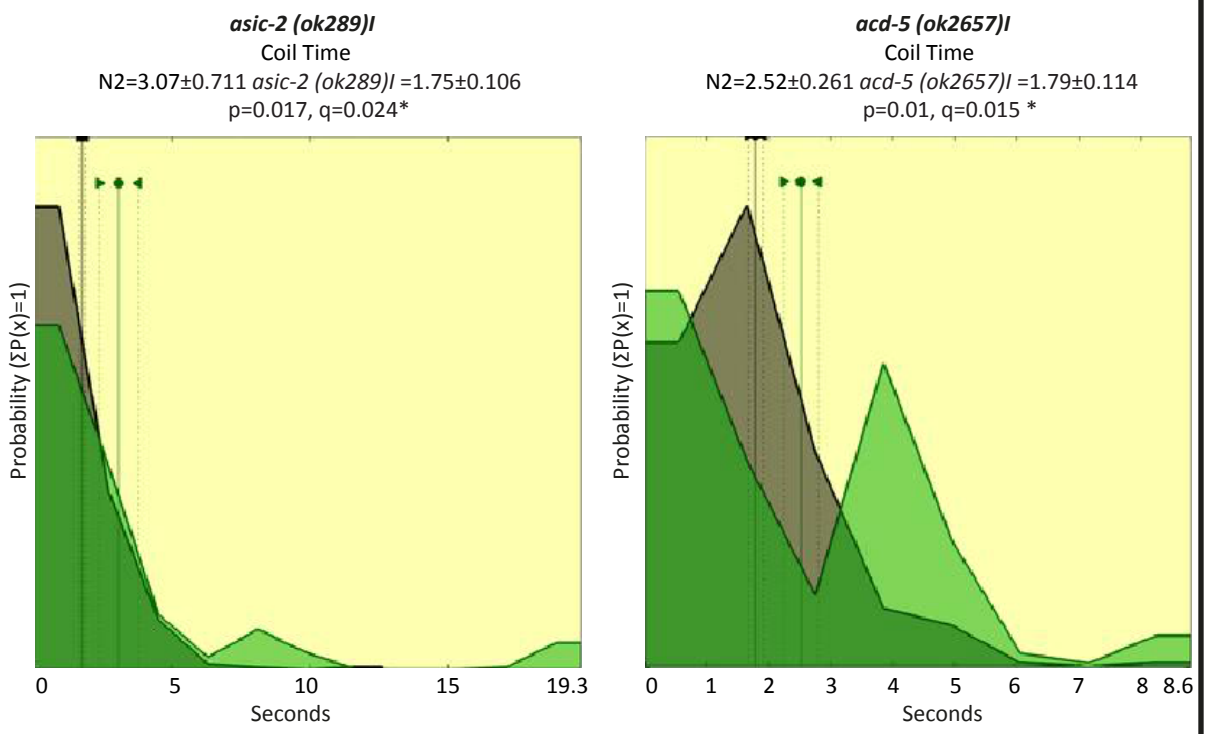

Fig.2.15: The coil time of *asic-2 (ok289)I* and *acd-5 (ok2657)I*. Graphs show the time mutant worms spent in coils during recording. Results for 20 individuals of the *asic-2 (ok289)I* mutant and 21 individuals of the *acd-5 (ok2657)I* mutant allele strain are shown. The colour of the graph background represents the significance of the mutant result when compared to N2 individuals tracked on the same day. A white background denotes no siginificance, and shades pale yellow to purple display increasing levels of significance (as shown in the key). The grey shaded area of the graph shows the results for N2. The overlayed, green shaded area shows the result for the mutants. These results do not give an indication of the direction of entry into the coil, but show that the mutant spends more time in individual coiling events than N2.

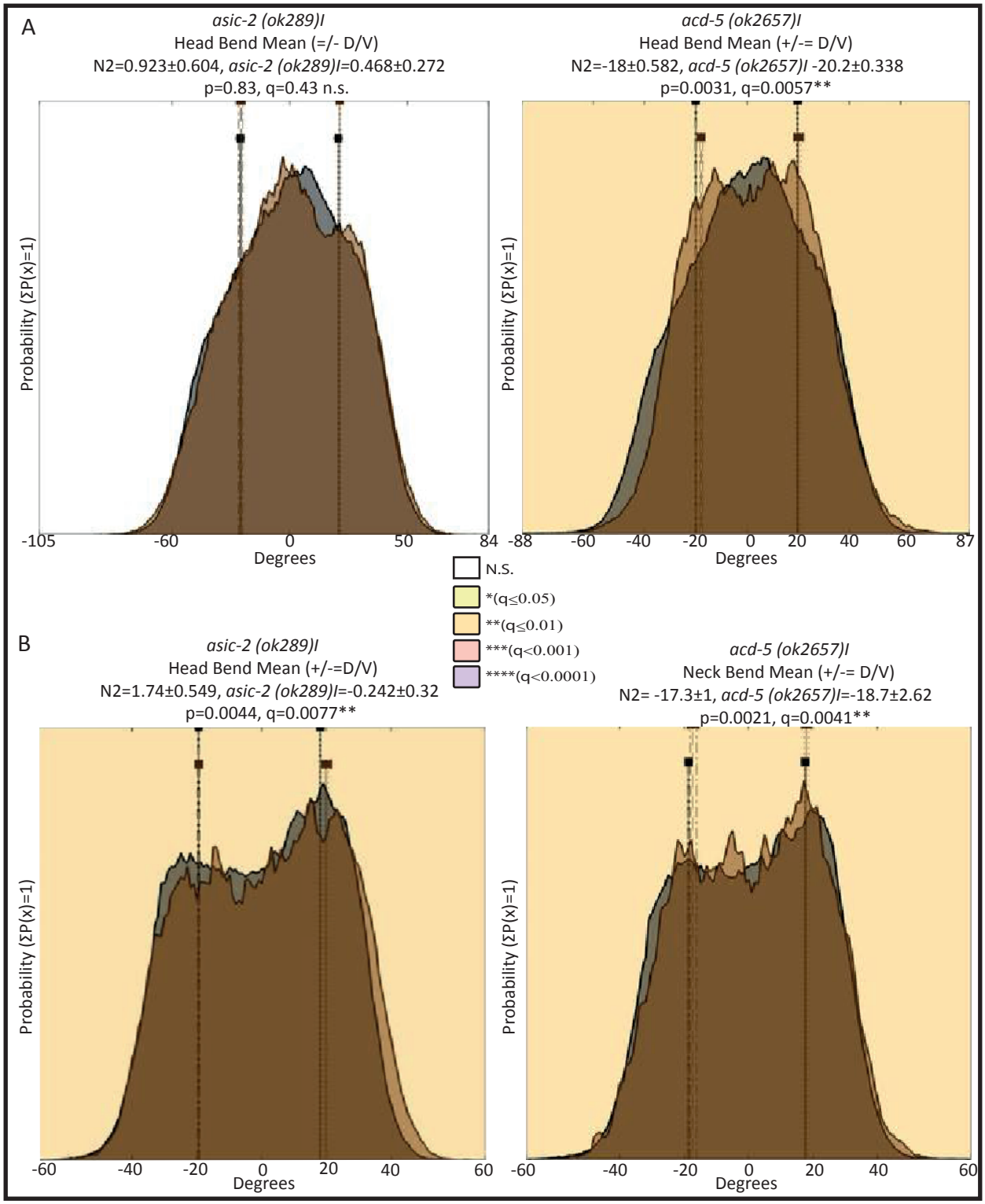

Fig.2.16: The Head and Neck Bend Means of *asic-2 (ok289)I* and *acd-5 (ok2657)I* Mutant Allele Strains. Graphs show the degree of bends mutant worms made at different body points during recording. Results for 20 individuals of the *asic-2 (ok289)I* mutant and 21 individuals of the *acd-5 (ok2657)I* mutant allele strain are shown. The colour of the graph background represents the significance of the mutant result when compared to N2 individuals tracked on the same day. A white background denotes no siginificance, and shades pale yellow to purple display increasing levels of significance (as shown in the key). The grey shaded area of the graph shows the results for N2. The overlayed, brown shaded area shows the result for the mutants. Positive results display the degree of the dorsal bends each strain performed, while negative results display the degree of the ventral bends each strain performed. A: The head bend mean of *asic-2 (ok289)I* and *acd-5 (ok2657)I* B: The neck bend means of *asic-2 (ok289)I* and *acd-5 (ok2657)I.*

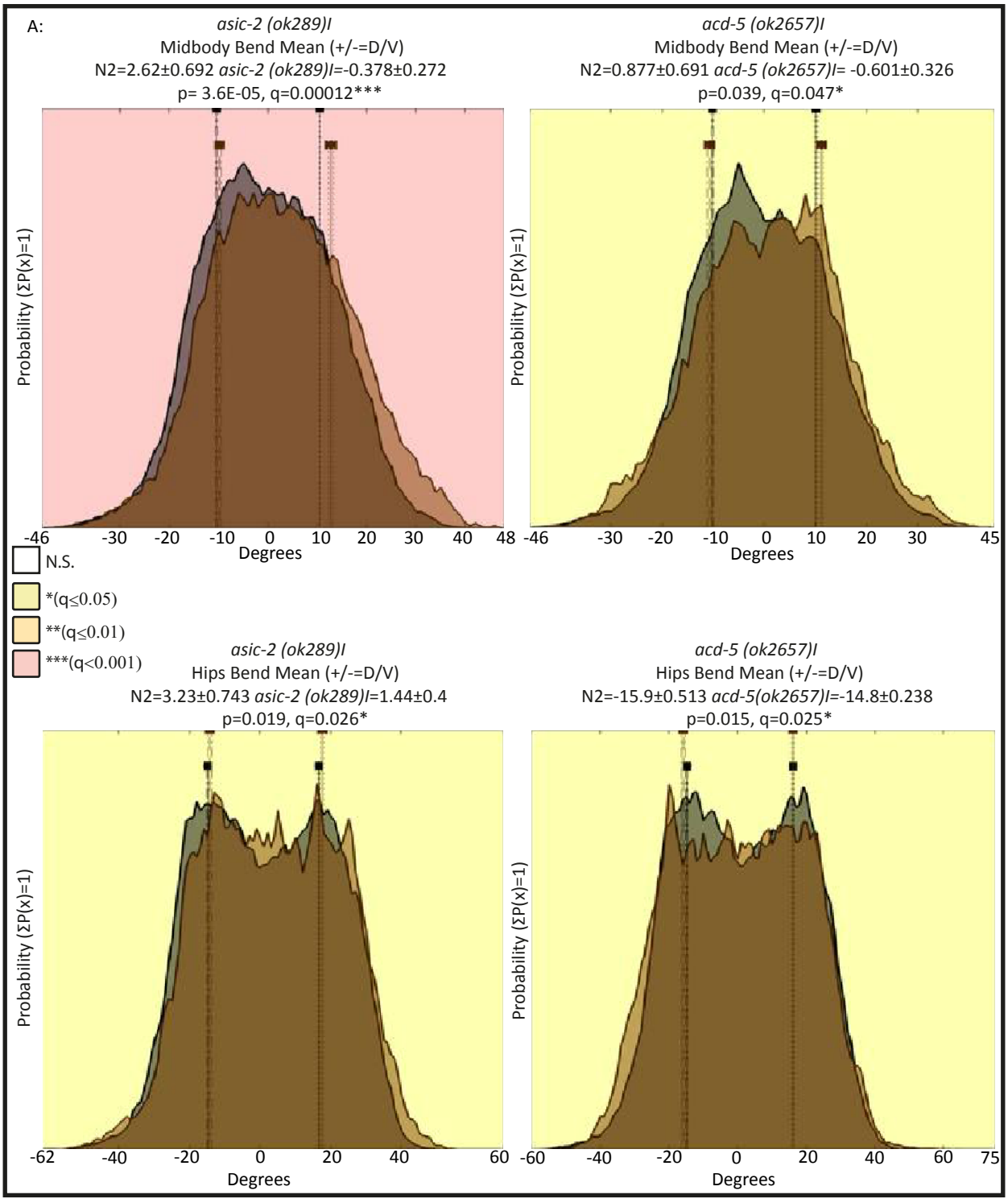

Fig.2.17: The Midbody and Hip Bend Means of *asic-2 (ok289)I* and *acd-5 (ok2657)I* Mutant Allele Strains.

Graphs show the degree of bends mutant worms made at different body points during recording. Results for 20 individuals of the *asic-2 (ok289)I* mutant and 21 individuals of the *acd-5 (ok2657)I* mutant allele strain are shown. The colour of the graph background represents the significance of the mutant result when compared to N2 individuals tracked on the same day. A white background denotes no siginificance, and shades pale yellow to purple display increasing levels of significance (as shown in the key). The grey shaded area of the graph shows the results for N2. The overlayed, brown shaded area shows the result for the mutants. Positive results display the degree of the dorsal bends each strain performed, while negative results display the degree of the ventral bends each strain performed. A: The midbody bend mean *asic-2 (ok289)I* and *acd-5 (ok2657)I* B: The hip bend mean of *asic-2 (ok289)I* and *acd-5 (ok2657)I.*

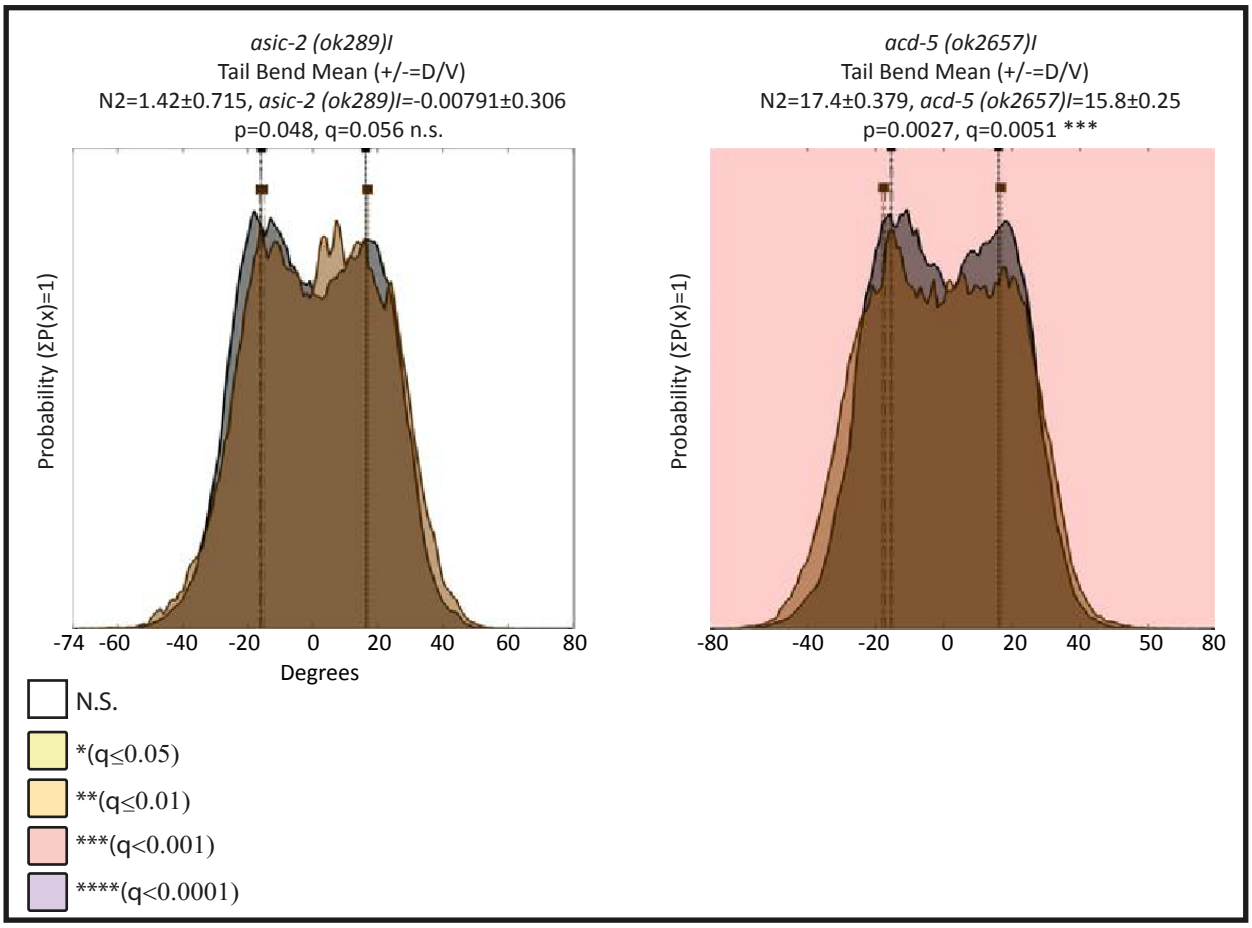

Fig.2.18: The Tail Bend Means of *asic-2 (ok289)I* and *acd-5 (ok2657)I* Mutant Allele Strains.
Graphs show the degree of bends mutant worms made at the tail during recording.
Results for 20 individuals of the *asic-2 (ok289)I* mutant and 21 individuals of the *acd-5 (ok2657)I* mutant allele strain are shown. The colour of the graph background represents the significance of the mutant result when compared to N2 individuals tracked on the same day. A white background denotes no siginificance, and shades pale yellow to purple display increasing levels of significance (as shown in the key). The grey shaded area of the graph shows the results for N2. The overlayed, brown shaded area shows the result for the mutants. Positive results display the degree of the dorsal bends each strain performed, while negative results display the degree of the ventral bends each strain performed.

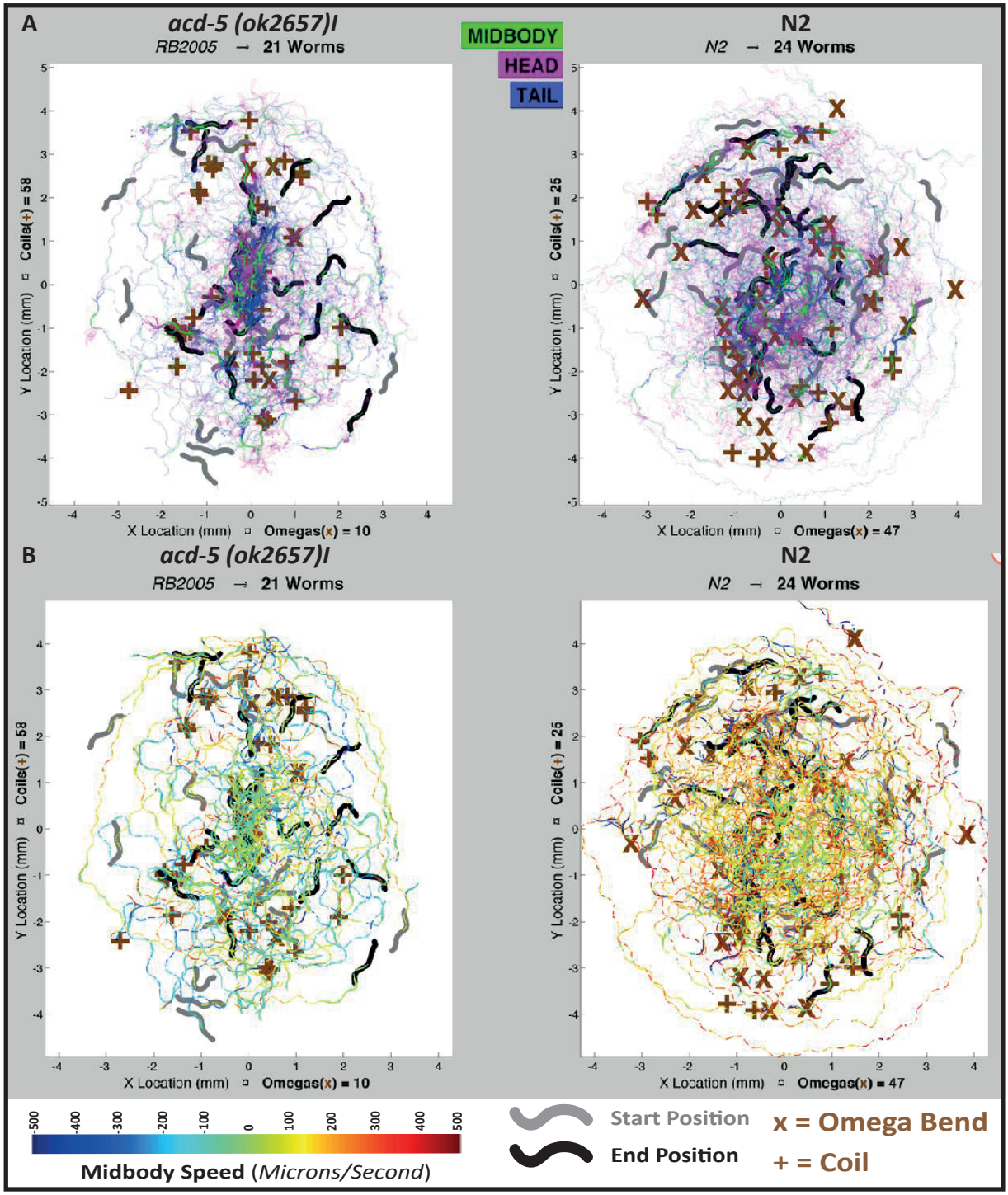

Fig.2.19: The position and speed of individual worms over the time course of recording A: The position of worms, recordings are over-layed ontop of one another. The left schematic shows the tracks of the mutant stain *acd-5 (ok2567)I* and the right, N2 controls recorded on the same day. Brown + denotes the point where a worm coiled, brown x denotes the point where a worm performed an omega bend. The total number of omega turns for all recordings is shown below the X-axis and the total number of coils for all recordings is shown to the left of the Y-axis. Green tracks show the poisiton of the midbody, pink the head position and blue the tail position. grey worm shapes show where the worm was when recording commenced, black worm shapes show the position of the worm at the end of the recording. B: The speed of individual worms over the time course of recording, as previously recordings are overlayed, the image on the left is *acd-5 (ok2567)I* and right the N2 controls. Brown +, x grey worm shapes and black worm shapes are as described previously. The colour of the tracks, from blue to red, indicates the speed of the worm at that position. Green is non-moving, yellow-red is slow to fast forward locomotion, pale-dark blue is slow to fast reverse locomotion.

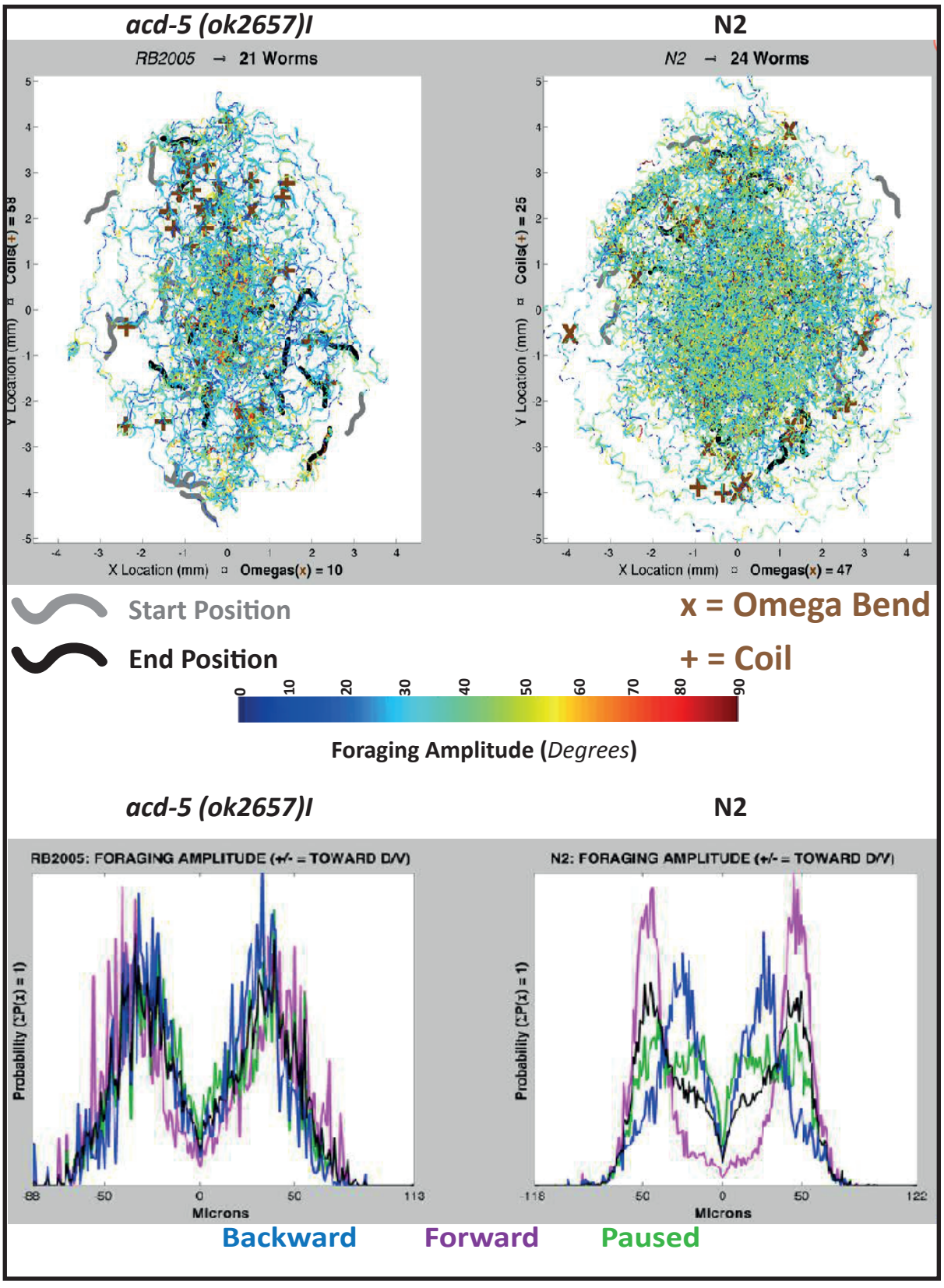

Fig.2.20: A: The foraging amplitude of *C. elegans* mutant strain *acd-5 (ok2657)I* and N2. Tracks are coloured blue where a worms foraging amplitude is 0 degrees through to red where the foraging amplitude is 90 degrees. Tracks for individual recordings are overlayed on top of one another. Grey worm shapes denote the position ofthe worm at the start of recording, the black worm shape denotes the position of the worm at the end of recording. B: The average foraging amplitude probability ($\Sigma P(x)=1$) for backward, forward and paused locomotion for the *C. elegans* mutant strain *acd-5 (ok2657)I* and N2. Foraging amplitude for backward locomotion is shown in blue, forward in purple and paused in green.

2.3.2.2 Turning Analysis

In order to characterise these turning behaviours in greater detail, turning events were explored in depth by Tadas Jucikas. The entirety of the Bristol N2 recordings was assessed for the number, type, duration and magnitude of turns. Over the 1,218 good quality N2 recordings, 6416 turning event were recorded, 4543 of these were omega bends and the remaining 1873 turns had a similar magnitude but the worm posture did not satisfy the criteria set for an omega bend. The percentage of these turns that were entered in the dorsal or ventral direction is shown in Fig.2.21. There is a clear bias in *C. elegans* wild-type worms for entering turns in the ventral direction. When comparing this to the percentage of turns made by all of either *acd-5 (ok2657)I* or *asic-2 (ok289)I* in the dorsal or ventral direction, this bias is switched to dorsally entered turns, although the bias is not as strong as in N2 for ventral turns. In addition the average length of omega turns in N2 worms was 4.5±2 (± SD) seconds, and other turns were found to have similar durations. In the *acd-5* mutant, omega bends had an average duration of 6.2±4 seconds while in the *asic-2* mutant, average omega bend duration was 4.7±3.

Omega bends in N2 worms were shown to have a high correlation with reversal events, 97±1% of wild-type omega bends are correlated with reversals (Jucikas, 2013). Other turns were correlated with reversals in 77±1.9% of turning events. The mean distance of reversals correlated with omega bends and other turns was found to be larger than the mean distance of all of the reversals that the animal makes. A mean reversal distance for wild type strain is 255±238.5 (±SD) µm and 586.5±446.3 µm (±SD) and 555.3±396.3 µm (±SD) for omega and other turns respectively (Jucikas, 2013).

The variability in the DEG/ENaC family members in comparison to wild-type on turning features alone was assessed by Tadas Jucikas and it was found that, along with the loss of ventral bias on turning, the correlation between reversals and turns was lost (significance calculated using Chi-Square test with Bonferroni correction, significance was set at $p \leq 0.05$). The heat map in figure 2.22 shows that ventral bias is significantly less in the mutants than the mean in N2 and long reversals are significantly increased in the mutants compared to N2.

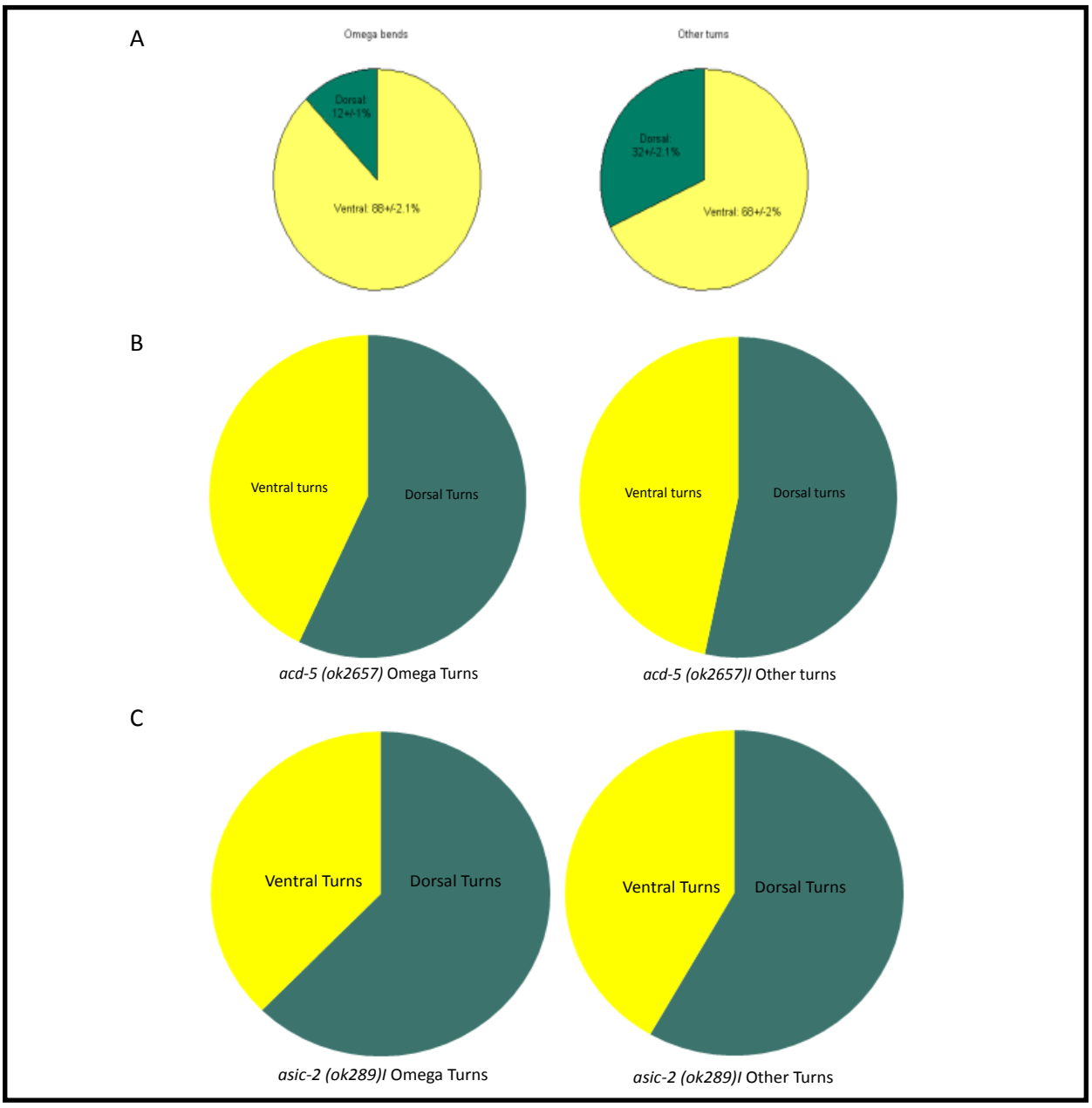

Fig.2.21: Pie Charts Showing the Percentage of Omega and Other Turns Performed In Different *C. elegans* Genotypes In The Dorsal or Ventral Direction. A: Pie charts showing the percentage of omega turns (left) and other turns (right) made by N2 in the dorsal or ventral direction (T. Jucikas 2013). B: Pie charts showing the percentage of omega turns (left) and other turns (right) made by *acd-5 (ok2657)I* in the dorsal or ventral direction. C: Pie charts showing the percentage of omega turns (left) and other turns (right) made by *asic-2 (ok289)I* in the dorsal or ventral direction.

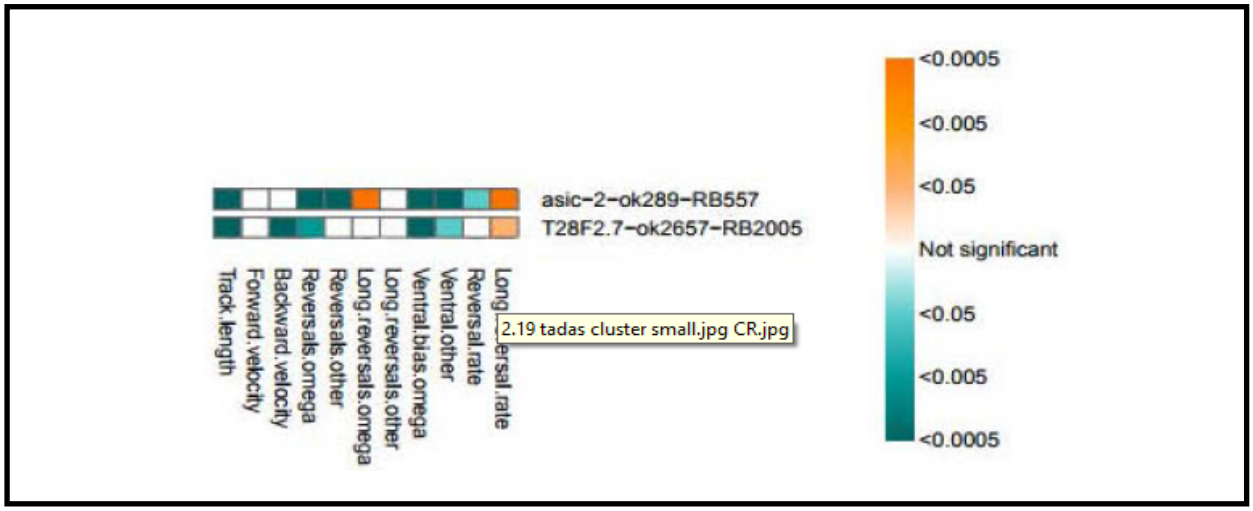

Fig.2.22: Heatmaps For Turning Related Phenotypes in *acd-5 (ok2657)I* and *asci2 (ok289)I.* Turning related phenotypes are listed at the bottom of the figure, colouration represents significance of the mutant mean from the N2 mean for each feature, blue scale colours denote results that were significantly less than the N2 mean,. Red scale colours denot results that were significantly higher than the mean. Significance level and colour is shown in the key. Significance was established using Chi-Square test with Bonferroni correction (T. Jucikas 2013).

2.4 Discussion

2.4.1 Comparison of Clustering Techniques

Both the motif clustering and features clustering techniques show promising results, with many of the mutants from the same, known pathways clustering together. There are, however, some differences in the clustering of unknown mutants. This may be because the clustering techniques were selected on their ability to cluster known mutants together, and assessed as viable if this was the case.

Both clustering techniques have their advantages and disadvantages. The features clustering method is useful if the researcher needs to compare results from the high-throughput tracking project to previously observed data. The features extracted and analysed for this method of clustering are already well characterised in *C. elegans*. This allows for comparisons between the tracked strains and mutant strains that have yet to be tracked. For example, if an increase in reversals is observed in a mutant strain that has not been tracked one could search the open access database to find tracked strains that also display this phenotype. Similarly, if the tracked strain exhibits a set of features these can then be compared to previously observed features of strains postulated to have a similar function.

The motif method of clustering is useful for detecting novel behaviours. In previous studies all features extracted from recordings of *C. elegans* had to be predetermined. This could mean that some important behavioural phenotypes were being missed. By using the data set to discover behavioural motifs a brand new set of phenotypes can be analysed. This type of clustering could be useful when no comparison to previous studies is required and when the researcher is interested in novel behaviours.

For the tracking project itself it is useful to have two methods of clustering to compare. Connections that are found in both sets of results are likely to have some functional similarity.

The DEG/ENaC mutants *acd-5 (ok2657)I* and *asic-2 (ok289)I* did not cluster together in the feature based clustering performed by Ev Yemini. This could be an indication that the two genes are not as alike as the motif based clustering suggests. However, it is noteworthy that the monoamine signalling pathway mutants do not show as close clustering in the feature based analysis as they do when using behavioural motifs, so it is unclear which of the two methods can most effectively cluster mutant strains of genes working in the same pathways.

2.4.2 DEG/ENaC Clustering

asic-2 (ok289)I and *acd-5 (ok2657)I* cluster only in the motif clustering analysis. Results from the features clustering suggest that the pair is not all that alike. Table 2.1 shows 60 features that are significantly different from wild type in both mutants. However, there are 274 extra features for *acd-5 (ok2657)I* that are significantly different from wild type that are not shared with *asic-2 (ok289)I.* Similarly *asic-2 (ok289)I* has 54 extra features that are significantly different from N2 that are not shared with *acd-5 (ok2657)I.*

Since the motif method of clustering creates novel behaviours it is difficult to know what the significance of these behaviours are. When looking at phenotypes that have been previously described there is some knowledge as to the molecular functioning behind the mutant phenotype. When using the motif clustering data no such knowledge exists. For the DEG/ENaC subunit pair *asic-2 (ok289)I* and *acd-5 (ok2657)I* the shared motifs of a forward bout of locomotion or a prolonged pause

in a curved shape give no hint as to how the genes are functioning, only that they may function together. Similarly the mutant tendency to bend dorsally while N2 tends to bend ventrally gives little insight into the functioning of these DEG/ENaC subunits. At present there is no research into why N2 worms have a ventral bend preference, therefore it is difficult to elucidate why the mutant may display the opposite tendency. Further investigation into the functioning of these genes is required for any conclusions to be made as to whether the pair are functionally similar.

2.4.3 Troubleshooting

For the first year of tracking experiments mutants were tracked on a group by group basis. For example, all G-protein coupled receptor mutants were obtained and tracked together over a period of around 2 weeks. Once enough videos for each strain of a gene family had been collected, a new gene family would be tracked. In hindsight this could lead to some families appearing to cluster more strongly together simply because they were tracked at the same time. The data in Fig 2.4a and b suggest that there are seasonal differences in the N2 tracking results. It is feasible, in this case, that mutants tracked in August may behave in a different way to those tracked in December, even with normalisation to their N2 counterparts. This would mean that the mutants tracked in August would cluster strongly together and mutants tracked in December would cluster together. In later experiments efforts were made to spread gene families out across longer time periods and to mix them with other gene families. It would be interesting to see if any genes from different families that are known to work together still cluster despite being tracked in different seasons.

2.4.4 Applications of the Tracking System

Since its development, worm tracker 2 has been successfully used for a number of experiments.

2.4.4.1 Neon-Green Validation

mNeon-Green is a fluorescent molecule that can be used in the same way as GFP, but has a 3-5 fold increase in fluorescence in comparison to GFP. mNeon-Green has successfully been used in *C. elegans* to determine expression patterns of genes. Specifically the gene *F21D12.3,* a predicted transmembrane amino acid transporter related to the GABA transporter UNC-47 (Edwards et al. 1997). Using mNeon-Green it was established that *F21D12.3* is expressed in motor neurons and muscles, suggesting a role in the modulation of locomotion. WT2 was used to track the locomotory behaviour of the mutant, resulting in significant features in curvature, speed and posture, suggesting that, like other fluorescence-based reporters, mNeon-Green can be used successfully to guide the discovery of gene functions (Hostettler et al. 2017).

2.4.4.2 Tracking Postural Changes On and Off Food

Using the WT2 system it is possible to identify 90 postures for the worm that can offer a compact data set explaining *C. elegans* locomotion. These postures explain not only worm locomotion on food but also off food and in response to the chemoattractant benzaldehyde. The locomotory behaviour of *C. elegans* off food and during chemotaxis varies significantly to that on food. As the compact data set can identify all postures in these conditions, it would be possible to use the single worm trackers to identify anomalies in mutant behaviours in a food-free environment and also while the worm taxes towards attractants. This is particularly interesting for research into mutants that show chemotactic defects, as it may be possible to identify changes in micro-behaviours in the mutant that would usually occur in the local search behaviour (Schwarz et al. 2015).

2.4.4.3 Determining Neurons Involved In Locomotion

The neuron PDB had previously not been implicated in locomotory modulation, but was predicted to play a role in locomotion. Predictions were made by analysing the connectome network of *C. elegans*

and determining which neurons showed characteristic connectivity in line with locomotion modulators. WT2 was used to track single worms with the PDB ablated, alongside mock ablated worms. For analysis, only the eigenworm data was used, rather than the entire feature dataset. PDB ablated worms were found to have significantly different results in eigenworm projection 1, a posture that represents large body bends. Interestingly, worms with DD4 and DD5 ablated, but not DD2 or DD3 ablated, were found to have significantly different absolute eigenworm 4 projections during forward locomotion, compared with mock-ablated controls, correlating with a reduction in tail movement during forward locomotion. These results suggest a role for PDB and particular DD neurons in locomotion, as predicted (Yan et al. 2017).

2.4.5 Future experiments

Investigation into the possible interaction between *asic-2* and *acd-5* has been discussed in detail in chapter 3 of this thesis. There are a number of unknown genes that clustered strongly together when looking at similarity between phenotypes, one pair of these is *delm-2 (ok1822)I* and *acd-2 (ok1237)I*, another pair of DEG/ENaC subunits (AU=99.1%). These genes have a similar phenotypic fingerprint, both share many features that are significantly different to wild type. Of these shared significant features most trend away from N2 in same direction. For example, both mutants have an increased pathlength in comparison to N2 and both have a decreased primary wavelength in comparison to N2 and an investigation into the functioning of these two genes could be carried out, as it has been for *acd-5* and *asic-2* mutants, in order to determine if one form of clustering is able to identify mutants working in the same pathway better than the other.

2.5 References

Albert, P.S. & Riddle, D.L., 1983. Developmental alterations in sensory neuroanatomy of the *Caenorhabditis elegans* dauer larva. *The Journal of Comparative Neurology*, 219(4), pp.461–481. Available at: http://doi.wiley.com/10.1002/cne.902190407 [Accessed September 29, 2017].

Alkema, M.J. & Hunter-Ensor, M., 2005. Tyraminefunctionsindependently of octopamine in the *Caenorhabditis elegans* nervous system. *Neuron*, 46, pp.247–260. Available at: http://ac.els-cdn.com/S0896627305001674/1-s2.0-S0896627305001674-main.pdf?_tid=d95b8670-881c-11e7-a5da-00000aab0f6b&acdnat=1503504495_15b3813e1307f67a54da89de7ef58631 [Accessed August 23, 2017].

Altun, Z.F. et al., 2009. High resolution map of *Caenorhabditis elegans* gap junction proteins. *Developmental dynamics : an official publication of the American Association of Anatomists*, 238(8), pp.1936–50. Available at: http://www.ncbi.nlm.nih.gov/pubmed/19621339 [Accessed September 18, 2017].

Baek, J.-H. et al., 2002. Using machine vision to analyze and classify *Caenorhabditis elegans* behavioral phenotypes quantitatively. *Journal of neuroscience methods*, 118(1), pp.9–21. Available at: http://www.ncbi.nlm.nih.gov/pubmed/12191753 [Accessed September 18, 2017].

Bargmann, C.I., 1998. Neurobiology of the *Caenorhabditis elegans* genome. *Science*, 282(5396), pp.2028–2033.

Berri, S. et al., 2009. Forward locomotion of the nematode *C. elegans* is achieved through modulation of a single gait. *HFSP journal*, 3(3), pp.186–93. Available at: http://www.ncbi.nlm.nih.gov/pubmed/19639043 [Accessed September 18, 2017].

Brenner, S., 1974. The genetics of *Caenorhabditis elegans*. *Genetics*, 77(1), pp.71–94. Available at: http://www.ncbi.nlm.nih.gov/pubmed/4366476 [Accessed September 11, 2017].

Brown, A.E.X. et al., 2013. A dictionary of behavioral motifs reveals clusters of genes affecting *Caenorhabditis elegans* locomotion. *Proceedings of the National Academy of Sciences of the United States of America*, 110(2).

Brown, A.E.X. et al., 2013. A dictionary of behavioral motifs reveals clusters of genes affecting Caenorhabditis elegans locomotion. *Proceedings of the National Academy of Sciences of the United States of America*, 110(2), pp.791–6. Available at: http://www.pubmedcentral.nih.gov/articlerender.fcgi?artid=3545781&tool=pmcentrez&rendertype=abstract.

Butler, V.J., 2012. Molecular and neuromuscular mechanisms underlying locomotion and proprioception in *Caenorhabditis elegans*. Available at: http://www2.mrc-lmb.cam.ac.uk/groups/wschafer/VictoriaButler.pdf [Accessed October 1, 2017].

Chalfie, M. & Sulston, J., 1981. Developmental genetics of the mechanosensory neurons of Caenorhabditis elegans. *Developmental biology*, 82(2), pp.358–70. Available at: http://www.ncbi.nlm.nih.gov/pubmed/7227647 [Accessed September 18, 2017].

Chen, B.L., Hall, D.H. & Chklovskii, D.B., 2006. Wiring optimization can relate neuronal structure and function. *Proceedings of the National Academy of Sciences of the United States of America*, 103(12), pp.4723–8. Available at: http://www.ncbi.nlm.nih.gov/pubmed/16537428 [Accessed September 18, 2017].

Coulson, A. et al., 1986. Toward a physical map of the genome of the nematode *Caenorhabditis elegans* (ordered clone bank/genomic data base/clone matching). *Genetics*, 83, pp.7821–7825.

Available at: https://www.ncbi.nlm.nih.gov/pmc/articles/PMC386814/pdf/pnas00324-0265.pdf [Accessed September 6, 2017].

Cox, G.N. et al., 1989. Sequence comparisons of developmentally regulated collagen genes of *Caenorhabditis elegans*. *Gene*, 76(2), pp.331–344. Available at: http://www.sciencedirect.com/science/article/pii/037811198990173X [Accessed September 18, 2017].

CROLL, N.A., 1975. Components and patterns in the behaviour of the nematode *Caenorhabditis elegans. Journal of Zoology*, 176(2), pp.159–176. Available at: http://onlinelibrary.wiley.com/doi/10.1111/j.1469-7998.1975.tb03191.x/abstract;jsessionid=E9ABD2EF5ACBE631A8ECE02EF6EA6BC5.f01t02.

Croll, N.A. & Smith, J.M., 1978. Integrated behaviour in the feeding phase of *Caenorhabditis elegans* (Nematoda). *Journal of Zoology*.

Culetto, E. et al., 2004. The *Caenorhabditis elegans unc-63* gene encodes a levamisole-sensitive nicotinic acetylcholine receptor α subunit. *Journal of Biological Chemistry*, 279(41), pp.42476–42483. Available at: http://www.ncbi.nlm.nih.gov/pubmed/15280391 [Accessed October 19, 2017].

Duerr, J.S. et al., 2008. Identification of major classes of cholinergic neurons in the nematode *Caenorhabditis elegans*. *The Journal of Comparative Neurology*, 506(3), pp.398–408. Available at: http://doi.wiley.com/10.1002/cne.21551 [Accessed September 30, 2017].

Dunsenbery, D.B., 1985. Video camera-computer tracking of nematode *Caenorhabditis elegans* TO record behavioral responses. *Journal of Chemical Ecology*, 11(9). Available at: https://link.springer.com/content/pdf/10.1007/BF01024112.pdf [Accessed July 28, 2017].

Dusenbery, D.B., 1974. Analysis of chemotaxis in the nematode *Caenorhabditis elegans* by countercurrent separation. *Journal of Experimental Zoology Part A: Ecological Genetics and Physiology*, 188(1), pp.41–47. Available at: http://onlinelibrary.wiley.com/doi/10.1002/jez.1401880105/abstract [Accessed September 18, 2017].

Dusenbery, D.B., 1980. Journal of Comparative Physiology. A Appetitive Response of the Nematode *Caenorhabditis elegans* to Oxygen. *Physiol*, 136, pp.333–336.

Dusenbery, D.B., 1985. Using a microcomputer and video camera to simultaneously track 25 animals. *Computers in Biology and Medicine*.

Epstein~ ’~, H.P., Waterston~~, R.H. & Brennee ’, S., 1974. A Mutant Affecting the Heavy Chain of Myosin in *Caenorhabditis elegans*. *J. Mol. Bi0.l*, 90, pp.291–300.

Feng, Z. et al., 2004. An imaging system for standardized quantitative analysis of *C. elegans* behavior. *BMC Bioinformatics*, 5(1), p.115. Available at: http://bmcbioinformatics.biomedcentral.com/articles/10.1186/1471-2105-5-115 [Accessed October 1, 2017].

Frey, B.J. & Dueck, D., 2008. Response to Comment on “Clustering by Passing Messages Between Data Points.” *Science*.

Fujiwara, M., Sengupta, P. & McIntire, S.L., 2002a. Regulation of body size and behavioral state of *C. elegans* by sensory perception and the EGL-4 cGMP-dependent protein kinase. *Neuron*, 36(6), pp.1091–102. Available at: http://www.ncbi.nlm.nih.gov/pubmed/12495624 [Accessed October 2, 2017].

Gao, S. & Zhen, M., 2011. Action potentials drive body wall muscle contractions in *Caenorhabditis elegans*. *Proceedings of the National Academy of Sciences of the United States of America*, 108(6), pp.2557–62. Available at: http://www.ncbi.nlm.nih.gov/pubmed/21248227 [Accessed September 18, 2017].

Geng, W. et al., 2004. Automatic tracking, feature extraction and classification of *C. elegans* phenotypes. *IEEE Transactions on Biomedical Engineering*, 51(10), pp.1811–1820.

Geng, W. et al., 2005. *Caenorhabditis elegans* egg-laying detection and behavior study using image analysis. *EURASIP Journal on Applied Signal Processing*, 14, pp.2229–2240.

George-Raizen, J.B. et al., 2014. Dynamically-expressed prion-like proteins form a cuticle in the pharynx of *Caenorhabditis elegans*. *Biology Open*, 3(11), pp.1139–1149. Available at: http://www.ncbi.nlm.nih.gov/pubmed/25361578 [Accessed October 2, 2017].

Gray, J. & Lissmann, H.W., 1964. The locomotion of nematodes. *J. Exp. Biol*, 41, pp.3–4.

Gray, J.M., Hill, J.J. & Bargmann, C.I., 2005. A circuit for navigation in *Caenorhabditis elegans*. *Proceedings of the National Academy of Sciences of the United States of America*, 102(9), pp.3184–91. Available at: http://www.ncbi.nlm.nih.gov/pubmed/15689400 [Accessed October 1, 2017].

Hardaker, L.A. et al., 2001. Serotonin modulates locomotory behavior and coordinates egg-laying and movement in *Caenorhabditis elegans*. *J Neurobiol*, 49, pp.303–313. Available at: http://www.mrc-lmb.cam.ac.uk/wormtracker/pdf/Hardaker2001.pdf [Accessed July 28, 2017].

Hart, A.C., 2006. Behavior. *WormBook*. Available at: http://www.wormbook.org/chapters/www_behavior/behavior.html [Accessed September 18, 2017].

Hostettler, L. et al., 2017. The bright fluorescent protein mNeonGreen facilitates protein expression analysis In Vivo. *G3 (Bethesda, Md.)*, 7(2), pp.607–615. Available at: http://www.ncbi.nlm.nih.gov/pubmed/28108553 [Accessed October 19, 2017].

Huang, K.M., Cosman, P. & Schafer, W.R., 2006. Machine vision based detection of omega bends and reversals in *C. elegans*. *Journal of Neuroscience Methods*.

Hutter, H. et al., 2000. Conservation and novelty in the evolution of cell adhesion and extracellular matrix genes. *Science (New York, N.Y.)*, 287(5455), pp.989–94. Available at: http://www.ncbi.nlm.nih.gov/pubmed/10669422 [Accessed September 14, 2017].

Illinois State University, Molecular neothology lab . https://about.illinoisstate.edu/avidal/Pages/AGVG_Res.aspx

Johnathon Hodgkin, Jonathan Hodgkin (person) - WormBase : Nematode Information Resource. Available at: http://www.wormbase.org/resources/person/WBPerson261#01--10 [Accessed September 18, 2017].

Jucikas, T., An online database for behavioural phenotypes of the nematode *Caenorhabditis elegans*. Available at: http://www2.mrc-lmb.cam.ac.uk/groups/wschafer/tjucikas_phd_thesis.pdf [Accessed October 19, 2017].

Kagawa, H. et al., 1989. Paramyosin gene (*unc-15*) of *Caenorhabditis elegans*. Molecular cloning, nucleotide sequence and models for thick filament structure. *Journal of molecular biology*, 207(2), pp.311–33. Available at: http://www.ncbi.nlm.nih.gov/pubmed/2754728 [Accessed September 18, 2017].

Kim, J. et al., 2001. Genes affecting the activity of nicotinic receptors involved in *Caenorhabditis*

elegans egg-laying behavior. *Genetics*, 157(4), pp.1599–610. Available at: http://www.ncbi.nlm.nih.gov/pubmed/11290716 [Accessed September 18, 2017].

LeDoux, M., 2005. *Animal models of movement disorders*, Elsevier Academic Press. Available at: https://books.google.co.uk/books?id=Qq0SfGR_R_QC&pg=PA219&lpg=PA219&dq=c+elegans+lay+around+300+eggs&source=bl&ots=HZ1RZ8Qn4R&sig=HQQqbo1504Y5hIFs1dRnt1bOKzA&hl=en&sa=X&ved=0ahUKEwifrf_doPzVAhUoK8AKHebqAWgQ6AEIYDAH#v=onepage&q=300 eggs&f=false [Accessed August 29, 2017].

Lee, B.H. et al., 2011. Hyperactive neuroendocrine secretion causes size, feeding, and metabolic defects of *C. elegans* Bardet-Biedl Syndrome Mutants S. K. Kim, ed. *PLoS Biology*, 9(12), p.e1001219. Available at: http://dx.plos.org/10.1371/journal.pbio.1001219 [Accessed October 10, 2017].

Lewis, J.A. & Hodgkin, J.A., 1977. Specific neuroanatomical changes in chemosensory mutants of the nematode *Caenorhabditis elegans*. *The Journal of Comparative Neurology*, 172(3), pp.489–510. Available at: http://www.ncbi.nlm.nih.gov/pubmed/838889 [Accessed July 24, 2017].

Li, W., Herman, R.K. & Shaw, J.E., 1992. Analysis of the *Caenorhabditis elegans* axonal guidance and outgrowth gene unc-33. *Genetics*, 132(3), pp.675–89. Available at: http://www.ncbi.nlm.nih.gov/pubmed/1468626 [Accessed September 18, 2017].

Loer, C.M. & Kenyon, C.J., 1993. Serotonin-deficient mutants and male mating behavior in the nematode *Caenorhabditis elegans*. *The Journal of neuroscience : the official journal of the Society for Neuroscience*, 13(12), pp.5407–17. Available at: http://www.ncbi.nlm.nih.gov/pubmed/8254383 [Accessed October 19, 2017].

Macleod, A.R. et al., 1977. Identification of the Structural Gene for a Myosin Heavy-chain in *Caenorhabditis elegans*. *J. Mol. Biol*, 114, pp.133–140.

Nagy, S. et al., 2015. *Caenorhabditis elegans* exhibit a coupling between the defecation motor program and directed locomotion. *Scientific reports*, 5, p.17174. Available at: http://www.ncbi.nlm.nih.gov/pubmed/26597056 [Accessed July 28, 2017].

Ogura, K. et al., 1997. The UNC-14 protein required for axonal elongation and guidance in *Caenorhabditis elegans* interacts with the serine/threonine kinase UNC-51. *Genes & development*, 11(14), pp.1801–11. Available at: http://www.ncbi.nlm.nih.gov/pubmed/9242488 [Accessed September 18, 2017].

Ogura, K.-I. & Goshima, Y., 2006. The autophagy-related kinase UNC-51 and its binding partner UNC-14 regulate the subcellular localization of the Netrin receptor UNC-5 in *Caenorhabditis elegans*. *Development (Cambridge, England)*, 133(17), pp.3441–50. Available at: http://www.ncbi.nlm.nih.gov/pubmed/16887826 [Accessed September 18, 2017].

Ono, K. et al., 2003. Specific requirement for two ADF/cofilin isoforms in distinct actin-dependent processes in *Caenorhabditis elegans*. *Journal of cell science*, 116(Pt 10), pp.2073–85. Available at: http://www.ncbi.nlm.nih.gov/pubmed/12679387 [Accessed September 18, 2017].

Otsuka, A.J. et al., 1995. An ankyrin-related gene (unc-44) is necessary for proper axonal guidance in *Caenorhabditis elegans*. *The Journal of cell biology*, 129(4), pp.1081–92. Available at: http://www.ncbi.nlm.nih.gov/pubmed/7744957 [Accessed September 18, 2017].

Peng, H., Long, F. & Ding, C., 2005. Feature selection based on mutual information: criteria of max-dependency, max-relevance, and min-redundancy. *IEEE transactions on pattern analysis and machine intelligence*, 27(8), pp.1226–38. Available at: http://www.ncbi.nlm.nih.gov/pubmed/16119262 [Accessed September 18, 2017].

Pierce-Shimomura, J.T. et al., Genetic analysis of crawling and swimming locomotory patterns in *C. elegans.* Available at: http://www.pnas.org/content/105/52/20982.full.pdf [Accessed September 18, 2017].

Pierce-Shimomura, J.T., Morse, T.M. & Lockery, S.R., 1999. The fundamental role of pirouettes in *Caenorhabditis elegans* chemotaxis. *The Journal of neuroscience : the official journal of the Society for Neuroscience*, 19(21), pp.9557–69. Available at: http://www.ncbi.nlm.nih.gov/pubmed/10531458 [Accessed September 18, 2017].

Rajaram, S., Sedensky, M.M. & Morgan, P.G., 1998. *unc-1*: a stomatin homologue controls sensitivity to volatile anesthetics in *Caenorhabditis elegans*. *Proceedings of the National Academy of Sciences of the United States of America*, 95(15), pp.8761–6. Available at: http://www.ncbi.nlm.nih.gov/pubmed/9671752 [Accessed September 28, 2017].

Ramot, D. et al., 2008. The parallel worm tracker: A platform for measuring average speed and drug-induced paralysis in nematodes R. Aramayo, ed. *PLoS ONE*, 3(5), p.e2208. Available at: http://dx.plos.org/10.1371/journal.pone.0002208 [Accessed October 5, 2017].

Rankin, C.H. et al., 1990. *Caenorhabditis elegans*: a new model system for the study of learning and memory. *Behavioural Brain Research*, 37, pp.89–92.

Riddle, D.L., 1997. *C. elegans II*, Cold Spring Harbor Laboratory Press.

Rose, C.R. & Konnerth, A., 2001. NMDA Receptor-mediated Na+ signals in spines and dendrites. *Journal of Neuroscience*, 21(12). Available at: http://www.jneurosci.org/content/21/12/4207.long [Accessed September 14, 2017].

Sawin, E.R., Ranganathan, R. & Horvitz, H.R., 2000. *C. elegans* locomotory rate is modulated by the environment through a dopaminergic pathway and by experience through a serotonergic pathway. *Neuron*, 26(3), pp.619–31. Available at: http://www.ncbi.nlm.nih.gov/pubmed/10896158 [Accessed October 10, 2017].

Schwarz, R.F. et al., 2015. Changes in postural syntax characterize sensory modulation and natural variation of *C. elegans* Locomotion. *PLoS Computational Biology*, 11(8).

Srinivasan, J. et al., 2008. A blend of small molecules regulates both mating and development in *Caenorhabditis elegans*. *Nature*, 454(7208), pp.1115–1118. Available at: http://www.ncbi.nlm.nih.gov/pubmed/18650807 [Accessed October 2, 2017].

Stephens, G.J. et al., 2008. Dimensionality and dynamics in the behavior of *C. elegans.* O. Sporns, ed. *PLoS Computational Biology*, 4(4), p.e1000028. Available at: http://dx.plos.org/10.1371/journal.pcbi.1000028 [Accessed December 15, 2016].

Sulston, J., Dew, M. & Brenner, S., 1975. Dopaminergic neurons in the nematode *Caenorhabditis elegans*. *The Journal of Comparative Neurology*, 163(2), pp.215–226. Available at: http://doi.wiley.com/10.1002/cne.901630207 [Accessed October 10, 2017].

Trent, C., Tsuing, N. & Horvitz, H.R., 1983. Egg-laying defective mutants of the nematode *Caenorhabditis elegans*. *Genetics*, 104(4), pp.619–47. Available at: http://www.ncbi.nlm.nih.gov/pubmed/11813735 [Accessed July 24, 2017].

Varshney, L.R. et al., 2011. Structural Properties of the *Caenorhabditis elegans* neuronal network. O. Sporns, ed. *PLoS Computational Biology*, 7(2), p.e1001066. Available at: http://dx.plos.org/10.1371/journal.pcbi.1001066 [Accessed September 1, 2017].

Vidal-Gadea, A. et al., 2011. *Caenorhabditis elegans* selects distinct crawling and swimming gaits via dopamine and serotonin. *Proceedings of the National Academy of Sciences of the United States*

of America, 108(42), pp.17504–9. Available at: http://www.ncbi.nlm.nih.gov/pubmed/21969584 [Accessed September 18, 2017].

Waggoner, L.E. et al., 1998. Control of alternative behavioral states by serotonin in *Caenorhabditis elegans*. *Neuron*, 21(1), pp.203–214. Available at: http://linkinghub.elsevier.com/retrieve/pii/S0896627300805279 [Accessed August 17, 2017].

Ward, A. et al., 2008. Light-sensitive neurons and channels mediate phototaxis in *C. elegans*. *Nature neuroscience*, 11(8), pp.916–22. Available at: http://dx.doi.org/10.1038/nn.2155.

Ward, S. et al., 1975. Electron microscopical reconstruction of the anterior sensory anatomy of the nematode *Caenorhabditis elegans*. *Journal of Comparative Neurology*.

White, J.G. et al., 1986. The structure of the nervous system of the nematode *Caenorhabditis elegans*. *Philosophical transactions of the Royal Society of London. Series B, Biological sciences*, 314(1165), pp.1–340. Available at: http://www.ncbi.nlm.nih.gov/pubmed/22462104 [Accessed September 18, 2017].

Winnier, A.R. et al., 1999. UNC-4/UNC-37-dependent repression of motor neuron-specific genes controls synaptic choice in *Caenorhabditis elegans*. *Genes & development*, 13(21), pp.2774–86. Available at: http://www.ncbi.nlm.nih.gov/pubmed/10557206 [Accessed October 19, 2017].

Yan, G. et al., 2017. Network control principles predict neuron function in the *Caenorhabditis elegans* connectome. *Nature*. Available at: http://www.nature.com/doifinder/10.1038/nature24056 [Accessed October 19, 2017].

Yeh, E. et al., 2008. A putative cation channel, NCA-1, and a novel protein, UNC-80, transmit neuronal activity in *C. elegans*. M. de Bono, ed. *PLoS Biology*, 6(3), p.e55. Available at: http://www.ncbi.nlm.nih.gov/pubmed/18336069 [Accessed July 24, 2017].

Yemini, E. et al., 2013. A database of *Caenorhabditis elegans* behavioral phenotypes. *Nature Methods*, 10(9).

Yemini, E., 2011a. High-throughput, single-worm tracking and analysis in *Caenorhabditis elegans.* Available at: http://www2.mrc-lmb.cam.ac.uk/groups/wschafer/EvYemini.pdf [Accessed September 18, 2017].

Chapter 3: Determining the Functional Links Between the DEG/ENaC Genes *asic-2* and *acd-5*

3.1 Introduction

In the previous chapter, a number of unknown mutants were tracked in order to identify phenotypes that may lead to identification of the mutated gene's function. As expected, several of the mutants in genes with a known function clustered together with those from the same pathways. In this chapter I sought to determine whether a pair of unknown genes that clustered together are functioning in the same pathway: specifically, *asic-2* (Acid-sensing Amilioride-Sensitive Ion Channel) and *acd-5* (ACid-sensing Degenerin). These mutant strains cluster together strongly when sorting by behavioural motifs, specifically a dorsal bend bias on turning (Fig.3.1A) and loss of reversals related to turns. These features alone do not point to a specific function therefore further investigation was necessary.

3.1.1 DEG/ENaC Family

Both *asic-2* and *acd-5* are members of the DEG/ENaC super-family, a large group of Na^+ channel subunits found in a variety of organisms including nematodes, snails, flies and humans. The name derives from the initial two identified subfamilies, the *C. elegans* degenerins (encoded by *deg-1, mec-4, mec-10, del-1, unc-8* and *unc-108*) and the vertebrate epithelial amilioride-sensitive Na^+ channel (ENaC) (Mano & Driscoll 1999). Members of the super-family have two membrane spanning domains, intracellular N- and C-termini and an extracellular domain with a cysteine-rich region (Renard et al. 1994) (Fig. 3.1B). Despite the highly conserved topology, DEG/ENaCs have been implicated in a variety of functions in different cell types. These include mechanosensation, specifically proprioception and pain sensation, gametogenesis and epithelial Na^+ transport, in cells such as kidney epithelia, muscle cells and neurons (Mano & Driscoll 1999).

Figure 3.1C shows a phylogenetic tree for representative members of the family from non-nematode sources and all of the putative *C. elegans* DEG/ENaC channels in the nematode genome. This shows the various DEG/ENaC sub-families, each sharing a more highly conserved DNA sequence (Syntichaki & Tavernarakis 2004)(Fig.3.1C). These different families tend to have different cellular functions and gating properties: the almost constitutively active Na^+ preferring/selective channels found in vertebrates (ENaC channels) (Garty & Palmer 1997), those activated by mechanical stimulus (*C. elegans* degenerins) (Syntichaki & Tavernarakis 2004; Gu et al. 1996) or activated by proton binding (acid sensing ion channels)(Waldmann & Lazdunski 1998).

In *C. elegans* there are 30 genes postulated to code for DEG/ENaC channels (Syntichaki & Tavernarakis 2004) and at present, many of these do not have defined functions. Those that have a proven function are the mechanosensory degenerins. The name degenerin originates from these genes as they were the first in the family to be classified in *C. elegans*, and all have an unusual property; the gain of function mutations in *deg-1, mec-4, mec-10, del-1, unc-8* and *unc-108* can induce swelling and subsequent necrotic cell death (degeneration) of the neurons in which they are expressed (Chalfie & Wolinsky 1990).

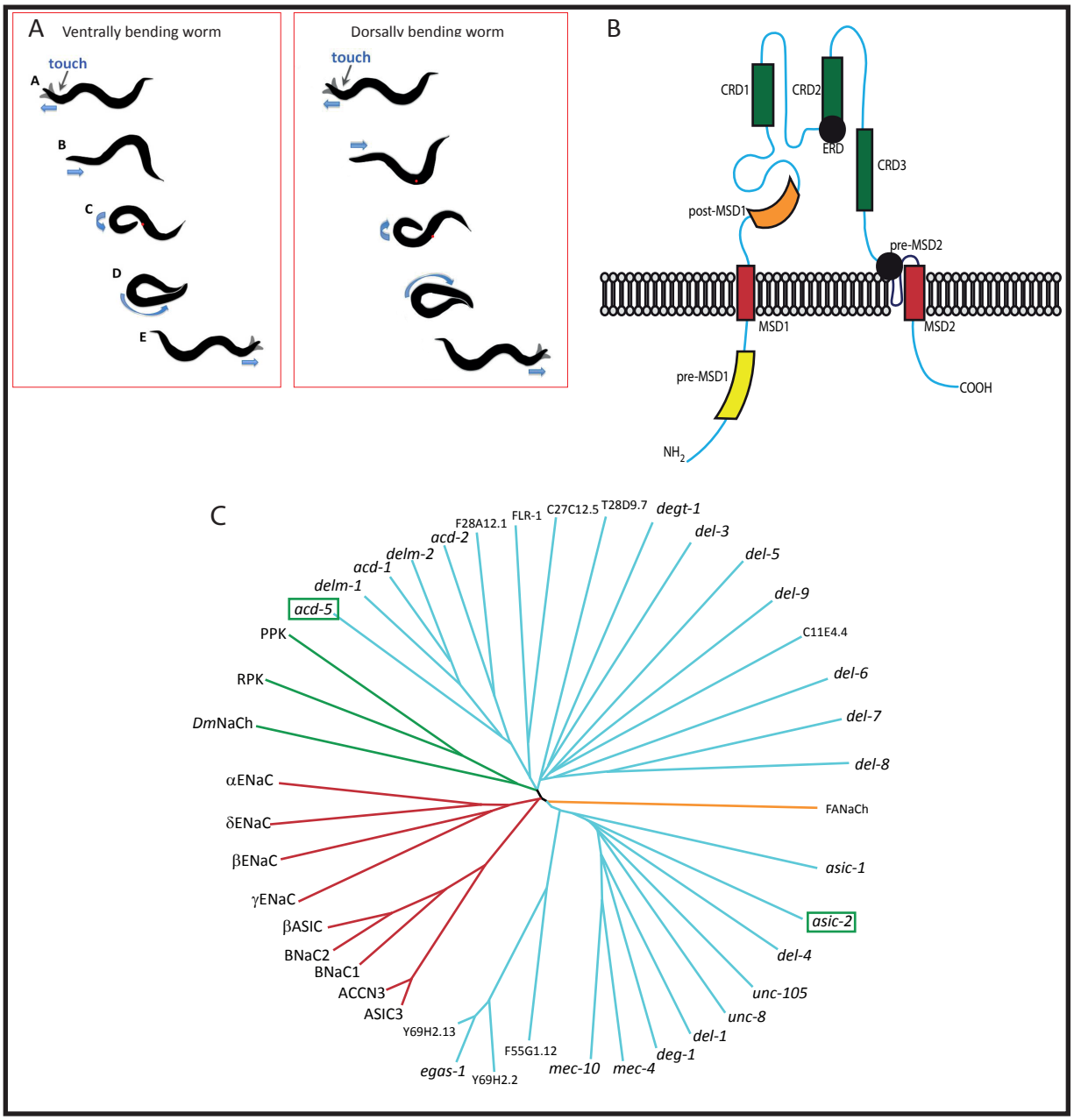

Fig.3.1: DEG/ENaC Family and Topolgy

A: The more common form of turning executed by *C. elegans*, entered ventrally (vulva on the inside of the turn, Donnelly et. al 2013) in comparison to the dorsally entered turn more commonly executed by *asic-2* and *acd-5.* B: A *C. elegans* degenerin subunit is depicted to show the general topology of a DEG/ENaC subunit. Top is extracellular; bottom is intracellular. MSD, membrane spanning domain; CRD, cysteine-rich domain; ERD, extracellular regulatory domain. CRD1 and ERD are ony present in degenerins, and CRD2 is only partially conserved across subfamilies (Mano and Driscoll 1999). C: Concensus tree for the Deg/ENaC family, nematode degenerins are shown with blue lines, Mammalian with red lines, Fly with green lines and snail with orange *asic-2* and *acd-5* are highlighted in green boxes (Syntichaki and Taverinakis 2004).

The DEG/ENaC subunit encoding genes *mec-4* and *mec-10* are important in touch transduction in *C. elegans.* The MEC-4 protein is expressed in the TRNs (Touch Receptor Neurons) and is required for gentle touch-evoked calcium transients and mechanical currents in these neurons (Suzuki et al. 2003; O'Hagan et al. 2005); MEC-4 is also essential for the behavioural response to gentle touch. MEC-10 plays an important role in touch transduction, but it is not essential for behavioural or calcium responses (M. Chatzigeorgiou et al. 2010). MEC-10 is not sufficient to induce mechanoreceptor currents in the absence of MEC-4 (O'Hagan et al. 2005), and is also known to function in harsh touch, in PVD and FLP, along with DEGT-1 (M Chatzigeorgiou et al. 2010). When expressed together MEC-4 and MEC-10 form a trimer (Chen et al. 2015). MEC-4 co-localises with extracellular matrix components and therefore may be anchored to it, however, the ends of the microtubules previously thought to anchor the channel intracellularly do not co-localise with MEC-4, suggesting that the complex is not anchored here (Cueva et al. 2007).

DEG/ENaCs in *C. elegans* have also been implicated in proprioception, the ability of an organism to sense its posture. Worms carrying a mutation in *unc-8* have disruptions in the normal sinusoidal crawling motion, and are expressed in some ventral cord motorneurons that control locomotion (Tavernarakis et al. 1997). The particular neurons that *unc-8* is expressed in in *C. elegans* have chemical connectivity reminiscent of motorneurons in the nematode *Ascaris suum.* In *A. suum* these specific neurons have been shown to be stretch responsive, and are therefore postulated to be involved in proprioception (Davis & Stretton 1996). Based on these similarities, it is thought that *unc-8* plays a role in a stretch receptor complex in the motorneurons in *C. elegans*. Two other DEG/ENaCs, *del-1* and *unc-1*, are almost exclusively co-expressed with *unc-8*, leading to the theory that these three DEG/ENaC subunits may also be involved in the proprioception complex (Rajaram et al. 1998; Tavernarakis et al. 1997).

The *C. elegans* DEG/ENaC genes of unknown function have been placed into sub-families based on sequence similarities to one another, and others within the larger family. These sub-groups are; ACid sensing Degenerin (*acd*), the Acid-sensing amilioride-Sensitive Ion Channels (*asic*), DEGenerin Linked to Mechanosensation (*delm*), DEGenerin Like (*del*), DEGenerin related Touch involved (*degt*), EGF plus ASC domain ion channel (*egas*) and DEGeneration of certain Neurons (*deg*) (Syntichaki & Tavernarakis 2004).

The sequences of both *acd-5* and *asic-2* suggest that the channels they form a part of are gated by protons. In mammals the ASIC genes play a role in sensing localised drops in pH, that then induce a pain response in nociceptive cells (Waldmann & Lazdunski 1998). In *C. elegans* it has yet to be proven that *asic/acd* genes are acid sensing.

3.1.2 Expression Patterns

It was found that *asic-2* is expressed in the 6 IL2 neurons only, while *acd-5* is expressed in an individual head neuron, ASI, and gut muscles (3.3.4 Expression Patterns).

3.1.3 Function of the IL2 Neurons

3.1.3.1 IL2 Anatomy

The IL2 neuron class consists of three symmetrical pairs of neurons, the dorsal, ventral and lateral pairs. All three pairs have similar structure and express many of the same genes; however the lateral IL2 pair has different neuronal connectivity and morphology in comparison to the ventral and dorsal pairs (Wang et al. 2010). The IL2s release acetylcholine and synapse onto several sensory, motor and inter-neurons (Duerr et al. 2008)(Fig.3.2A). The IL2 cell bodies are located just posterior to the

anterior pharyngeal bulb, and have axonal projections to the nose tip and around the nerve ring (Fig.3.22D). The IL2 dendrite ending is open to the outside environment, as it protrudes through the hole in the socket cell (Fig.3.22G) (Bae & Barr 2008). In *C. elegans*, neurons with external cilia are most often involved in sensing cues from the external environment. For this reason it has been postulated that the IL2s are involved in chemosensation; however, laser ablation of the IL2s does not result in any apparent defect in the worms ability to sense chemical cues (C.L. Bargmann et al. 1993).

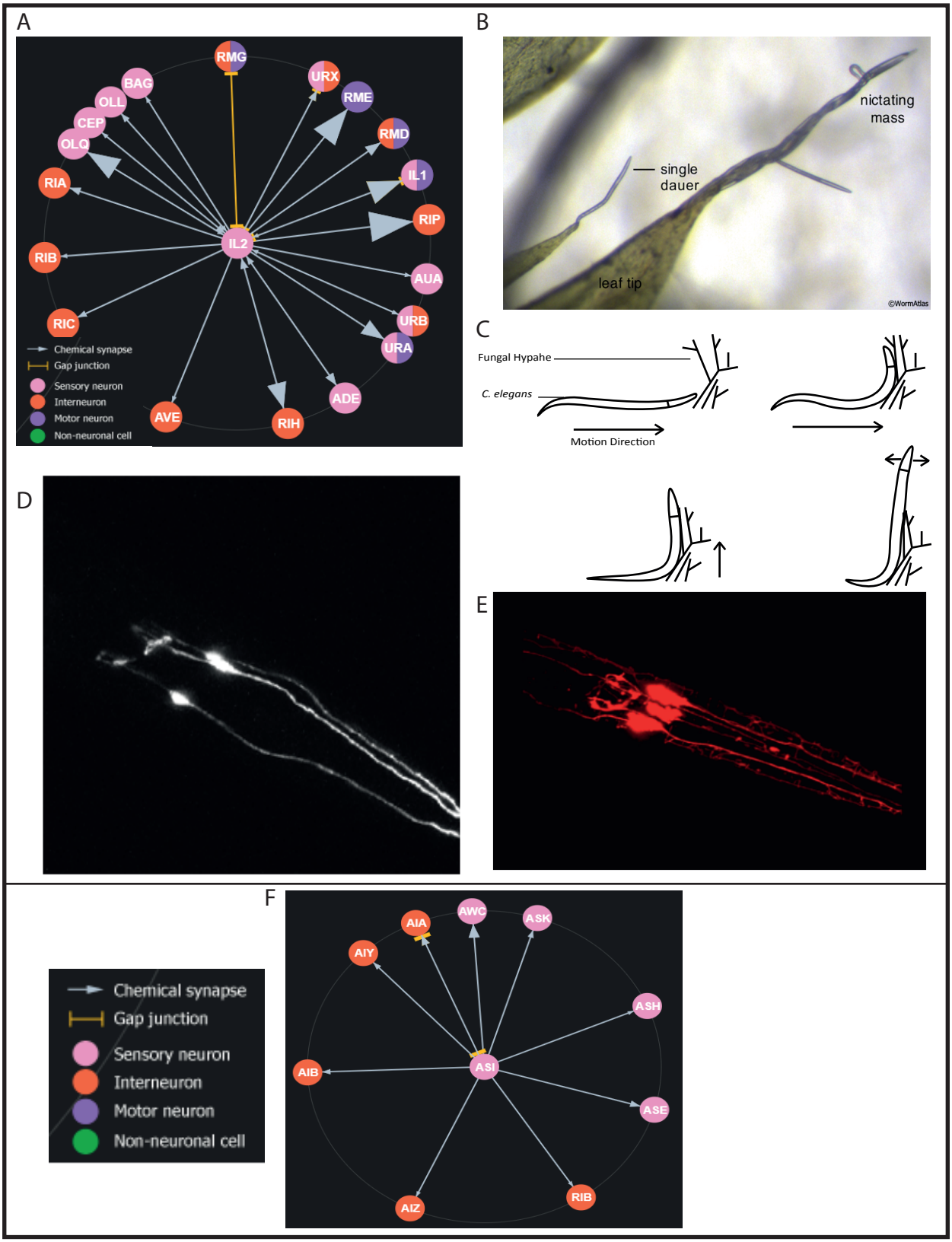

Fig.3.2: Connectivity of *asic-2* and *acd-5*
A: A diagram of the connections that the IL2s make to other neurons. Pink are sensory neurons, red inter-neurons and purple motor neurons (Wormweb). B: A photograph of *C. elegans* dauers nictating, Image source: Wolkow, C.A. and Hall, D.H. 2011. Dauer Behavior. In WormAtlas. C: A schematic of a *C.elegans* dauer nictating (Lee et at. 2015). D: The IL2 neurons in an L4 worm that has never entered dauer stage E: The IL2 neurons in a dauer worm. F: A diagram of the connections that ASI makes to other neurons, colour codes are the same as before (Wormweb).

3.1.3.2 IL2 Function in Dauer Dispersal

The IL2s play a fundamental role in dauer larvae dispersal. The dauer larval stage is induced in *C. elegans* when worms in larval stage one, L1, encounter unfavourable environmental conditions (Fig 1.1). When there is no food, poor quality food or high population density an individual will enter larval arrest in order for the worm to survive and disperse to a favourable environment. A high ambient temperature combined with these factors will increase the number of dauers produced in a population (Golden & Riddle 1982). In this way *C. elegans* can survive starvation for up to 6 months. Various specific anatomical changes occur in the worm upon entry into dauer, morphological changes include restriction of the worm's body width (Cassada & Russell 1975), pharyngeal restriction (Vowels & Thomas 1992) coupled with a lack of pharyngeal pumping (Cassada & Russell 1975) and a blocked mouth hole (Riddle et al. 1981). Many other changes occur within the worm when entering dauer arrest, including the onset of a behaviour known as nictation. This behaviour is not usually seen in *C. elegans* wild-type larvae or adults and is characterised by the lifting of the worm's head away from the surface that it is crawling on (Fig.3.2B (Lee et al. 2015) and C) (Croll & Matthews 1977). In laboratory conditions, this behaviour is usually seen on older plates with fungal contamination, where the fungal hyphae act as projections for the dauers to nictate from. Parasitic nematodes are known to exhibit this behaviour during normal larval stages, and it is thought that it enhances the parasite's infection efficiency (Gaugler & Campbell 1993). Although *C. elegans* are not parasitic, it is thought that this conserved behaviour is also used to increase dispersal, by attaching the worm to larger, more mobile creatures, such as small insects (Croll & Matthews 1977). For nictation to occur in *C. elegans* dauers, the ciliated endings of the IL2s must be functional and cholinergic transmission from the IL2s must be present (H. Lee et al. 2011). Artificial activation of the IL2s does not lead to nictation in non-dauer larvae; this may be because the anatomy of the IL2s is transformed upon entry into dauer stage, which may contribute to the activation of nictation (Albert & Riddle 1983).

3.1.3.3. IL2 Dendrite Arborisation in Dauer Worms

Upon entry into dauer stage the IL2s undergo stage-specific remodelling; in non-dauer larvae and adults the IL2s have single, unbranched primary dendrites. Upon entering dauer arrest dorsal and ventral IL2s go through dendrite arborisation, increasing dendrite length 3-fold. Axon remodelling also takes place through axons branching and thickening (Fig. 3.2D and E). The lateral IL2s also undergo the same transformations, but to a lesser extent. Once dauers are returned to favourable environmental conditions the dendrite arbours retract but leave remnant branches in post-dauer L4s and adults that are not observed in adults that have not been through dauer stage (Schroeder et al. 2013).

3.1.4 Function of the ASI Neurons

The ASI neurons appear to be involved in a number of behavioural aspects in *C. elegans.* It is thought that the ASI may work to integrate information about the worm's external environment. The ASIs are the only producers of the neurotransmitter DAF-7, a member of the TGF-β (Transforming Growth Factor-β) superfamily that has numerous effects on *C. elegans* behaviour and physiology (Ren et al. 1996; Schackwitz et al. 1996).

3.1.4.1 ASI Anatomy

acd-5 is expressed in the ASIs. The ASI neuron class constitutes one pair of neurons, ASIL and ASIR (ASI Left and ASI Right), both of which express a large number of receptors and release a large number of neurotransmitters. Just under a half of these transmitters are insulin related. Both

neurons have single ciliated endings and are un-branched. The cell bodies of the ASIs are located just anterior, and to the left/right of the terminal pharyngeal bulb, with axonal projections to the nose tip and around the nerve ring (Fig.3.24E). The ciliated endings of the ASIs are open to the external environment through the amphid sensilla (Fig.3.24F). The main synaptic outputs of the ASIs are the AIA inter-neurons, which also have electrical synapses with ASI (White & Jorgensen 2012). ASI is also pre-synaptic to a number of sensory and inter-neurons (Fig 3.2F).

3.1.4.2 ASI Function in Chemotaxis

Chemosensation is a fundamental process for many different organisms, from bacteria to vertebrates, allowing the individual to seek out food and to avoid toxins (van Haastert et al. 1982; Finger et al. 2000; Adler 1975). *C. elegans* can sense a wide range of attractive and aversive stimuli and have a much simpler nervous system in which to research these neuronal pathways. The ciliated neurons of the amphid and inner labial sensilla are the neurons responsible for the detection of the various chemicals recognised by the worm (Lewis & Hodgkin 1977; Perkins et al. 1986). The various classes of ciliated neurons in *C. elegans* are known to respond to specific chemical stimuli. For example the AWCs recognise attractive concentrations of benzaldehyde, butanone, isoamyl alcohol, 2,3-pentanedione, and 2,4,5-trimethylthiazole, AWB responds to volatile repellents, such as 2-nonanone (C I Bargmann et al. 1993), and ASH responds to the repellents copper, detergents, bitter alkaloids such as quinine and acid pH (Hilliard et al. 2004; Hilliard et al. 2002; Ward 1973). ASIs participate in chemosensation as they sense lysine and play a residual role in chemotactic response to cAMP, biotin, Cl^-, and Na^+ after ASE neurons are killed (Bargmann & Horvitz 1991). The TGF-β gene DAF-7 expressed in ASI also has an effect on chemosensation; the expression of a subset of chemoreceptor genes is regulated by the *daf-7*/ TGF-β pathway in favourable conditions (Nolan et al. 2002).

3.1.4.3 ASI Function in Locomotion

C. elegans exhibit different patterns of locomotion when on food and during various stages once removed from their food source. When crawling on a good food source worms will mostly dwell and forage, reversals are short and turns are irregular. Immediately after removal from food, worms placed on an un-seeded NGM plate will begin the 'local search' pattern of behaviour. Omega turns, coils and pirouettes are greatly increased in number, as are reversals, particularly of an extended distance, all in order for the worm to find its food source. Local search behaviour is modulated by the sensory neurons AWC, ASK and the inter-neuron AIB. AWC, an olfactory neuron, and ASK, a gustatory neuron, enhance the number of omega bends and reversals in response to the absence of food. After a period of around 10-15 minutes without food individuals cease the local search behaviour, and begin to disperse. Dispersal is characterised by long runs of forward locomotion, reversals and turns are rare. In worms with ablated ASI neurons this dispersal behaviour is inhibited and local search behaviour is prolonged (Gray et al. 2005); suggesting that ASI is involved in promoting dispersal behaviour. ASI has several synapses onto AWC, leading to the theory that ASI actively inhibits AWC after the worm has been without food for a prolonged time.

3.1.4.4. ASI Function in Temperature Sensation

C. elegans can be conditioned to associate environmental cues with the availability of food. For instance, worms grown on a good food source at 20°C will tax towards this temperature when placed on a thermal gradient. This phenomenon has been tested with worms grown at various temperatures with the same result (Hedgecock & Russell 1975). The AFD neurons are known to be the major thermosensory neuronal class in *C. elegans* (Mori & Ohshima 1995), and respond to temperatures above cultivation temperature (Tc) (Ryu et al. 2002; Kimura et al. 2004). The AWC neurons also show

responses to temperatures higher or lower than Tc, and modulate negative thermotaxis (Biron et al. 2008; Kuhara et al. 2008). The ASI neurons also play a role in thermal sensing; specifically, the ASIs are active at temperatures in a particular range. Temperatures not too far from Tc and those not too close to Tc activate the ASIs. AFD determines Tc, and regulates the bounds in which ASI is responsive to temperature (Beverly et al. 2011).

3.1.4.5 ASI Function in Dauer Formation

DAF-7 is a signalling molecule that is responsible for suppressing entry into dauer phase, in favourable environments DAF-7 is continuously released by ASI to promote sexual growth of the worm (Ren et al. 1996). Because ASI is the only producer of this molecule it is not surprising that ablation of ASI is sufficient, at 27°C, to induce dauer arrest (Ailion & Thomas 2000). At the normal growth temperature of 20-22°C ablation of both ASI and ADF is required for dauer arrest (Bargmann & Horvitz 1991).

The transmembrane guanylate cyclase DAF-11 is expressed in the cilia of ASI and ASJ neurons and is required for normal chemosensation (Birnby et al. 2000). It is also known to promote the transcription of *daf-7* and *daf-28* in response to favourable conditions (Murakami et al. n.d.). DAF-28 is an insulin-like peptide expressed in ASI and ASJ and is thought to transduce environmental signals in order to antagonise dauer formation (Li et al. 2003).

3.1.4.6. ASI Function in Pheromone Sensing

C. elegans, like many other organisms, release and sense pheromones. Dauer entry, male sexual attraction to hermaphrodites and social behaviour are all modulated by pheromones (Jeong et al. 2005; Srinivasan et al. 2008; Macosko et al. 2009). *C. elegans* pheromones are composed of derivatives of the dideoxysugar ascarylose, known as ascarosides. The ascarosides C3, C6, C7 and C9 are known components of the dauer pheromone (Butcher et al. 2007).

3.1.4.6.1 Dauer

The receptors for the ascaroside C6, and C3 are expressed in ASI. DAF-37/GPCR binds C6 in a heterodimeric complex with DAF-38, to suppress ASI activity and promote entry into dauer arrest (Park et al. 2012). SRG-36/-37 heterodimreic receptors in ASI bind the ascaroside C3 to have the same effect (McGrath et al. 2011). The ASK neurons suppress ASI in response to C6 and thus promote dauer entry (Kim et al. 2009).

3.1.4.6.2 Male Attraction

The male sexual mating behaviour elicited by the hermaphrodite pheromone is genetically present in both males and hermaphrodites but this behaviour is suppressed in hermaphrodites by ASI activity, specifically the release of TGF-β represses male mating behaviour. ASI ablation during development (before L4 stage) is sufficient to induce male mating behaviour in hermaphrodites, but this can be rescued by expression of DAF-7/TGF-β in the AWC and ASE, indicating that the ASIs main role in suppressing sexual attraction is the release of DAF-7. For male mating behaviour to be suppressed in *C. elegans*, ASI neurons must be present during development, active and capable of detecting the external environmental cues (White & Jorgensen 2012).

3.1.4.7 ASI Function in Response to Pathogens

In *C. elegans,* upon infection with a pathogen, the unfolded protein response (UPR) or ER stress response is triggered. The neuron classes ASH, ASI, AQR, PQR and URX control UPR in the worm. In ASI this control is asserted through the protein OCTR-1 (octopamine G protein-coupled

catecholamine receptor -1). The *octr-1* gene is expressed in ASI and ASH, and actively suppresses innate immune responses in *C. elegans* by down-regulating the expression of the genes *pqn/abu* (prion-like glutamine[Q]/asparagine[N]-rich domain-bearing protein/ activated in blocked unfolded protein response) in non-neuronal tissues. *pqn/abu* are non-canonical components of the unfolded protein response (Sun et al. 2011).

The p38 mitogen-activated protein kinase (p38-MAPK) signalling pathway, conserved from nematodes to humans, is also required for innate immunity; it has been shown that this pathway is under the control of OCTR-1, and therefore ASI and ASH (Sun et al. 2012).

3.1.4.8 ASI Function in Lifespan

ASI and ASG neuron classes shorten lifespan by suppressing ASJs and ASKs, and ablation of the ASIs increases *C. elegans* lifespan. Most likely the ASIs impact lifespan by modulating the DAF-2 pathway (Alcedo & Kenyon 2004). In the wild-type worm, DAF-2 is involved in a number of functions including adult longevity and stress resistance. In favourable living conditions the transcription factor DAF-16 is phophorylated by DAF-2, rendering it inactive (Lin et al. 2001). In its non-phosphorylated state, DAF-16 promotes the transcription of around 100 genes that protect the worm's cells from stressors, such as heat shock or oxidative stress (Murphy et al. 2003). *daf-2* mutants display higher expression of *daf-16* and have an extended lifespan; conversely, *daf-16* mutants have a shortened lifespan (Lin et al. 2001). In parallel to this pathway is the p38 MAPK pathway, which also plays a role in regulating the oxidative stress response. The gene *skn-1* is a bZIP transcription factor in this pathway and is phosphorylated by the AKT-1, AKT-2 and SGK-1 kinases, which are downstream of *daf-2* in the insulin signalling pathway (Tullet et al. 2008; Bowerman et al. 1992); expression of the *skn-1* gene is enhanced in *daf-2* mutants (Tullet et al. 2008). In *skn-1* mutants, the p38 MAPK pathway is disrupted and individuals are susceptible to oxidative stress, resulting in a shortened lifespan. In L4 and adult *C. elegan,s skn-1* is expressed in the ASI pair and intestinal cells (An & Blackwell 2003).

3.1.4.9 ASI Function in Satiety Quiescence

Like many organisms, *C. elegans* enters a quiescent state after eating a surfeit of food. Quiescence is a locomotory state defined by a lack of movement and a lack of eating, measured by a lack of pharyngeal pumping (You et al. 2008). Two other locomotory states are ppresent in the worm, roaming and dwelling. Roaming occurs when the worm is searching for food, and dwelling occurs when the worm is on food but still moving and eating (You et al. 2008; Fujiwara et al. 2002a). ASI promotes satiety quiescence by actively inhibiting the switch from quiescence to dwelling, and promoting the switch from dwelling to quiescent (Gallagher et al. 2013). ASI is activated by nutrition, and in favourable conditions releases TGF-β; TGF-β is at its highest level when worms show the most consistent quiescence. The satiety quiescence defect of cGMP pathway mutants is rescued by restoring cGMP signalling in ASI, indicating that both TGF-β and cGMP signalling in ASI are responsible for entry and sustainability of satiety quiescence in *C. elegans* (Gallagher et al. 2013).

3.1.5 Genetic Screens

A number of reverse genetics screens have been performed on various *C. elegans* genes, some of these experiments have elucidated some potential roles for *asic-2* and *acd-5*.

***asic-2*:**

Genes found to be regulated in *daf-16(mgDf50)* by reservatrol treatment with $p<0.01$ (Viswanathan et al. 2005).

DAF-16 binding DNA target identified by chromatin profiling by adenine methyltransferase identification (DamID) (Schuster et al. 2010).

Increase in expression after incubation with *E. faecalis*, or *P. luminescens*. Decrease in expression after incubation with *S. marcescens* or *D. conios* (Engelmann et al. 2011).

Potential DAF-12 target identified by ChIP-chip analysis performed on strain ALF4 (Hochbaum et al. 2011).

Genes with significantly increased expression in N2 animals after 4 hours of starvation (Mueller et al. 2014).

Transcripts that showed significantly altered expression with 500mM salt (NaCl) vs 100 mM salt when food was present (Burton et al. 2017).

Expression climbs from embryo stage to L1, after which it steadily reduces until adulthood (WormBase).

acd-5:

Increase in expression on incubation with *E. faecalis*, *P. luminescens*, *S. marcescens* and *B. pseudomallei*. Decrease in expression on incubation with *B. thuringiensis* (Engelmann et al. 2011).

Upregulated during L4 lethargus (George-Raizen et al. 2014).

Genes regulated by DAF-16, according to whole transcriptome profiling to compare genome-wide regulatory influences of DPY-21 and SET-4 to those of key transcription factors controlling dauer arrest in *eak-7;akt-1* animals (Delaney et al. 2017).

Genes that were repressed by a glucose rich diet (2%) in an SBP-1/MDT-15 dependent manner (Lee et al. 2015).

Expression levels are highest in dauer worms, and lowest in the embryo. From hatching to adulthood the gene is expressed at a steady rate (WormBase).

These results suggest that both DEG/ENaC mutants are regulated by *daf-16*, suggesting a possible role in the stress pathway. This is supported by the finding that *asic-2* is a potential *daf-12* target as *daf-12* is known to affect gonad –dependent adult longevity along with *daf-16*.

Both genes show altered expression with changes in nutrition availability, starvation and increased levels of salt influence the expression of *asic-2* and high glucose concentration reduces the expression of *acd-5*. Expression is also altered on incubation with pathogens. These environments are all stressful for the worm, again suggesting a possible role for both genes in stress response.

3.2 Materials and Methods

Mutant strains used in these experiments were obtained frozen from CGC at the commencement of this section of work. These were RB557-*asic-2 (ok289)I*, and RB2005-*acd-5 (ok2657)I*.

3.2.1 Confocal Microscopy

Worms were either picked as L4s the day before experimentation, or, in the case of dye filled worms, used directly after the dye filling protocol was finished. Day 1 adult worms were picked onto a flattened agarose pad (2% agarose in M9) on a microscope slide. In order to paralyse the worm, 7µl 75mM sodium azide was added over the worm, followed by a cover-slip. The cover-slip is then held in place by painting clear nail varnish around its entire edge. Once dry the worm was imaged.

All confocal data was acquired on a Zeiss 780 confocal microscope using a 60x objective with oil immersion. Image processing was performed with Zen software (Zeiss).

3.2.2 Dye Filling

DiO fluorescent dye (Molecular probes, D-275) stock solution, 2mg/ml in dimethyl formamide was diluted 1:200 in M9. An aliquot of 150µl of working solution was added to a 1.5ml eppendorf tube, and to this ten individual day 1 adult *Pacd-5::SL2-tagRFP*::*UTR* worms were added. The worms were incubated for 3 hours at room temperature, in the dark. After this time period the worms were centrifuged for 1min in a set speed MINI microfuge, and the loose worm pellet was pipetted onto a fresh, seeded 6cm NGM plate. Dyed worms were allowed to crawl on the plate for 3 hours to remove excess DiO.

Individuals were then mounted as previously described for confocal microscopy.

3.2.3 Reporter Constructs

Reporter constructs were produced for each of the mutants to be tested. A region of 2kb upstream of the desired gene was amplified from genomic DNA using Q5 PCR mix with primers including the attb sites for position 1 of gateway (Table A6, Appendix). Promoter sequences were gel extracted and cloned into pDONR P4-P1r, transformed using Ecloni® Chemically Competent Cells and Kanamycin selection. Plasmid extraction was achieved using a Quiagen® QiaQUICK mini-prep kit.

Gateway was used to produce the constructs *Pasic-2::GFP-stop::*UTR, *Pasic-2::mcherry-stop*::UTR, *Pacd-5::GFP-stop*::UTR and *Pacd-5::mcherry-stop*::UTR.

All reporter constructs were injected at 50ng/µl along with 50ng/µl *Punc-122::GFP,* 0.4µl 500ng/µl 1kb ladder and made up to 4µl with water. (A full list of primers, plasmids and strains can be found in Tables A6, A8 and A9 respectively, Appendix)

3.2.4 Rescue Constructs

cDNA for the gene of interest was amplified by RT-PCR using superscript® III RT-PCR system with platinum® *Taq* DNA polymerase. Primers for these reactions can be found in appendix A6.

Genomic DNA gene fragments were produced using Q5® PCR enzyme. Both forms of the gene were amplified for cloning into pDONR221 for MultiSite Gateway® Three-Fragment Vector Construction Kit (Invitrogen).

Promoter plasmids used in the reporter constructs were used to drive expression of their corresponding gene, each with a *tag-RFP* expressed in the third position of gateway (a list of rescue constructs can be found in Table A8, Appendix). Rescue plasmids were then injected into the

corresponding mutant strain at 50ng/µl, + 50ng/µl *Punc-122::GFP*, 50ng/µl 1kb ladder and made up to 4µl with water.

Once it had been elucidated which cells the reporters were expressing in, cell specific promoters were used to direct expression of the plasmids in those cells. For verification of *asic-2* expression in the IL2s, GFP expression was driven by the IL2 specific kinesin gene promoter *Pklp-6* (Peden & Barr 2005) to make *Pklp-6::GFP-stop*::UTR. For *Pklp-6,* a region of 2kb upstream of the gene was amplified and cloned as previously described for reporter. For *acd-5,* the cell specific promoter *Pdaf-7* (Schackwitz et al. 1996) was used for rescue of *acd-5* in ASI. *Pdaf-7* first position plasmid was created using Q5 PCR of *Pdaf-7::GCaMP3* (provided by the Lockery Lab) and cloning of the product into pDONR P4-P1r. To identify any connection between these two genes *asic-2* was also expressed under *Pdaf-7* and *acd-5* under *Pklp-6*. This was to determine whether the rescue of the gene in either of these cells caused a difference in the worms' phenotype, suggesting a functional overlap.

See Table A8 (Appendix) for a full list of rescue constructs.

3.2.5 Chemotaxis Experiments

3.2.5.1 Salt

Nine cm quadrant plates containing 7ml 100µM NaCl in CTX agar in opposite quadrants, and 7ml CTX agar containing no NaCl in the other quadrants were poured 2 days prior to experimentation (see Fig 3.3A). The following day a thin layer of CTX agar was poured over the top of the quadrants to create a flat connecting surface. These were left to dry for a second night while the salt diffuses into the CTX agar layer.

Around 100 L4 animals of each genotype were picked to a fresh 6cm, seeded plate and left overnight.

Young adult worms were washed off of the 6cm plate using 1.5ml of S-Basal (Appendix, Recipes, S-Basal) in a 2ml eppendorf tube and centrifuged in a set speed MINI microfuge. Excess S-Basal was pipetted off and 1ml of fresh S-Basal was added. Washing was repeated 3 times, after the final wash worms were pelleted and excess supernatant pipetted off.

Ten µl of the worm pellet were then pipetted onto the middle of the 9cm quadrant plates. After 15 minutes the number of worms within each quadrant was counted. A chemotaxis index can then be calculated using the following calculation:

$$CI = \frac{\text{Total number worms in test quadrants} - \text{Total number of worms in control quadrants}}{\text{Total number of worms on plate}}$$

Statistical analysis was conducted using a two-way ANOVA and Dunnet's multiple comparisons test.

3.2.5.2 Odorants

Nine cm plates containing 30ml CTX agar were dried for 2 days at room temperature.

On the day of testing, plates were prepared as described by Margie et al 2013 (Margie et al. 2013). Briefly, the plate was divided into quadrants, opposite quadrants contained either the odorant spot or control spot, both equidistant from the centre. At the centre a 1 cm diameter circle marked the origin, where worms were placed Fig.3.3B.

Approximately 200 worms were picked as L4s onto a 6cm, OP50 seeded plate the day before experimentation. On the day of experiment young adult worms were washed from the plates as described for salt chemotaxis and 10µl of worm pellet was pipetted into the centre of the origin circle.

Immediately after this 2µl the odorant was pipetted at the test spots, and ethanol at the controls. 2µl 0.5M sodium azide was then added to all four spots. The worms were allowed to chemotax for 60 minutes, from the time that the S-basal dried, at room temperature on the bench.

At this point the number of worms in the control quadrant, test quadrant and origin were counted. The chemotaxis index (CI) is calculated with the following calculation.

$$CI = \frac{\text{Total number worms in test quadrants} - \text{Total number of worms in control quadrants}}{\text{Total number of worms on plate}}$$

Concentrations of odorant for repellent and attractant responses were as follows:

Benzaldehyde and diacetyl, 2 µl 1% in ethanol for attractant, 2µl 100% for repellent.

Isoamyl alcohol, 2 µl 1% in ethanol attractant, 5 µl 100% repellent.

1-Octonol 2 µl 100% repellent.

Control spots were matched for the quantity of ethanol at test spots.

Statistical analysis was conducted using a two-way ANOVA and Dunnet's multiple comparisons test, with N2 as the control on GraphPad Prism 7.02.

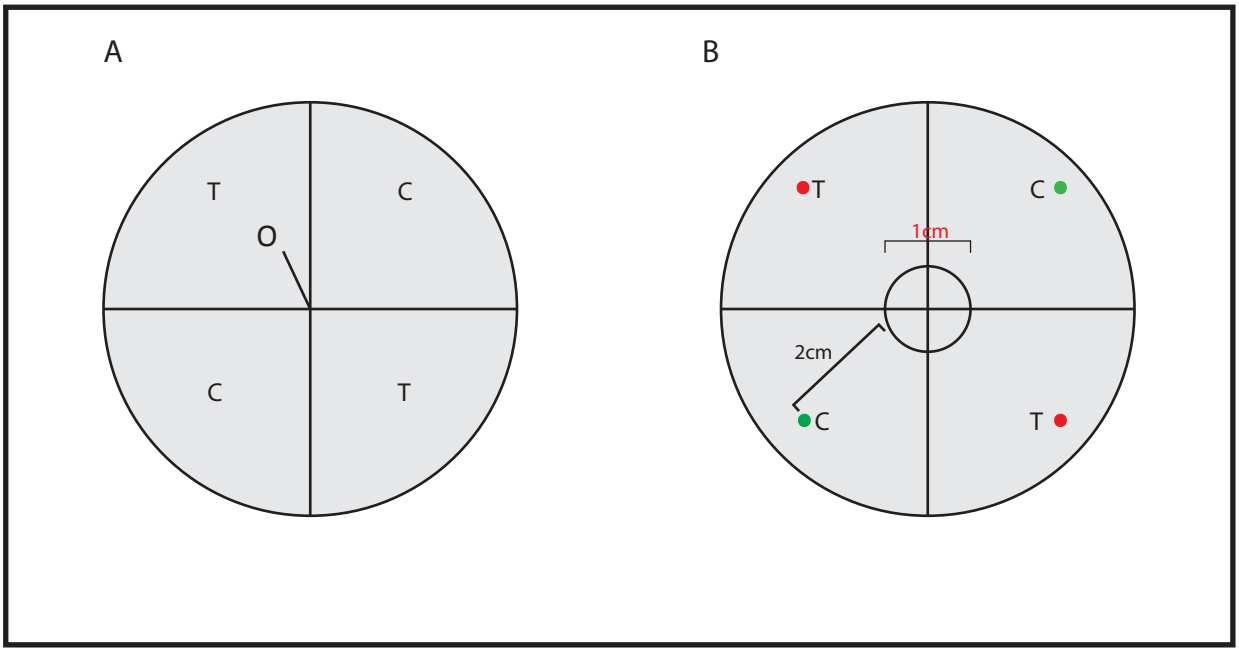

Fig. 3.3: Quadrant Set Up Of Chemotaxis Plates
A: A 9cm quadrant plate. Quadrants labelled C (control) contain CTX agar, quadrants labelled T (test) contain 100mM NaCl2 in CTX agar. Worms are placed at the centre labelled O. B: A 9cm CTX plate, red spots labelled T indicate where test solutions were place, green dots labelled C indicate where control solutions were placed. The circle at the center was the area considered the origin, and worms were placed at the centre of this circle. Unlike plates in figure A, quadrants on plates in figure B were not physically divided by plastic walls, and all agar was the same across the plate. Quadrant divisions were marked on the bottom of the plate, as was the circle of origin.

3.2.5.3. Calcium Imaging

Worms were picked as L4 larvae to 6cm seeded plates 16-20 hours before experimentation.

A 2% solution of Hi-Pure™ low EEO agarose in M9 buffer (Appendix, Recipes, M9) was made and around 50µl was pipetted onto a microscope slide. A cover slip was then placed on top of the agarose droplet in order to make a pad. Once set, the cover slip was removed and the pad was allowed to dry for around 15 minutes

Approximately 10 minutes prior to experimentation, the worms were transferred onto 6cm un-seeded plates, and allowed to crawl for 5 minutes to remove excess food. The worm was then picked from this plate and placed onto the agarose pad.

A small ice bath was made in the lid of a petri dish and the slide was placed over this. When cooled the worms become immobile and could be glued, as straight as possible, onto the pad. Glue was applied down the right had side of the worm from nose to tail tip. Care was taken to not glue over the mouth, as this can result in poor responses or the death of the worm. Dermabond® topical skin adhesive was used for gluing.

On the day of experimentation, solutions were made consisting of 1% benzaldehyde in CTX buffer (Appendix, Recipes, CTX buffer), 1% Diacetyl in CTX buffer and 1:25 OP50 over night culture:CTX buffer. CTX buffer containing no stimulant was persistently perfused over the worms throughout experimentation. During recording CTX buffer was perfused over the worm for 10 seconds, then perfusion was switched to the stimulant for 20 seconds, after which it was switched back to CTX. Recordings lasted 50 seconds in total.

All perfusions were performed using gravity fed perfusion with the excess solutions were aspirated with a vacuum pump set at >5 (units).

3.2.6 Dauer Experiments

3.2.6.1 IL2 Dauer Fluorescence

Six L4 worms were picked to a fresh, seeded 6cm NGM plate and allowed to starve for 2 weeks. Dauer worms expressing *Pklp-6::Mcherry-stop::unc-54 5'UTR* were then prepared for confocal imaging.

3.2.6.2 Dauer Assay

Ascarosides C3, C6 and C9 were obtained from the Butcher lab at the University of Florida.

Crude dauer pheromone was produced following the method described by Zhang et al. 2013 (Zhang et al. 2013).

Dauer assays were performed following the method developed by the Butcher lab (Appendix) using synthetically produced ascarosides.

3.2.7 Tracking

Single worm tracking was carried out as described in the previous chapter for each mutant, N2 and rescue. The data was also analysed as described in the previous chapter.

Multi-worm tracking was carried out using an in house developed system. A Dinolite AM413T microscope camera was mounted on a clamp stand 15 cm above a 6 cm plate-holding hoop. The LED

lights on the Dinolite camera were switched off for recording. Illumination comes from below in the form of a Heathrow Scientific light box.

The Dinolite video recording software is used for the video recording interface, with exposure set at 29.

Multi-worm videos were analysed using the Goodman lab multi-worm analysis MATLAB script (Ramot et al. 2008).

3.2.8 Speed On and Off Food

The day prior to experimentation ~200 L4 worms were picked to a seeded 6cm plate. On the same day a 6cm low peptone NGM plate was seeded with 200 µl of OP50.

The following day the worms were washed from the plates using 1ml S-Basal and washed as described for salt chemotaxis assays. Washed worms were placed onto an un-seeded 6cm low peptone NGM plate and allowed to acclimatise for 30 minutes. After this time the speed of the worms was measured using the multi-worm tracker. After recording the worms were washed from the plate in the same manner as previously described. The worms were then pipetted onto one of the plates seeded the previous day, allowed to rest for 30 minutes, then recorded on the multi-worm tracker.

Statistical significance was determined using an unpaired t-test on GraphPad Prism 7.02.

3.2.9 Egg Laying Off Food

Twenty L4 worms were picked to a fresh, seeded, 6cm NGM plate the day before experimentation. The following day all worms were picked to un-seeded plates and allowed to crawl for 10 minutes to remove food. Following this, ten worms were picked to individual, un-seeded, 3cm NGM plates and 10 worms were picked to individual, seeded, 3 cm NGM plates. All plates were left for 6 hours and the number of eggs laid on each plate was counted.

Statistical analysis was performed using one-way ANOVA with Sidak correction of multiple comparisons on GraphPad Prism 7.02.

3.2.10 Lifespan Experiments

3.2.10.1 Rate of Death

C. elegans strains were cultivated for 3 generations in well fed conditions and 20 L4s were picked from the final generation to a 6 cm plate seeded with a thick lawn of OP50. Worms were then moved to a new plate daily and the number of deceased worms was noted on each day. Worms that had crawled up the sides of plates and subsequently desiccated were not included in the data.

The rate of death was calculated using Kaplan-Meier survival analysis on GraphPad Prism 7.02. Statistical significance was determined using both the log-rank (Mantel-Cox) test and Gehan-Breslow-Wilcoxon test.

3.2.10.2 Locomotion Speed over Lifespan

On each day, 1 hour after worms were moved to new plates, the speed of individuals was measured using the multi-worm tracker. The average speed for each genotype on each day was plotted and a best-fit, straight line, non-linear regression was calculated in prism for each genotype. The slope for

each mutant regression was compared to that of N2 and significance was calculated using the Extra sum-of-squares F test.

3.2.10.3 Pharyngeal Pumping Rate

Following speed measurements, the number of pharyngeal pumps in 6 randomly chosen individuals of each strain was counted over 10 seconds, on food, and then multiplied by 6 to equate the number of pumps per minute. The average pharyngeal pumping rate for each genotype on each day was plotted and a best-fit, straight line, non-linear regression was calculated in prism for each genotype. The slope for each mutant regression was compared to that of N2 and significance was calculated using the Extra sum-of-squares F test.

3.2.11 CRISPR Protocol

sgRNAs were designed for both genes (*asic-2* and *acd-5)* using the Meyer lab protocol (B. Farboud & B, Meyer 2015). sgRNAs were then ligated into EcoRI-digested Prpr-1 expression vector using a Gibson Assembly® Master Mix (NEB) to make guide vectors. Positive clones were selected for on ampicillin plates.

An injection mix consisting of 30ng/µl of Cas9 plasmid, 100ng/µl of guide vector and 50ng/µl of unc-122::GFP was made and injected into day 1 adults. F1 animals from injected worms were selfed at L4 and were lysed as day 2 adults. A region around the CRISPR site was amplified from worm lysate using KOD polymerase. The PCR product was purified using a PCR Purification kit (Invitrogen) and sent for sequencing by Eurofins. Worms containing an edit were identified by a disruption to sequencing around the PAM site. At this stage all worms with an edit are heterozygous WT/CRISPR edit. L4 worms from plates where the parent had a suspected edit were selfed (16 individuals from each plate), lysed, PCRed and sequenced as before. Homozygotes were identified by clean sequences prior to and immediately after the PAM site. Plates from homozygous adults were kept and were considered as a new mutant strain.

3.2.12 RNAi Constructs

A short region (200bp) of coding DNA for the genes *asic-2* and *acd-5* was amplified in the 3'-5' direction using PCR with taq polymerase. The same short sequence was amplified in the 5'-3' direction (for primers see Appendix table A6). Each of these PCR products was cloned into position 2 of Gateway. Constructs were made, using Gateway, that expressed the sequences under the gene's own promoter and the cell specific promoter appropriate to the gene (*Pacd-5* and *Pdaf-7* for *acd-5* and *Pasic-2* and *Pklp-6* for *asic-2)* with SL2-tagRFP in the third position (see table A8 for a list of constructs). Constructs were then injected, in pairs, into day 1 adult N2s. The pairings were as follows: *Pacd-5::acd-5forward::SL2-tagRFP* and *Pacd-5::acd-5reverse::SL2-tagRFP*, *Pdaf-7::acd-5forward::SL2-tagRFP* and *Pdaf-7::acd-5reverse::SL2-tagRFP, Pasic-2::asic-2forward::SL2-tagRFP* and *Pasic-2::asic-2reverse::SL2-tagRFP* and *Pklp-6::asic-2forward::SL2-tagRFP* and *Pklp-6::asic-2reverse::SL2-tagRFP.*

3.3 Results

3.3.1 Tracking Results For *acd-5 (ok2657)I* and *asic-2 (ok289)I* Are Reproducible

The tracking experiments were reproduced using freshly ordered mutants, *asic-2 (ok289)* and *acd-5 (ok2657)I* from CGC, and were assayed and analysed as previously described (2.2. Tracking Materials and Methods).

3.3.1.1 *asic-2*

Repeat experiments with *asic-2 (ok289)I* animals gave many of the same significant features as previously described. A dorsal bend bias upon entering omega turns was still significant, and upon re-experimentation there was a more pronounced dorsal bend bias upon entering upsilon turns. Mid-body bends were still more dorsally biased whereas other bends, head, neck, hips and tail remained comparable to wild type (Fig.3.8). Foraging amplitude was still the same for all directions of locomotion, unlike wild type, where the amplitude differs for the forwards, paused and reverse locomotion. In this set of experiments the length of time that animals spent in a coiled posture was not longer than expected, but rather, comparable to wild-type.

3.3.1.2 *acd-5*

The newly tracked *acd-5 (ok2657)I* mutants exhibited the same dorsal bend bias upon turning as described in the previous chapter. Upon re-tracking this mutant, the dorsal bend bias in head, neck mid-body, hips and tail were more pronounced during crawling (Fig.3.4 and 3.5) as well as upon entering omega and upsilon bends (Fig.3.6 A and B).

Many of the other existing significant features were more pronounced upon re-tracking. Time spent in a paused or backward motion was still increased in comparison to wild type, but with a larger effect size. Time spent travelling in a forward direction and total path range also became significantly reduced and time spent dwelling in the mutant was significantly increased in comparison to wild type. The speed of the mutant was still reduced and foraging amplitude remained the same in all directions of locomotion (Fig.3.7). The number of coils was still increased in comparison to wild type and the number of omegas reduced.

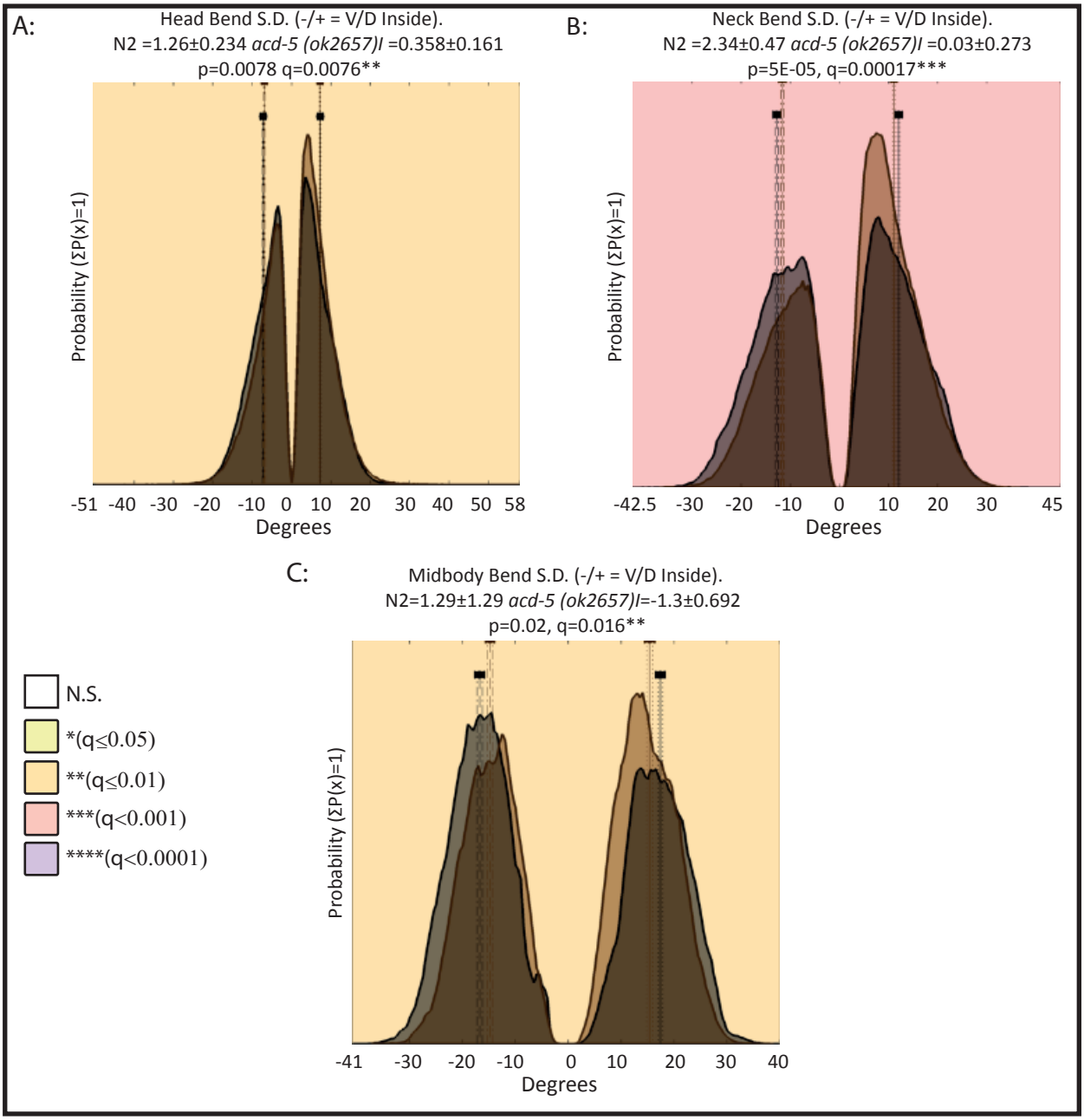

Fig.3.4: Body Bend S.D. For *acd-5 (ok2657)I.*

Graphs A-C show the the body bend standard deviations for 27 individuals of the *acd-5 (ok2657)I* mutant allele strain. The colour of the graph background represents the significance of the mutant result when compared to N2 individuals tracked on the same day. A white background denotes no siginificance, and shades pale yellow to purple display increasing levels of significance (as shown in the key). The grey shaded area of the graph shows the results for N2. The overlayed, brown shaded area shows the result for *acd-5 (ok2657)I*. Positive results display the degree of bending in the dorsal direction, while negative results display the degree of bending in the ventral direction.

A: Head bend S.D. for *acd-5 (ok2657)I.* B: Neck bend S.D for *acd-5 (ok2657)I*. C: Midbody bend S.D for *acd-5 (ok2657)I*

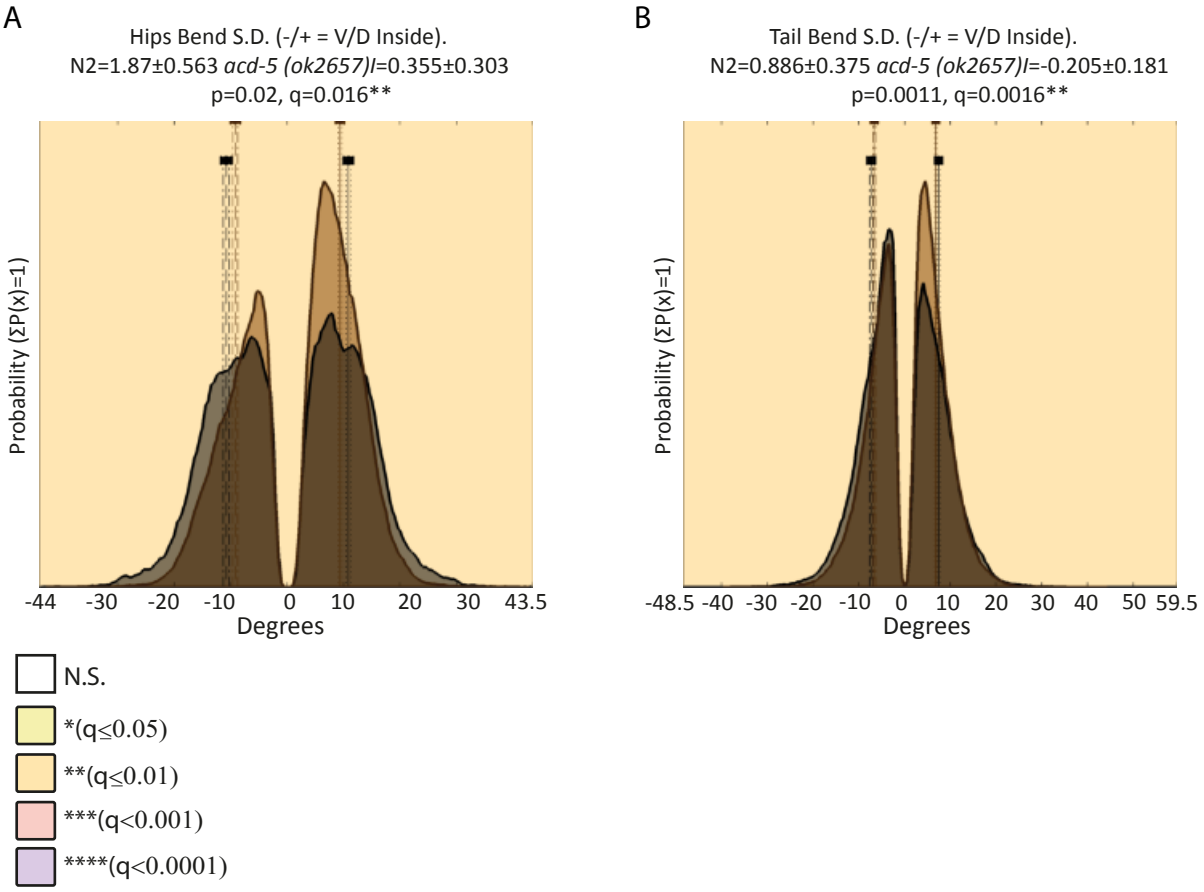

Fig.3.5: Body Bend S.D. For *acd-5 (ok2657)I.*
Graphs A-B show the the body bend standard deviations for 27 individuals of the *acd-5 (ok2657)I* mutant allele strain. The colour of the graph background represents the significance of the mutant result when compared to N2 individuals tracked on the same day. A white background denotes no siginificance, and shades pale yellow to purple display increasing levels of significance (as shown in the key). The grey shaded area of the graph shows the results for N2. The overlayed, brown shaded area shows the result for *acd-5 (ok2657)I*. Positive results display the degree of bending in the dorsal direction, while negative results display the degree of bending in the ventral direction.
A: Hips bend S.D. for *acd-5 (ok2657)I.* B: Tail bend S.D for *acd-5 (ok2657)I*.

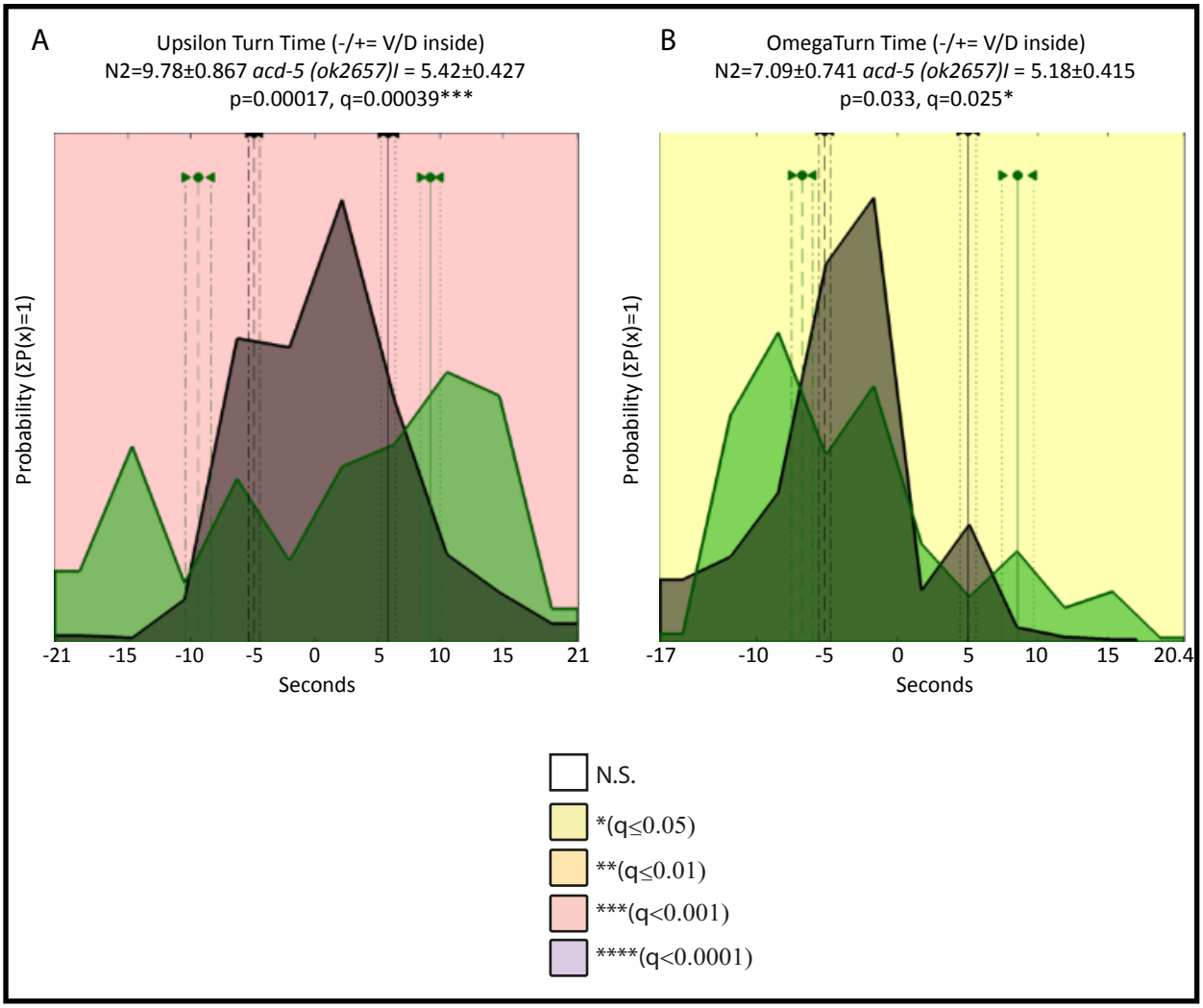

Fig.3.6: Upsilon and Omega Turns In *acd-5 (ok2657)I* Repeat Tracking Experiments.
A: The Upsilon turn time of *acd-5 (ok2657)I*. Background colours represent degrees of significance. Grey shading shows the results for N2 and green shading shows the results for *acd-5 (ok2657)I.* Positive results denote bends made dorsally and negative results denote bends made ventrally.
B: The omega turn time of *acd-5 (ok2657)I*. Graph parameters are the same as for upsilon turn time. The key shows the colouration of the degrees of significance.

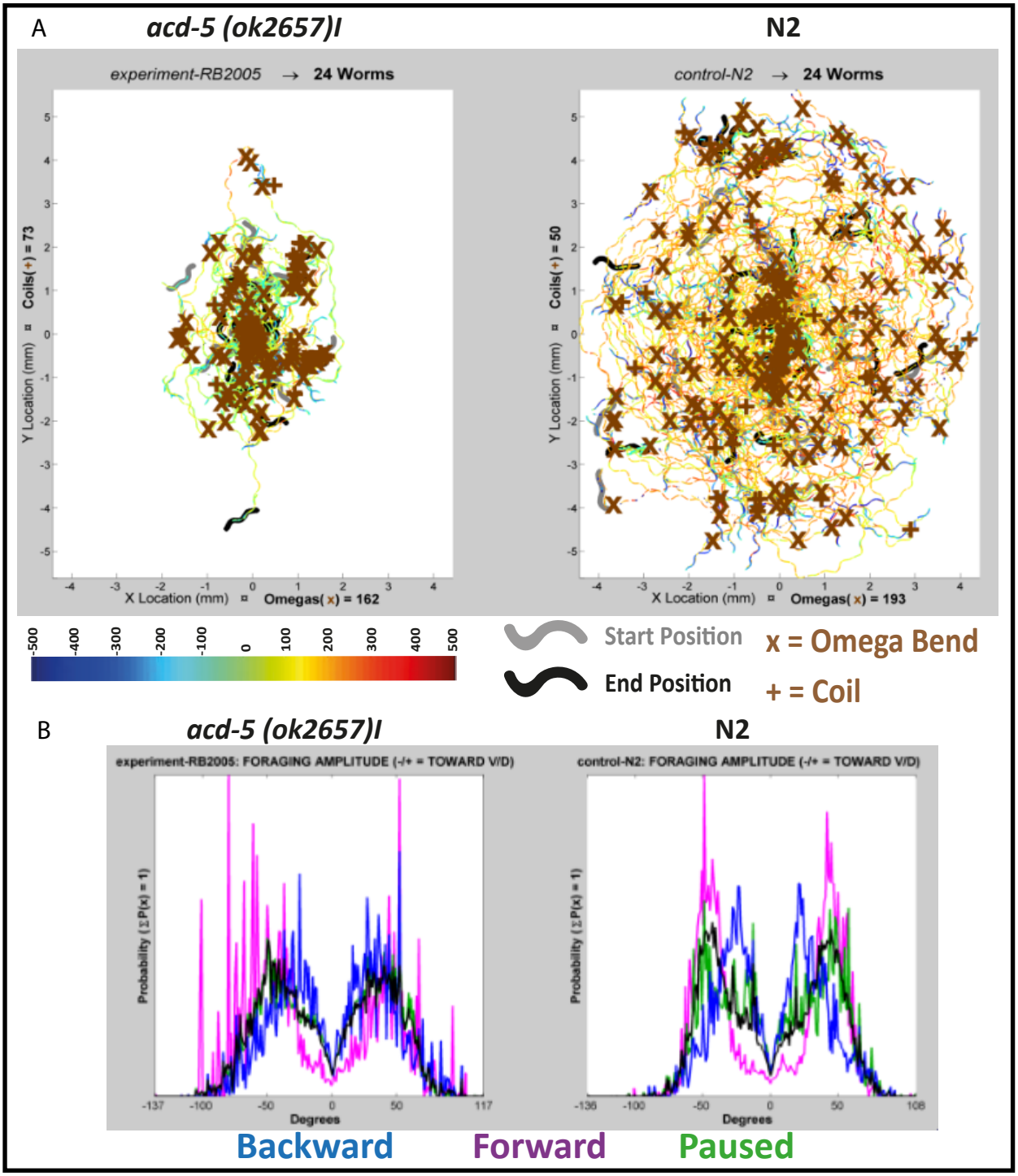

Fig: 3.7: The Speed and Foraging Amplitue Of *acd-5 (ok2657)I* Repeat Tracking.
A:The speed of individual worms over the time course of recording, recordings are overlayed, the image on the left is *acd-5 (ok2567)I* and right the N2 controls. Brown +, x grey worm shapes show where the worm was positioned at the beginning of recording, black worm shapes show the position of the worm at the end of recording. The colour of the tracks, from blue to red, indicates the speed of the worm at that position. Green is non-moving, yellow-red is slow to fast forward locomotion, pale-dark blue is slow to fast reverse locomotion. B: The foraging amplitude of *acd-5 (ok2657)I* mutants in compariosn to N2. Backward foraging amplitude is shown in blue, forward in purple and paused in green. The foraging amplitude in the mutant is more pronounced during forward locomotion and less pronounced during reverse locomotion and whilst paused. This results in similar foraging amplitudes for all locomotory states.

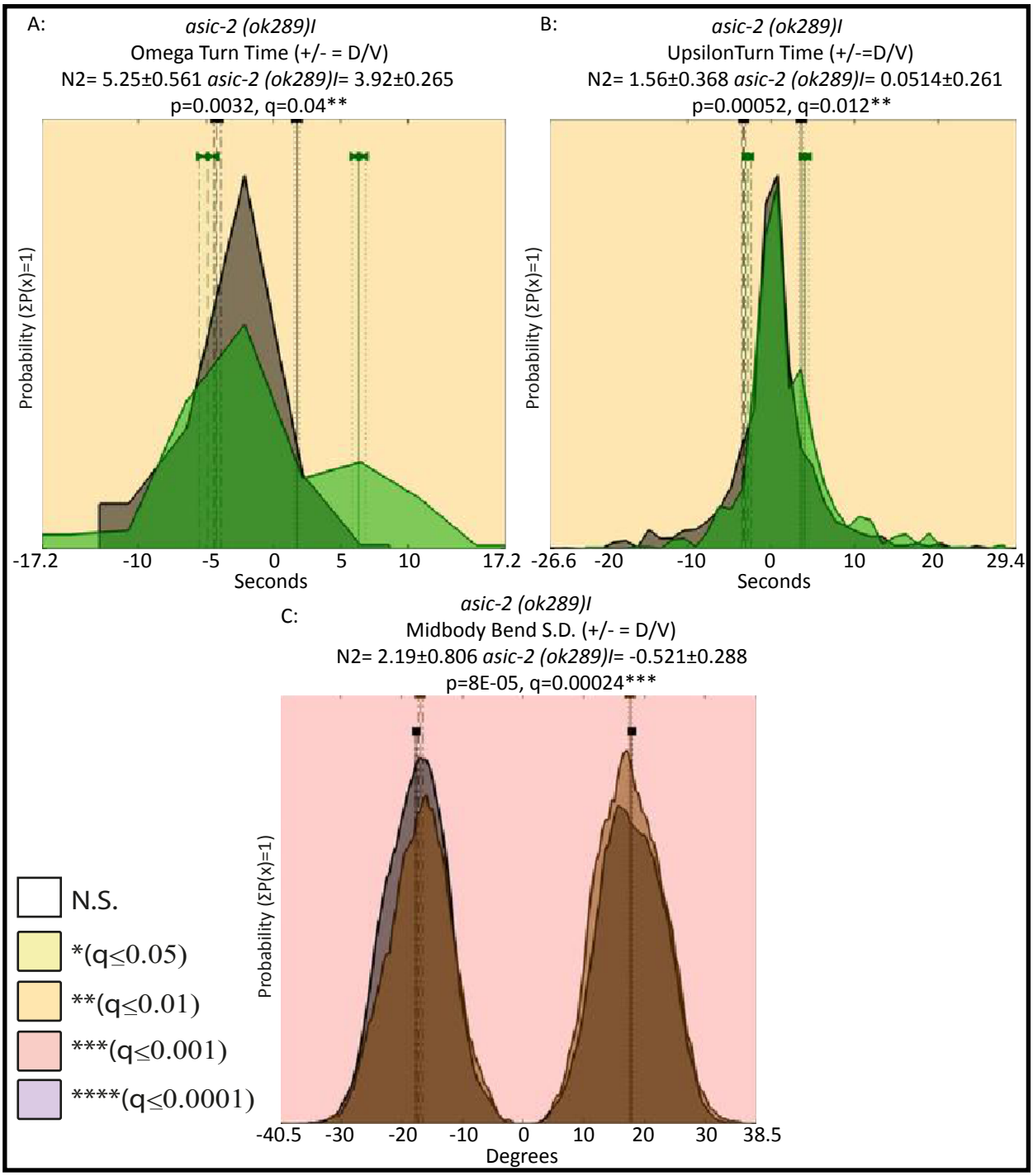

Fig.3.8: The Omega and Upsilon Turn Time and Midbody Bend S.D. of the *asic-2 (ok289)I* Mutant Allele Strain.

Graphs show the time mutant worms spent in omega and upsilon bends during recording. Results for 20 individuals of the *asic-2 (ok289)I* mutant allele strain are shown. The colour of the graph background represents the significance of the mutant result when compared to N2 individuals tracked on the same day. A white background denotes no siginificance, and shades pale yellow to purple display increasing levels of significance (as shown in the key). The grey shaded area of the graph shows the results for N2. The overlayed, brown or green shaded area shows the result for the mutants. Positive results display the time spent by each strain in turns performed in the dorsal direction, while negative results display the time spent by each strain in turns performed in the ventral direction.

A: The omega turn time of *asic-2 (ok289)I* B: The upsilon turn time of *asic-2 (ok289)I* C: The midbody bend S.D. for *asic-2 (ok289)I*

3.3.2 Tracking Mutant Rescue Lines

Rescue lines were created for both *asic-2 (ok289)I* and *acd-5 (ok2657)I*, by expressing the cDNA of the gene under its own promoter and under a promoter specific for the cell in which the gene is expressed (3.3.4 Reporter Constructs).

For both genes, only a small number of features identified as significantly different in the mutant in comparison to N2 were rescued by expression of the rescue constructs. In both mutants, the features that were rescued were involved in head and neck bending. Table 3.1 lists the features that are rescued in the mutant background lines of *asic-2 (ok289)I* and *acd-5 (ok2657)I* by exogenous expression of the gene cDNA under their own promoters and promoters that are cell specific to the IL2 (*for asic-2)* and ASI (*for acd-5*). Only a fraction of the features that are significantly different from wild type in the CGC mutants are rescued. In *acd-5 (ok2657)I* 334 features were significantly different in comparison to wild type. In the rescue under *Pacd-5* 254 features were still significantly different in comparison to wild type. These numbers were similar for the rescue under *Pdaf-7*. Likewise, *asic-2 (ok289)I* had 115 significant features in comparison to N2, whereas the rescue under *Pasic-2* had 131 and under *Pklp-6* there were 179.

These results suggest two explanations. Either the rescue constructs used did not rescue the genes as they should, perhaps because the cDNA did not express properly, or because the original mutants were not outcrossed and the features that did not rescue were being caused by background mutations. To test this hypothesis I created CRISPR mutants for these genes.

Table 3.1 Significant Features in CGC Mutants that are Rescued By Expression of Rescue Constructs In The Mutant Bacground.

Pacd-5::acd-5 cDNA rescue	
Feature rescued in *acd-5 (ok2657)I* background by *Pacd-5::acd-5 cDNA*	P value in *acd-5 (ok2657)I*
'Neck Bend Mean (+/- = D/V Inside)'	2.80163E-05
'Positive Backward Head Bend Mean (+/- = D/V Inside)'	0.00208576
'Head Bend Mean (+/- = D/V Inside)'	0.00441524
'Negative Neck Bend Mean (+/- = D/V Inside)'	0.00682085
'Positive Neck Bend Mean (+/- = D/V Inside)'	0.00757836
'Paused Neck Bend Mean (+/- = D/V Inside)'	0.0101794
'Positive Paused Head Bend Mean (+/- = D/V Inside)'	0.0125861
'Positive Paused Neck Bend Mean (+/- = D/V Inside)'	0.0326966
'Absolute Forward Head Bend Mean (+/- = D/V Inside)'	0.0348972
Pdaf-7::acd-5 cDNA rescue	
Feature rescued in *acd-5 (ok2657)I* background by *Pdaf-7::acd-5 cDNA*	P value in *acd-5 (ok2657)I*
'Neck Bend Mean (+/- = D/V Inside)'	2.80163E-05
'Backward Neck Bend Mean (+/- = D/V Inside)'	0.00193125
'Absolute Backward Head Bend Mean (+/- = D/V Inside)'	0.00273088
'Head Bend Mean (+/- = D/V Inside)'	0.00441524
'Negative Neck Bend Mean (+/- = D/V Inside)'	0.00682085
'Positive Neck Bend Mean (+/- = D/V Inside)'	0.00757836
'Paused Neck Bend Mean (+/- = D/V Inside)'	0.0101794

'Positive Paused Head Bend Mean (+/- = D/V Inside)'	0.0125861
'Forward Head Bend Mean (+/- = D/V Inside)'	0.017289
'Positive Paused Neck Bend Mean (+/- = D/V Inside)'	0.0326966
'Absolute Forward Head Bend Mean (+/- = D/V Inside)'	0.0348972
midbody bend (+/-=d/v inside)	0.0468507
Pklp-6::asic-2 cDNA rescue	
Feature rescued in *asic-2 (ok289)I* background by *Pklp-6:: asic-2 cDNA*	P value in *asic-2 (ok289)I*
midbody bend (+/-=d/v inside)	0.000388658
'Positive Forward Head Bend Mean (+/- = D/V Inside)'	0.00525915
'Negative Backward Head Bend Mean (+/- = D/V Inside)'	0.00820158
'Absolute Backward Head Bend Mean (+/- = D/V Inside)'	0.0100132
'Positive Paused Head Bend Mean (+/- = D/V Inside)'	0.0215798
'Forward Head Bend Mean (+/- = D/V Inside)'	0.0244216
Pasic-2::asic-2 cDNA rescue	
Feature rescued in *asic-2 (ok289)I* background by *Pasic-2:: asic-2 cDNA*	P value in *asic-2 (ok289)I*
midbody bend (+/-=d/v inside)	0.000388658
'Negative Backward Head Bend Mean (+/- = D/V Inside)'	0.00820158
'Absolute Backward Head Bend Mean (+/- = D/V Inside)'	0.0100132
'Positive Paused Head Bend Mean (+/- = D/V Inside)'	0.0215798

3.3.3 CRISPR Induced Mutations In *asic-2* and *acd-5*

As conventional rescue techniques do not produce wild type worms, outcrossing of the mutants was proving difficult and there was only one mutant allele available for each gene, attempts were made to produce new alleles using CRISPR (Clustered Regularly Interspaced Short Palindromic Repeats) gene editing. CRISPR/*cas-9* gene editing is a technique that manipulates the bacterial CRISPR/*cas-9* prokaryotic immune system in order to make double stranded breaks at specific sites in an organism's genome (Friedland et al. 2013). The double stranded break is then fixed by the organism's cellular machinery. On occasion, the repair of the DNA is not perfect and base pairs are deleted or added. This can be checked in *C. elegans,* lysation of the worm after the CRISPR/*cas-9* reaction, and sequencing of the DNA will prove whether a modification has been made to the genome.

Targeted breaks can only be made in the gene of question where there is a PAM (Protospacer adjacent motif) site in the coding DNA. PAM sequences are 3-5 base pair sequences at which the *cas-9* enzyme will cut. Three PAM sites were identified in each gene; an effort was made to choose sites spaced out over the gene. In *asic-2* there were only 3 PAM sites, 2 of which were positioned at the very start of the gene (Fig.3.9) In *acd-5* there were more PAM sites to choose from, sites were chosen in exon 6, 8 and 9 (Fig.3.10) CRISPR/*cas-9* reactions were performed and the resultant worms selfed and sequenced several times until mutant homozygotes were isolated.

The resultant mutations for *asic-2* were at PAM sites 1 and 2 (Fig. 3.9), unfortunately they only resulted in 3bp excisions or insertions (Fig.3.9). The lack of frame shift in these mutants may cause the resultant protein to be almost identical as the wild type, as only one amino acid residue will be altered. This may have little to no effect on the functioning of the ASIC-2 protein encoded by the

CRISPR mutant. If the single residue alteration is in a conserved region of the gene it is more likely to affect the protein's function. Sequence analysis of a number of DEG/ENaC subunit genes highlighted regions of the genes that are conserved within the family (Fig.3.11 and 3.12). Unfortunately none of the CRISPR mutations lie within a conserved region (Fig.3.13). The 3D structure of the wild type ASIC-2 protein and CRISPR mutant proteins showed no disruption to the protein resulting from the CRISPR mutations (Fig.3.14). This would suggest that they are unlikely to have a phenotype any different to the wild type, and certainly not as severe as *asic-2 (ok289)* which has a stop codon introduced at amino acid position 4. However, each of the three mutations removes or repositions a glycine residue. Glycine is unique as it contains a hydrogen as its side chain, this means that there is much more conformational flexibility in glycine and as a result of this it can reside in parts of protein structures that are forbidden to all other amino acids (Betts, M.J. & Russell, R.B. 2003). This may mean that the functioning of the protein is, in fact, effected by these mutations.

Mutations resulting from CRISPR in *acd-5* were more promising. Excisions were created at position 2 and 3 in the gene. Two of the excisions at position 2 delete base pairs in multiples of three, *acd-5 (lj108)* and *(lj109)* (Fig.15.4), and the deletion at position 3, *acd-5 (lj110),* is a 3 bp deletion (Fig.3.15). None of these deletions will cause a frame shift and must be in a conserved position to have an effect on gene structure and function. The deletion for allele *acd-5 (lj107)* does cause a frame shift, causing missence mutations from amino acid position 546 to 583 and introducing a stop codon at position 584 of an 804 amino acid gene (Fig.3.16). PAM site 2 falls in a region conserved in the DEG/ENaC family, therefore the modifications at this site are expected to have an effect in protein function (Fig.3.15). Sequence guided 3D structure predictions show that sections of the 2nd transmembrane domain are missing, or the domain is shortened in the CRISPR alleles. In *acd-5 (ok2657)I* the 2nd transmembrane domain is missing (Fig.3.17.)

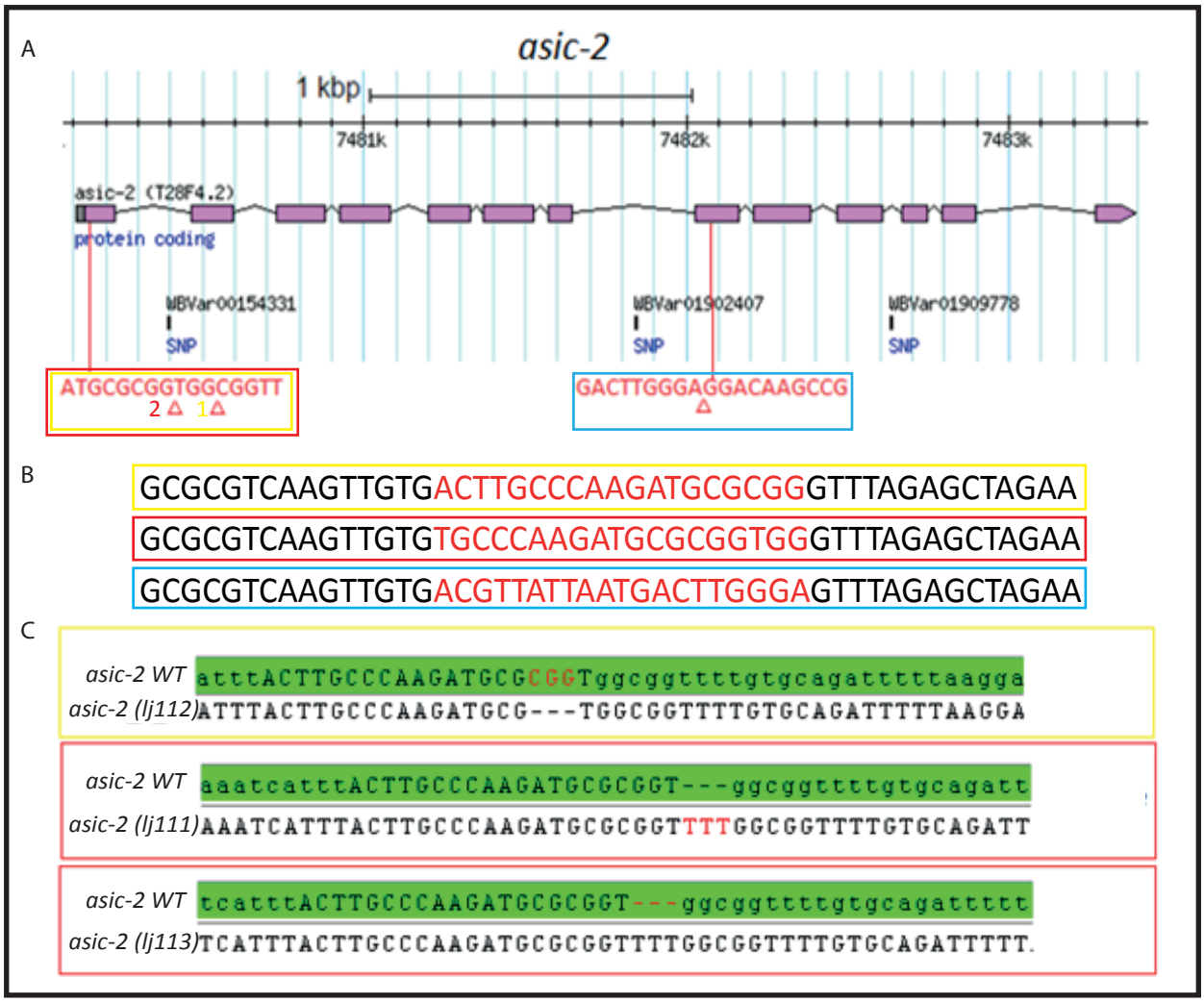

Fig.3.9: The Genetic Position and Alterations In *asic-2* CRISPR Alleles.
A: The genetic map of *C. elegans* wild type *asic-2*, purple boxes indicate exons and black lines indicate introns. Short DNA sequences show where PAM sites were identified, the yellow box is PAM site 1, red is PAM site 2 and blue is PAM site 3. Red arrows indicate where the *cas-9* enzyme will cut. B: Position 1, 2and 3 primers used for CRISPR reaction. C: The resultant modifications at each PAM site.

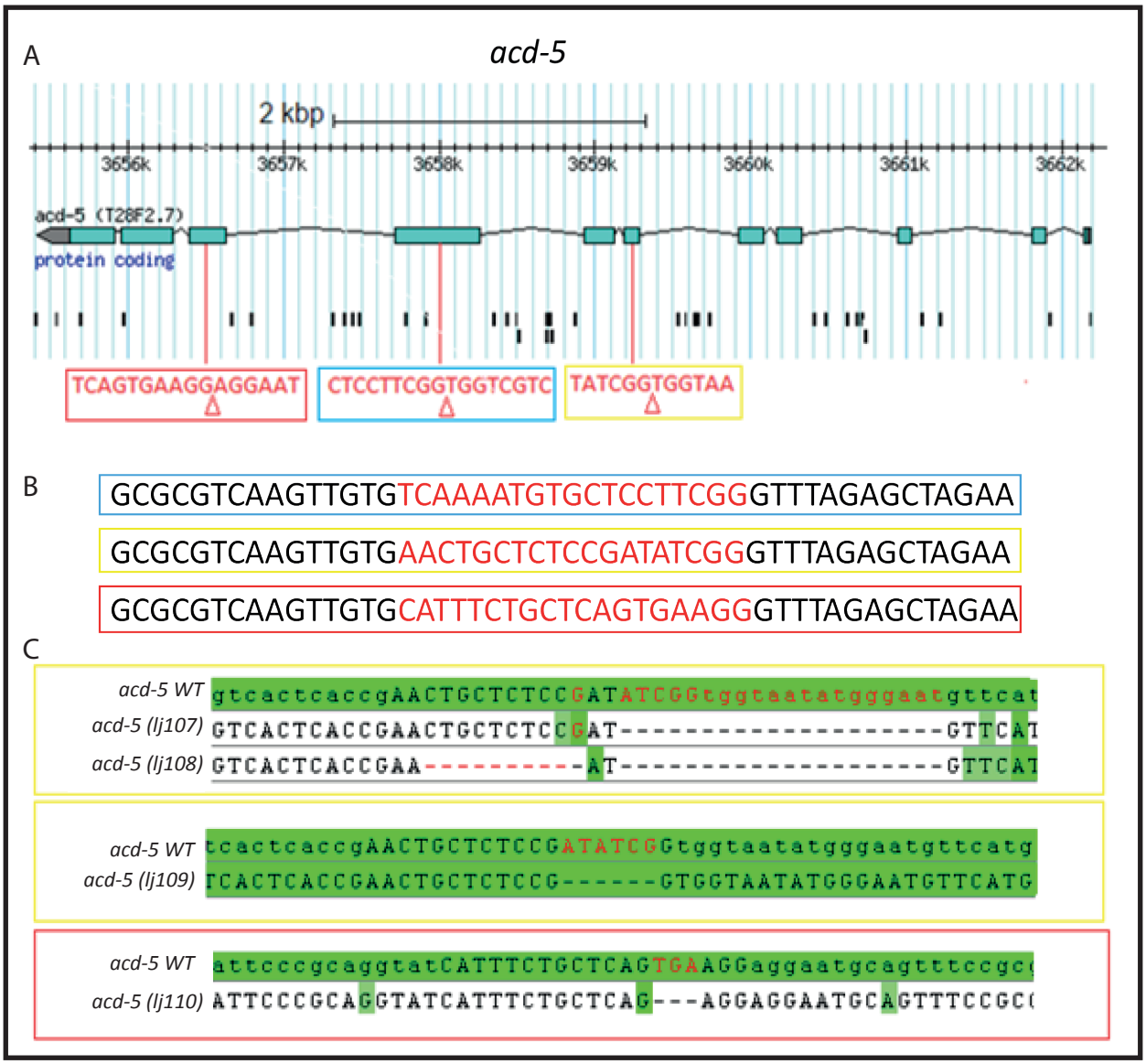

Fig.3.9: The genetic position of CRISPR mutations and their deletions.
A: The genetic map of *C. elegans* wild type *acd-5*, blue boxes indicate exons and black lines indicate introns. Short DNA sequences show where PAM sites were identified, The blue boxed sequence is PAM site 1, yellow is PAM site 2 and red is PAM site 3. Red arrows indicate where the *cas-9* enzyme will cut. B: Position 1, 2 and 3 primers used for CRISPR reaction. C: The resultant excisions created for each PAM site.

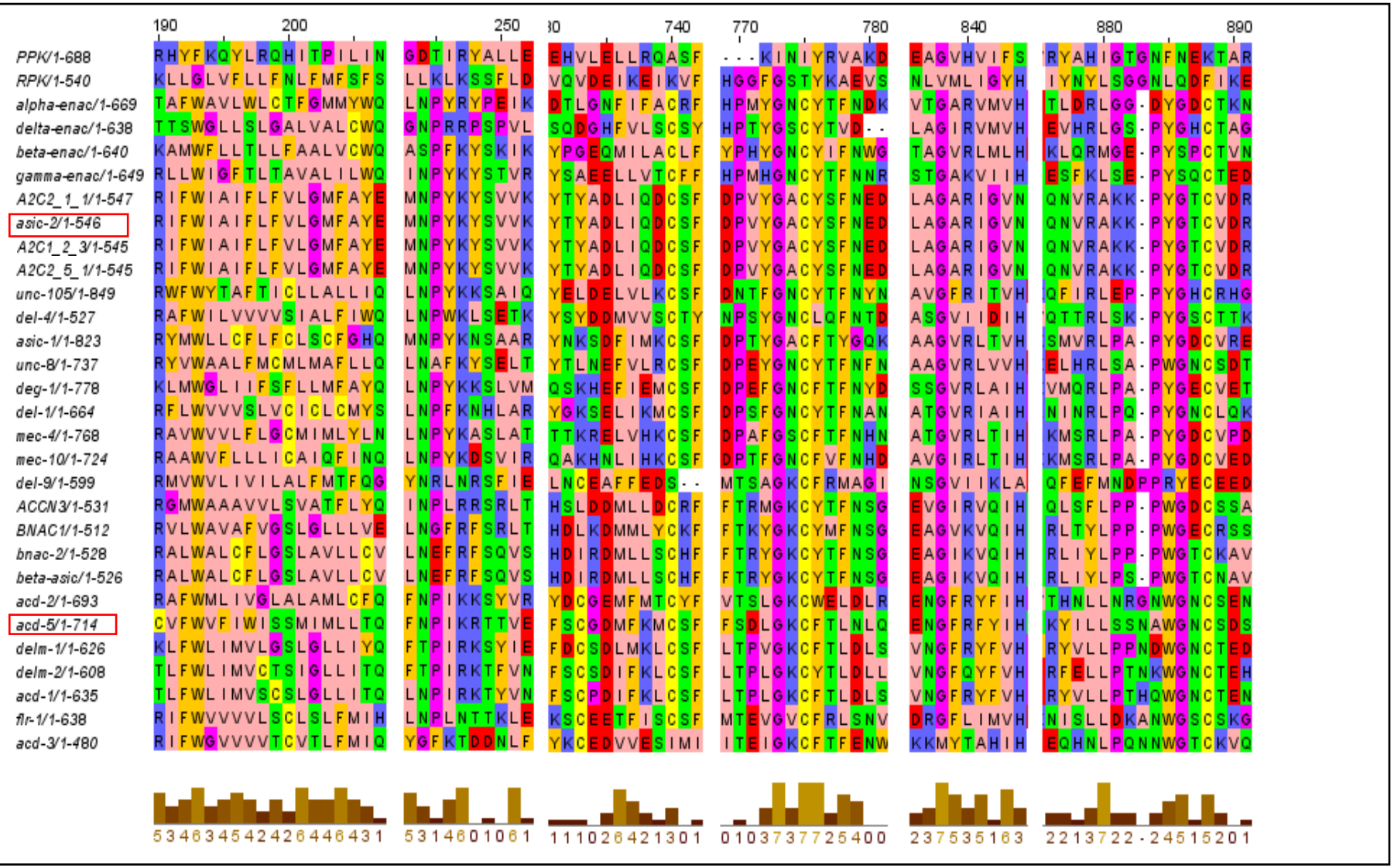

Fig. 3.11: Regions of the DEG/ENaC family that are conserved to some level throughout the family. colour coding is zappo, pink residues are hydrophobic/aliphatic, orange are aromatic, blue are positive, red are negative, green are hydrophillic, magenta are conformationally special and yellow is cysteine. White boxes with dashes are gaps in the conservation, amino acid position is labelled at the top of the regions. Alignments were performed in Jalview and conservation was calculated using the AMAS method of multiple sequence alignment analysis, also in Jalview.

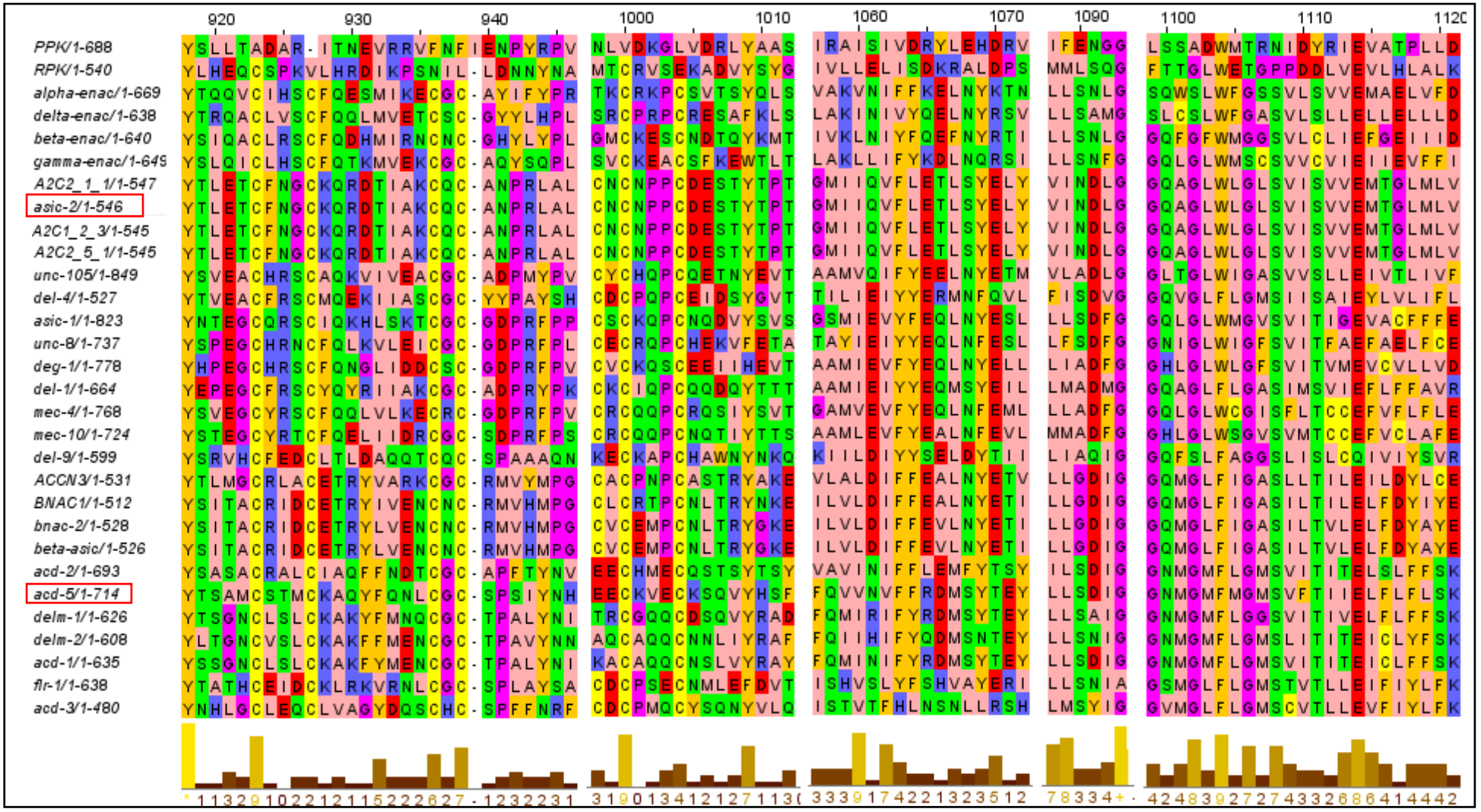

Fig. 3.12: Regions of the DEG/ENaC family that are conserved to some level throughout the family. colour coding is zappo, pink residues are hydrophobic/ aliphatic, orange are aromatic, blue are positive, red are negative, green are hydrophillic, magenta are conformationally special and yellow is cysteine. White boxes with dashes are gaps in the conservation, amino acid position is labelled at the top of the regions. Alignments were performed in Jalview and conservation was calculated using the AMAS method of multiple sequence alignment analysis, also in Jalview.

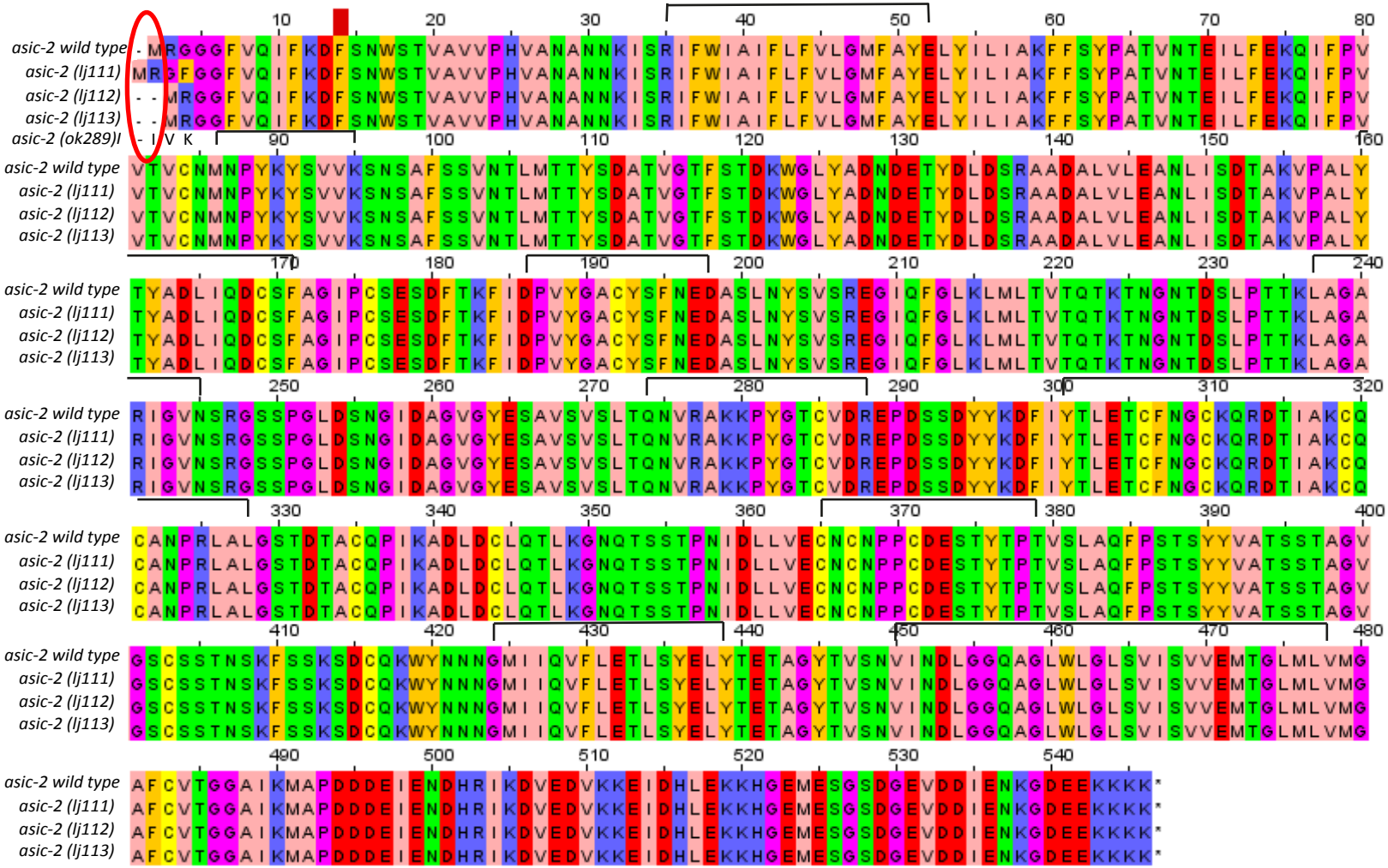

Fig.3.13: **The alignment of *C. elegans* wild-type *asic-2* alongside CRISPR alleles *asic-2 (lj111), asic-2 (lj112)* and *asic-2 (lj113)***. Grey bars indicate the regions of the wild-type gene that are conserved in the DEG/ENaC family. White boxes with a dash indicate regions where there is no alignment and asterisks show the stop codon. Colour coding of amino acids is Zappo, pink residues are hydrophobic/aliphatic, orange are aromatic, blue are positive, red are negative, green are hydrophillic, magenta are conformationally special and yellow is cysteine. CRISPR mutations are seen as unconserved residues or residues that show no alignment. All three CRISPR mutants of *asic-2* have a deletion or addition within the first 2 amino acid positions. Alignments were produced using Jalview.

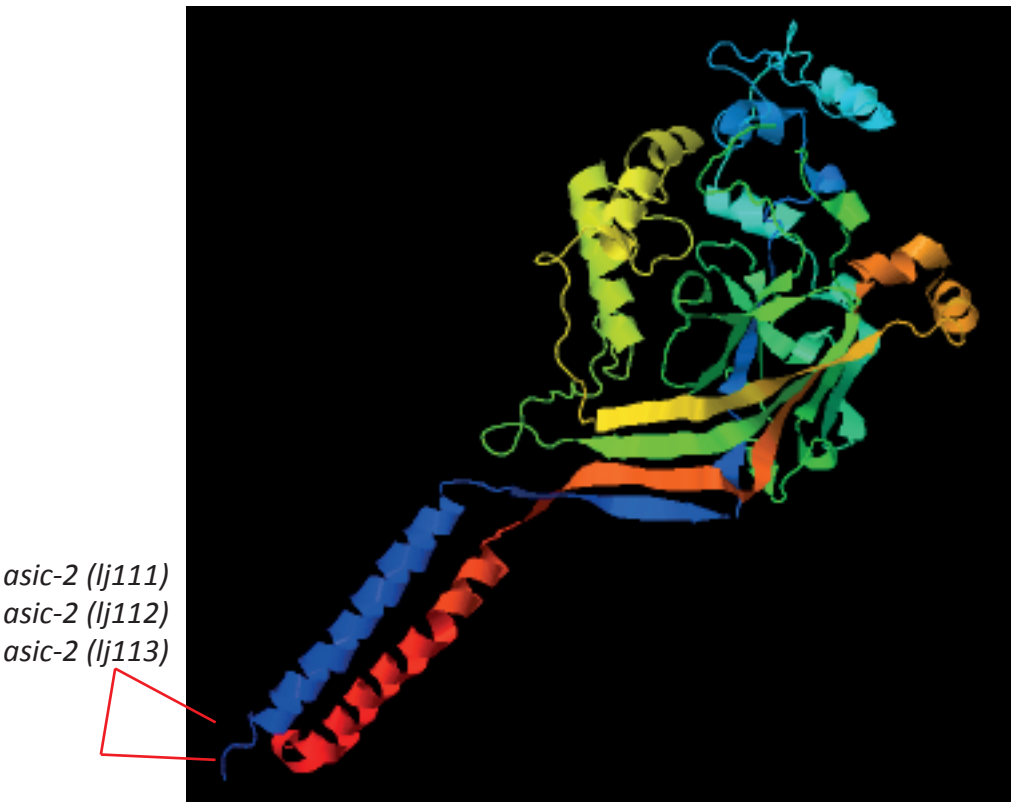

Fig.3.14: The predicted tertiary structure of ASIC-2. Image coloured by rainbow from blue to red, N- C terminus. N and C termini are located cytoplasmically, red and blue helixes indicate the two transmembrane domains, and the large loop is located extracellularly. amino acid sequence analysis was performed using Phyre2, a program which compares sequence domians of known genes to predict 3D structure of unknowns. The positionof the CRISPR mutations is labelled, none of the CRISPR mutants result in variable tertiary structure. The asic-2(ok289)I mutation results in a 3 amino acid sequence followed by a stop codon. No tertiary structure in made.

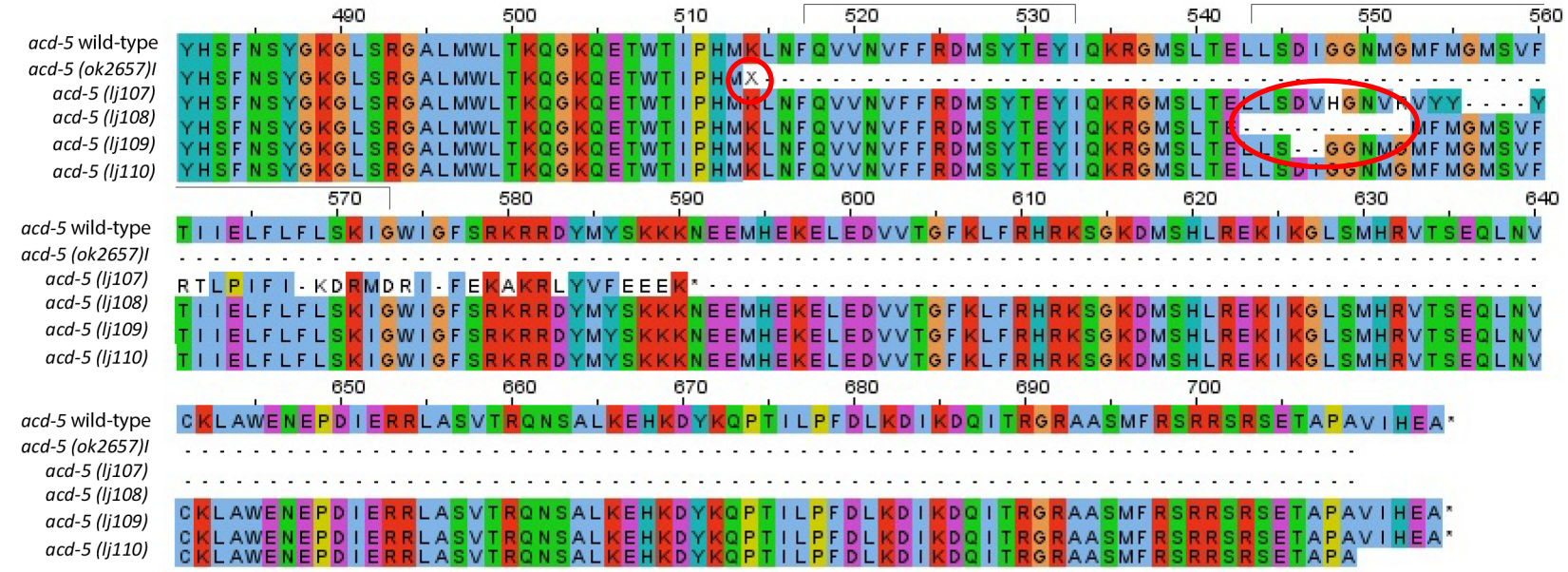

Fig.3.15: The alignment of *C. elegans* wild-type *acd-5* alongside CRISPR alleles *acd-5 (lj107)*, *acd-5 (lj108)* *acd-5 (lj109)* and *acd-5 (lj110)*. Grey bars indicate the regions of the wild-type gene that are conserved in the DEG/ENaC family. White boxes with a dash indicate regions where there is no alignment and asterisks show the stop codon. Colour coding of amino acids is Clustal, hydrophobic residues are blue, positively charged are red, negatively charged are magenta, polar resdiues are green, Cysteines are pink, Glycines are orange, prolines are yellow, aromatic are cyan and unconserved are white. CRISPR mutations are seen as unconserved residues or residues that show no alignment, mutants *acd-5 (lj107)- acd-5 (lj109)* have mutations within the final region that is conserved in the DEG/ENaC family. Alignments were produced using Jalview.

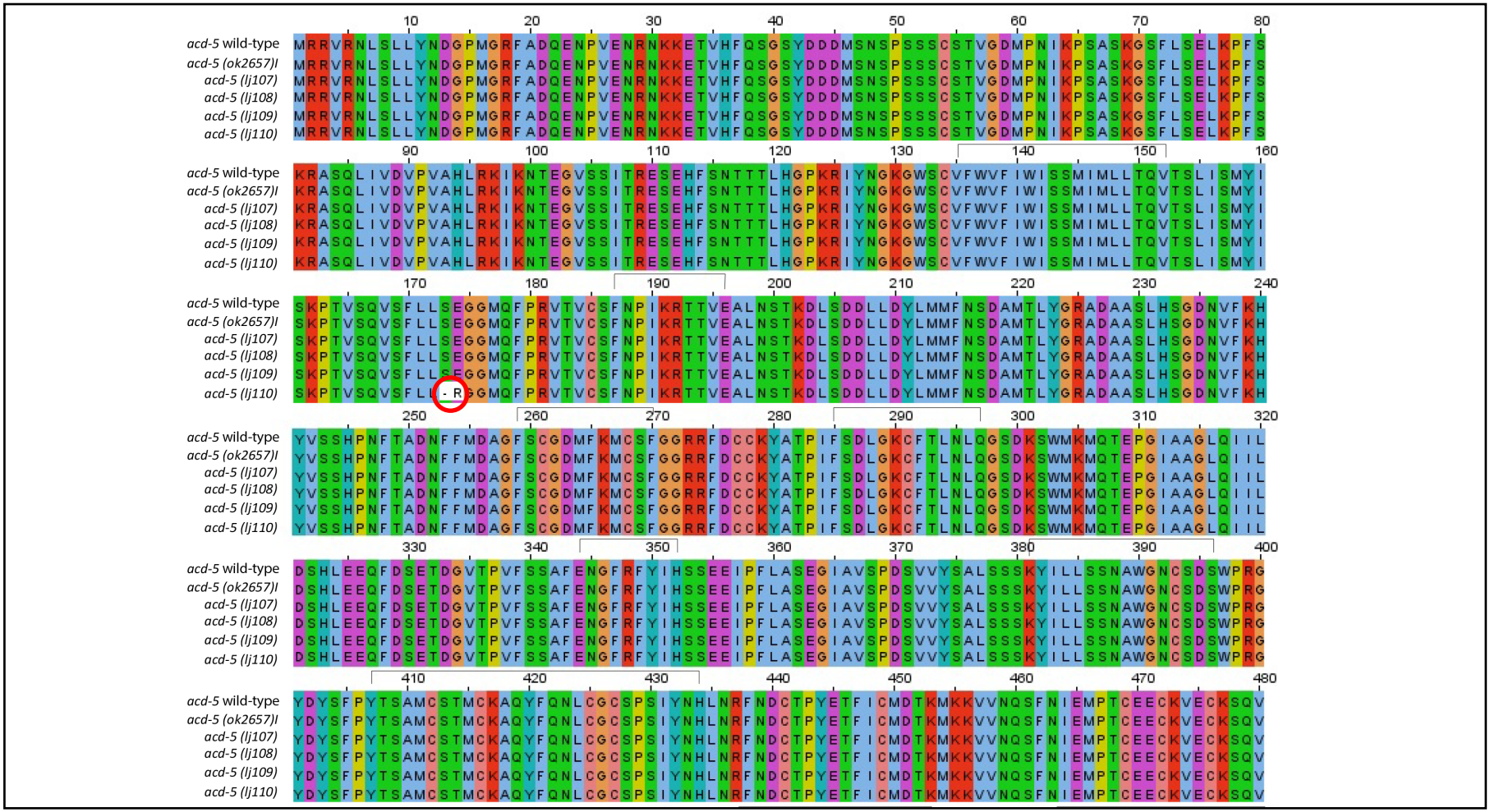

Fig.3.16: The alignment of *C. elegans* wild-type *acd-5* alongside *acd-5 (ok2657)*I CRISPR alleles *acd-5 (lj107), acd-5 (lj108) acd-5 (lj109)* and *acd-5 (lj110)*. Grey bars indicate the regions of the wild-type gene that are conserved in the DEG/ENaC family. White boxes with a dash indicate regions where there is no alignment and asterisks show the stop codon. Colour coding of amino acids is Clustal, hydrophobic residues are blue, positively charged are red, negatively charged are magenta, polar resdiues are green, Cysteines are pink, Glycines are orange, prolines are yellow, aromatic are cyan and unconserved are white. CRISPR mutations are seen as unconserved residues or residues that show no alignment, mutants, *acd-5 (lj110)* mutation is shown in a region not conserved with other members of the DEG/ENaC family.Alignments were produced using Jalview.

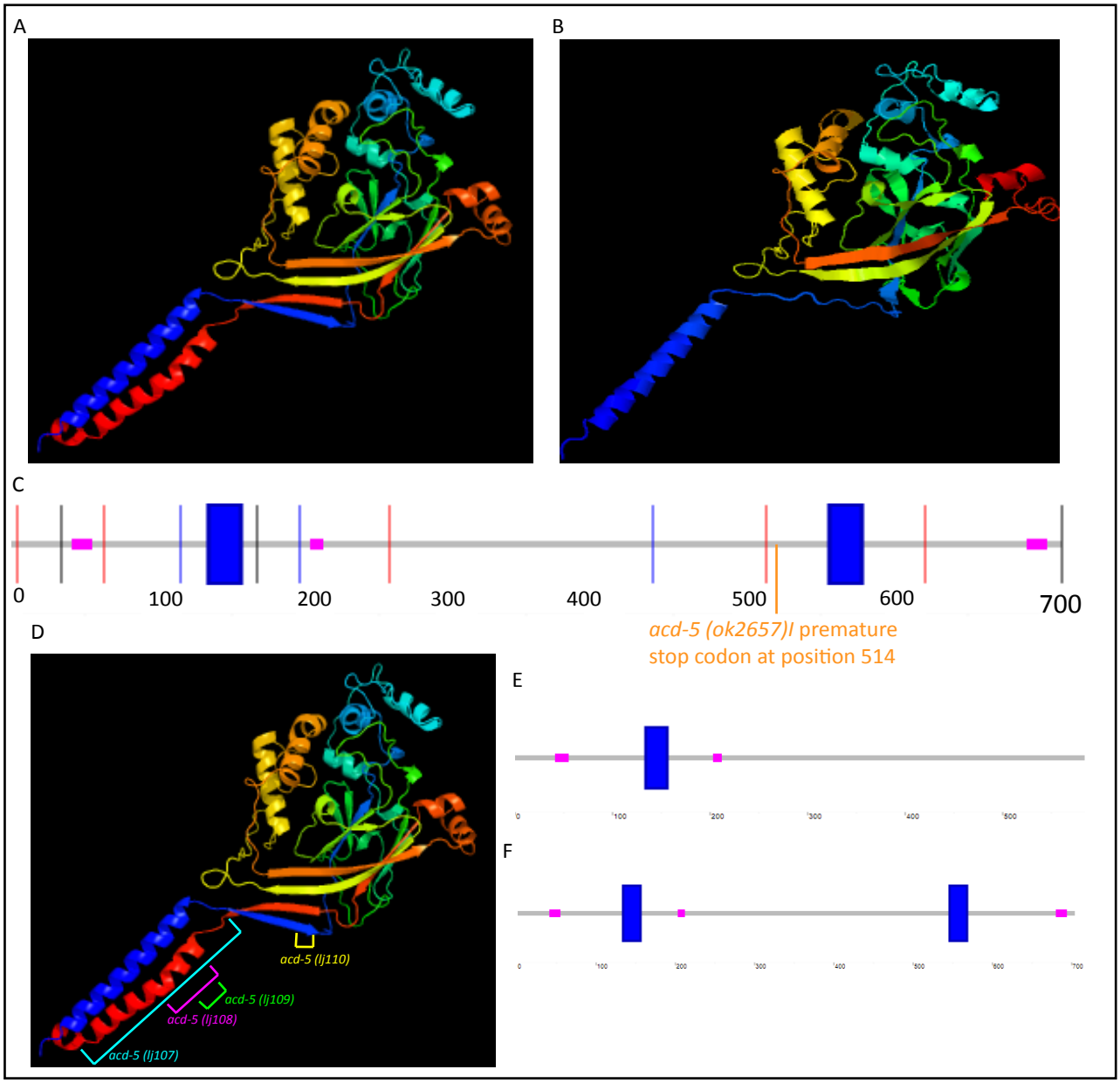

Fig. 3.17: 3D structures of *acd-5* mutants A: The predicted tertiary structure of wild-type ACD-5, image coloured by rainbow from blue to red, N- C terminus. N and C termini are located cytoplasmically, red and blue helixes indicate the two transmembrane domains, and the large loop is located extracellularly. Protein sequence analysis was performed using Phyre2, a program which compares sequence domians of known genes to predict 3D structure of unknowns. B: The tertiary structure of *acd-5 (ok2657)I*, image properties are the same as the wild-type image. In the mutant the 2nd transmembrane domain is no longer present. C: Predicted schematic of the wild-type *acd-5* protein, blue boxes indicate transmembrane positions, red lines indicate introns and pink boxes indicate low complexity regions. Annotated in orange is the point where the *acd-5 (ok2657)I* mutant protein is truncated. D: The predicted tertiary structure of wild-type *acd-5* annotated to show the regions affected by the various CRISPR mutations. *acd-5 (lj108)* has a 10 amino acid deletion from position 543 to 552, which is located in the 2nd transmembrane domain. *acd-5 (lj109)* has a 2 amino acid deletion at positions 546 and 547, also in the 2nd transmembrane domain. *acd-5 (lj110)* has a 1 amino acid deletion at poisiton 173 and is followed by a substitution of glutamic acid for argenine at position 174 E: Predicted schematic of *acd-5 (lj107)* CRISPR mutant, the deletion results in a short span of frame-shift from position 546 to a premature stop codon at position 584. F: Predicted schematic of *acd-5 (lj108), acd-5 (lj109)* and *acd-5 (lj110)*.

3.3.3.1 *acd-5* CRISPR Mutant Tracking

The CRISPR mutants were tracked in the same manner as all previous single worm tracking assays. In addition to the new CRISPR strains N2 and the original CGC mutants were also tracked simultaneously. Features of interest were analysed using a multiple t-test with no correction for multiple comparisons. Table 3.2 lists the features that were significantly different in the CRISPR mutants and *acd-5 (ok2657)I* in comparison to N2s tracked on the same days. Numbers listed in the table are the P values for each feature for each mutant. Empty boxes signify that this feature was not significantly different in the mutant in comparison to wild type.

Features labelled positive or negative specifically show the results for dorsally or ventrally directed actions. For example, 'positive upsilon turn time' gives the result for the amount of time a worm has spent in an upsilon turn event entered into from the dorsal direction. Forward and backward features specifically give results for an action performed during forward or backward locomotion, e.g. 'backward head speed' gives the result for the speed at which the worms head is travelling when performing a reversal. Inter upsilon and omega turn time/distance shows the length of time or distance travelled by the worm in between upsilon and omega turn events. 'Absolute' features are the result of adding together the result for positive/negative or forward/backward results.

There are fewer significant features for the CRISPR mutant than for the CGC mutants. This is to be expected as the CGC mutant has a large portion of the 2nd transmembrane domain is missing while the CRISPR mutant alleles *acd-5 (lj108), acd-5 (lj109)* and *acd-5 (lj110)* have only a small number of amino acid residues altered. The protein is more likely to still be functioning in this case. Although there are a number of features that are significantly different from wild type in each CRISPR mutant, few are shared between the three CRISPR alleles.

3.3.3.1.1 Significant Features For *acd-5 (lj107)*

The mutant *acd-5 (lj107)* is significantly different from wild type in its upsilon turning behaviour. On average the worm travels a greater distance before performing an upsilon turn in the ventral direction than the wild type (Fig.3.18A), the mutant also travels further in between upsilon turn events in the dorsal direction than wild type, but the result is not significant (data not shown). The same is true, in this mutant, for the distance travelled between omega turn events (Fig.3.18B). This would suggest that these behaviours occur less regularly in this mutant than in the wild type. The Upsilon frequency result confirms this theory for these events, the frequency of upsilon turns in significantly reduced in *acd-5 (lj107)* animals (Fig.3.18C). Additionally the mean time in between upsilon turn events entered into in the dorsal direction is significantly higher in the mutant in comparison to N2 (Fig.3.18D).

There are also significant differences in this mutant in the amplitude at which it crawls, when travelling in a forward direction, the amplitude of dorsal bends is much reduced in comparison to the wild type (Fig.3.18E). Conversely, when reversing, the amplitude of dorsal bends in the mutant is significantly higher than N2 (Fig.3.18F).

3.3.3.1.2 Significant Features For *acd-5 (lj108)*

This strain also has a pronounced increase in the amount of time in between upsilon turn events. Here both the time between ventrally entered upsilon bends (Fig.3.18D) and the time between all upsilon turns is longer (Fig.3.19A).

3.3.3.1.3 Significant Features For *acd-5 (lj109)*

This mutant is another with significance in upsilon turn features. Here the mean duration of an upsilon turn is greater than in wild type (Fig.3.19D), time spent specifically in dorsally entered upsilon turns is significantly higher than wild type (Fig.3.19C). Once again the distance travelled in between upsilon turns is significantly increased (Fig.3.19B).

	Features that are significantly different from N2 in *acd-5 (lj107)* mutants
	Features that are significantly different from N2 in *acd-5 (lj108)* mutants
	Features that are significantly different from N2 in *acd-5 (lj109)* mutants
	Features that are significantly different from N2 in *acd-5 (lj110)* mutants

Table 3.2 Significant Features in CRISPR Mutants of *acd-5*

Feature	*acd-5 (lj107)*	*acd-5 (lj108)*	*acd-5 (lj109)*	*acd-5 (lj110)*
'Negative Inter Upsilon Distance (+/- = Previous D/V)'	0.02			
'Upsilon Turns Frequency'	0.03			
'Positive Forward Midbody Crawling Amplitude (+/- = D/V Inside)'	0.04			
'Negative Inter Omega Distance (+/- = Previous D/V)'	0.04			
'Positive Backward Head Crawling Amplitude (+/- = D/V Inside)'	0.04			
'Positive Inter Upsilon Time (+/- = Previous D/V)'	0.05	0.04		
'Absolute Inter Upsilon Time (+/- = Previous D/V)'		0.03		
'Positive Upsilon Turn Time (+/- = D/V Inside)'			0.01	
'Inter Upsilon Distance (+/- = Previous D/V)'			0.01	
'Upsilon Turn Time (+/- = D/V Inside)'			0.04	0.038
'Positive Backward Head Motion Direction (+/- = Toward D/V)'				0.003
'Absolute Backward Head Motion Direction (+/- = Toward D/V)'				0.004
'Absolute Backward Midbody Motion Direction (+/- = Toward D/V)'				0.005
'Absolute Forward Head Crawling Amplitude (+/- = D/V Inside)'				0.006
'Absolute Backward Head Tip Speed (+/- = Forward/Backward)'				0.007
'Negative Backward Head Tip Speed (+/- = Forward/Backward)'				0.007
'Positive Forward Head Crawling Amplitude (+/- = D/V Inside)'				0.007
Absolute Head Crawling Amplitude (+/- = D/V Inside)'				0.008
'Positive Head Crawling Amplitude (+/- = D/V Inside)'				0.011
'Positive Head Bend Mean (+/- = D/V Inside)'				0.013
'Negative Backward Head Speed (+/- = Forward/Backward)'				0.019
'Absolute Backward Head Speed (+/- = Forward/Backward)'				0.02
'Absolute Neck Bend Mean (+/- = D/V Inside)'				0.02
'Absolute Head Bend Mean (+/- = D/V Inside)'				0.023
'Positive Forward Head Motion Direction (+/- = Toward D/V)'				0.024

'Positive Backward Midbody Motion Direction (+/- = Toward D/V)'				0.025
'Track Length'				0.027
'Absolute Forward Head Motion Direction (+/- = Toward D/V)'				0.029
'Absolute Forward Midbody Motion Direction (+/- = Toward D/V)'				0.03
'Backward Track Length'				0.03
'Negative Forward Head Speed (+/- = Forward/Backward)'				0.032
'Absolute Midbody Motion Direction (+/- = Toward D/V)'				0.033
'Absolute Midbody Crawling Frequency (+/- = D/V Inside)'				0.034
'Positive Head Motion Direction (+/- = Toward D/V)'				0.035
'Absolute Head Motion Direction (+/- = Toward D/V)'				0.035
'Backward Head Speed (+/- = Forward/Backward)'				0.037
'Backward Midbody Speed (+/- = Forward/Backward)'				0.038
'Forward Track Length'				0.038
'Backward Head Tip Speed (+/- = Forward/Backward)'				0.039
'Positive Midbody Motion Direction (+/- = Toward D/V)'				0.04
'Absolute Backward Head Crawling Frequency (+/- = D/V Inside)'				0.041
'Negative Head Tip Speed (+/- = Forward/Backward)'				0.041
'Paused Track Length'				0.043
'Positive Backward Head Crawling Frequency (+/- = D/V Inside)'				0.047
'Positive Tail Tip Speed (+/- = Forward/Backward)'				0.047

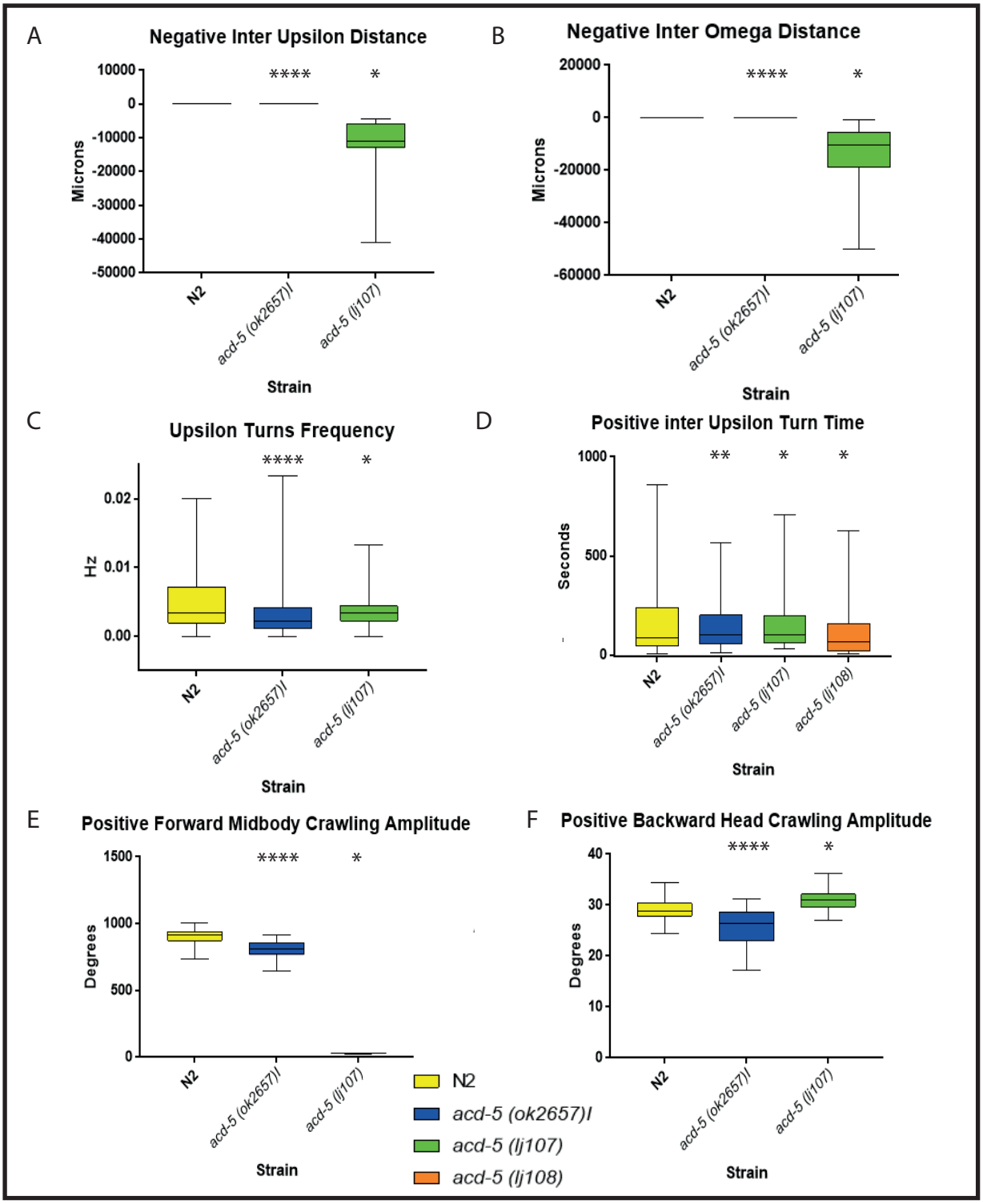

Fig.3.18: Box and Whisker plots of The Statistically Significant Features of *acd-5* CRISPR mutants. A:A box and whisker plot of the negative inter upsilon distance for the mutant *acd-5 (lj107)* in comparison to N2 and *acd-5 (ok2657)I*. B: A box and whisker plot of the negative inter omega distance for the mutant *acd-5 (lj107)* in comparison to N2 and *acd-5 (ok2657)I*. C: A box and whisker plot of the upsilon turns frequency for the mutant *acd-5 (lj107)* in comparison to N2 and *acd-5 (ok2657)I*. D: A box and whisker plot of the positive inter upsilon turn time for the mutants *acd-5 (lj107)* and *acd-5 (lj108)* in comparison to N2 and *acd-5 (ok2657)I*. E: A box and whisker plot of the positive forward midbody crawling amplitude for the mutant *acd-5 (lj107)* in comparison to N2 and *acd-5 (ok2657)I*. F: A box and whisker plot of the positive backward head crawling amplitude for the mutant *acd-5 (lj107)* in comparison to N2 and *acd-5 (ok2657)I*.For all plots error bars represent standard deviation, box intersections represent the mean and the box represents the interquartile range. The key shows the colouration of the different genotypes. *=p≤0.05, **=p≤0.01, ***=p≤0.001 ****=p≤0.0001

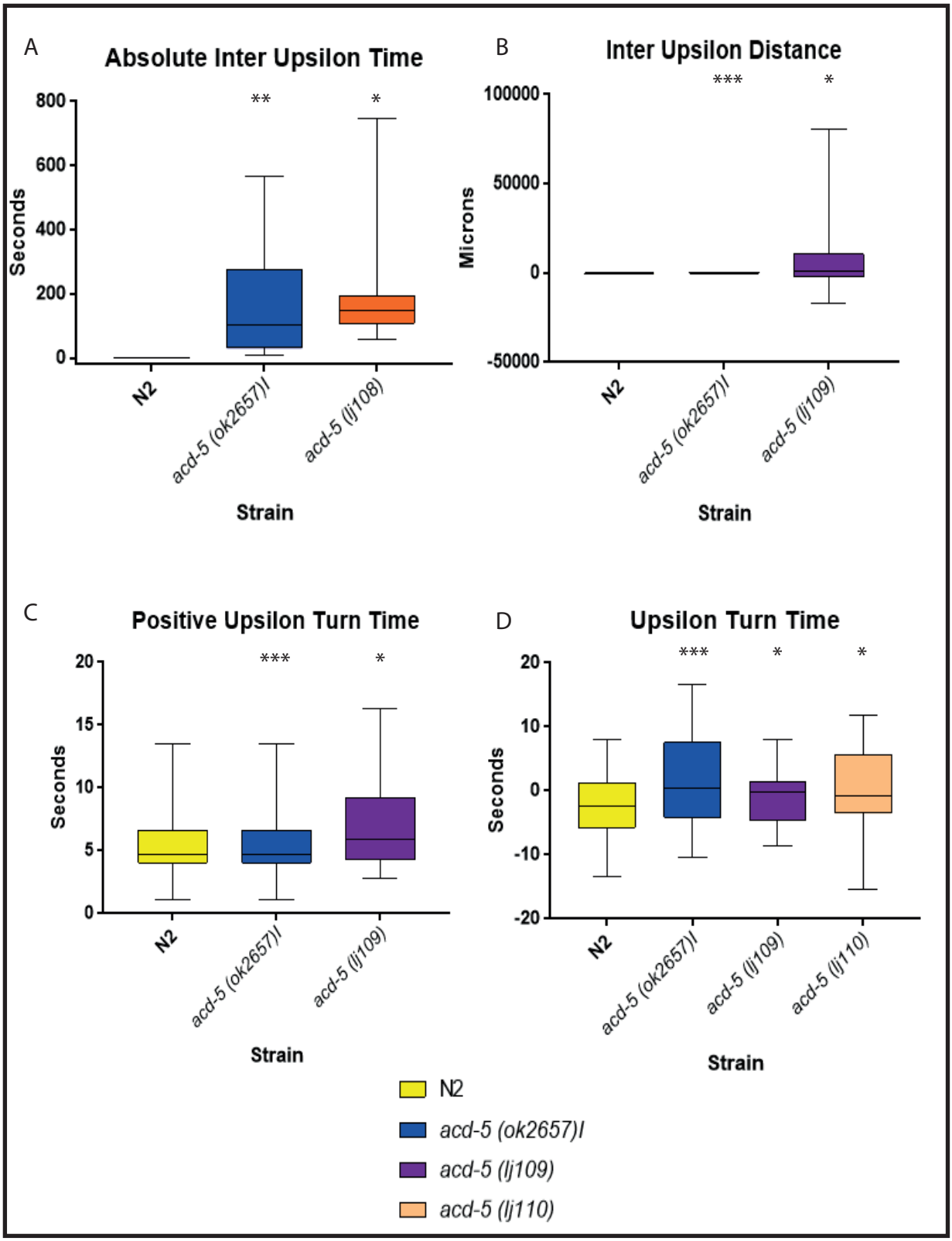

Fig.3.19: Box and Whisker plots of The Statistically Significant Features of *acd-5* CRISPR mutants. A: A box and whisker plot of the absolute inter upsilon time for the mutant *acd-5 (lj108)* in comparison to N2 and *acd-5 (ok2657)I*. B: A box and whisker plot of the inter upsilon distance for the mutant *acd-5 (lj109)* in comparison to N2 and *acd-5 (ok2657)I*. C: A box and whisker plot of the positive upsilon turn time for the mutant *acd-5 (lj109)* in comparison to N2 and *acd-5* D: A box and whisker plot of the upsilon turn time for the mutant *acd-5 (lj109)* in comparison to N2 and *acd-5 (ok2657)I*. For all plots error bars represent standard deviation, box intersections represent the mean and the box represents the interquartile range. The key shows the colouration of the different genotypes. *=p≤0.05, **=p≤0.01, ***=p≤0.001,****=p≤0.0001

3.3.3.1.4 Significant Features For *acd-5 (lj110)*

Surprisingly, the mutant *acd-5 (lj110)* has many more significantly different features than any of the other CRISPR mutants. This is the mutant with a single amino acid deletion and substitution in a non-conserved region of the protein. A possible reason that this mutant allele has a more severe effect is that its position is slightly different that the CGC mutant and other CRISPR mutants. This mutation is in the extracellular domain as opposed to the transmembrane domain. This could affect the gating properties of the channel.

The significant features fall into six categories, The speed the worm is travelling at, time spent in upsilon turn events, the distance that the worms travels over the course of recording, the frequency and amplitude of crawling, the head and neck bend means and finally the motion direction during crawling.

Speed: Predominantly the speed of the different bodily sections during reversals in the mutant is slower than wild type (Fig.3.20A). Also, the speed at which the head travels in the ventral direction during forward locomotion is significantly reduced (Fig.3.20B).

Upsilon Turns: The time spent in an omega or upsilon turn is increased (Fig.3.19D).

Track Length: The distance that the mutant worms travel over the course of the assay is significantly reduced (Fig.3.20C), in both the forward and reverse crawling directions.

Frequency and Amplitude of crawling: The frequency (number of events) of reversals is decreased in the mutant for several sections of the body, when compared to wild type (Fig.3.20E). The amplitude of the head and midbody during forwards locomotion is decreased in the mutant (Fig.3.20D), as is the amplitude in the dorsal direction while crawling, indicating that bends are more shallow in these instances.

Head and Neck Bending: In the mutant the mean head and neck bend is shallower than in the wild type, predominantly when the worm is bending its head in the dorsal direction (Fig.3.20F).

Motion Direction: The mutant has a number of significant defects in the motion direction of the head and midbody, for both dorsal direction and absolute direction of motion. The direction of motion in the dorsal direction is reduced, as is the overall direction of motion (Fig.3.21A and B). Indicating the worm is bending its head and midbody at a significantly slower rate than wild type, specifically in the dorsal direction.

In most circumstances the CRISPR mutant features are not as severe as the CGC mutant. However, the fact that each new allele is showing similar deficiencies to each other and the original mutant engenders confidence that the phenotypes are linked to mutations in these genes.

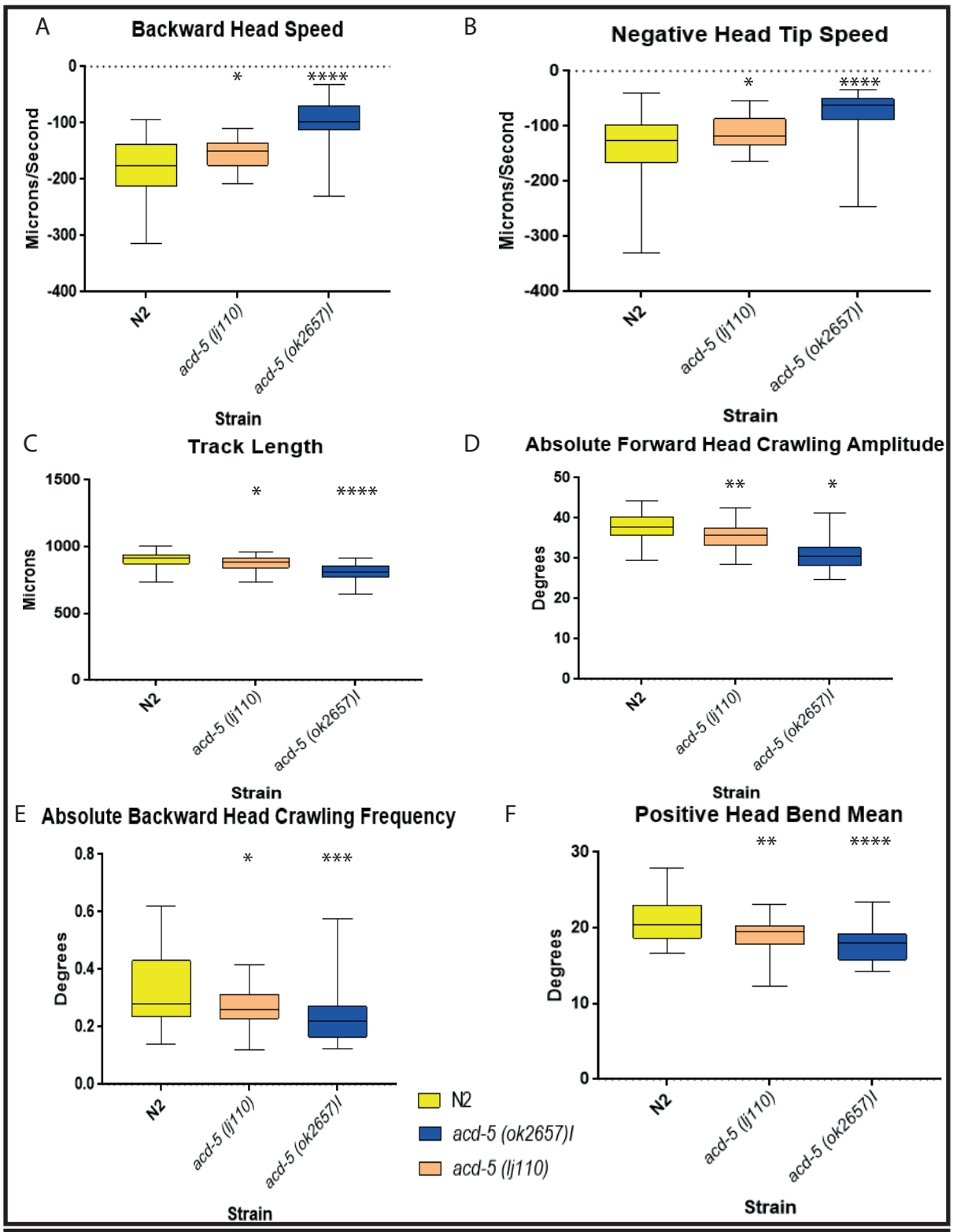

Fig.3.20: Box and Whisker plots of The Statistically Significant Features of *acd-5* CRISPR mutants. A: A box and whisker plot of the backwards head speed for the mutant *acd-5 (lj110)* in comparison to N2 and *acd-5 (ok2657)I*. B: A box and whisker plot of the negative head tip speed for the mutant *acd-5 (lj110)* in comparison to N2 and *acd-5 (ok2657)I*. C: A box and whisker plot of the track length for the mutant *acd-5 (lj110)* in comparison to N2 and *acd-5 (ok2657)I*. D: A box and whisker plot of the absolute forward head crawling amplitude for the mutant *acd-5 (lj110)* in comparison to N2 and *acd-5 (ok2657)I*. E: A box and whisker plot of the absolute backward head crawling frequency for the mutant *acd-5 (lj110)* in comparison to N2 and *acd-5 (ok2657)I*.F: A box and whisker plot of the positive head bend mean for the mutant *acd-5 (lj110)* in comparison to N2 and *acd-5 (ok2657)I*. For all plots error bars represent standard deviation, box intersections represent the mean and the box represents the interquartile range. The key shows the colouration of the different genotypes. *=p≤0.05, **=p≤0.01, ***=p≤0.001,****=p≤0.0001

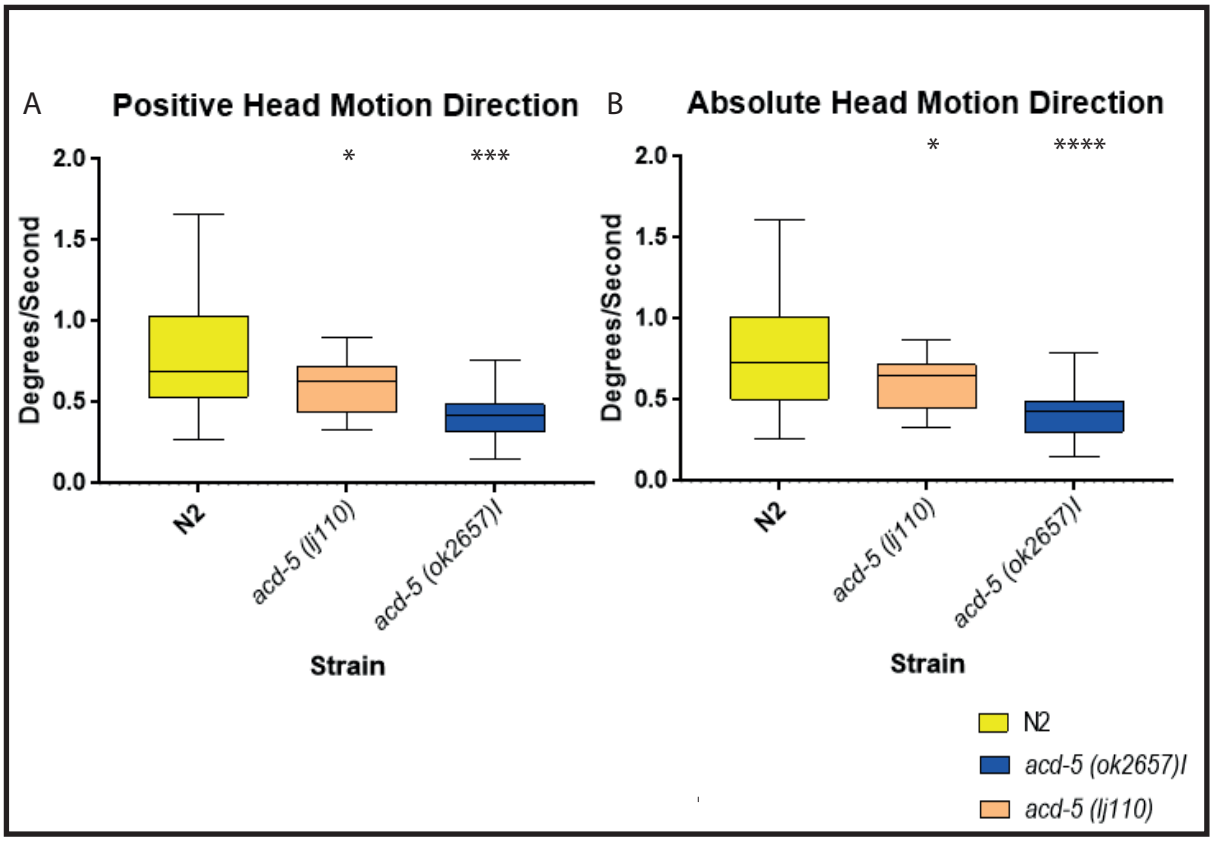

Fig.3.21: Box and Whisker Plots For CRISPR Mutant *acd-5 (lj110)* A: A box and whisker plot of the positive head motion direction of the CRISPR mutant *acd-5 (lj110)* in comparison to N2 and *acd-5 (ok2657)I.* B: A box and whisker plot of the absolute head motion direction of the CRISPR mutant *acd-5 (lj110)* in comparison to N2 and *acd-5 (ok2657)I*. For all plots error bars represent standard deviation, box intersections represent the mean and the box represents the interquartile range. The key shows the colouration of the different genotypes.
*=p≤0.05, **=p≤0.01, ***=p≤0.001,****=p≤0.0001

3.3.2.2 *asic-2* CRISPR Mutant Tracking

Table 3.3 lists the significant features for CRISPR mutants of *asic-2.* Although there are a number of features that are significantly different from wild type in each CRISPR mutant, few are shared between the three CRISPR alleles.

3.3.2.2.1 Significant Features For *asic-2 (lj111)*

All the significant features for this mutant involve bending means, amplitude changes or bend counts.

Bend means for several parts of the worm's body, during forward, reverse and paused locomotion were increased in the mutant, so the mutant bends significantly deeper than the wild type (Fig.3.22A). Based on this it is not surprising that the amplitude of the worm's movements were significantly increased in the mutant during forward locomotion (Fig.3.22B). The time spent in upsilon bends was also increased (Fig.3.22C).

3.3.2.2.2 Significant Features For *asic-2 (lj112)*

For this mutant bend means were significantly higher for the hips and tail of the worm, meaning that the worm bends its tail and hips more deeply than N2 (Fig.3.22D).. Also the foraging amplitude during forward locomotion was deeper (Fig.3.23A).

3.3.2.2.3 Significant Features For *asic-2 (lj113)*

The significant features in this mutant also involved aberrations in the bending behaviour of the worm, predominantly during reversals. Bending during reversals was less deep in the mutant than in wild type, and bending during forward locomotion was deeper than in the wild type (Fig.3.23A and B).

	Features that are significantly different from N2 in *asic-2 (lj111)* mutants
	Features that are significantly different from N2 in *asic-2 (lj112)* mutants
	Features that are significantly different from N2 in *asic-2 (lj113)* mutants

Table 3.3 Significant Features in CRISPR Mutants of *asic-2*

Feature	*asic-2 (lj111)*	*asic-2 (lj112)*	*asic-2 (lj113)*
'Absolute Backward Hips Bend Mean (+/- = D/V Inside)'	0.001674778	0.038499373	
'Absolute Backward Midbody Bend Mean (+/- = D/V Inside)'	0.030711349		0.020214161
'Absolute Forward Head Crawling Amplitude (+/- = D/V Inside)'	0.042991823		
'Absolute Forward Hips Bend Mean (+/- = D/V Inside)'	0.042155152		
'Absolute Forward Midbody Bend Mean (+/- = D/V Inside)'	0.001872807		
'Absolute Midbody Bend Mean (+/- = D/V Inside)'	0.001861413		
'Absolute Paused Hips Bend Mean (+/- = D/V Inside)'	0.036290667		
'Absolute Paused Midbody Bend Mean (+/- = D/V Inside)'	0.025856026		
'Backward Head Bend Mean (+/- = D/V Inside)'			0.036630328
'Backward Head Crawling Amplitude (+/- = D/V Inside)'			0.04448831
'Backward Midbody Crawling Amplitude (+/- = D/V Inside)'			0.024724024
'Backward Neck Bend Mean (+/- = D/V Inside)'			0.038039681
'Midbody Crawling Amplitude (+/- = D/V Inside)'			0.022081838
'Forward Bend Count'	0.048136954		
'Forward Max Amplitude'	0.030597183		

'Forward Time'	0.046003628		
'Negative Forward Head Crawling Amplitude (+/- = D/V Inside)'	0.039909981		
'Negative Forward Midbody Bend Mean (+/- = D/V Inside)'	0.028644893		
'Negative Midbody Bend Mean (+/- = D/V Inside)'	0.041668785		
'Negative Paused Hips Bend Mean (+/- = D/V Inside)'	0.020528016		
'Paused Max Amplitude'	0.042441743		
'Positive Backward Midbody Bend Mean (+/- = D/V Inside)'			0.015032777
'Positive Forward Head Crawling Amplitude (+/- = D/V Inside)'	0.047847974		
'Positive Forward Hips Bend Mean (+/- = D/V Inside)'	0.027745752		
'Positive Forward Foraging Amplitude (+/- = Toward D/V)'	0.040396064	0.040396064	
'Positive Hips Bend Mean (+/- = D/V Inside)'	0.028416007	0.028416007	
'Positive Forward Midbody Bend Mean (+/- = D/V Inside)'	0.003763437		0.036654107
'Positive Forward Tail Bend Mean (+/- = D/V Inside)'	0.007505657		
'Positive Hips Bend Mean (+/- = D/V Inside)'	0.002851994		
'Positive Paused Tail Bend Mean (+/- = D/V Inside)'		0.016186012	
'Positive Tail Bend Mean (+/- = D/V Inside)'		0.022967581	
'Positive Upsilon Turn Time (+/- = D/V Inside)'	0.017495322		
'Tail Bend Mean (+/- = D/V Inside)'			0.040604083

It is surprising that such small changes in the amino acid sequences of *asic-2* and *acd-5* can cause noticeable phenotypes in the worms expressing them. It is promising however, that these small changes result in phenotypes that correspond to the tracking data collated for the original CGC mutants.

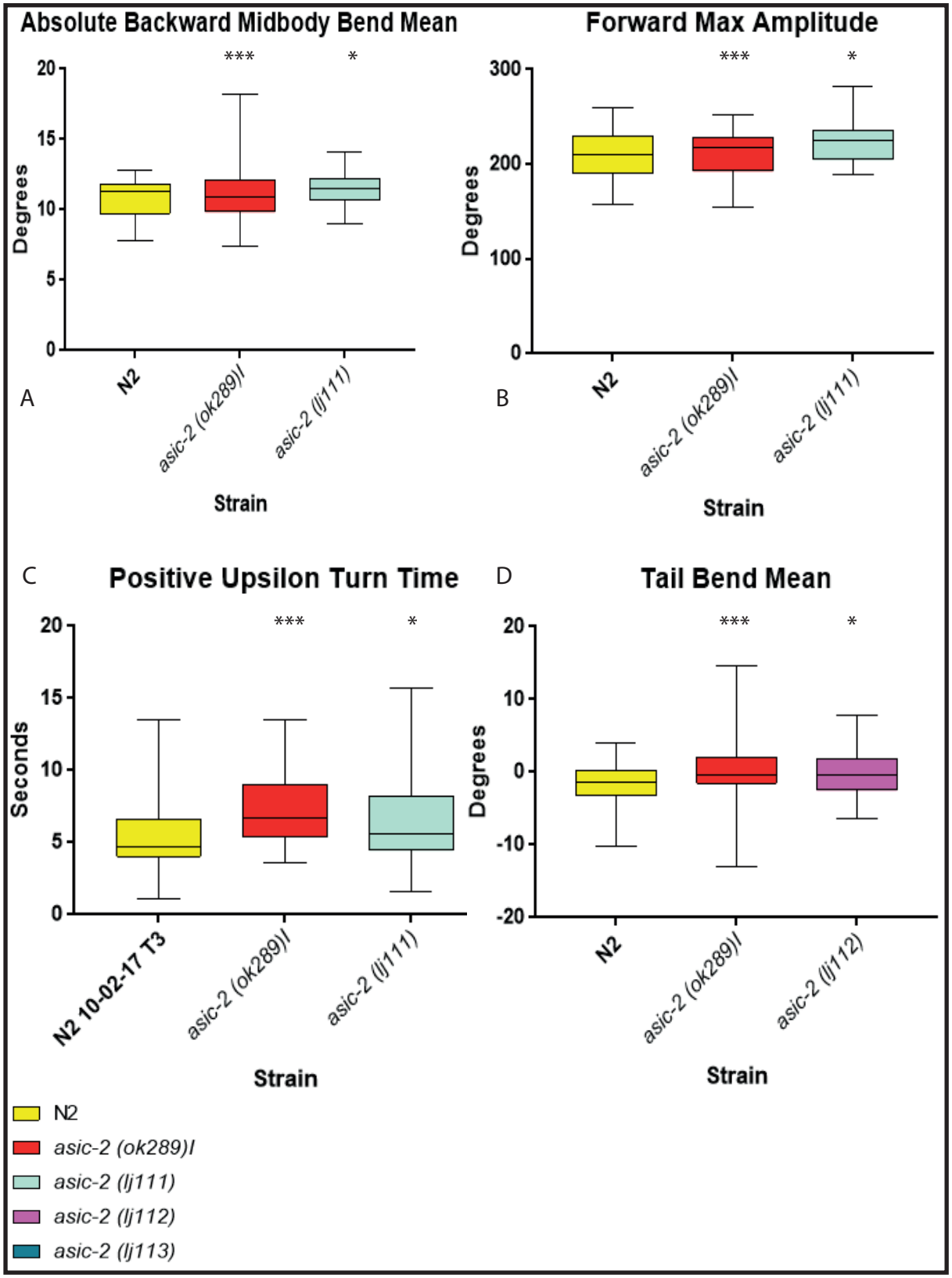

Fig.3.22: Box and whisker plots for the CRISPR mutants of *asic-2*. A: The absolute backward mid-body bend mean of the CRISPR mutant *asic-2 (lj111)* along side N2 and *asic-2 (ok289)I* tracked on the same days. Error bars show the standard deviation of the mean and boxes show the interquartile range of results. Box intersections denote the mean result. B: The maximum amplitude of worms during forward locomotion, graph parameters are as graph A. C: The mean time spent in a dorsally entered upsilon turn, graph parameters are as graph A. D: The tail bend means for worms, graph parameters are as graph A. The key explains the colouration of graph boxes. *=p≤0.05, **=p≤0.01, ***=p≤0.001,****=p≤0.0001

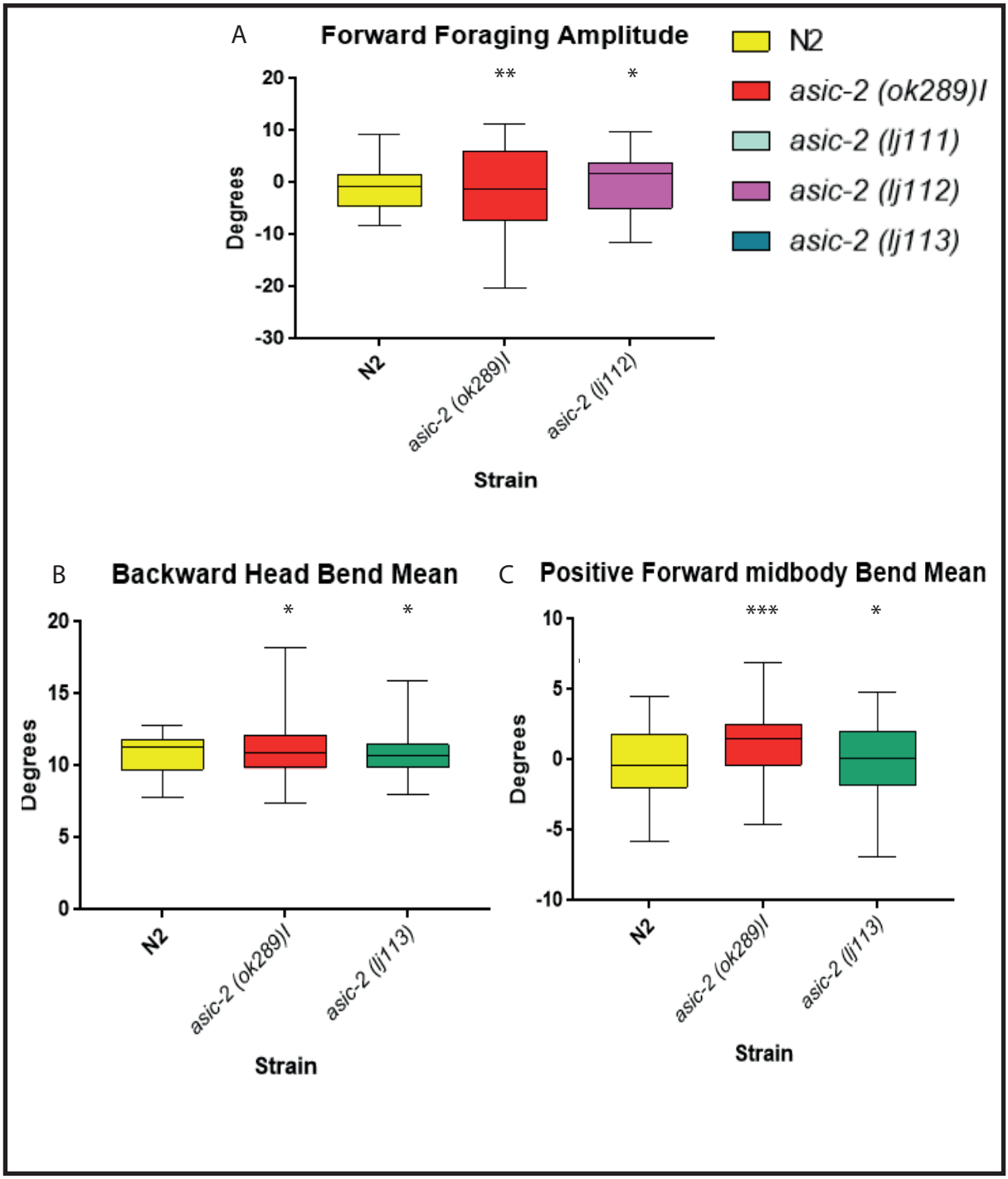

Fig.3.23: Box and Whisker Plots For The CRISPR Mutants Of *asic-2*. A: A box and whisker plot of the forward foraging amplitude of the mutant *asic-2 (lj112)* along-side N2 and *asic-2 (ok289)I*. Error bars show the standard devition of the mean, boxes show the interquartile range, box intersections show the mean result. B: A box and whisker plot of the backward head bend mean for *asic-2 (lj113)* along-side N2 and *asic-2 (ok289)I*. Graph parameters are as graph A. C: A box and whisker plot of the positive forward midbody bend mean for *asic-2 (lj113)* along-side N2 and *asic-2 (ok289)I*. Graph parametes are as graph A. Graph coloration is explined in the key. *=p≤0.05, **=p≤0.01, ***=p≤0.001,****=p≤0.0001

3.3.4 Reporter Expression

As previously shown with the DEG/ENaC pairs *mec-4* and *mec-10*, and *del-1* and *unc-8*, the cellular expression of the gene can help identify gene function. Therefore the logical first step towards establishing functionality is to map the expression pattern of the two genes. A promoter-GFP construct for *asic-2* and a promoter-RFP construct for *acd-5* was produced and co-injected to look for co-expression. It was found that *asic-2* is expressed in the IL2 neurons (Fig.3.24A and B), while *acd-5* is expressed in an individual head neuron and gut muscles. Dye filling *Pacd-5*::RFP worms with DiO, identified the neuron as ASI (Fig.3.24C). The ASI and IL2 neurons are both ciliated neuron classes located in the head of the worm (Fig. 3.24D and E). The ASIs are found in the amphid sensilla (Fig.3.24F) and the IL2s are located in the inner labial sensilla (Fig.3.24G), both neuron classes have distinct functions.

Figure references: (Bae & Barr 2008)(Perkins et al. 1986)

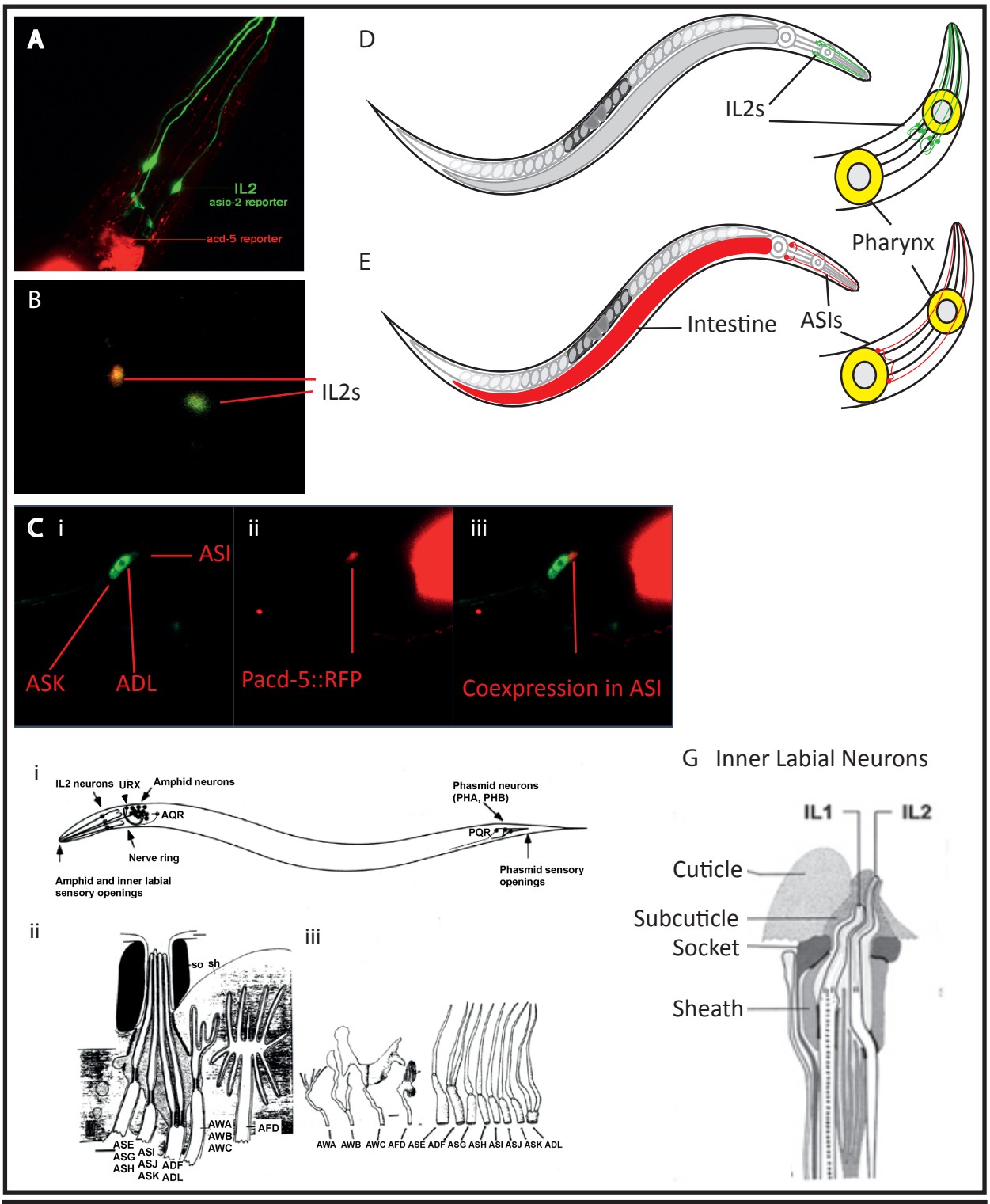

Fig.3.24: Expression patterns of *asic-2* and *acd-5*

A: The head of a worm expressing *Pasic-2::GFP-stop::UTR* and *Pacd-5::mcherry-stop::UTR*. B: A close up of the IL2 neurons expressing *Pklp-6::GFP-stop::UTR* and *Pasic-2::mcherry-stop::UTR*, the yellow hue shows co-expression. Ci: A dye filled worm expressing DiO (green). ii: The expression pattern of *Pacd-5::mcherry-stop::UTR.* iii: A dye filled worm expressing *Pacd-5::mcherry-stop::UTR* showing co-expression in ASI. D: A schematic of the expression of *Pasic-2::GFP-stop::UTR*. E: A schematic of the expression pattern of *Pacd-5::mcherry-stop::UTR.* Fi: The position of the inner labial neurons, amphid sensilla and nerve ring in the worm. Fii: A cross section of the amphid sensilla opening showing the socket (so), sheath (sh) and cilliated nerve endings. Fiii: the structre of the ciliated endings in different neuron classes (Perkins 1986). G: The structure of the inner labial sensilla (Bae and Barr 2008).

3.3.5 *acd-5 (ok2657)I* Worms Show Reduced Dispersal Behaviour Compared to N2 and *asic-2* Mutants.

In *C. elegans* dispersal after 10-15 minutes off of food is a behaviour known to be modulated by ASI. As *acd-5* is expressed in ASI, the dispersal of *acd-5* mutants was assayed. The speed of *acd-5 (ok2657)I* on food is already shown to be slower than that of N2, and dwelling is significantly increased in the mutant (Fig. 3.7). In order to test whether *acd-5* mutants are able to disperse normally, well fed worms were placed on plates with no food and recorded after half an hour. At this point N2 worms should be exhibiting dispersal behaviours: long forward runs and a reduction in turns. This can be measured by tracking the worms speed over a 5 minute window, a worm attempting to disperse will be moving faster than worms that are dwelling or locally searching. The original mutant allele of *acd-5* was tracked on the same days as the wild type, *acd-5* CRISPR alleles, rescues and RNAi strains. Worms were tracked using the multi-worm tracker and the mean of 8 assay repeats was plotted (Fig.3.25A). There was no significant difference in the speeds of the mutant strains off of food in comparison to the wild type. For each mutant strain there was a significant difference between the speeds in crawling off food and the speeds in crawling on food, P values were set at $P \leq 0.05$. Speed in rescue animals was further decreased and speed in RNAi animals was increased in comparison to wild type.

To elucidate whether 30 mins is the optimum wait time in for observation of a difference between local search behaviour and dispersal, the speed of *acd-5 (ok2657)I* and N2 worms was measured over 180 minutes from introduction to a food-free environment (Fig.3.25B). This shows that the speed in N2 worms does not reach its peak until the worms have been without food for 60 minutes. The assays were repeated in the same way as before but with a 1 hour wait off food before tracking (Fig.3.25C). After a wait of 60 minutes the speed of *acd-5 (ok2657)I* and *acd-5 (lj109)* mutants is significantly slower off food in comparison to wild type of the same condition (*acd-5 (ok2657)I* P=0.019, *acd-5 (lj109)* P=0.029). Also, although the speed of all mutants off food is higher than that of animals of the same strain on food, in *acd-5 (ok2657)* and *acd-5 (lj109)* mutants there is no significant difference between when they are off food compared to on food after 60mins.

This suggests that *acd-5* may be playing a role in the ASI-induced modulation of dispersal behaviour in *C. elegans*, either by helping to inhibit the AWC after extended periods without food, or helping ASI to recognise that the nutritional state of the worm has become less favourable.

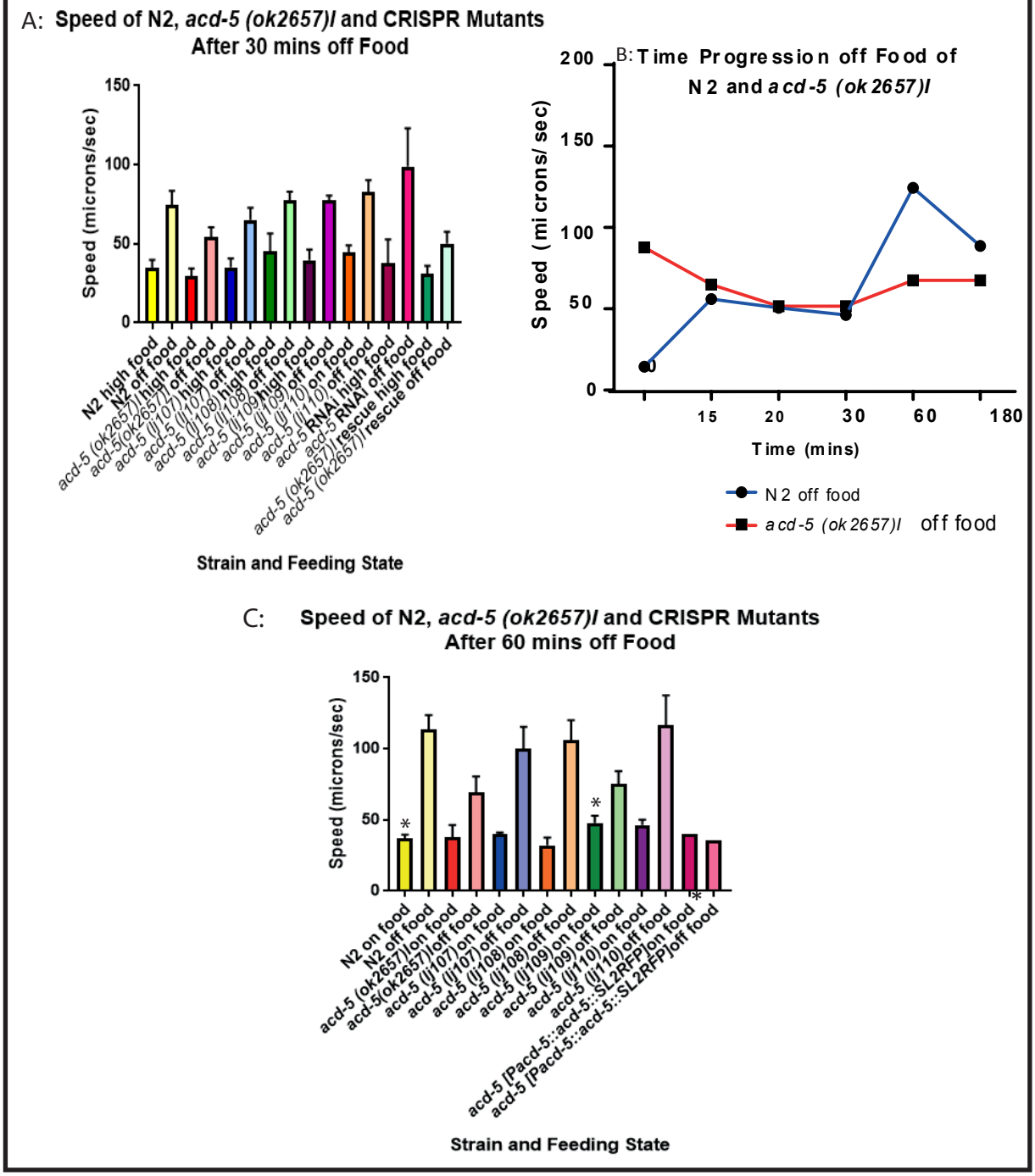

Fig.3.25: The speeds on and off of food for *acd-5* muants and N2 A: The average speed (microns/sec) of *C. elegans,* N2 and *acd-5* mutants on high food and after 30 mins off food. Error bars indicate the Standard Error of the Mean (SEM), bars indicate the average speed of 8 assays for each strain in each condition. Significance was calculated using a two tailed, unpired t-test, none of the mutantstrains moved significantly faster off food in comparison to N2. Only the RNAi and rescue did not move significantly faster off food in comparison to on food. B: The average speed of N2 and *acd-5 (ok2657)I* after set time intervals after moving from a food-rich plate to a plate with no food. C: The average speed (microns/sec) of*C. elegans,* N2 and *acd-5* mutants on high food and after 60 mins off food. Significance is shown with * above the bar in question, *= P,0.05. Significance was calculated using a two tailed, unpaired t-test comparing each mutant reslult with the N2 result under the same condition.Not shown on the graph is the significance between the on food and off food result for each strain. *acd-5 (ok2657)I* and *acd-5 (lj109)* are the only strins where the difference in speed between the two states is not signifcant.

3.3.6 ACD-5 is involved in chemosensation

Chemosensation and the sensing of the nutritional state of the worm is another process in which ASI is implicated. To test whether *acd-5* plays a role in chemosensation, mutant strains were tested alongside N2 for their ability to chemotax towards attractants, and to avoid repellents. Benzaldehyde, diacetyl and isoamyl alcohol (IAA) are known food cues in *C. elegans* (Bargmann & Horvitz 1991). Attractive and repellent concentrations of these odourants were added to plates and the chemotaxis index of the strains to, or away from them was measured. 1-octonol is a known repellent and repulsion to it is enhanced during starvation. So this was tested as well (Fig.3.25).

The chemotaxis index for *acd-5 (ok2657)*I was significantly reduced for attraction (P=0.0008) and repulsion to benzaldehyde (P=0.0001), and the mutant *acd-5 (lj109)* was significantly less repelled by a high concentration of benzaldehyde (P=0.0146). Although the difference was not significant*, acd-5 (ok2657)I* trends toward being more repelled by 1-octonol than any other strain.

Lysine is reported to be sensed by the ASI class of neurons, in preliminary experiments assaying the chemotaxis towards salt, tryptophan or lysine, *acd-5 (ok2657)I* is significantly less attracted to lysine than N2 (P=0.0022) (Fig.3.27).

Calcium imaging was used to determine if the behavioural anomaly in *acd-5 (ok2657)I* response to benzaldehyde can be seen on the cellular level. The response in ASI to 1:25 OP50:CTX buffer, 1% diacetyl in CTX and 1% benzaldehyde in CTX was tested by perfusion of the stimulus over glued worms . In N2 the ASI neurons responded well to OP50, this response was greatly reduced but still present in *acd-5 (ok2657)I* worms (Fig.3.28A and B). As expected from the behavioural data, no response in either N2 or *acd-5 (ok2657)I* ASI to diacetyl was seen (Fig.3.28C and D). The imaging data for benzaldehyde responses confirms the behavioural results; N2 ASI responded well to 1% benzaldehyde, but *acd-5 (ok2657)I* ASIs did not respond to benzaldehyde (Fig.3.28E and F). It has previously been shown that the AWC neurons are responsible for detecting benzaldehyde. Because dispersal behaviour and benzaldehyde responses are known to be triggered by AWC, it may be the case that the signalling between ASI and AWC is effected in *acd-5 (ok2657)I* mutants.

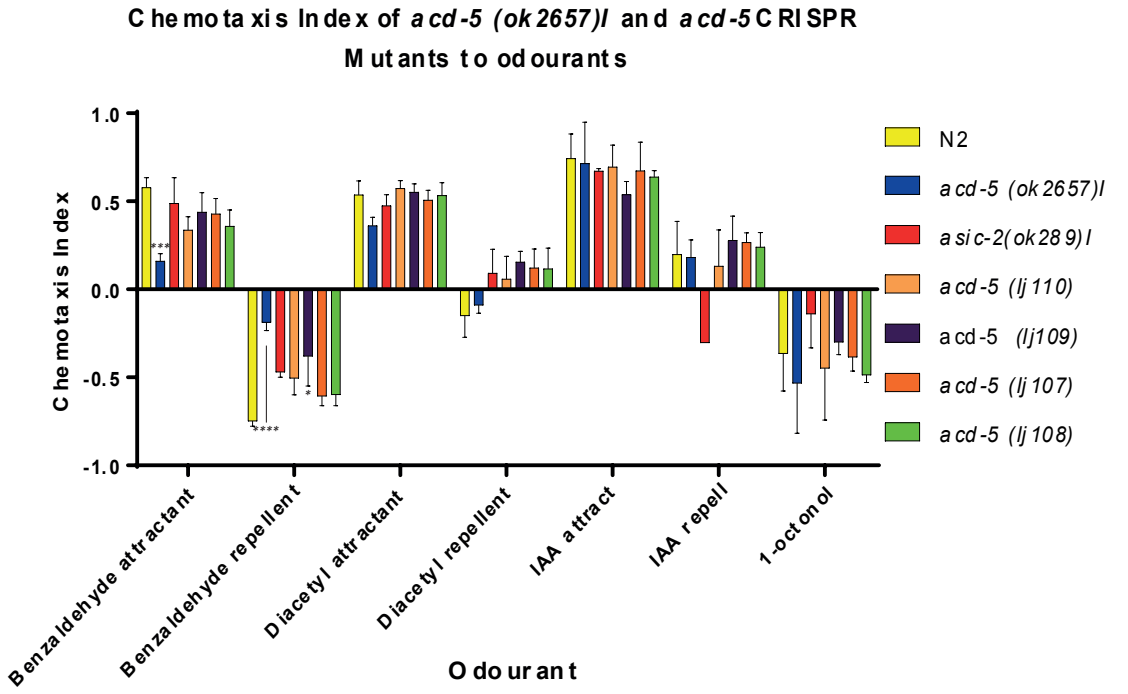

Fig.3.26: The chemotaxis Index of *C. elegans* N2 and *acd-5* mutants to attrative and repellant concentrations of Benzaldehyde, Diacetyl and Isoamyl aclohol, and a repellant concentration of 1-octonol. Bar colouration is indicated in the key, bars show the mean Chemotaxis Index (CI) of 8 assays each, for each strain and each condition. Error bars show the Standard Error of the Mean (SEM). Positive CIs indicate chemoattraction, while negative results indicate avoidance of the chemical. Significance is shown by stars above the result in question; *= P<0.05, **= P<0.01, ***= P<0.001 and ****= P<0.0001. Significance was calculated using a 2 way ANOVA, each mutant strain result was compared to the N2 result for the same condition.

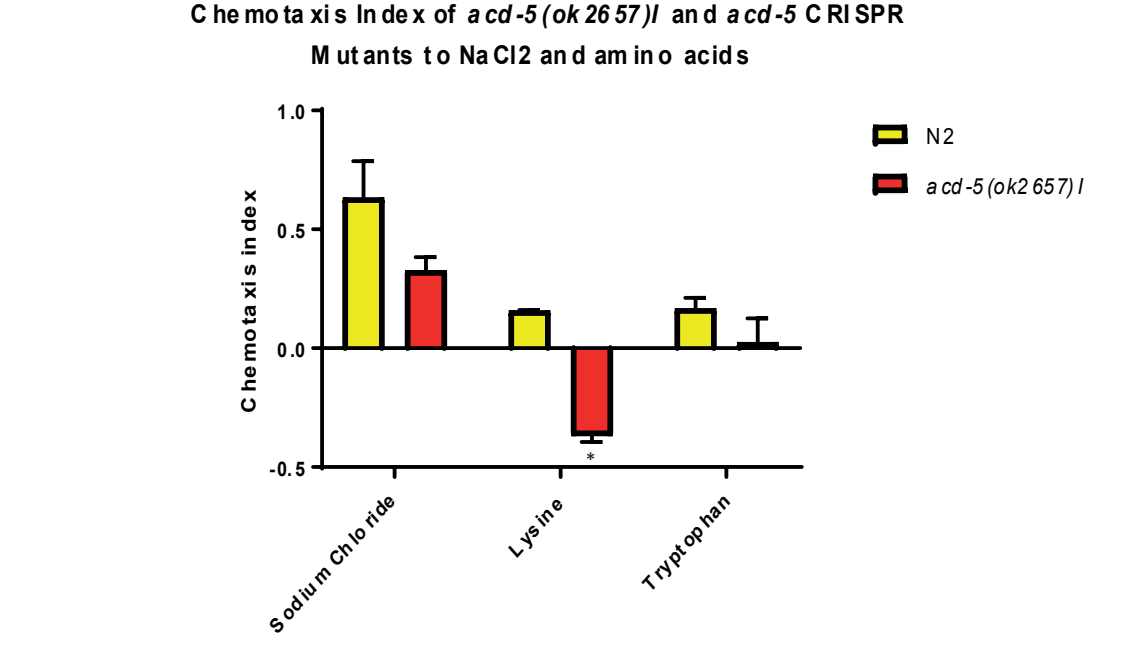

Fig.3.27: The Chemotaxis Index of *C. elegans* N2 and *acd-5* mutants to attractive concentrations of sodium chloride, Lysine and Tryptophan. Bar colouration is indicated in the key, bars show the mean of 3 assays each for each strain, in each condition. Error bars indicate SEM. Positive and negative results show chemoattraction and avoidance respectively. Significance is shown by stars above the resultin question; *= P<0.05, **= P<0.01, ***= P<0.001 and ****= P<0.0001.

A: N2 ASI mean trace in response to OP50

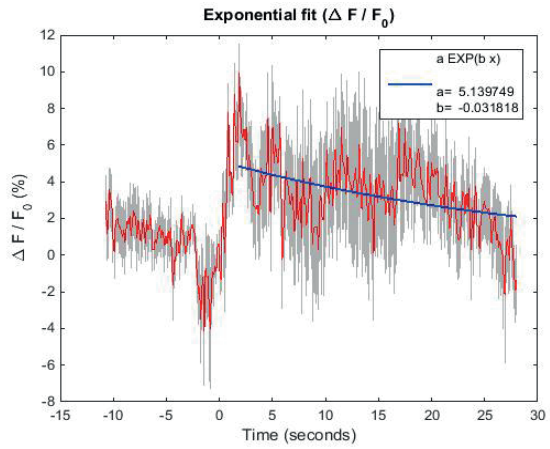

B: *acd-5 (ok2657)I* mean trace in response to OP50

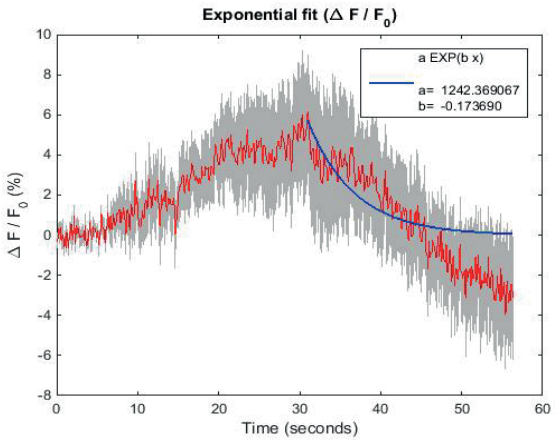

C: N2 ASI mean trace in response to Diacetyl

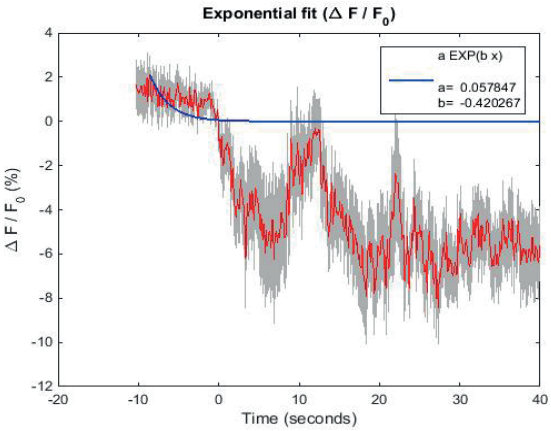

D: *acd-5 (ok2657)I* mean trace in response to Diacetyl

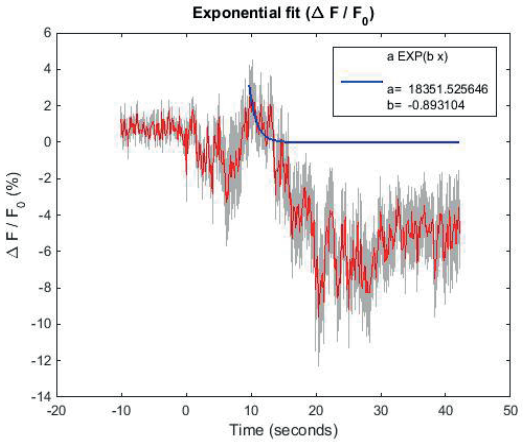

E: N2 ASI mean trace in response to Benzaldehyde

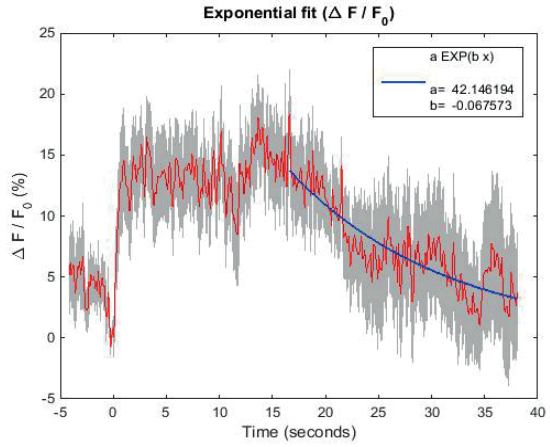

F: *acd-5 (ok2657)I* mean trace in response to Benzaldehyde

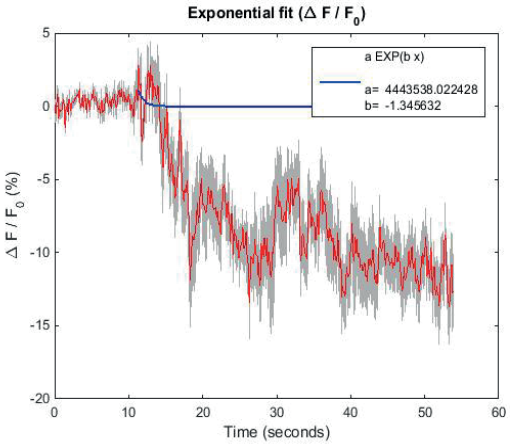

Fig.3.28: Calcium Imaging Results For ASI in *acd-5 (ok2657)I* A: Mean trace of the response in ASI N2 to 1:25 OP50 overnight culture:CTX buffer. Red line is the mean, grey shaded area is response range, blue line is the best fit exponential degradation of the calcium dissociation. Stimulus is applied a 0s and lasts 15s. Recordings lasted for 50s. B: Mean trace of the response in *acd-5 (ok2657)I*ASI in response to 1:25 OP50 overnight culture:CTX buffer. C: Mean trace of the response in N2 ASI in response to 1% Diacetyl in CTX. D: Mean trace of the response in *acd-5 (ok2657)I* in response to 1% Diacetyl in CTX. E: Mean trace in N2 ASI in response to 1% Benzaldehyde in CTX. F: Mean trace in *acd-5 (ok2657)I* ASI in response to 1% Benzaldehyde in CTX.

3.3.7 Mutations in *asic-2* Do Not Affect Chemosensation

The IL2s have also been suggested to have a role in chemosensation, therefore *asic-2 (ok289)I* was assayed alongside the *acd-5* mutants (Fig.3.26). The *asic-2* mutant does not respond to any of the odourant conditions in a significantly different manner to N2. There is an avoidance trend to repelling concentrations of IAA where there is not in any other strain, but there was no significant difference.

3.3.8 Mutations in *acd-5* and *asic-2* Do Not Affect Egg Laying Rates On and Off Food.

As nutritional state affects the rate at which wild type *C. elegans* lay eggs, *acd-5* and *asic-2* mutants were assayed to see if there were any difference from wild type in the rate of egg laying on and off food. Ten individuals of each strain were allowed to crawl on seeded and un-seeded plates for 6 hours and the number of eggs was counted after this time (Fig.3.29). There was no significant difference between the numbers of eggs that mutants laid on food in comparison to the number laid on food by N2. Similarly there was no significant difference between the numbers of eggs laid off food by mutant strains than laid by N2 off food. This shows that *acd-5 (ok2657)I* mutants are able to detect the difference in nutritional state between and on food and off food environment.

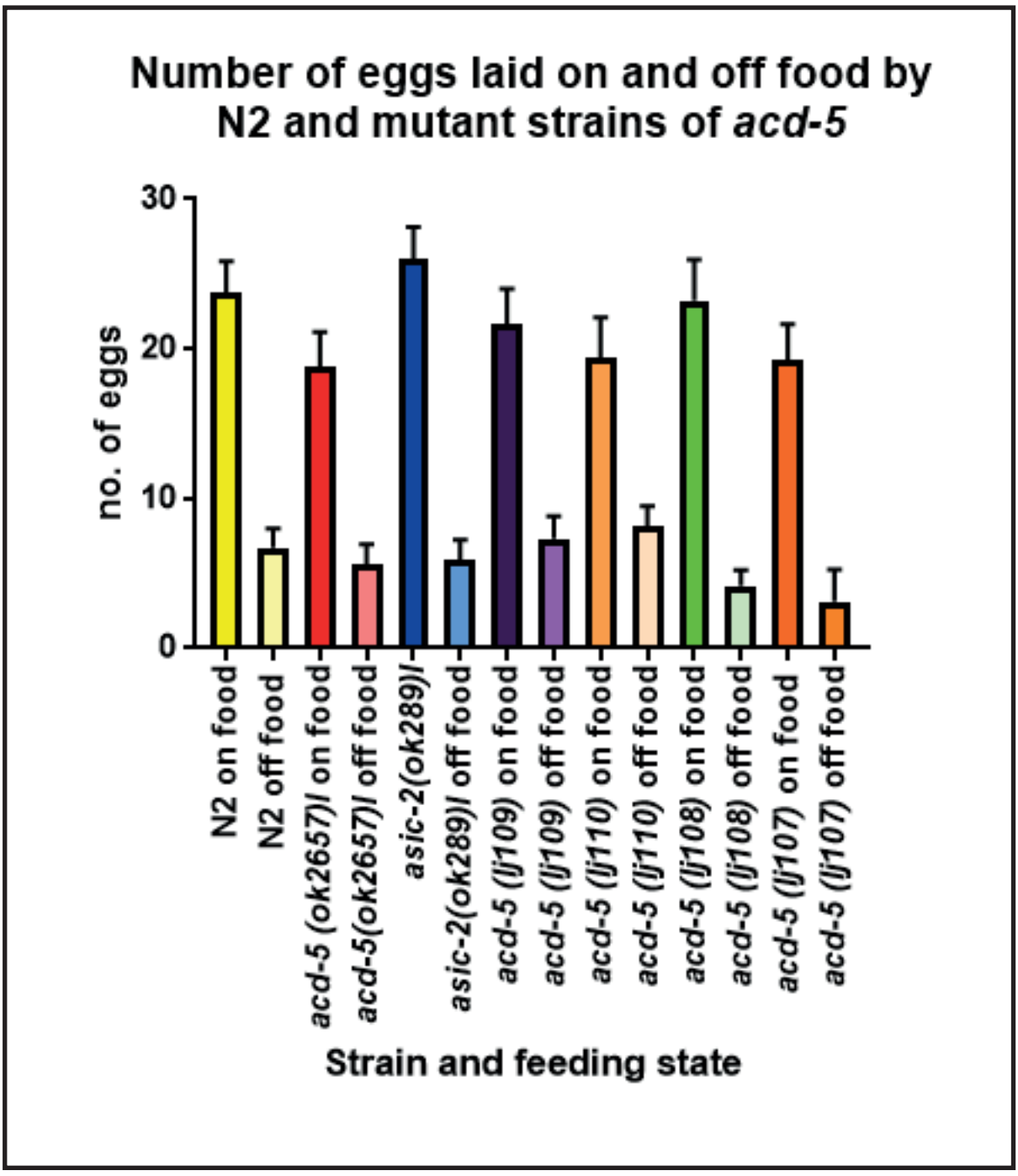

Fig.3.29: The mean number of eggs laid on and off food by *C. elegans,* N2, *asic-2 (ok289)I* and mutant strains of *acd-5*. Darker shades of alloted colour per strain are for results on food, pale shades are for results off food. Error bars indicate the SEM (Standard Error of the Mean). Eggs were laid over a period of 6 hours for both on and off food conditions for each strain, all experiments were run in parallel.

3.3.9 ACD-5 and ASIC-2 Affect Dauer Entry

Preliminary data suggests that both ACD-5 and ASIC-2 play a role in dauer arrest. In a previous screen of expression levels of different genes throughout *C. elegans* development, *acd-5* was expressed at its highest level in the dauer worm. It has also been found that receptors for C3 and C6 are expressed in ASI. *asic-2*, on the other hand, is highly expressed in L1 worms, the stage at which the decision to enter dauer arrest is made. As the IL2s are greatly influenced by the dauer stage, there is a chance that *asic-2* affects dauer entry.

A dauer assay was run per the method developed by the Butcher lab; N2, *acd-5 (ok2657)I* and *asic-2 (ok289)I* were assayed on two plates each of either control plates, containing no exogenous dauer pheromone, or plates containing crude dauer pheromone, C3 ascaroside, C6 ascaroside or C9 ascaroside. The number of dauer worms was counted after 9 days and the mean of the repeats was plotted (Fig.3.30). Both genes seem to have some effect on dauer entry, but the effects are different and only one result is significant. *acd-5 (ok2657)I* worms arrest in dauer stage at equivalent levels to N2 on control plates and plates containing C9. On crude pheromone plates dauer arrest is mildly reduced in *acd-5 (ok2657)I* mutants in comparison to N2. Interestingly, dauer arrest is increased in the *acd-5* mutant on plates containing C3 or C6, the two ascarosides that ASI is known to express receptors for.

Conversely, *asic-2 (ok289)I* mutants have greatly reduced dauer entry on plates containing any of the ascarosides, but equivalent levels in control and crude conditions. This may mean that *asic-2* mutant animals fail to detect the three ascarosides tested, but are able to detect other components of the pheromone that are present in the crude conditions.

Further experimentation is required in order to draw confident conclusions here as only two repeats were performed, each with large SEM.

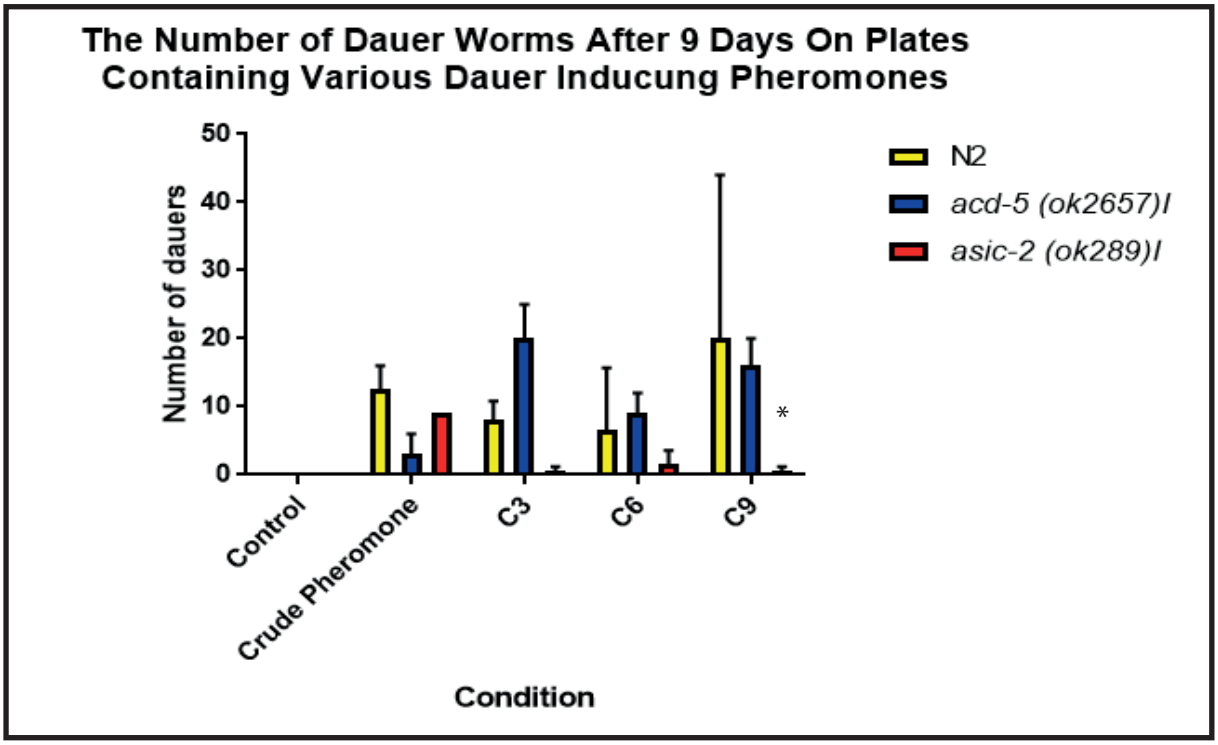

Fig.3.30: The number of dauers for N2, *asic-2 (ok289)I* and *acd-5 (ok2657)I* on plates containing crude dauer pheromone or the ascarosides C9, C6 or C3. A star above the approprate bar indicates significance, * = P<0.05.Significance is calculated using 2 way ANOVA and comparing each mutant strain to the N2 result under the same condition.

3.3.10 ACD-5 and ASIC-2 Affect Lifespan in Opposite Ways

As discussed in the introduction, the ASI plays an important role in modulating longevity in worms. The *acd-5* mutants were tested for abnormalities in lifespan. To provide more information, the health-span of the worms was also tested. The IL2s also have a role in dauer formation, since dauer pathways and longevity tend to be linked; *asic-2* mutants were also tested for health and lifespan. Worms were assessed on a daily basis from day 1 adults to death; the percentage of live worms left on each day is plotted in Fig.3.30. The speed and pumping rate of 6 individuals for each strain was tested daily as a measure of health-span, these are plotted in Fig.3.32.

The lifespan of *acd-5 (ok2657)I* was significantly reduced in comparison to wild type N2s. The pumping rate of the mutant was comparable to wild type in the early stages of life, but the rate declined significantly faster than in N2, suggesting that both health-span and lifespan are in some way controlled by ACD-5. The CRISPR mutants *acd-5 (lj108), acd-5 (lj109)* and *acd-5 (lj110)* had only a slightly reduced lifespan, none were significantly different to wild type, the same is true for pharyngeal pumping rate in these mutants.

The decline in speed over the worm's lifetime can be used as another measure of health-span. The decline in speed over the lifetime of *acd-5* mutants was not significantly different to wild type. The mutant has a slower rate of speed in early life stages in comparison to N2, which may reduce the rate of decline in speed over the mutant lifetime, giving a false representation of the mutant health-span. There are also some constraints with the multi-worm tracker when analysing slow or paralysed worms; non-moving worms are considered to be debris or dents on the agar and are automatically excluded from the results by the analysis program. It was noted that *acd-5 (ok2657)I* mutant worms stop moving at around 9 days, while N2 worms are still mobile until around 18 days. The data collected by the multi-worm tracker does not reflect these observations.

The *asic-2 (ok289)I* mutant had a significantly increased lifespan in comparison to N2; the pumping rate remained high for longer than in N2 and the rate of decline was significantly slower. This suggests that ASIC-2 is having the opposite effect on health and lifespan in wild type individuals. The CRISPR mutant asic-2 (lj112) also has an increased life and health-span, although this is not significantly different to the wild type. . The CRISPR mutants *asic-2 (lj111)* and *asic-2 (lj113)* also had a lifespan comparable to, but slightly shorter than, N2; however, their pumping rate was slightly higher than N2 over the latter stages of life, suggesting an increased health-span in these worms.

A surprising result is that the CRISPR mutant *acd-5 (lj107)* had a significantly increased health and lifespan in comparison to wild type. As the structural change in the ACD-5 channel subunit mutant is fairly comparable to that of *acd-5 (ok2657)I* it would be expected to have a similar phenotype. This may suggest that ACD-5 is playing some role in the modulation of longevity, but if different alleles are resulting in opposite effects on lifespan, this role is not entirely clear.

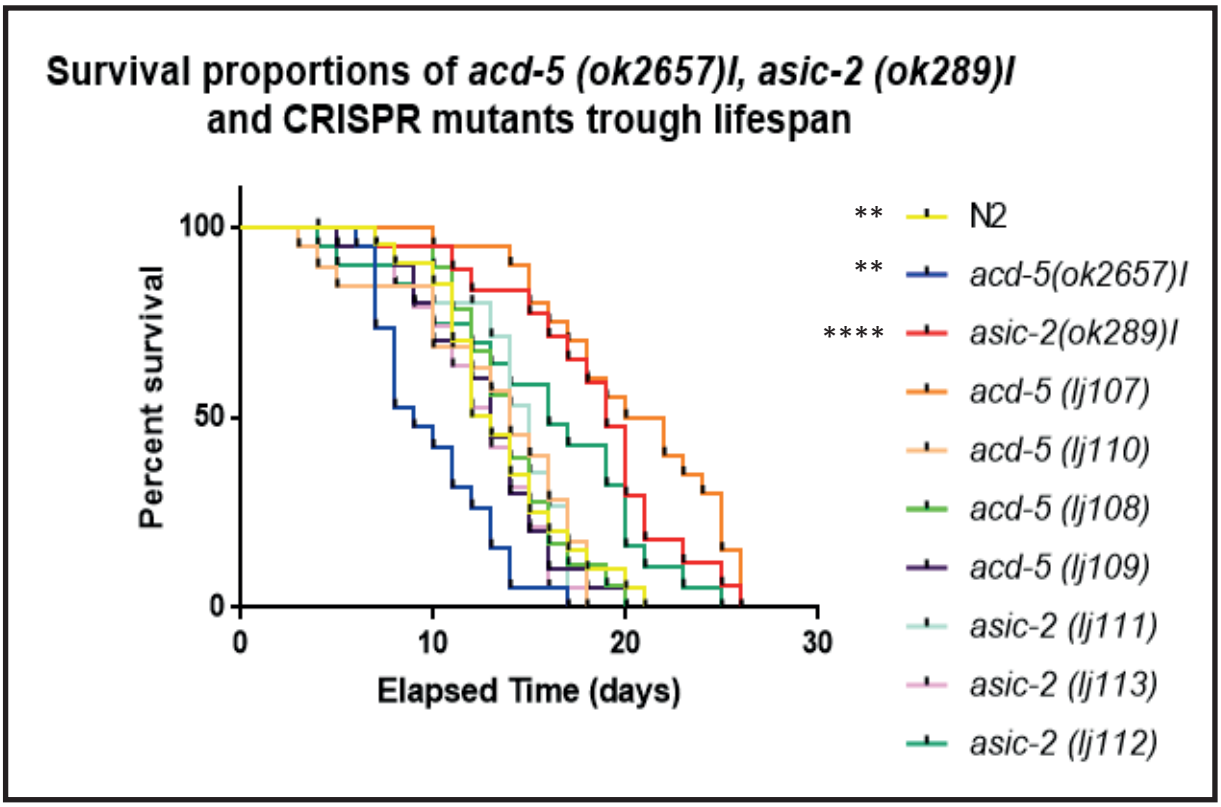

Fig.3.31: The percentage survival of N2 and mutants strains of *acd-5* and *asic-2*. Each strain began with 20 live individuals on day 1, L4 larvae were picked on day 0. The number of surviving adults was counted on each subsequent day, and the percentage of live worms left was calculated and plotted. Survival plot colours are as detailed in the key. Significance is denoted by stars next to strain names in the key, *= P<0.05, **= P<0.01, ***= P<0.001, ****= P<0.0001. All strains were compared to N2 to determine significance. The Log-rank (Cox-Mantel) test was used to determine significance between survival plots.

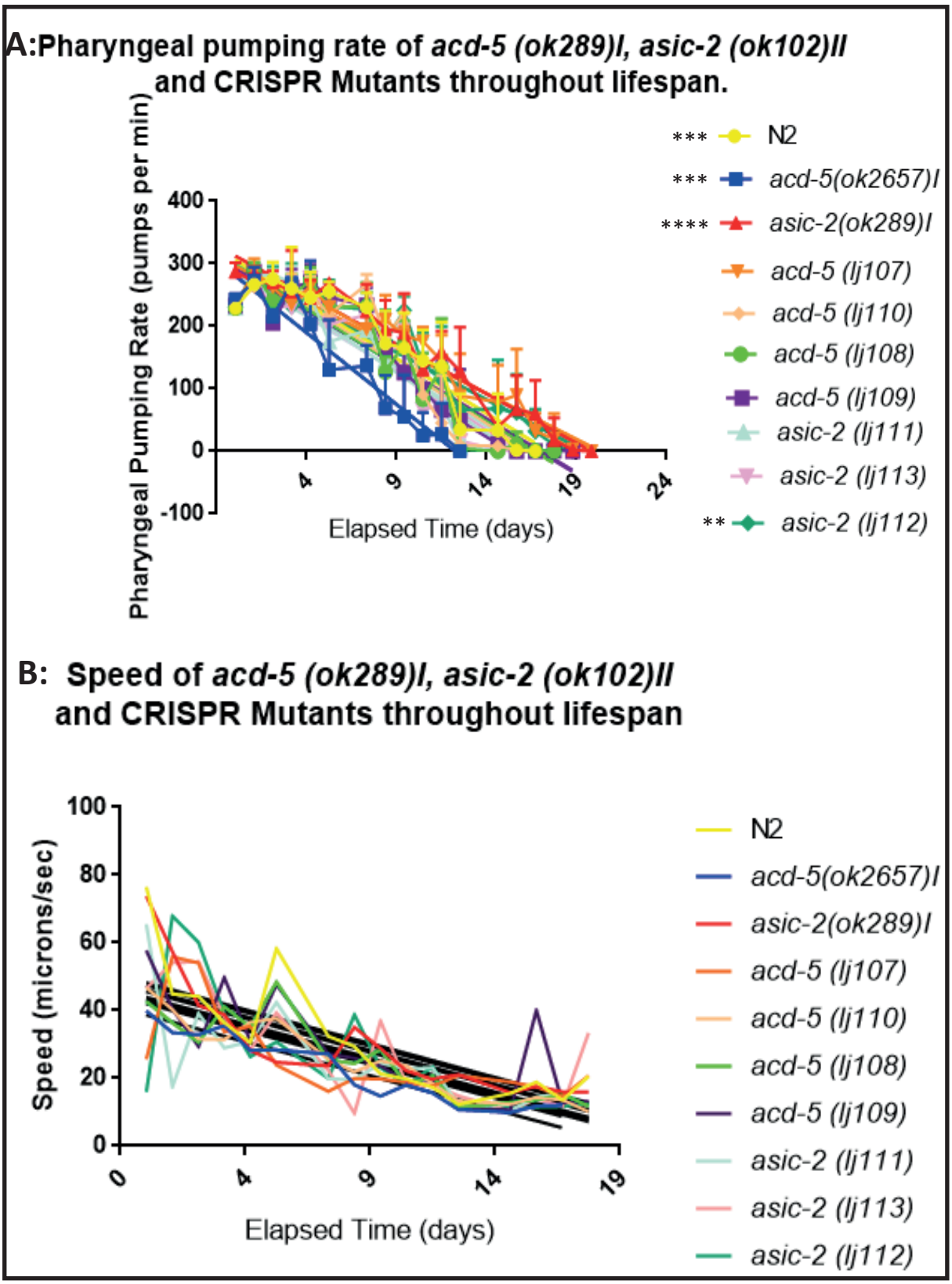

Fig.3.32: Healthspan measurements for mutants of *asic-2* and *acd-5.* A: The rate of pharyngeal pumping over the lifespan of *C. elegans* N2 and mutants of *acd-5* and *asic-2*. Non-linear regressions are fit to each degradation, colours match the regression for each strain (see key). For comparison the slope of each non-linear regression was compared to the slope for N2, significance is shown as a* next to the appropriate strain in the key. * = P<0.05, ** = P<0.01, *** = P<0.001, **** = P<0.0001 B: The meanspeed of the strains over their lifespan, for coloration of lines see the key. Non-linear regressions are fit to each degradation, shown in black. For comparison the slope of each non-linear regression was compared to the slopefor N2. None were significant.

3.4 Discussion

Both mutant genes examined appear to have aberrations in functions that fit with those already known about the neurons in which they express and, although these genes do not seem to be acting in the same genetic pathways, there is some overlap in their effects.

3.4.1 *acd*-5 Functionality

acd-5 seems to be involved in a number of functions controlled in part by ASI, suggesting a function in the over-all working of the neuron. A number of the functions that *acd-5* mutants display abnormal phenotypes for seem to insinuate a gain of function for ASI in the mutant.

3.4.1.1 Lifespan

The shortened lifespan of *acd-5* mutants may be explained by over-active ASI neurons. It has been show previously that DAF-2 induces phosphorylation of DAF-16 (Lin et al. 2001), a gene important for stress response, rendering it inactive. DAF-16 stimulates the transcription of a number of genes involved in the stress response pathway, including *skn-1*, also important for stress response (Murphy et al. 2003). DAF-2 expression is modulated by DAF-7/TGF-β, which is released from ASI (Murakami et al. n.d.), if the ASI neurons in *acd-5* mutants were over-active the levels of DAF-7/TGF-β would be expected to be higher, and in turn DAF-2 expression would be heightened. This would lead to the increase in phosphorylation of DAF-16 and a reduction in expression of stress response genes like *skn-1*. As depletion of *skn-1* and *daf-16* result in a shortened lifespan (Tullet et al. 2008), it can be theorised that *acd-5* mutants may have a shorter lifespan due to an over-production of DAF-7 causing an inhibited stress response. This would also explain the reduction in health-span of the mutant. In order to test this theory, plasmids have been made expressing a *daf-7::mcherry* fusion under *Pdaf-7*, a cell specific promoter for ASI. Neurotransmitters in *C. elegans* are collected in the coelomocytes after action, and the intensity in brightness of fluorescently tagged neurotransmitters in the coelomocytes can be used as a measure of the level of expression of that transmitter (Lee et al. 2011). These fusions will be injected into the mutant and wild type worm to identify any difference in the expression levels of DAF-7 in the transgenics.

Another theory is that ACD-5 itself is involved in the stress response. Previous studies have determined that ACD-5 may be regulated by DAF-16 (Delaney et al. 2017), indicating that it is part of the stress response pathway. It is also up regulated in bacterial infection, a stressful condition, and dauer larve, where the worm is under considerable stress (Engelmann et al., 2011, WormBase). ACD-5 also shares an expression pattern with SKN-1, known to work in p38-MPAK pathway (Bowerman et al. 1992). This theory does not explain the multiple other phenotypes that *acd-5 (ok2657)I* mutants exhibit. A test for this idea would be to cross *acd-5 (ok2657)I* worms with *daf-16* mutant worms. If the two genes are having the same effect, no change in phenotype would be expected. If they are not, rescue of the shortened lifespan would be seen.

3.4.1.2 Chemosensation

In DAF-7/TGF-β pathway mutants the expression levels of a subset of chemoreceptors in ASI are altered. Expression of the receptors SRA-6, STR-1 and STR-3 are significantly reduced in the ASIs of TGF- β pathway mutants, whereas STR-2 expression is strongly up regulated (Nolan et al. 2002). In wild-type animals STR-1 and STR-3 are strongly expressed in ASI and STR-2 is only weakly expressed in this class of neurons, but is expressed strongly in either the left or right AWC; the expression levels in AWC remains unchanged in TGF- β signalling pathway mutants (Nolan et al. 2002). STR-2 is

involved in the chemotaxis towards attractive concentrations of benzaldehyde, therefore a reduction in attractive response to 1% benzaldehyde in *acd-5* worms may be explained by a reduction in expression of this receptor in ASIs if they are producing higher amounts of DAF-7; the maintenance in STR-2 levels in AWC would explain why attraction to benzaldehyde in the mutant is not lost completely.

STR-2 is only involved in chemotaxis to attractive concentrations of benzaldehyde, so decreased expression of this protein cannot explain the significant reduction in *acd-5* mutant's avoidance of high concentrations of benzaldehyde. The receptor ODR-3, along with GPCRs, is responsible for the avoidance of noxious concentrations of volatile odorants, such as benzaldehyde and IAA, and is expressed in AWC (Roayaie et al. 1998). These receptors are also involved in chemotaxis towards attractive concentrations of these substances. The reduction in attraction and avoidance to benzaldehyde could be explained by a reduction in signalling between AWC and ASI. AWC makes many connections to ASI (White et al. 1986), and ASI is known to have an inhibitory effect on AWC after the prolonged absence of food (Gray et al. 2005). In this case, the same reduction in responsiveness would be expected in chemotaxis towards/away from attractive/repulsive concentration of IAA, yet no such reduction is observed.

A further, different, explanation could be that ASI has the capability to detect both attractive and repulsive concentrations of benzaldehyde and this is why the reduction in response in *acd-5* mutants is unique to this odorant. Further investigation of this network is needed to establish the true role of ACD-5 in the response to benzaldehyde. Calcium imaging shows that ASI does respond to benzaldehyde in wild type worms, and that this response is depleted in *acd-5 (ok2657)I* mutants. A strain expressing Cameleon in AWC has been produced and the next step of experimentation will be to test the responsiveness of AWC to benzaldehyde at attractive and repellent concentrations in the wild type and *acd-5* mutant worm. If the response is the same in both genotypes then inhibition of the AWCs by an over-active ASI can be ruled out.

AWC is not known to have any presynaptic connections to ASI, making it unlikely that a reduction in benzaldehyde responsiveness is due to a fault in signals provided from AWC to ASI. AWC only expresses two neurotransmitters, *nlp-1* and glutamate, and has no gap junction connections (White et al. 1986). To test whether AWC is signalling to ASI during benzaldehyde sensation, the responsiveness of the ASI to benzaldehyde can be tested in animals with knockdown of *nlp-1* and *eat-4* in AWC (*eat-4* mutants are defective in glutamate signalling). If a reduction in benzaldehyde responses in ASI in knockdown animals is observed then it is possible that AWC can convey messages to ASI in response to odourants. In this case the mutation in *acd-5* could cause a signalling defect between AWC and ASI. The expression levels of STR-2 should also be examined in the *acd-5* mutant to determine if the expression level of this receptor is reduced in *acd-5 (ok2657)I*.

The decrease in chemoattraction to lysine and the decrease in calcium transients in response to OP50 cannot be explained by this model as ASI is involved in the sensation of lysine and nutritional state. If the neuron were hyper-active this response would be expected to be higher.

3.4.1.3 Male Attraction

Male attraction in hermaphrodites was not observed in *acd-5* mutants. If the ASI was over-active in these worms this phenotype would not be expected, as suppression of the behaviour would be increased. To elucidate if this is the case *acd-5* mutant males could be examined to determine if male attraction in these animals is reduced.

3.4.1.3 Locomotion

The locomotion of *acd-5* mutants is changed significantly from wild type, although it is still not clear how the gene could be modulating some of the behaviours. The dorsal bend bias of this mutant is consistently observed, but there is no obvious biological explanation for this phenotype. Bending phenotypes could be caused by a number of defects, in musculature, neuronal signalling or perturbations in proprioception. Since ASI is not directly involved in any of these functions it is unclear what role the ACD-5 protein could be playing.

ASI is responsible for gathering information on the nutritional state of the worm, and modulating responses to favourable/poor environmental conditions (You et al. 2008). In unfavourable conditions DAF-7 is suppressed and dauer arrest or stress responses are triggered. If the ASI were constantly telling the worm that conditions are favourable the impetus to seek out a food source would be down regulated. The low speed of *acd-5 (ok2657)I* off food can be explained by this scenario, the ASI could be signalling that the environment is favourable and therefore food is not sought so avidly as it is in wild type. If this were the case it would be expected that *acd-5* mutants would show a higher rate in egg laying off food than wild type, however, this result is not observed in the egg laying assay. Once again, this theory can be tested by quantifying the level of DAF-7 expression in the mutant. Further experiments could be performed looking at *daf-28* and *daf-11* expression; DAF-28 is a neurotransmitter released from ASI when conditions are favourable (Li et al. 2003). A *Pdaf-7::daf-28no stop::Mcherry* fusion plasmid has been created and injection into both mutant and wild type worms will be used to see if accumulation of DAF-28 in the coelomocytes is greater in the mutant than the wild type. DAF-11 is a receptor expressed in ASI that is also involved in determining if environmental conditions are favourable (Murakami et al. n.d.). Fusions of this gene expressed under *Pdaf-7* may indicate whether the expression level of the receptor is higher in the mutant.

If ASI were over-reactive in general, but not the DAF-7/TGF- β pathway specifically, a reduction in local search behaviour when removed from food would be expected, as would an increase in dispersal behaviour. This does not seem to be the case, as the speed of *acd-5 (ok2657)I* off of food is slower than wild type, suggesting that AWC is not being over-inhibited by ASI. Additional testing for this could be carried out by tracking *acd-5* mutants off of food on the single worm tracker. If ASI were over-active in general, it would suppress the number of omega turns and reversals within a 30 minute range of the worm being removed from food, and dispersal would be expected to begin within a shorter time frame.

The situation on food is different; AWC does not induce a higher number of turns and reversals when there are favourable conditions (Gray et al. 2005). On food omega and upsilon turn events are reduced in number in the *acd-5 (ok2657)I* mutants in comparison to N2, but the duration of each individual event is lengthened. Also, reversals are more common and the distance travelled in backwards locomotion is increased over the time of recording. Speed is decreased and time spent dwelling is greater. It has previously been shown that dwelling on food is up regulated in mutants with ciliated neuron defects (Fujiwara et al. 2002b), which may be the reason ASI defective mutants dwell more. Also, this behaviour could be explained if the worms are experiencing a higher rate of satiety in the mutant than the wild type. As previously discussed (3.1.4.9), ASI regulates satiety quiescence, promoting entry into a quiescent state (Gallagher et al. 2013). Increased DAF-7/TGF- β signalling could induce more regular bouts of sleep on food in *acd-5* mutants than seen in wild-type. As the assay for satiety quiescence is very sensitive, the best way to determine if this is the case

would be to send to worms to the You lab for them to determine if *acd-5 (ok2657)I* worms have a satiety quiescence phenotype.

3.4.1.4 Dauer

If it is the case that ASI is over-promoting signalling for favourable conditions in the mutant worm it is to be expected that the mutant would have a dauer defective phenotype. As discussed in the introduction (3.1.4.5) ASI has receptors for the ascarosides C3 and C6 (Park et al. 2012), preliminary dauer assay results show a larger number of dauer larvae upon introduction of the ascaroside to well fed *acd-5 (ok2657)I* worms than do wild type worms. This implies that DAF-7 signalling is not hyper-aroused in *acd-5* mutants, unless exogenous ascarosides exert a more powerful affect on the worm than the TGF-β signalling pathway. An interesting experiment to run with these worms would be to observe the number of dauers produced during starvation, rather than upon introduction of exogenous dauer pheromone. If the mutant worms produce significantly fewer dauers in these conditions than wild type it could be determined if they have a dauer defective phenotype. Further evidence for a role in dauer arrest for ACD-5 is the fact that its expression is down regulated by a glucose rich diet (Lee et al. 2015) and that expression levels are highest in the dauer worm (WormBase). The lack of ACD-5 in the mutant worm may cause problems in the maintenance of the dauer arrest if it is so highly expressed at this stage. To test whether maintenance of dauer arrest is problematic for the mutant, dauer stage could be induced with C3 or C6 ascaroside and once dauer arrest is achieved the worms could be washed and allowed to self fertilise on unseeded plates. The duration of dauer arrest in N2 and mutant could be compared to determine whether the mutant cannot maintain the state.

3.4.2 ASIC-2 Functionality

Dauer formation and lifespan are the two areas where the phenotypes of the two DEG/ENaC subunits overlap, if in opposite ways. ASIC-2 mutants display a pronounced reduction in dauer arrest induced by the individual ascarosides and exhibit a lengthened lifespan in comparison to wild type. At present there is no evidence to suggest that the IL2s play a role in the lifespan of *C. elegans,* but genes involved in the dauer pathway often have an effect on longevity. Further evidence to suggest that ASIC-2 is involved in the dauer pathway in some way is that the gene is highly expressed at L1 stage, the time at which the decision to enter dauer arrest is made (WormBase) and expression is increased in the adult after starvation (Mueller et al. 2014).

There is still no clue as to why a mutation in this gene would induce a dorsal bend bias, or why this locomotory phenotype would be linked to a defect in dauer arrest. It is also not clear whether the two genes are working together. It is possible to surmise from the data collected that, although the tracking system does not always cluster together genes working in the same pathway, it is able to cluster genes together that work in similar pathways.

3.4.3 Troubleshooting

3.4.3.1 Rescues

Many of the phenotypes observed in *acd-5 (ok2657)I* worms could not be rescued using cDNA expressed cell specifically in ASI or under its own promoter. The reasons for this are still unknown, but one explanation could be that the unusual introns in the gene are having some sort of regulatory function. *acd-5* is unlike many genes in that it has a number of large introns at the beginning of the gene (Fig.3.24A), with the main coding sections confined to the last quarter. Such large introns shortly after the start of the coding region are frequently important for regulatory control. For this reason the full gene has been amplified from genomic DNA, rather than cDNA, and plasmids have

been made expressing this under both *Pacd-5* and *Pdaf-7*. It is hoped that inclusion of the introns in the rescue will result in a full rescue of the various phenotypes of *acd-5 (ok2657)I.*

Another cause of the lack of rescue could be that background mutations are causing the phenotypes rather than mutations in *acd-5*. If this were the case expression of the cDNA would not eradicate the aberrations.

If the loss of the 2nd transmembrane domain in *acd-5 (ok2657)I* mutants results in a dominant gain-of-function for ASI signalling there may be a chance that expressing the rescue construct in a mutant background does not rescue mutant phenotypes as many irregular channels still exist. There is a chance that the combination of mutant and wild-type DEG/ENaC subunits could exacerbate the existing problem and could explain why phenotypes became more pronounced upon expression of the rescue. This may also explain why RNAi of the *acd-5* gene resulted in an opposing phenotype, as the channel subunits would not be expressed in these worms, perhaps creating a loss of function mutation.

3.4.3.2 Outcrossing

Due to the possible contributions of background mutations, many attempts were made to outcross the *acd-5 (ok2657)I* mutants with no success. Outcrossing is a process by which background mutations in a mutant strain can be bred out of a population. Many mutation techniques can cause a number of genes to be mutated in the worm, and without outcrossing, it cannot be certain that the phenotypes observed are caused by mutations in the gene being analysed. In *C. elegans* research it is customary to outcross a mutant 6 times to the wild-type strain; this involves mating wild type males to mutant hermaphrodites resulting in heterozygote F1s, genotyping of the F1s is used to confirm heterozygosity. The F1s are then mated with N2 males to create a population with the expected offspring ratios of ¼ wild type homozygote, ½ heterozygote and ¼ mutant homozygote. Males from this cross are then mated with N2 hemaphrodites and a number of the F1s are selfed to individual plates and allowed to lay eggs. Once the F1 has laid sufficient eggs it is lysed and genotyped to confirm heterozygosity. Heterzygotes are then mated with N2 males and the procedure is repeated twice more. In *acd-5 (ok2657)I* mutants heterozygosity is lost in between the first genotyping and second, even when large numbers of F1s are selfed. This could be explained if the *acd-5* mutant males do show a reduction in male mating behaviour, as the homozygote N2 males created in the first cross would win out against the dysfunctional *acd-5* mutant males in the second cross.

The fact that many of the phenotypes observed in *acd-5 (ok2657)I* mutants are in processes in which ASI is involved is promising. Also the fact the CRISPR mutations in this gene regularly result in similar phenotypes, if greatly reduced in severity, points toward *acd-5* mutations causing the phenotypes observed. To prove this, further attempts will be made to rescue the phenotypes and outcross the mutants, but new methods must be used to overcome previous issues.

3.4.3.3 Dauer Numbers

An issue that arose from experimentation with *asic-2* mutants was the low number of dauers that could be produced to use for experiments. Attempts were made to observe fluorescent IL2 neurons in the dauer *asic-2 (ok289)I* animals to determine whether or not the neurons are still able to branch as they do in wild type. However, the lack in number of dauers and low transmission rate of *Pklp-6::mcherry*, meant that at no point was a dauer *asic-2 (ok289)I* with fluorescent IL2s produced. The proof that *asic-2* mutants do not have a defect in nictation suggests that the IL2 dendrites in the few

dauers produced are probably arborised, as this process has been found to be necessary for nictation.

3.4.3.4 Differences in Tracking Repeats

Some differences were observed in the original tracking data collected in 2011 when compared to the repeat tracking experiments performed in 2016 and 2017. This can be explained by the different environments in which the trackers were housed in these two periods. In 2011 the trackers were housed in a non-air-conditioned room with large south-east facing windows. As *C. elegans* do not like high temperatures or sunlight the amount of time spent coiled in the older experiments may be a reflection of the less favourable experimental conditions. In 2013 the LMB moved to new premises, and the trackers were housed in an air-conditioned room with no windows. These conditions are likely to have been more favourable for the worms and a reduction in speed and coils in most mutants was observed.

3.5 References

Adler, J., 1975. Chemotaxis in Bacteria. *Annual Review of Biochemistry*, 44(1), pp.341–356. Available at: http://www.annualreviews.org/doi/10.1146/annurev.bi.44.070175.002013 [Accessed October 1, 2017].

Ailion, M. & Thomas, J.H., 2000. Dauer formation induced by high temperatures in *Caenorhabditis elegans*. *Genetics*, 156(3), pp.1047–67. Available at: http://www.ncbi.nlm.nih.gov/pubmed/11063684 [Accessed October 2, 2017].

Albert, P.S. & Riddle, D.L., 1983. Developmental alterations in sensory neuroanatomy of the *Caenorhabditis elegans* dauer larva. *The Journal of Comparative Neurology*, 219(4), pp.461–481. Available at: http://doi.wiley.com/10.1002/cne.902190407 [Accessed September 29, 2017].

Alcedo, J. & Kenyon, C., 2004. Regulation of *C. elegans* longevity by specific gustatory and olfactory neurons. *Neuron*, 41(1), pp.45–55. Available at: http://www.ncbi.nlm.nih.gov/pubmed/14715134 [Accessed October 2, 2017].

An, J.H. & Blackwell, T.K., 2003. SKN-1 links *C. elegans* mesendodermal specification to a conserved oxidative stress response. *Genes & development*, 17(15), pp.1882–93. Available at: http://www.ncbi.nlm.nih.gov/pubmed/12869585 [Accessed October 2, 2017].

Angstadt, J.D. & Stretton, A.O., 1989. Slow active potentials in ventral inhibitory motor neurons of the nematode *Ascaris*. *Journal of comparative physiology. A, Sensory, neural, and behavioral physiology*, 166(2), pp.165–77. Available at: http://www.ncbi.nlm.nih.gov/pubmed/2607486 [Accessed October 13, 2017].

Bae, Y.-K. & Barr, M.M., 2008. Sensory roles of neuronal cilia: cilia development, morphogenesis, and function in *C. elegans*. *Frontiers in bioscience : a journal and virtual library*, 13, pp.5959–74. Available at: http://www.ncbi.nlm.nih.gov/pubmed/18508635 [Accessed September 29, 2017].

Bargmann, C.I., 1998. Neurobiology of the *Caenorhabditis elegans* genome. *Science*, 282(5396), pp.2028–2033.

Bargmann, C.I., Hartwieg, E. & Horvitz, H.R., 1993. Odorant-selective genes and neurons mediate olfaction in *C. elegans*. *Cell*, 74(3), pp.515–27. Available at: http://www.ncbi.nlm.nih.gov/pubmed/8348618 [Accessed September 29, 2017].

Bargmann, C.I. & Horvitz, H.R., 1991. Chemosensory neurons with overlapping functions direct chemotaxis to multiple chemicals in *C. elegans*. *Neuron*, 7(5), pp.729–42. Available at: http://www.ncbi.nlm.nih.gov/pubmed/1660283 [Accessed October 1, 2017].

Betts, M.J. & Russell, R.B. 2003. Amino acid properties and consequences of substitutions. *Bioinformatic for Geneticists.* Chapter 14. pp 289-316.

Beverly, M., Anbil, S. & Sengupta, P., 2011. Degeneracy and neuromodulation among thermosensory neurons contribute to robust thermosensory behaviors in *Caenorhabditis elegans*. *The Journal of neuroscience : the official journal of the Society*

for Neuroscience, 31(32), pp.11718–27. Available at: http://www.ncbi.nlm.nih.gov/pubmed/21832201 [Accessed October 1, 2017].

Birnby, D.A. et al., 2000. A transmembrane guanylyl cyclase (DAF-11) and Hsp90 (DAF-21) regulate a common set of chemosensory behaviors in *Caenorhabditis elegans*. *Genetics*, 155(1), pp.85–104. Available at: http://www.ncbi.nlm.nih.gov/pubmed/10790386 [Accessed October 2, 2017].

Biron, D. et al., 2008. An olfactory neuron responds stochastically to temperature and modulates *Caenorhabditis elegans* thermotactic behavior. *Proceedings of the National Academy of Sciences of the United States of America*, 105(31), pp.11002–7. Available at: http://www.ncbi.nlm.nih.gov/pubmed/18667708 [Accessed October 1, 2017].

Bowerman, B., Eaton, B.A. & Priess, J.R., 1992. skn-1, a maternally expressed gene required to specify the fate of ventral blastomeres in the early *C. elegans* embryo. *Cell*, 68(6), pp.1061–75. Available at: http://www.ncbi.nlm.nih.gov/pubmed/1547503 [Accessed October 2, 2017].

Burton, N.O. et al., 2017. Insulin-like signalling to the maternal germline controls progeny response to osmotic stress. *Nature Cell Biology*, 19(3), pp.252–257. Available at: http://www.nature.com/doifinder/10.1038/ncb3470 [Accessed October 2, 2017].

Butcher, R.A. et al., 2007. Small-molecule pheromones that control dauer development in *Caenorhabditis elegans*. *Nature Chemical Biology*, 3(7), pp.420–422. Available at:

Cassada, R.C. & Russell, R.L., 1975. The Dauerlarva, a Post-Embryonic Developmental Variant of the Nematode *Caenorhabditis elegans*. *DEVELOPMENTAL BIOLOGY*, 46, pp.326–342. Available at: http://ac.els-cdn.com/0012160675901098/1-s2.0-0012160675901098-main.pdf?_tid=da4af008-8ca3-11e7-b1ca-00000aacb35e&acdnat=1504002283_0a98d9cb69a872239e3b2a17613c3e15 [Accessed August 29, 2017].

Chalfie, M. & Sulston, J., 1981. Developmental genetics of the mechanosensory neurons of *Caenorhabditis elegans*. *Developmental biology*, 82(2), pp.358–70. Available at: http://www.ncbi.nlm.nih.gov/pubmed/7227647 [Accessed September 18, 2017].

Chalfie, M. & Wolinsky, E., 1990. The identification and suppression of inherited neurodegeneration in *Caenorhabditis elegans*. *Nature*, 345(6274), pp.410–416. Available at: http://www.ncbi.nlm.nih.gov/pubmed/2342572 [Accessed September 28, 2017].

Chatzigeorgiou, M. et al., 2010. Spatial asymmetry in the mechanosensory phenotypes of the *C. elegans* DEG/ENaC gene mec-10. *Journal of Neurophysiology*, 104(6).

Chatzigeorgiou, M. et al., 2010. Specific roles for DEG/ENaC and TRP channels in touch and thermosensation in *C. elegans* nociceptors. *Nature Neuroscience*, 13(7), pp.861-U106.

Chelur, D.S. et al., 2002. The mechanosensory protein MEC-6 is a subunit of the *C. elegans* touch-cell degenerin channel. *Nature*, 420(6916), pp.669–673. Available at: http://www.ncbi.nlm.nih.gov/pubmed/12478294 [Accessed October 24, 2017].

Chen, B.L., Hall, D.H. & Chklovskii, D.B., 2006. Wiring optimization can relate neuronal structure and function. *Proceedings of the National Academy of Sciences of the United*

States of America, 103(12), pp.4723–8. Available at: http://www.ncbi.nlm.nih.gov/pubmed/16537428 [Accessed September 18, 2017].

Chen, Y. et al., 2015. Subunit composition of a DEG/ENaC mechanosensory channel of *Caenorhabditis elegans*. *Proceedings of the National Academy of Sciences*, 112(37), pp.11690–11695. Available at: http://www.ncbi.nlm.nih.gov/pubmed/26324944 [Accessed October 5, 2017].

Coulson, A. et al., 1986. Toward a physical map of the genome of the nematode *Caenorhabditis elegans* (ordered clone bank/genomic data base/clone matching). *Genetics*, 83, pp.7821–7825. Available at: https://www.ncbi.nlm.nih.gov/pmc/articles/PMC386814/pdf/pnas00324-0265.pdf [Accessed September 6, 2017].

Croll, N.A. & Smith, J.M., 1978. Integrated behaviour in the feeding phase of *Caenorhabditis elegans* (Nematoda). *Journal of Zoology*.

Cueva, J.G., Mulholland, A. & Goodman, M.B., 2007. Nanoscale Organization of the MEC-4 DEG/ENaC Sensory Mechanotransduction Channel in *Caenorhabditis elegans* Touch Receptor Neurons. *Journal of Neuroscience*, 27(51), pp.14089–14098. Available at: http://www.ncbi.nlm.nih.gov/pubmed/18094248 [Accessed October 5, 2017].

Davis, R.E. & Stretton, A.O., 1996. The motornervous system of *Ascaris*: electrophysiology and anatomy of the neurons and their control by neuromodulators. *Parasitology*, 113 Suppl, pp.S97-117. Available at: http://www.ncbi.nlm.nih.gov/pubmed/9051930 [Accessed September 28, 2017].

Delaney, C.E. et al., 2017. A histone H4 lysine 20 methyltransferase couples environmental cues to sensory neuron control of developmental plasticity. *Development (Cambridge, England)*, 144(7), pp.1273–1282. Available at: http://www.ncbi.nlm.nih.gov/pubmed/28209779 [Accessed October 2, 2017].

Duerr, J.S. et al., 2008. Identification of major classes of cholinergic neurons in the nematode *Caenorhabditis elegans*. *The Journal of Comparative Neurology*, 506(3), pp.398–408. Available at: http://doi.wiley.com/10.1002/cne.21551 [Accessed September 30, 2017].

Edwards, R.H. et al., 1997. Identification and characterization of the vesicular GABA transporter. *Nature*, 389(6653), pp.870–876. Available at: http://www.ncbi.nlm.nih.gov/pubmed/9349821 [Accessed October 19, 2017].

Ellis, H.M. & Horvitz, H.R., 1986. Genetic control of programmed cell death in the nematode *C. elegans*. *Cell*, 44(6), pp.817–29. Available at: http://www.ncbi.nlm.nih.gov/pubmed/3955651 [Accessed December 15, 2016].

Engelmann, I. et al., 2011. A Comprehensive Analysis of Gene Expression Changes Provoked by Bacterial and Fungal Infection in *C. elegans* B. Lehner, ed. *PLoS ONE*, 6(5), p.e19055. Available at: http://dx.plos.org/10.1371/journal.pone.0019055 [Accessed October 2, 2017].

Farboud, B. & Meyer, B. 2015. Dramatic enhancement of genome editing by CRISPR/Cas9 through improved guide RNA design. *Genetics,* 208 (1)

Finger, T.E., Silver, W.L. & Restrepo, D., 2000. *The neurobiology of taste and smell*, Wiley-

Liss.

Friedland, A.E. et al., 2013. Heritable genome editing in *C. elegans* via a CRISPR-Cas9 system. *Nature Methods*, 10(8), pp.741–743. Available at: http://www.nature.com/doifinder/10.1038/nmeth.2532 [Accessed December 15, 2016].

Fujiwara, M., Sengupta, P. & McIntire, S.L., 2002a. Regulation of body size and behavioral state of *C. elegans* by sensory perception and the EGL-4 cGMP-dependent protein kinase. *Neuron*, 36(6), pp.1091–102. Available at: http://www.ncbi.nlm.nih.gov/pubmed/12495624 [Accessed October 2, 2017].

Fukushige, T. et al., 1999. MEC-12, an alpha-tubulin required for touch sensitivity in *C. elegans. Journal of cell science*, 112 (Pt 3), pp.395–403. Available at: http://www.ncbi.nlm.nih.gov/pubmed/9885292 [Accessed September 18, 2017].

Gallagher, T. et al., 2013. ASI regulates satiety quiescence in *C. elegans*. *The Journal of neuroscience : the official journal of the Society for Neuroscience*, 33(23), pp.9716–24. Available at: http://www.ncbi.nlm.nih.gov/pubmed/23739968 [Accessed October 2, 2017].

Gao, S. & Zhen, M., 2011. Action potentials drive body wall muscle contractions in *Caenorhabditis elegans*. *Proceedings of the National Academy of Sciences of the United States of America*, 108(6), pp.2557–62. Available at: http://www.ncbi.nlm.nih.gov/pubmed/21248227 [Accessed September 18, 2017].

Garty, H. & Palmer, L.G., 1997. Epithelial sodium channels: function, structure, and regulation. *Physiological reviews*, 77(2), pp.359–96. Available at: http://www.ncbi.nlm.nih.gov/pubmed/9114818 [Accessed September 27, 2017].

Gaugler, R. & Campbell, J.F., 1993. Nictation Behaviour and Its Ecological Implications in the Host Search Strategies of Entomopathogenic Nematodes (Heterorhabditidae and Steinernematidae). *Behaviour*, 126(3), pp.155–169. Available at: http://booksandjournals.brillonline.com/content/journals/10.1163/156853993x00092 [Accessed September 29, 2017].

George-Raizen, J.B. et al., 2014. Dynamically-expressed prion-like proteins form a cuticle in the pharynx of *Caenorhabditis elegans*. *Biology Open*, 3(11), pp.1139–1149. Available at: http://www.ncbi.nlm.nih.gov/pubmed/25361578 [Accessed October 2, 2017].

Golden, J.W. & Riddle, D.L., 1982. A pheromone influences larval development in the nematode *Caenorhabditis elegans*. *Science (New York, N.Y.)*, 218(4572), pp.578–80. Available at: http://www.ncbi.nlm.nih.gov/pubmed/6896933 [Accessed September 29, 2017].

Goodman, M.B. et al., 2002. MEC-2 regulates *C. elegans* DEG/ENaC channels needed for mechanosensation. *Nature*, 415(6875), pp.1039–1042.

Gray, J.M., Hill, J.J. & Bargmann, C.I., 2005. A circuit for navigation in *Caenorhabditis elegans. Proceedings of the National Academy of Sciences of the United States of America*, 102(9), pp.3184–91. Available at: http://www.ncbi.nlm.nih.gov/pubmed/15689400 [Accessed October 1, 2017].

Gu, G., Caldwell, G.A. & Chalfie, M., 1996. Genetic interactions affecting touch sensitivity in *Caenorhabditis elegans*. *Proceedings of the National Academy of Sciences of the United States of America*, 93(13), pp.6577–82. Available at: http://www.ncbi.nlm.nih.gov/pubmed/8692859 [Accessed September 27, 2017].

van Haastert, P.J., De Wit, R.J. & Konijn, T.M., 1982. Antagonists of chemoattractants reveal separate receptors for cAMP, folic acid and pterin in Dictyostelium. *Experimental cell research*, 140(2), pp.453–6. Available at: http://www.ncbi.nlm.nih.gov/pubmed/7117406 [Accessed October 1, 2017].

Hart, A.C., 2006. Behavior. *WormBook*. Available at: http://www.wormbook.org/chapters/www_behavior/behavior.html [Accessed September 18, 2017].

Hedgecock, E.M. & Russell, R.L., 1975. Normal and mutant thermotaxis in the nematode *Caenorhabditis elegans. Genetics*, 72(10), pp.4061–4065. Available at: http://www.pnas.org/content/72/10/4061.full.pdf [Accessed September 1, 2017].

Hilliard, M.A. et al., 2005. In vivo imaging of *C. elegans* ASH neurons: cellular response and adaptation to chemical repellents. *The EMBO journal*, 24(1), pp.63–72. Available at: http://www.ncbi.nlm.nih.gov/pubmed/15577941 [Accessed September 14, 2017].

Hilliard, M.A. et al., 2004. Worms taste bitter: ASH neurons, QUI-1, GPA-3 and ODR-3 mediate quinine avoidance in *Caenorhabditis elegans*. *The EMBO Journal*, 23(5), pp.1101–1111. Available at: http://www.ncbi.nlm.nih.gov/pubmed/14988722 [Accessed October 1, 2017].

Hilliard, M.A., Bargmann, C.I. & Bazzicalupo, P., 2002. *C. elegans* responds to chemical repellents by integrating sensory inputs from the head and the tail. *Current biology : CB*, 12(9), pp.730–4. Available at: http://www.ncbi.nlm.nih.gov/pubmed/12007416 [Accessed October 1, 2017].

Hochbaum, D. et al., 2011. DAF-12 Regulates a Connected Network of Genes to Ensure Robust Developmental Decisions S. K. Kim, ed. *PLoS Genetics*, 7(7), p.e1002179. Available at: http://dx.plos.org/10.1371/journal.pgen.1002179 [Accessed October 2, 2017].

Hutter, H. et al., 2000. Conservation and novelty in the evolution of cell adhesion and extracellular matrix genes. *Science (New York, N.Y.)*, 287(5455), pp.989–94. Available at: http://www.ncbi.nlm.nih.gov/pubmed/10669422 [Accessed September 14, 2017].

Jeong, P.-Y. et al., 2005. Chemical structure and biological activity of the *Caenorhabditis elegans* dauer-inducing pheromone. *Nature*, 433(7025), pp.541–545. Available at: http://www.ncbi.nlm.nih.gov/pubmed/15690045 [Accessed October 2, 2017].

Johnathon Hodgkin, Jonathan Hodgkin (person) - WormBase : Nematode Information Resource. Available at: http://www.wormbase.org/resources/person/WBPerson261#01--10 [Accessed September 18, 2017].

Kamath, R.S. et al., 2003. Systematic functional analysis of the *Caenorhabditis elegans* genome using RNAi. *Nature*, 421(6920), pp.231–237. Available at:

http://www.nature.com/doifinder/10.1038/nature01278 [Accessed July 24, 2017].

Kaplan, J.M. & Horvitz, H.R., 1993. A dual mechanosensory and chemosensory neuron in *Caenorhabditis elegans. Proceedings of the National Academy of Sciences of the United States of America*, 90(6), pp.2227–31. Available at: http://www.ncbi.nlm.nih.gov/pubmed/8460126 [Accessed October 10, 2017].

Kim, J. et al., 2001. Genes affecting the activity of nicotinic receptors involved in *Caenorhabditis elegans* egg-laying behavior. *Genetics*, 157(4), pp.1599–610. Available at: http://www.ncbi.nlm.nih.gov/pubmed/11290716 [Accessed September 18, 2017].

Kim, K. et al., 2009. Two chemoreceptors mediate developmental effects of dauer pheromone in *C. elegans*. *Science (New York, N.Y.)*, 326(5955), pp.994–8. Available at: http://www.ncbi.nlm.nih.gov/pubmed/19797623 [Accessed October 2, 2017].

Kimura, K.D. et al., 2004. The *C. elegans* thermosensory neuron AFD responds to warming. *Current biology : CB*, 14(14), pp.1291–5. Available at: http://www.ncbi.nlm.nih.gov/pubmed/15268861 [Accessed September 14, 2017].

Kuhara, A. et al., 2008. Temperature sensing by an olfactory neuron in a circuit controlling behavior of *C. elegans. Science (New York, N.Y.)*, 320(5877), pp.803–7. Available at: http://www.ncbi.nlm.nih.gov/pubmed/18403676 [Accessed October 1, 2017].

LeDoux, M., 2005. *Animal models of movement disorders*, Elsevier Academic Press. Available at: https://books.google.co.uk/books?id=Qq0SfGR_R_QC&pg=PA219&lpg=PA219&dq=c+elegans+lay+around+300+eggs&source=bl&ots=HZ1RZ8Qn4R&sig=HQQqbo1504Y5hIFs1dRnt1bOKzA&hl=en&sa=X&ved=0ahUKEwifrf_doPzVAhUoK8AKHebqAWgQ6AEIYDAH#v=onepage&q=300 eggs&f=false [Accessed August 29, 2017].

Lee, B.H. et al., 2011. Hyperactive Neuroendocrine Secretion Causes Size, Feeding, and Metabolic Defects of *C. elegans* Bardet-Biedl Syndrome Mutants S. K. Kim, ed. *PLoS Biology*, 9(12), p.e1001219. Available at: http://dx.plos.org/10.1371/journal.pbio.1001219 [Accessed October 10, 2017].

Lee, D. et al., 2015. SREBP and MDT-15 protect *C. elegans* from glucose-induced accelerated aging by preventing accumulation of saturated fat. *Genes & development*, 29(23), pp.2490–503. Available at: http://www.ncbi.nlm.nih.gov/pubmed/26637528 [Accessed October 2, 2017].

Lee, H. et al., 2011. Nictation, a dispersal behavior of the nematode *Caenorhabditis elegans,* is regulated by IL2 neurons. *Nature Neuroscience*, 15(1), pp.107–112. Available at: http://www.nature.com/doifinder/10.1038/nn.2975 [Accessed September 29, 2017].

Lewis, J.A. & Hodgkin, J.A., 1977. Specific neuroanatomical changes in chemosensory mutants of the nematode *Caenorhabditis elegans. The Journal of Comparative Neurology*, 172(3), pp.489–510. Available at: http://www.ncbi.nlm.nih.gov/pubmed/838889 [Accessed July 24, 2017].

Li, W. et al., 2006. A *C. elegans* stretch receptor neuron revealed by a mechanosensitive TRP channel homologue. *Nature*, 440(7084), pp.684–7. Available at: http://www.ncbi.nlm.nih.gov/pubmed/16572173 [Accessed October 11, 2017].

Li, W., Kennedy, S.G. & Ruvkun, G., 2003. daf-28 encodes a *C. elegans* insulin superfamily member that is regulated by environmental cues and acts in the DAF-2 signaling pathway. *Genes & development*, 17(7), pp.844–58. Available at: http://www.ncbi.nlm.nih.gov/pubmed/12654727 [Accessed October 2, 2017].

Lin, K. et al., 2001. Regulation of the *Caenorhabditis elegans* longevity protein DAF-16 by insulin/IGF-1 and germline signaling. *Nature Genetics*, 28(2), pp.139–145. Available at: http://www.ncbi.nlm.nih.gov/pubmed/11381260 [Accessed October 2, 2017].

Loer, C.M. & Kenyon, C.J., 1993. Serotonin-deficient mutants and male mating behavior in the nematode *Caenorhabditis elegans*. *The Journal of neuroscience : the official journal of the Society for Neuroscience*, 13(12), pp.5407–17. Available at: http://www.ncbi.nlm.nih.gov/pubmed/8254383 [Accessed October 19, 2017].

Macosko, E.Z. et al., 2009. A hub-and-spoke circuit drives pheromone attraction and social behaviour in *C. elegans*. *Nature*, 458(7242), pp.1171–5. Available at: http://www.ncbi.nlm.nih.gov/pubmed/19349961 [Accessed October 2, 2017].

Mano, I. & Driscoll, M., 1999. DEG/ENaC channels: A touchy superfamily that watches its salt. *BioEssays*, 21(7), pp.568–578.

Margie, O., Palmer, C. & Chin-Sang, I., 2013. *C. elegans* chemotaxis assay. *Journal of visualized experiments : JoVE*, (74), p.e50069. Available at: http://www.ncbi.nlm.nih.gov/pubmed/23644543 [Accessed September 7, 2017].

McGrath, P.T. et al., 2011. Parallel evolution of domesticated *Caenorhabditis* species targets pheromone receptor genes. *Nature*, 477(7364), pp.321–5. Available at: http://www.ncbi.nlm.nih.gov/pubmed/21849976 [Accessed October 2, 2017].

Mori, I. & Ohshima, Y., 1995. Neural regulation of thermotaxis in *Caenorhabditis elegans.* *Nature*, 376(6538), pp.344–348. Available at: http://www.ncbi.nlm.nih.gov/pubmed/7630402 [Accessed October 1, 2017].

Mueller, M.M. et al., 2014. DAF-16/FOXO and EGL-27/GATA promote developmental growth in response to persistent somatic DNA damage. *Nature Cell Biology*, 16(12), pp.1168–1179. Available at: http://www.nature.com/doifinder/10.1038/ncb3071 [Accessed October 2, 2017].

Murakami, M., Koga, M. & Ohshima, Y., DAF-7/TGF-b expression required for the normal larval development in *C. elegans* is controlled by a presumed guanylyl cyclase DAF-11. Available at: https://ac.els-cdn.com/S092547730100507X/1-s2.0-S092547730100507X-main.pdf?_tid=ae6154e4-a758-11e7-8e64-00000aab0f6b&acdnat=1506938678_aa35b159829c5e62e8b533890bd4f0d7 [Accessed October 2, 2017].

Murphy, C.T. et al., 2003. Genes that act downstream of DAF-16 to influence the lifespan of *Caenorhabditis elegans*. *Nature*, 424(6946), pp.277–283. Available at: http://www.nature.com/doifinder/10.1038/nature01789 [Accessed October 2, 2017].

Nolan, K.M. et al., 2002. The DAF-7 TGF-beta signaling pathway regulates chemosensory receptor gene expression in *C. elegans*. *Genes & development*, 16(23), pp.3061–73. Available at: http://www.ncbi.nlm.nih.gov/pubmed/12464635 [Accessed October 2,

2017].

O'Hagan, R., Chalfie, M. & Goodman, M.B., 2005. The MEC-4 DEG/ENaC channel of *Caenorhabditis elegans* touch receptor neurons transduces mechanical signals. *Nature neuroscience*, 8(1), pp.43–50.

Ono, K. et al., 2003. Specific requirement for two ADF/cofilin isoforms in distinct actin-dependent processes in *Caenorhabditis elegans*. *Journal of cell science*, 116(Pt 10), pp.2073–85. Available at: http://www.ncbi.nlm.nih.gov/pubmed/12679387 [Accessed September 18, 2017].

Otsuka, A.J. et al., 1995. An ankyrin-related gene (unc-44) is necessary for proper axonal guidance in *Caenorhabditis elegans*. *The Journal of cell biology*, 129(4), pp.1081–92. Available at: http://www.ncbi.nlm.nih.gov/pubmed/7744957 [Accessed September 18, 2017].

Park, D. et al., 2012. Interaction of structure-specific and promiscuous G-protein-coupled receptors mediates small-molecule signaling in *Caenorhabditis elegans*. *Proceedings of the National Academy of Sciences*, 109(25), pp.9917–9922. Available at: http://www.ncbi.nlm.nih.gov/pubmed/22665789 [Accessed October 2, 2017].

Peden, E.M. & Barr, M.M., 2005. The KLP-6 Kinesin Is Required for Male Mating Behaviors and Polycystin Localization in *Caenorhabditis elegans*. *Current Biology*, 15(5), pp.394–404. Available at: http://www.ncbi.nlm.nih.gov/pubmed/15753033 [Accessed

Perkins, L.A. et al., 1986. Mutant sensory cilia in the nematode *Caenorhabditis elegans*. *Developmental biology*, 117(2), pp.456–87. Available at: http://www.ncbi.nlm.nih.gov/pubmed/2428682 [Accessed September 29, 2017].

Pierce-Shimomura, J.T., Morse, T.M. & Lockery, S.R., 1999. The fundamental role of pirouettes in *Caenorhabditis elegans* chemotaxis. *The Journal of neuroscience : the official journal of the Society for Neuroscience*, 19(21), pp.9557–69. Available at: http://www.ncbi.nlm.nih.gov/pubmed/10531458 [Accessed September 18, 2017].

Ramot, D. et al., 2008. The Parallel Worm Tracker: A Platform for Measuring Average Speed and Drug-Induced Paralysis in Nematodes R. Aramayo, ed. *PLoS ONE*, 3(5), p.e2208. Available at: http://dx.plos.org/10.1371/journal.pone.0002208 [Accessed October 5, 2017].

Rankin, C.H. et al., 1990. *Caenorhabditis elegans*: a new model system for the study of learning and memory. *Behavioural Brain Research*, 37, pp.89–92.

Ren, P. et al., 1996. Control of *C. elegans* larval development by neuronal expression of a TGF-beta homolog. *Science (New York, N.Y.)*, 274(5291), pp.1389–91. Available at: http://www.ncbi.nlm.nih.gov/pubmed/8910282 [Accessed October 1, 2017].

Renard, S. et al., 1994. Biochemical analysis of the membrane topology of the amiloride-sensitive Na+ channel. *The Journal of biological chemistry*, 269(17), pp.12981–6. Available at: http://www.ncbi.nlm.nih.gov/pubmed/8175716 [Accessed September 27, 2017].

Riddle, D.L., 1997. *C. elegans II*, Cold Spring Harbor Laboratory Press.

Riddle, D.L., Swanson, M.M. & Albert, P.S., 1981. Interacting genes in nematode dauer larva formation. *Nature*, 290(5808), pp.668–71. Available at: http://www.ncbi.nlm.nih.gov/pubmed/7219552 [Accessed September 29, 2017].

Roayaie, K. et al., 1998. The G alpha protein ODR-3 mediates olfactory and nociceptive function and controls cilium morphogenesis in *C. elegans* olfactory neurons. *Neuron*, 20(1), pp.55–67. Available at: http://www.ncbi.nlm.nih.gov/pubmed/9459442 [Accessed October 10, 2017].

Rose, C.R. & Konnerth, A., 2001. NMDA Receptor-Mediated Na+ Signals in Spines and Dendrites. *Journal of Neuroscience*, 21(12). Available at: http://www.jneurosci.org/content/21/12/4207.long [Accessed September 14, 2017].

Ryu, W.S. et al., 2002. Thermotaxis in *Caenorhabditis elegans* analyzed by measuring responses to defined Thermal stimuli. *The Journal of neuroscience : the official journal of the Society for Neuroscience*, 22(13), pp.5727–33. Available at: http://www.ncbi.nlm.nih.gov/pubmed/12097525 [Accessed October 1, 2017].

Savage, C. et al., 1989. *mec-7* is a beta-tubulin gene required for the production of 15-protofilament microtubules in *Caenorhabditis elegans*. *Genes & development*, 3(6), pp.870–81. Available at: http://www.ncbi.nlm.nih.gov/pubmed/2744465 [Accessed September 28, 2017].

Schackwitz, W.S., Inoue, T. & Thomas, J.H., 1996. Chemosensory neurons function in parallel to mediate a pheromone response in *C. elegans*. *Neuron*, 17(4), pp.719–28. Available at: http://www.ncbi.nlm.nih.gov/pubmed/8893028 [Accessed October 1, 2017].

Schroeder, N.E. et al., 2013. Dauer-specific dendrite arborization in *C. elegans* is regulated by KPC-1/Furin. *Current biology : CB*, 23(16), pp.1527–35. Available at: http://www.pubmedcentral.nih.gov/articlerender.fcgi?artid=4671503&tool=pmcentrez&rendertype=abstract [Accessed February 10, 2016].

Schuster, E. et al., 2010. DamID in *C. elegans* reveals longevity-associated targets of DAF-16/FoxO. *Molecular systems biology*, 6(1), p.399. Available at: http://www.ncbi.nlm.nih.gov/pubmed/20706209 [Accessed October 2, 2017].

Schwarz, R.F. et al., 2015. Changes in Postural Syntax Characterize Sensory Modulation and Natural Variation of *C. elegans* Locomotion. *PLoS Computational Biology*, 11(8).

Srinivasan, J. et al., 2008. A blend of small molecules regulates both mating and development in *Caenorhabditis elegans. Nature*, 454(7208), pp.1115–1118. Available at: http://www.ncbi.nlm.nih.gov/pubmed/18650807 [Accessed October 2, 2017].

Stephens, G.J. et al., 2008. Dimensionality and Dynamics in the Behavior of *C. elegans* O. Sporns, ed. *PLoS Computational Biology*, 4(4), p.e1000028. Available at: http://dx.plos.org/10.1371/journal.pcbi.1000028 [Accessed December 15, 2016].

Sun, J. et al., 2011. Neuronal GPCR controls innate immunity by regulating noncanonical unfolded protein response genes. *Science (New York, N.Y.)*, 332(6030), pp.729–32. Available at: http://www.ncbi.nlm.nih.gov/pubmed/21474712 [Accessed October 2, 2017].

Sun, J., Liu, Y. & Aballay, A., 2012. Organismal regulation of XBP-1-mediated unfolded

protein response during development and immune activation. *EMBO reports*, 13(9), pp.855–60. Available at: http://www.ncbi.nlm.nih.gov/pubmed/22791024 [Accessed October 2, 2017].

Syntichaki, P. & Tavernarakis, N., 2004. Genetic Models of Mechanotransduction: The Nematode *Caenorhabditis elegans*. *Physiological Reviews*, 84(4), pp.1097–1153. Available at: http://www.ncbi.nlm.nih.gov/pubmed/15383649 [Accessed September 27, 2017].

Tavernarakis, N. et al., 1997. *unc-8*, a DEG/ENaC family member, encodes a subunit of a candidate mechanically gated channel that modulates *C. elegans* locomotion. *Neuron*, 18(1), pp.107–119.

Thomas, J.H., 1993. Chemosensory regulation of development in *C. elegans. BioEssays*.

Tullet, J.M.A. et al., 2008. Direct Inhibition of the Longevity-Promoting Factor SKN-1 by Insulin-like Signaling in *C. elegans*. *Cell*, 132(6), pp.1025–1038. Available at: http://www.ncbi.nlm.nih.gov/pubmed/18358814 [Accessed October 2, 2017].

Varshney, L.R. et al., 2011. Structural Properties of the *Caenorhabditis elegans* Neuronal Network O. Sporns, ed. *PLoS Computational Biology*, 7(2), p.e1001066. Available at: http://dx.plos.org/10.1371/journal.pcbi.1001066 [Accessed September 1, 2017].

Viswanathan, M. et al., 2005. A role for SIR-2.1 regulation of ER stress response genes in determining *C. elegans* life span. *Developmental cell*, 9(5), pp.605–15. Available at: http://www.ncbi.nlm.nih.gov/pubmed/16256736 [Accessed October 2, 2017].

Vowels, J.J. & Thomas, J.H., 1992. Genetic analysis of chemosensory control of dauer formation in *Caenorhabditis elegans*. *Genetics*, 130(1), pp.105–23. Available at: http://www.ncbi.nlm.nih.gov/pubmed/1732156 [Accessed September 29, 2017].

Waldmann, R. & Lazdunski, M., 1998. H(+)-gated cation channels: neuronal acid sensors in the NaC/DEG family of ion channels. *Current opinion in neurobiology*, 8(3), pp.418–24. Available at: http://www.ncbi.nlm.nih.gov/pubmed/9687356 [Accessed September 27, 2017].

Wang, J., Schwartz, H.T. & Barr, M.M., 2010. Functional specialization of sensory cilia by an RFX transcription factor isoform. *Genetics*, 186(4), pp.1295–1307. Available at: http://www.ncbi.nlm.nih.gov/pubmed/20923979 [Accessed September 29, 2017].

Ward, A. et al., 2008. Light-sensitive neurons and channels mediate phototaxis in *C. elegans. Nature neuroscience*, 11(8), pp.916–22. Available at: http://dx.doi.org/10.1038/nn.2155.

Ward, S., 1973. Chemotaxis by the nematode *Caenorhabditis elegans*: identification of attractants and analysis of the response by use of mutants. , 70(3), pp.817–821.

Ward, S. et al., 1975. Electron microscopical reconstruction of the anterior sensory anatomy of the nematode *Caenorhabditis elegans*. *Journal of Comparative Neurology*.

Way, J.C. & Chalfie, M., 1989. The *mec-3* gene of *Caenorhabditis elegans* requires its own product for maintained expression and is expressed in three neuronal cell types. *Genes & development*, 3(12A), pp.1823–33. Available at:

http://www.ncbi.nlm.nih.gov/pubmed/2576011 [Accessed October 10, 2017].

White, J.G. et al., 1986. The structure of the nervous system of the nematode *Caenorhabditis elegans*. *Philosophical transactions of the Royal Society of London. Series B, Biological sciences*, 314(1165), pp.1–340. Available at: http://www.ncbi.nlm.nih.gov/pubmed/22462104 [Accessed September 18, 2017].

White, J.Q. & Jorgensen, E.M., 2012. Sensation in a single neuron pair represses male behavior in hermaphrodites. *Neuron*, 75(4), pp.593–600. Available at: http://www.ncbi.nlm.nih.gov/pubmed/22920252 [Accessed October 2, 2017].

Yan, G. et al., 2017. Network control principles predict neuron function in the *Caenorhabditis elegans* connectome. *Nature*. Available at: http://www.nature.com/doifinder/10.1038/nature24056 [Accessed October 19, 2017].

You, Y. et al., 2008. Insulin, cGMP, and TGF-beta signals regulate food intake and quiescence in *C. elegans*: a model for satiety. *Cell metabolism*, 7(3), pp.249–57. Available at: http://www.ncbi.nlm.nih.gov/pubmed/18316030 [Accessed October 2, 2017].

Zhang, X. et al., 2013. Analysis of ascarosides from *Caenorhabditis elegans* using mass spectrometry and NMR spectroscopy. *Methods in Molecular Biology*.

Chapter 4: The Use of Novel Variants of The Calcium Indicator GCaMP5

4.1 Introduction

All organisms must be able to respond and adapt to changes in their external and internal environment, whether it be to escape toxins, recognise and seek out food sources or to regulate bodily functions. A large proportion of these responses are modulated by neurons. As discussed in previous chapters, *C. elegans* has a neuronal system capable of responding to a number of external stimuli, and of maintaining complex bodily functions. Many techniques have been developed for investigation into the connectivity and reactivity of neurons, one such technique is calcium imaging.

This technique allows changes in the concentration of free calcium ions in the cytoplasm of neuronal cells to be measured. Increases in calcium ion concentration show that a neuron is responding to stimuli, in the case of sensory neurons, or synaptic input from another neuron in the case of interneurons and motorneurons. The ability to detect impulses in *C. elegans* neurons is valuable in research as it allows the function of neurons to be determined. This then guides researchers to the possible function of particular channel subunits expressed in these neurons. For example, MEC-4, one of several channel proteins that are uniquely expressed in the touch neurons of *C. elegans*. This suggested a possible role for this protein in touch response. Upon mutation of the gene encoding this channel protein it was possible to detect a lack of calcium transients in the touch neurons in response to touch, verifying the gene's function as a mechanosensation channel subunit.

This chapter discusses some novel calcium indicators for use in *C. elegans*. It is hoped that the newly developed indicators can be used to detect rapid on/off responses and smaller changes in calcium ion concentration than previous indicators. Allowing for a more comprehensive understanding of *C. elegans* neuronal responses.

4.1.1 *C. elegans* Neuronal Function

As discussed in chapter 1 *C. elegans* have a number of classes of neuron and complex networks of these neurons modulate the behaviour in the worm. The functioning of the neurons *in C. elegans* is similar in some respect to that in mammals but there are some significant differences. There are no genes in the *C. elegans* genome encoding voltage gated sodium channels, and there is yet to be any proof that *C. elegans* displays any Na^+ transients in its neurons (Goodman et al. 1998). Action potentials are characterised by a regenerative all-or-nothing response that is propagated along a neuron in response to stimulus, they do not vary in strength in an individual neuron in response to a weak/strong stimulus, but in firing rate. There are three other types of regenerative signal propagation in neurons, gradient potentials, intrinsically oscillating potentials and plateau potentials. The former two have been observed in different neuron classes in the parasitic nematode *A. Suum*, as have calcium action potentials (Davis & Stretton 1996; Angstadt & Stretton 1989) but not in *C. elegans*. Plateau potentials however have been observed in *C. elegans*, they are characterised by prolonged all-or-none potentials that can be switched on or off by brief positive and negative charges respectively (Mellem et al. 2008; Lockery & Goodman 2009).

In mammalian neurons potassium/sodium pumps are responsible for polarising the cell membrane, by pumping 3 sodium ions out for every 2 potassium ions pumped in, maintaining a resting potential that is more negative than the extracellular space. This is not so in *C. elegans*, where most neurons are thought to be isopotential and signals are thought to arise from a simultaneous efflux of potassium ions and influx of calcium ions (Goodman et al. 1998). Mammalian neurons are much

larger than those in *C. elegans*, and action potentials are required for propagation of an electrical current along a much longer distance. There are many more sodium channels in a single mammalian neuron than in a neuron in *C. elegans* and several of these must be opened in mammals to reach the threshold potential to fire an action potential. As *C. elegans* neurons are so small, and contain only tens or hundreds of ion channels in the entire neuron, it is conceivable that opening just one of these channels can induce an electrical response.

4.1.2 The *C. elegans* Touch Neuron Circuit

In nature *C. elegans* is found in fruit, living on the bacteria and fungi growing on rotten vegetable matter. In this environment the worm must be able to respond to mechanosensory stimuli in the form of soil particles, other animals, its own body movements and surface tension. Mechanosensation responses in the worm are easily observed by applying mechanical stimuli to the worm's external cuticle. Different neurons have been shown to respond to different stimuli. Mild pressure, or brushing, to the outer cuticle of the body of the worm is known as gentle body touch (Chalfie & Sulston 1981; Sulston et al. 1975) and is sensed by the touch receptor neurons (TRNs). Harsh touch to the body, which is detected by the TRNs, PVD and FLP and harsh touch to the head or tail sensed by the BDU, SQR, AQR, ADE, PVD and PDE neurons (Way & Chalfie 1989; Li et al. 2011). Nose touch is detected by OLQ, FLP and ASH (Kaplan & Horvitz 1993). Texture, specifically the change in texture of the medium through which the worm is travelling when it enters a food lawn, results in slowing of locomotion rate upon lawn entry. This requires the dopaminergic neurons CEP, ADE and PDE (Sawin et al. 2000). Responses in *C. elegans* to tapping the exterior of a plate on which the worm is crawling require the TRNs (Chalfie & Sulston 1981)

Individuals will respond to these stimuli by performing an escape response, moving away from the stimulation. If the stimulation is applied to the anterior of the worm it will stop or reverse, if applied to the posterior, the worm will increase speed or move forward out of a reversal (Fig. 4.1A). In response to tapping the plate on which the worm is crawling, the worm will pause, perform a reversal or speed up in order to try to escape the vibration (Chalfie & Sulston 1981).

It is still not fully understood how *C. elegans* detect proprioception. Stretch receptors are believed to be responsible, in other organisms, for the detection of posture; for example, the stretch receptors in the motor neurons of *Ascaris Suum* (Davis & Stretton 1996). In *C. elegans* the only known stretch receptor is *trp-4*, expressed in the DVA neuron pair (Li et al. 2006). DVA positively and negatively modulates locomotion in response to stretching at its membrane, but is not required to generate a locomotion wave.

The non-ciliated mechanosensory neurons that detect touch to the cuticle of the worm along the body are the Touch Receptor neurons (TRNs) ALML, ALMR, PLML, PLMR, PVD and AVM. These neurons create robust and reliable escape responses to gentle body touch by triggering responses in a network of inter and motor neurons. A gentle stimulus delivered to the body of the worm, such as running an eyelash over the body, is sufficient to induce an escape response (Fig. 4.1B.) Gentle touch sensation requires the expression of a number of genes in the TRNs. As discussed in chapter 3, the DEG/ENaCs *mec-4* and *mec-10* are required for functional gentle touch sensation complexes in the TRNs. Several other genes play an important role in gentle touch transduction and form a part of the mechanotransduction complex. *mec-7* and *mec-12* both are β-tubulin genes required for 15-protofilament microtubule production in the gentle touch neurons (Savage et al. 1989; Fukushige et al. 1999). *mec-5* and *mec-9* encode putative extracellular proteins expressed in the TRNs that are required for gentle touch. MEC-5 is a collagen made by the epidermal cells that surrounds the touch

cells and MEC-9 is a protein with 5 Kunitz-type protease inhibitor domains, 6 EGF-like repeats (2 of the Ca(2+)-binding type), and a glutamic acid-rich region (Du et al. 1996). *mec-6* encodes a single-pass membrane-spanning protein expressed in muscle cells and the TRNs. MEC-6 increases amiloride-sensitive Na+ currents produced by MEC-4/MEC-10 and functions synergistically with MEC-2 to increase currents further (Chelur et al. 2002). MEC-2 is a stomatin-related protein that is also required for touch sensation (Goodman et al. 2002). Mutations in all of these genes cause mechanosensation phenotypes. As these neurons are easily and reliably stimulated during calcium imaging, by applying a gentle buzz to the worm's cutilcle (Suzuki et al. 2003), create robust responses and respond reliably, they offer a good control to test how well calcium indicators work within the neurons of *C.elegans.*

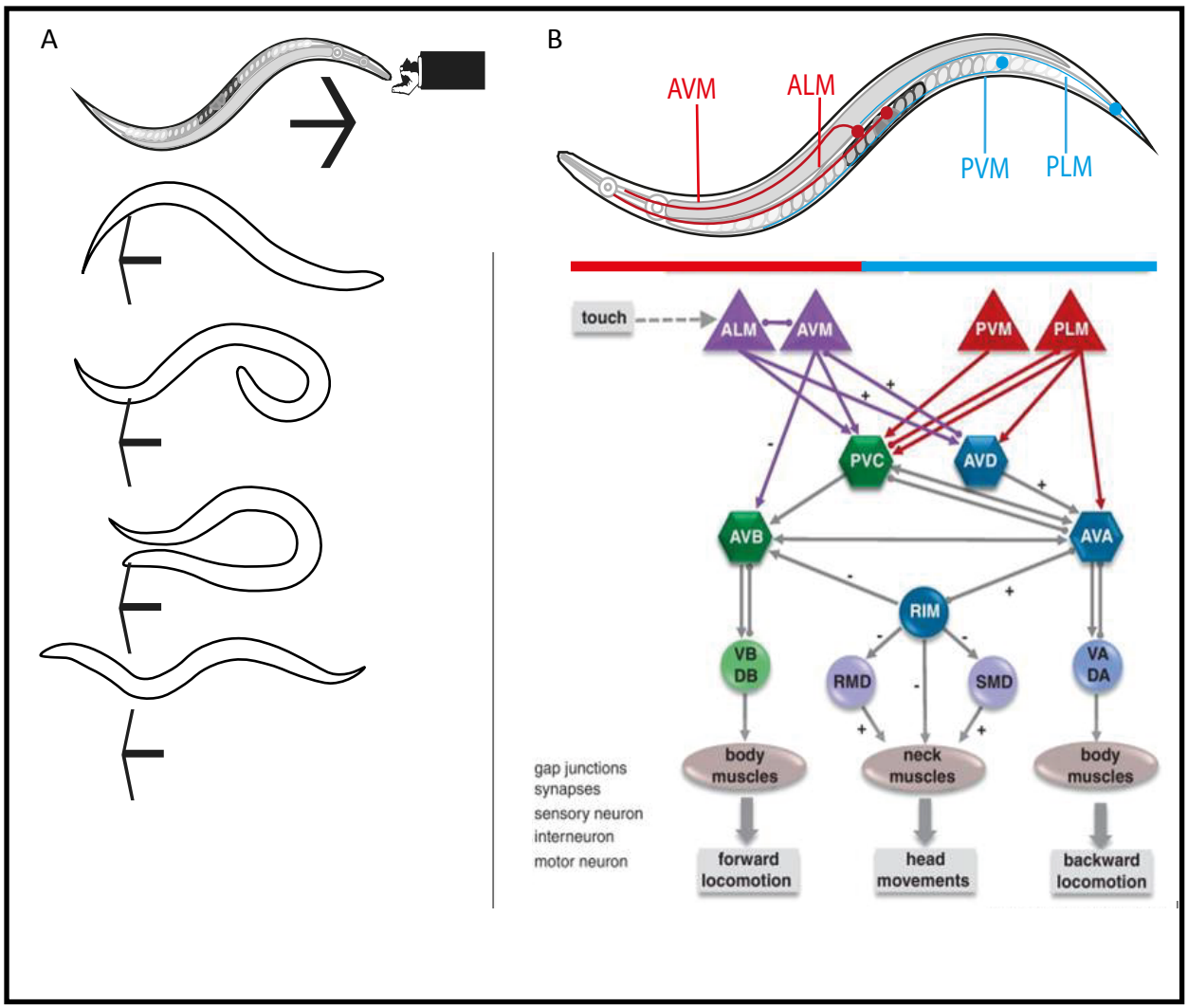

Fig.4.1: The Touch Response Circuit In *C. elegans.* A: The escape response exhibited by *C. elegans* in response to touch to the nose of the worm. B: The position of the TRNs in the worm. Below a schematic of the circuitry of the touch response in *C. elegans.* Neuronal classes in triangles are sensory neurons, classes in hexagons are interneurons and those in circles are motor neurons. Lines with arrow heads show synapses and those with circular ends show gap junctions (Image from the Alkema Lab).

4.1.3 Calcium Imaging

Calcium imaging is a valuable method for detecting the reactivity of all neurons in *C. elegans*. The absence of sodium-dependent action potentials in *C. elegans* means that electrical signals in most excitable cells in the worm are created by the influx of calcium ions into the neuron, rather than of sodium ions (Goodman et al. 1998). Calcium indicators can therefore be used in all neuronal classes to detect stimulation.

4.1.4 Organic Indicators and Genetically Encoded Calcium Indicators

A number of calcium indicators have been developed for use in calcium imaging. Small organic calcium indicators have been used successfully for some time, for example Oregon Green 488 BAPTA-1 (OGB-1), a visible light excitable calcium indicator. OBG-1 is particularly useful for quantitative, high signal-to-noise imaging, for example in imaging from living cardiac myocytes where calcium transients are fast and shortly spaced (Agronskaia et al.2004). These types of indicator must be injected directly into the cell of interest and imaged in the same worm as had been injected into. In *C. elegans* this method had several issues. By injecting directly into the cell of interest the experimenter is already interfering with the usual functioning of said cell. In *C. elegans* the neurons are small in comparison to higher organisms and the likelihood of damaging the cell is high. It is time consuming and challenging to inject enough individuals after damaged worms have been discounted. In order to overcome these issues Genetically Encoded Calcium Indicators (GECIs) were developed, the first of these was Cameleon, initially tested for appropriate functioning in HeLa cells (Miyawaki et al. 1997). Cameleon imaging has since been adapted for use in *C. elegans*, initially in the muscles of the pharynx and in all neurons (Kerr et al. 2000), and more recently in the TRNs (Suzuki et al. 2003). Cell specific promoters can be used to direct the expression of the calcium indicators to the cell of choice, requiring no damage to the cell to be imaged from.

4.1.5 Cameleon

Cameleon is a Förster Resonance Energy Transfer (FRET)-based indicator that relies on energy transfer from one of its fluorophores to the other (Miyawaki et al. 1997). Cameleon consists of Calmodulin (CaM), a calcium binding protein able to bind 4 calcium ions at once (Stevens 1983), two flurophores which are both modifications of GFP, shifted to different colours, one yellow (YFP) and one cyan (CFP), and the CaM binding protein M13. CaM is fused at the N terminus to the C terminus of CFP and at the C terminus to the N terminus of M13, and M13 is fused at the C terminus to the N terminus of YFP (Miyawaki et al. 1997) (Fig.4.2A). When bound to calcium CaM changes conformation, exposing hydrophobic methyl groups from methionine, increasing the binding affinity for target proteins. This conformational change involves a hinge like action of 2 EF hand domains that move so that the outer ends retract closer together once bound to calcium (Stevens 1983). M13 is a target protein for calcium-bound CaM and the M13 moves closer to CaM when calcium is present (Bayley et al. 1996). This, in turn, moves the CFP and YFP fluorophores closer together, which allows for energy transfer from the CFP to YFP molecule to occur. The ratio change in fluorescence between these two chromophores can then be used as a measure of calcium concentration (Miyawaki et al. 1997) (Fig.4.2A). Cameleon is very useful for imaging within the worm, where much of the imaging is performed in live animals and there is a possibility of small movements. For example, around the pharynx, even when a worm is glued the pharynx will continue to pump sporadically, causing movement in neighbouring neurons. FRET based indicators are advantageous in this instance since their output is a measure of ratio change rather than intensity change (Tsien 2009). Thus false negatives caused by small movements of the neuron are eradicated. In *C. elegans* Cameleon has been used heavily in a variety of different calcium imaging experiments. The down-side of Cameleon

is that the signal to noise ratio and kinetics are much reduced in comparison to molecules like OGB-1 (Zhao et al. 2011). Meaning that Cameleon cannot be used for fast, repeating neuronal activity, or for detecting excitation where the change in calcium concentration between resting potential and depolarisation is small.

4.1.6 GCaMP

Another widely used GECI in *C. elegans* is GCaMP. This molecule also contains Calmodulin, M13 and a fluorophore, however in this case there is just one and it is green. GCaMP contains a circularly permuted GFP that is fused at both ends. This creates a new terminus in the middle of the protein where M13 and Calmodulin are fused (Fig.4.2B). In its un-bound state the GFP fluorophore remains slightly open, allowing a solvent to quench the fluorescence. Upon binding with calcium the M13 and Calmodulin domains move together and cause the GFP barrel-like structure to close. The quenching solvent can no longer reach the centre of the fluorophore and the fluorescence increases (Fig.4.2B). In comparison to Cameleon, GCaMP has a much higher signal to noise ratio and its kinetics are faster (Nakai et al. 2001), opening up opportunities to use GECIs while still observing smaller and faster responses. Indicators like OGB-1 still out-compete GCaMP in these features and, unlike OGB-1, GCaMP fluorescence and calcium ion concentration is fairly non-linear. Quantification of calcium concentration using fluorescent emission levels from GCaMP is not as reliable as it is for small organic indicators or ratiometric GECIs like Cameleon (Zhao et al. 2011).

Cameleon and GCaMP only offer a small range of excitatory spectra, a larger range would be desirable for many techniques; for example, imaging from two, or more, neurons at the same time. A larger number of different coloured calcium indicators would allow for imaging the connectivity of networks, rather than just the activity of single neurons. The structure of GCaMP3 has been manipulated creating RCaMP (Red CaM Protein), G-GECO (Green-Genetically Encoded Calcium indicators for Optical imaging), R-GECO (Red-GECO) and B-GECO (Blue-GECO). GECOs are more recently developed GECIs that have almost comparable signal-to-noise ratios and kinetics to small organic indicators, and offer a wider range of excitation and emission spectra (Zhao et al. 2011), however, they are dimmer in the bound and unbound state than GCaMP3 and before this project was completed they had not been tested in neurons (Akerboom et al. 2012).

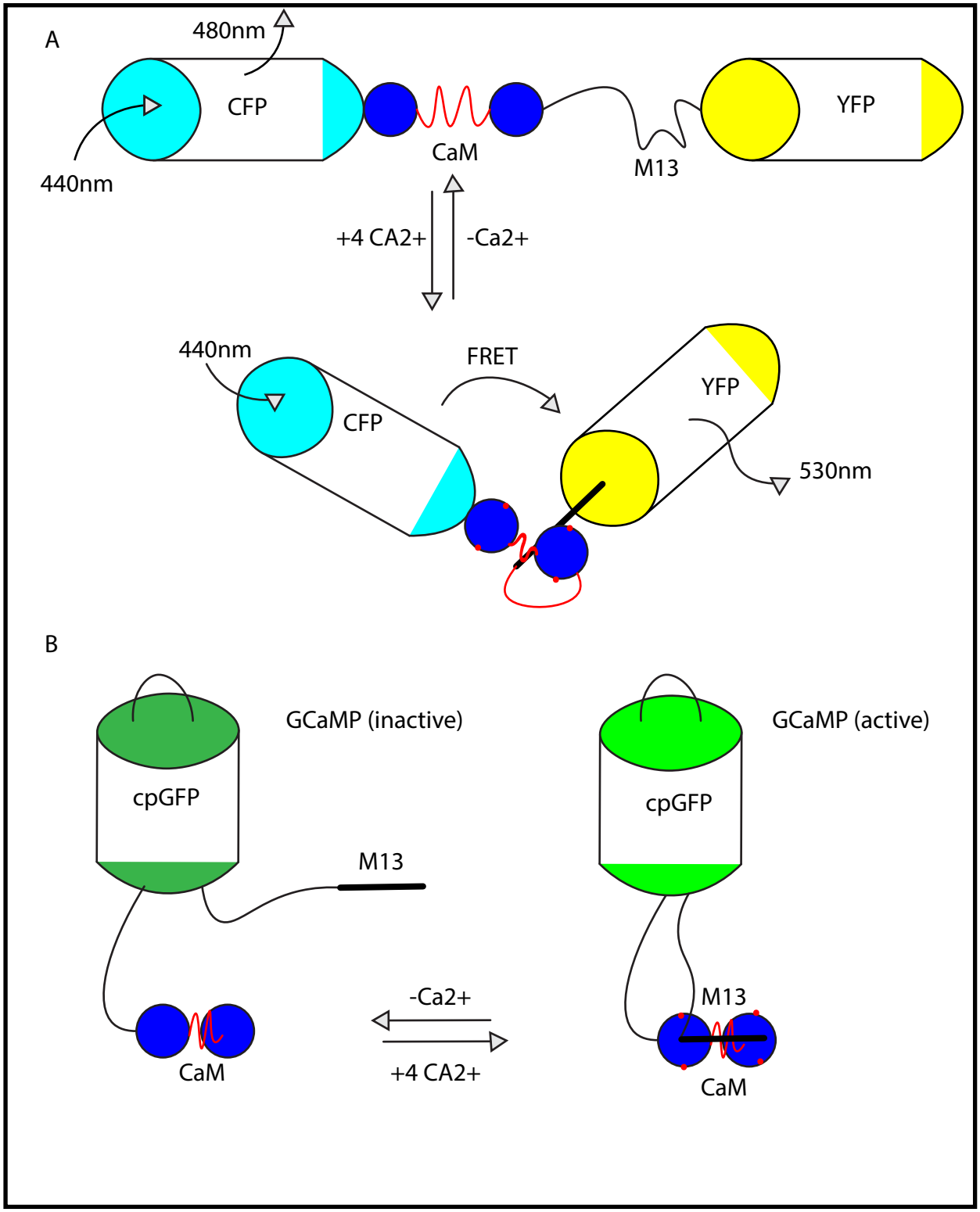

Fig.4.2: The Structures Of The GECIs Cameleon and GCaMP. A: A scematic of the structure of Cameleon. CFP and YFP are connected by the CaM and M13 domains, the top image shows Cameleon in the calcium unbound state and the lower image shows cameleon in the calcium bound state. (sung-kyun et. al 2011) B: A schematic of GCaMP, GFP is circularly permuted and M13 and CaM are fused to the internal C-terminus. The left hand picture shows GCaMP in the calcium unbound state and the right hand image shows GCaMP in the calcium bound state (Iino lab).

4.1.7 GCaMP5

The most commonly used GCaMP in *C. elegans* has been GCaMP3, which has an average fluorescence increase of 12x baseline and a *K*d (dissociation constant) of 542nM in *in vitro* testing (Zhao et al. 2011). A combination of structure-guided mutagenesis of the GCaMP3 cpGFP/CaM proto-interface, targeted library screening at the M13pep-cpGFP linker (linker 1) and cpGFP CaM linker (linker 2) and mutations in the M13 protein close to the third calcium binding site of calmodulin (Fig.4.3A) was used to produce GCaMP5 variants. Mutations in the interlobe linker of CaM (Fig.4.3A) were found to affect the solvent accessibility to the cpGFP chromophore in the calcium bound state, increasing the peak fluorescence 1.5 fold for GCaMP5A and 1.4 fold for GCaMP5G. Mutations in the linker 1 were found to increase the dynamic range GCaMP5B and GCaMP5C increases the range 2 or 3 fold respectively. Similar improvements were observed in linker 2 mutants; however these also displayed decreased affinity for calcium. The effects of these mutations were found to be additive in double and triple mutants. GCaMP5A and GCaMP5G were tested in *C. elegans* AWC neurons in response to IsoAmyl Alcohol (IAA). 5A showed a significantly improved dynamic range but slower dissociation constant and 5G had a similar dynamic range but slightly faster *K*d(Akerboom et al. 2012).

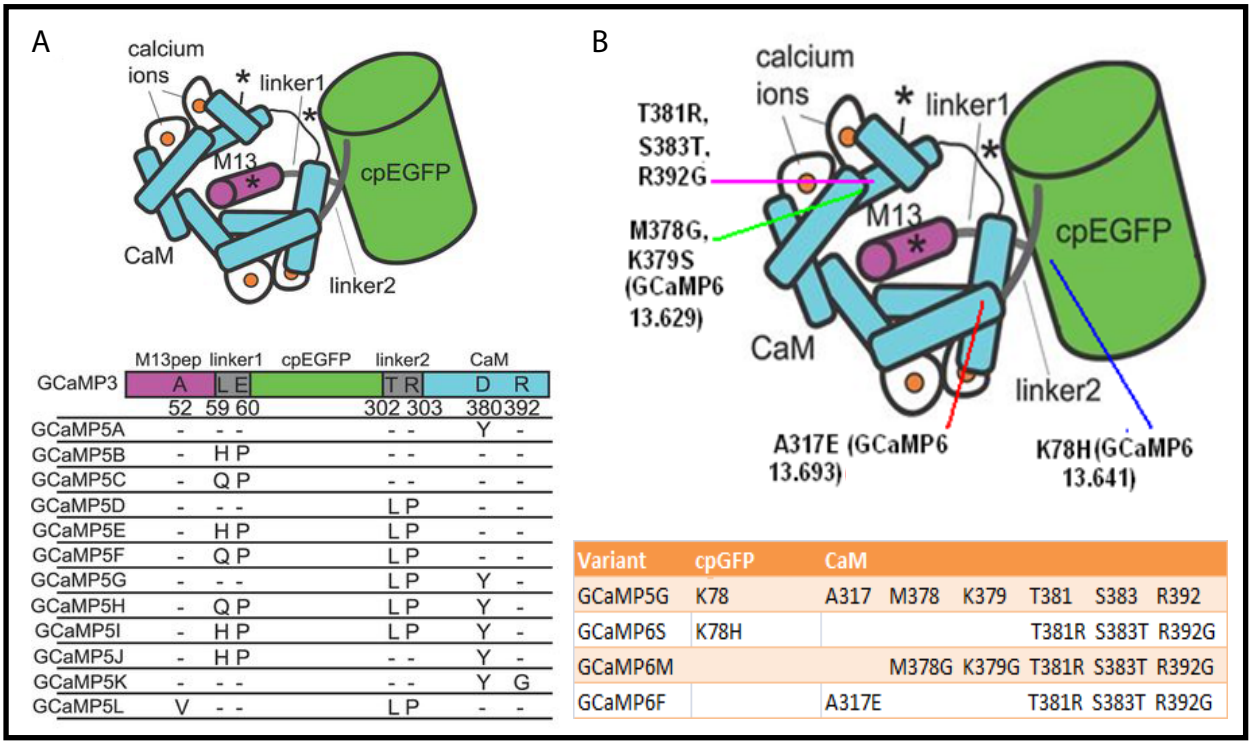

	M13pep	linker1		cpEGFP	linker2		CaM	
GCaMP3	A	L	E		T	R	D	R
	52	59	60		302	303	380	392
GCaMP5A	-	-	-		-	-	Y	-
GCaMP5B	-	H	P		-	-	-	-
GCaMP5C	-	Q	P		-	-	-	-
GCaMP5D	-	-	-		L	P	-	-
GCaMP5E	-	H	P		L	P	-	-
GCaMP5F	-	Q	P		L	P	-	-
GCaMP5G	-	-	-		L	P	Y	-
GCaMP5H	-	Q	P		L	P	Y	-
GCaMP5I	-	H	P		L	P	Y	-
GCaMP5J	-	H	P		-	-	Y	-
GCaMP5K	-	-	-		-	-	Y	G
GCaMP5L	V	-	-		L	P	-	-

Variant	cpGFP	CaM					
GCaMP5G	K78	A317	M378	K379	T381	S383	R392
GCaMP6S	K78H				T381R	S383T	R392G
GCaMP6M			M378G	K379G	T381R	S383T	R392G
GCaMP6F		A317E			T381R	S383T	R392G

Fig.4.3: The Mutations Added to GCaMP3 and GCaMP5G to Make GCaMP5 and GCaMP6 Variants. A: A schematic of the GCaMP3 protein showing CaM, M13 and GFP domains and linker 1 and 2 positions. The table below the schematic shows the position of mutations added to GCaMP3 for each variant (Akerboom et al. 2012). B: The tertiary structure of GCaMP5G, again showing M13, GFP and CaM domain and linker 1 and 2 positions. Labelled on the diagram are the positions in the structure where mutations were induced and the specific substitutions of amino acids that were made. The table below lists the individual mutations made to GCaMP5G that are present in each GCaMP6 variant.

4.1.8 GCaMP6

Mutations to GCaMP5G were performed in order to make the ultra-sensitive GCaMP6 variants. Numerous GCaMP6 variants were produced by focusing mutagenesis on the cpGFP and CaM interface at 16 amino acid positions. Mutations were also made at 18 additional sites at the M13-CaM interface, which can affect calcium affinity (Fig.4.3C). The mutation A317E, a mutation at the M13-CaM interface, accelerated kinetics four-fold in comparison to GCaMP3 but halved the dynamic range. Other mutations improved dynamic range but did not result in such fast kinetics. Once again combinations of the mutations resulted in the best compromise between increased kinetics and dynamic range. The variants GCaMP6S (Slow *K*d), GCaMP6M (Medium *K*d) and GCaMP6F (Fast *K*d) have varying kinetic speeds, and the slower the kinetics of the molecule the higher the sensitivity. These were tested *in vivo* in the presynaptic boutons of the *Drosophila* neuromuscular junctions, projection neurons of the *Drosophila* adult antennal lobe in response to odours and the neuropil and somata of the zebrafish tectum all were more sensitive and/or faster kinetically than GCaMP5G (Chen et al. 2013). Each variant has been shown to behave slightly differently in the neurons of different organisms. To determine how each works in the *C. elegans* neurons the indicators must be expressed and tested *in vivo*.

4.1.9 GECI Expression in *C. elegans*

Genes encoding GECIs can be introduced into worm in two distinct ways, either as extra-chromosomal arrays or integrated into the genome. The most common method for introducing new genetic material into the worm is by injecting into the gonad, where the DNA is taken up by the developing eggs in the form of an extra-chromosomal array. Arrays will be passed onto progeny at a rate dependent upon the construct that has been injected, both within the wider population and within individual worms. Two worms of the same genetic line can express different copy numbers of the same construct and some worms within the population will not express it at all. In integrated lines the DNA construct can be inserted into the genome of the worm and resultant populations will all express the same number of copies of the DNA construct. It is difficult to determine, in this situation, how many copies of the DNA have been inserted into the genome, so results may not be comparative between two different lines expressing the same gene. A method known as MosSCI can be used to insert a single copy of the DNA construct into the genome. This method harnesses the bacterial Mos-1 transposon, expressed at a specific site in the *C. elegans* genome. Excision of the Mos-1 transposon by Mos-1 transposase is used to introduce a double stranded break at a specific site and a single copy of the expression construct is inserted into this site (Frøkjaer-Jensen et al. 2008).

4.1.10 TMC Proteins

Mammalian TMC1 and TMC2 are proteins that are known to be involved in auditory transduction. TMC1 has been shown to be expressed in the post-natal mouse cochlear (Kurima et al. 2002) and knock-out mice for TMC1 and TM2 exhibit auditory and vestibular defects (Kawashima et al. 2011). It is thought that both TMC1 and TMC2 are pore forming subunits in the channel that responds to tip-link deflection on mammalian hair cells (Pan et al. 2013). In *C. elegans* the homologue *tmc-1* has been implicated in salt sensation in the ASH neurons (Chatzigeorgiou et al. 2013). There has been some contention as to whether this is actually the case, as reliable electrophysiology data for the *tmc-1* channel is not available.

4.1.11 Project Aims

This project aimed to determine which GCaMP6 variant provided the best dynamic range and kinetics in the *C. elegans* touch neuron circuit using gentle touch stimulus and calcium imaging. To determine whether GCaMP6 variants offer a means to observe changes in the free calcium ion concentration in the ER of pharyngeal cells upon muscle contraction. Finally to determine whether the higher sensitivity of GCaMP6 variants provides a useful application for determining the salt receptivity of *tmc-1.*

4.2 Materials and Methods

4.2.1 GCaMP6 Lines

GCaMP6 plasmids, as well as a GCaMP5 control, were obtained from the Looger lab at Janelia Research campus. GCaMP6 variants are listed in table A8.

4.2.2 Array Lines

Array lines were produced using the injection method described in chapter (general materials and methods). Worms were injected with: GCaMP plasmids at 50ng/µl, *Pymo-2* GFP or RFP at 50ng/µl, 1KB ladder at 50ng/µl and water up to 4µl, unless otherwise stated experiments were undertaken with the Bristol N2 line. (A list of GCaMP array lines can be found in Table A9, Appendix)

4.2.3 Single Copy Lines

Single copy lines were created using MosSCI, developed in the Jorgensen lab (Frøkjaer-Jensen et al. 2008; Frøkjær-Jensen et al. 2012). The plasmids required to complete this procedure were gifted from the Ch'ng lab at UCL.

For each GCaMP variant, a final concentration of 50ng/µl was coinjected with: 50ng/µl pCFJ601, 10ng/µl pMA122, 10ng/µl pGH8, 2.5ng/µl pCFJ90 and 5ng/µl pCFJ104. The mix was injected into *unc-119* mutant worms, containing the genomic Mos-1 transposon (strain number QL74). Approximately 100 animals were injected; 2-3 of each were placed on individual, seeded, 3cm NGM plates and left at 25°C for 7 days. Once fully starved, worms were heat shocked at 34°C for 2 hours. At least 4 hours after the heat shock ended, worms were screened for individuals with wild-type locomotion and no fluorescence from co-injection markers. These individuals were selfed onto seeded 3 cm NGM plates. After 4 days F1 animals were checked to ensure all progeny exhibited wild-type locomotion and free of co-injection markers. At this point expression of the GCaMP variant in touch neurons was verified by the detection of green fluorescence in PLM (A full list of single copy plasmids and strains can be found in Table A8, Appendix)

4.2.4 Introducing Point Mutations

Forward and reverse primers flanking the desired point of mutation were ordered from Sigma-Aldrich®. Each primer contained a modification to the triplet code for the amino acid of interest; see Table A6 (Appendix) lower case letters denote the modified triplet code. Phusion® high fidelity DNA polymerase was used to amplify the original plasmid prep to include the mutation within the primer. PCRs were run as per the recommended NEB method with a 58°C annealing temperature and 10 minute extension time for 10 cycles.

Reactions were purified using a QIAquick® PCR purification kit (Qiagen).

The original plasmid DNA, that did not contain the mutation, was digested using the restriction enzyme, DpnI (to specifically digest the methylated, bacterially-derived template). The resultant solution was run using gel electrophoresis and the DNA band was extracted using a QIAquick® Gel Extraction kit (Qiagen).

Gel extracts were transformed using Ecloni® Chemically Competent Cells and streaked onto TYE + Ampicillin plates. After a 16 hour, 37°C incubation, single colonies were inoculated into separate test tubes all containing 2ml LB + Ampicillin at 50µg/ml. Samples were incubated at 37°C for 16 hours then DNA was extracted using a QIAquick® miniprep kit (Qiagen).

For mutations in array plasmids, low affinity GCaMP6 variants were injected at 50ng/µl + pymo-2 GFP at 50ng/µl, 0.4µl 1KB ladder at 500ng/µl and water up to 4µl. Array plasmids were injected into Bristol N2.

Mutated MosSCI plasmids were injected at 50ng/µl +50ng/µl pCFJ601, 10ng/µl pMA122, 10ng/µl pGH8, 2.5ng/µl pCFJ90 and 5ng/µl pCFJ104, into QL74. The same procedure previously used to make single-copy lines was used in this instance. (A full list of primers, plasmids and strains can be found in Tables A6, A8 and A9 respectively) Table 4.1 shows the combination of mutations added to the different GCaMP6 variants.

Table 4.1: The mutations added to GCaMP5G to make GCaMP6 variants.

GCaMP6 variant	Mutations
13.641 (S)	K78H , T381R, S383T , R392G
13.693 (F)	A317E , T381R, S383T, R392G
13.629 (M)	M378G, K379S, T381R, S383T, R392G
13.649	K78H, A317E, T381R, S383T, R392G
13.643	K78H, A317E, K379S, T381R, S383T, R392G
13.646	K78H, A317E, M378G, T381R, S383T, R392G
13.629 (M) low affinity	D326L, M378G, K379S, T381R, S383T, R392G
13.641 (S) low affinity	K78H , D326L, T381R, S383T , R392G
13.629 (M) low affinity double	D324G, D326L, M378G, K379S, T381R, S383T, R392G
13.641 (S) low affinity 2	K78H , D326L, T381R, S383T , R392G , D397G

4.2.5 Calcium Imaging

Worms were picked as L4 larvae to 6cm seeded plates 16-20 hours before experimentation.

A 2% solution of agarose in M9 buffer (Appendix, Recipe, M9) was made and around 50µl was pipetted onto a microscope slide. A cover slip was then placed on top of the agarose droplet in order to make a pad. Once set, the cover slip was removed and the pad was allowed to dry for around 15mins

Approximately 10 minutes prior to experimentation the worms were transferred onto 6cm un-seeded plates, and allowed to crawl for 5 minutes to remove excess food. The worm was then picked from this plate and placed onto the agarose pad.

A small ice bath was made in the lid of a petri dish and the slide was placed over this. When cooled the worms become immobile and could be glued, as straight as possible, onto the pad. Glue was applied down the right had side of the worm from nose to tail tip. Care was taken to not glue over the mouth, as this can result in poor responses or the death of the worm. Dermabond® topical skin adhesive was used for gluing.

A buffer was then applied to the glued worms; the buffer used was dependent on the experiment taking place.

4.2.5.1 Gentle Touch

For gentle touch experiments Neuronal buffer was applied to the glued worms (Appendix, Recipes, Neuronal Buffer).

The fluorescent imaging microscope was set up as described in the general materials and methods section.

A blunted capillary needle was mounted into a PI micro-manipulator and was positioned around a quarter of the length of the worm anterior to the tail tip, with the needle almost touching the cuticle (Fig. 4.4A). The GFP filter emission pair was used for all GCaMP imaging. Recordings all lasted for 50 seconds; with stimulus being applied after 10 seconds. The stimulus was provided using the PI micro-manipulator set-up. A program was used on PI controller to deliver a 1 second buzz stimulus to the worm, the method for this program is detailed by Suzuki *et al.* 2003 (Suzuki et al. 2003).

4.2.5.2 Perfusion

All perfusion assays were performed using CTX buffer. Gluing was performed down both sides of the worm and the perfusion pen tip was positioned around three worm widths away from the worm's nose, ensuring the flow of perfusion passed across the nose of the worm (Fig. 4.4B).

4.2.5.3 Perfusion for ER Imaging

Calreticulin, a calcium binding molecule, is found at high concentrations in the ER lumen where it acts as a buffer for free calcium ions (Park et al. 2001). For this reason GCaMP was targeted to the ER using a calreticulin ER import signal sequence and an HDel calreticulin ER retention sequence. Primers containing these two sequences, and also the 2nd position gateway sites, were ordered from Sigma-Aldrich®. KOD® polymerase was used to amplify the GCaMP6 sequences from the original array plasmids. DNA fragments were cloned into Gateway pDONR221, and later transformed using Ecloni® Chemically Competent Cells and selected with Kanamycin. Plasmid DNA was isolated from cell culture using QIAquick® mini-prep.

Gateway was used to create plasmids *Pmyo-2*::ER retained GCaMP variant::*SL2-tagRFP*, and were transformed as before, but with Amplicillin selection. (A full list of plasmids and primers can be found in T6 and T8 respectively)

For imaging of the pharyngeal ER, an initial application of 20% digitonin was applied to the worms to permiabilise the cell membranes. During prolonged experimentation occasional additions of digitonin were used.

Worms were mounted for imaging as previously described but with additional gluing up the left hand side of the worm. Neuronal buffer containing 4mM EGTA was perfused over the worm at all times during experimentation when not applying calcium chloride solutions. During recording neuronal buffer + EGTA was perfused, using gravity fed perfusion, over the worm for 10s at which point perfusion was switched to either 2.5mM calcium chloride in neuronal buffer, 5mM calcium chloride in neuronal buffer, 10mM calcium chloride in neuronal buffer or 25mM calcium chloride in neuronal buffer for the remainder of recording. All recordings lasted 60 seconds.

In the case of decapitated worms, the worm head was severed and glued as described by Kerr et al. (Kerr et al. 2000).

For these experiments Intracellular Buffer containing 4mM EGTA was used to cover the worm instead of neuronal buffer. An initial dose of 20Mm digitonin was applied to permiablise the membrane.

4mM EGTA was perfused over the worm using gravity fed perfusion, after 10 seconds this was switched to either 2.5mM CaCl2, 5mM CaCl2, or 10mM CaCl2 for 70 seconds.

4.2.5.4 Sodium Perfusion in *tmc-1* expressing ASKs

Solutions of 1M Sucrose (in CTX buffer) and 0.5M sodium gluconate (in CTX buffer) were made and used for a maximum of 2 weeks. 1M sucrose has an osmolarity of 1osm and 0.5M sodium gluconate also has an osmolarity of 1osm, ruling out any responses in the neurons in response to changes in osmolarity.

During experimentation the sucrose/CTX solution was perfused over the worms for 10 seconds, then was switched to sodium gluconate for 50 seconds then returned to sucrose for 30s.

All perfusions were performed using gravity fed perfusion with the excess solutions were aspirated using a vacuum pump set at >5 (units).

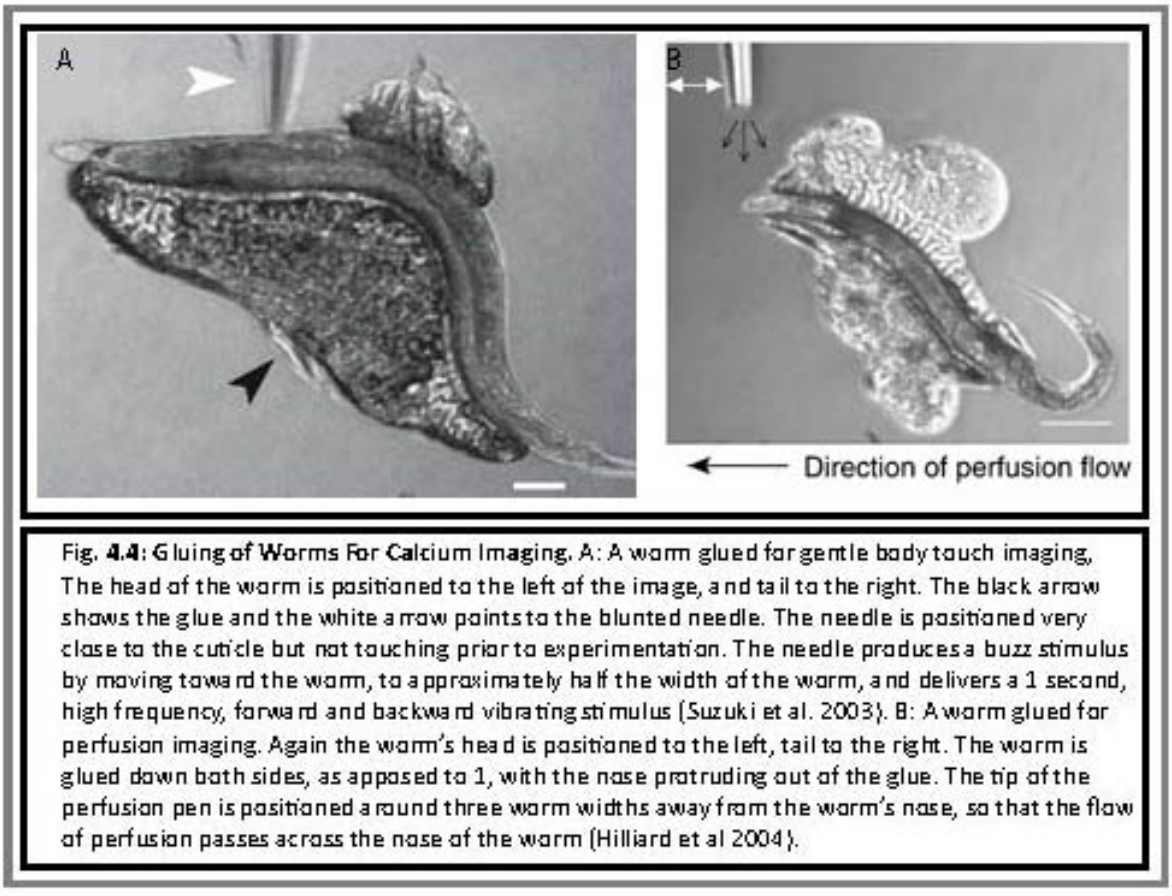

Fig. 4.4: Gluing of Worms For Calcium Imaging. A: A worm glued for gentle body touch imaging, The head of the worm is positioned to the left of the image, and tail to the right. The black arrow shows the glue and the white arrow points to the blunted needle. The needle is positioned very close to the cuticle but not touching prior to experimentation. The needle produces a buzz stimulus by moving toward the worm, to approximately half the width of the worm, and delivers a 1 second, high frequency, forward and backward vibrating stimulus (Suzuki et al. 2003). B: A worm glued for perfusion imaging. Again the worm's head is positioned to the left, tail to the right. The worm is glued down both sides, as apposed to 1, with the nose protruding out of the glue. The tip of the perfusion pen is positioned around three worm widths away from the worm's nose, so that the flow of perfusion passes across the nose of the worm (Hilliard et al 2004).

4.3 Results

4.3.1 GCaMP6F Has the Highest Dynamic Range and Kinetics When Expressed As an Array

The response of GCaMP6 variants in the PLM was tested using gentle touch to the worm's cuticle around ¼ of the worm's length anterior to the tail. GCaMP5G was tested in the same way along-side GCaMP6 variants for comparison. PLM was chosen as the GCaMP6 variants were so dim in the calcium unbound state that no other TRNs showed visible GCaMP expression. GCaMPs of all varieties were expressed under *Pmec-4* as arrays; this resulted in variable expression, and therefore variable baseline fluorescence in the PLM. The average traces and the correlation of baseline to peak fluorescence were plotted (Fig. 4.5 and 4.6). The GCaMP6 variants had varying dissociation rates, with GCaMP6M (GCaMP6 Medium *K*d) having the slowest exponential decay (71.26) (Fig. 4.5B), GCaMP6S (GCaMP6 Slow *K*d) having slightly improved kinetics (exp. decay= 91.33nM) (Fig. 4.6A) and GCaMP6F (GCaMP6 Fast *K*d) having further improved kinetics (exp. decay 195.56nM) (Fig. 4.6B). What is surprising is that both GCaMP6S and GCaMP6M, where kinetics are compromised for improved dynamic range, have lower peak fluorescence than GCaMP6F (149, 124 and 300 $\Delta F/F_0$ % respectively). None of the GCaMP6 variants matched the dissociation kinetics of GCaMP5 and only GCaMP6F surpassed GCaMP5 in dynamic range (exp. decay =296.29nM and peak fluorescence 199 $\Delta F/F_0$ %) (Fig. 4.5A). Although GCaMP6F had higher peak fluorescence than GCaMP5G, the results for GCaMP6F were much more variable, resulting in a reduced average trace for GCaMP6F in comparison to GCaMP5.

The correlations of baseline fluorescence to peak fluorescence imply that the lower the baseline fluorescence of the neuron, the higher the peak fluorescence. GCaMP6F has the lowest affinity for calcium out of all GCaMPs tested, which could explain why it has some of the highest peak fluorescent values recorded.

After initial testing with GCaMP6S, M and F three other GCaMP6 variants were tested in the same way as previously. These were GCaMP6.643, GCaMP6.646 and GCaMP6.649; these variants had different combinations of the aforementioned point mutations to S, M and F variants, in an effort to reduce their calcium affinity (Fig 4.7). Once again average traces and correlations of peak to baseline fluorescence were plotted. GCaMP6.643 and GCaMP6.646 only gave small responses to gentle touch in the PLM, and many time stimuli did not result in any response at all. Experimentation with these variants was discontinued at this point. GCaMP6.649 showed more promising results, with an exponential decay = 102.98nM and peak fluorescence of 205 $\Delta F/F_0$ % (Fig. 4.8).

As a lower affinity for calcium seemed to improve GCaMP6 dynamic range and exponential decay of traces in the *C. elegans* touch neuron PLM, further point mutations were added to GCaMP6S and GCaMP6M in an attempt to reduce their affinity for calcium. The point mutation D326L was added to both GCaMP6S and M, in the M13-calmodulin interface, a region previously shown to reduce CaM affinity for calcium. This point mutation swaps a negatively charged aspartic acid residue for an uncharged leucine residue. The mutations D324G and D397G, also trade a positive residue for an uncharged one. Both these mutations were added to GCaMP6M and the single D397G mutation was added to GCaMP6S (Fig 4.7). The modified indicators were imaged in the same way as previously and the average trace and peak to baseline correlation were plotted (Fig 4.9 and 4.10). The additional D326L mutation in GCaMP6M had a mildly improved exponential decay of 99.61nM an improved peak fluorescence of 225 $\Delta F/F_0$ % and a relatively unchanged average response of ~60 $\Delta F/F_0$ % (Fig 4.9A). The same mutation in GCaMP6S drastically reduces exponential decay and mildly reduces peak

fluorescence (27.21 and 110 $\Delta F/F_0$ % respectively). The responses were much more variable in this mutant so the peak fluorescence in the average trace is much reduced (Fig 4.9B).

The double mutation in GCaMP6M resulted in reduced exponential decay 42.99nM) and reduced peak fluorescence (100 $\Delta F/F_0$ %) (Fig. 4.10A). The single mutation D397G in GCaMP6S resulted in reduced kinetics (exp. decay 64.32nM) and peak fluorescence (78 $\Delta F/F_0$ %) (Fig 4.10B).

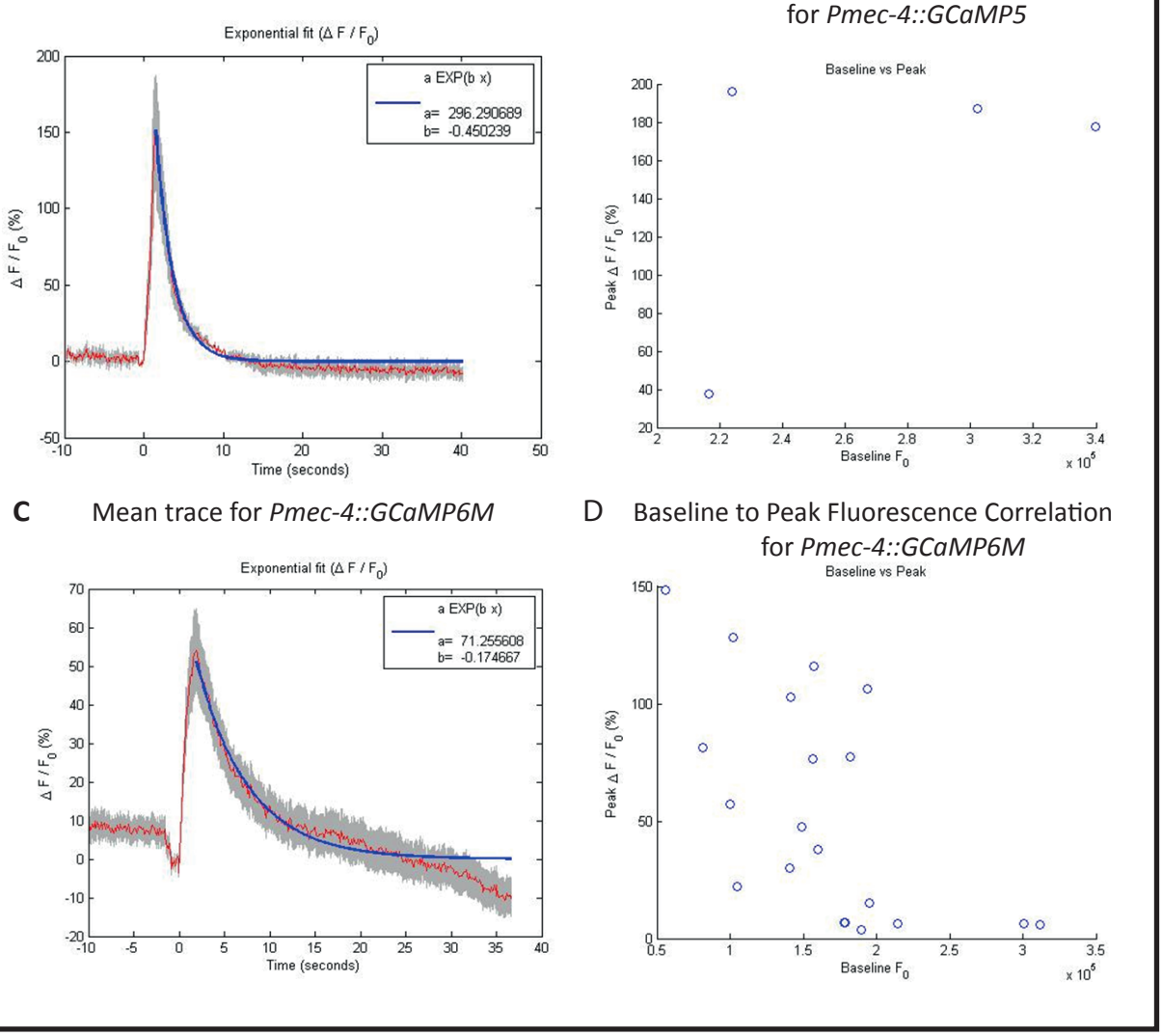

Fig.4.5: Calcium Imaging Results For PLM Expressing Multiple-Copy Arrays Of GCaMP6 Variants In Response To Gentle Touch. Figures A to D show the traces and baseline to peak fluorescence correlation for GCaMP variants in PLM. A: calcium trace for *Pmec-4::GCaMP5* B: Baseline fluorescence correlation to peak fluorescence of trace *Pmec-4:: GCaMP5*. C: Calcium trace for *Pmec-4::GCaMP6M* D: Baseline fluorescence correlation to peak fluorescence of trace *Pmec-4::GCaMP6M*. Calcium traces show the change in fluorescence over a set period of time divided by the peak fluorescence. The red line represents the mean of all traces, the grey shaded area shows the range of all traces. Dissociation rate is measured using the best fit exponential degradation shown with the blue line. Traces start at -10s as, for best analysis, the motion onset was set as the start of the trace. Motion onset is the time at which the stimulus was initiated, the stimulus lasted 1s.

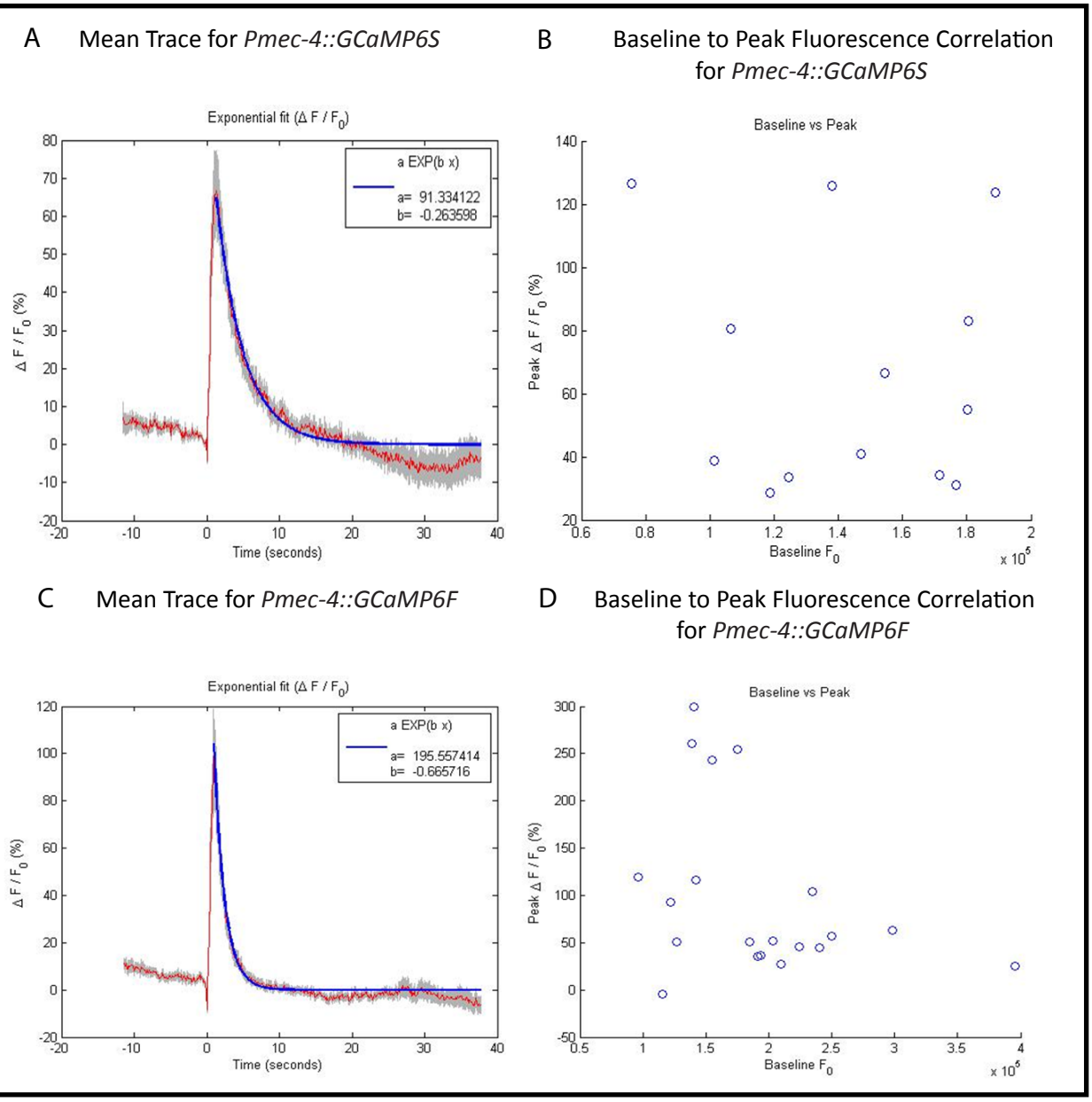

Fig.4.6: Calcium Imaging Results For PLM Expressing Multiple-Copy Arrays Of GCaMP6 Variants In Response To Gentle Touch. Figures A to D show the traces and baseline to peak fluorescence correlation for GCaMP variants in PLM. A: calcium trace for *Pmec-4::GCaMP6S* B: Baseline fluorescence correlation to peak fluorescence of trace *Pmec-4:: GCaMP6S*. C: Calcium trace for *Pmec-4::GCaMP6F* D: Baseline fluorescence correlation to peak fluorescence of trace *Pmec-4::GCaMP6F*. Calcium traces show the change in fluorescence over a set period of time divided by the peak fluorescence. The red line represents the mean of all traces, the grey shaded area shows the range of all traces. Dissociation rate is measured using the best fit exponential degradation shown with the blue line. Traces start at -10s as, for best analysis, the motion onset was set as the start of the trace. Motion onset is the time at which the stimulus was initiated, the stimulus lasted 1s.

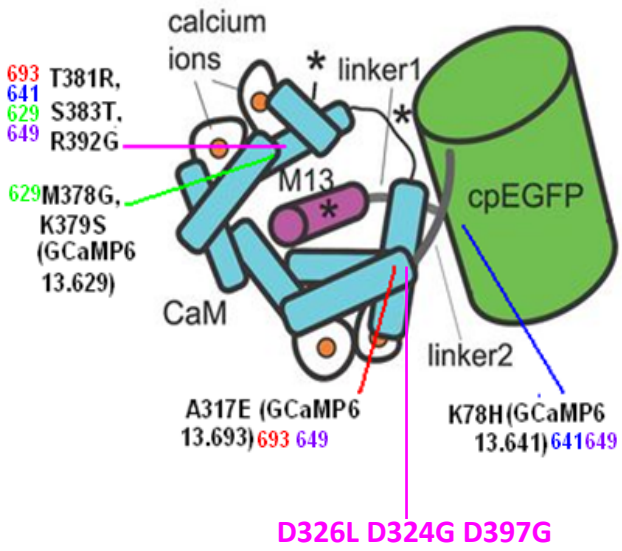

Fig.4.7: Additional Mutations Introduced In GCaMP6M and GCaMP6S. A schematic of the GCaMP6 molecule showing approximate sites of the mutations introduced in GCaMP5G, labelled in green, red, blue and purple are the mutations present in GCaMP6M, GCaMP6F, GCaMP6S and GCaMP6.649. In pink is labelled the approximate position of the mutations induced in GCaMP6M and GCaMP6S. Mutations at the CaM-GFP interface are hoped to reduce calcium affinity to the CaM molecule.

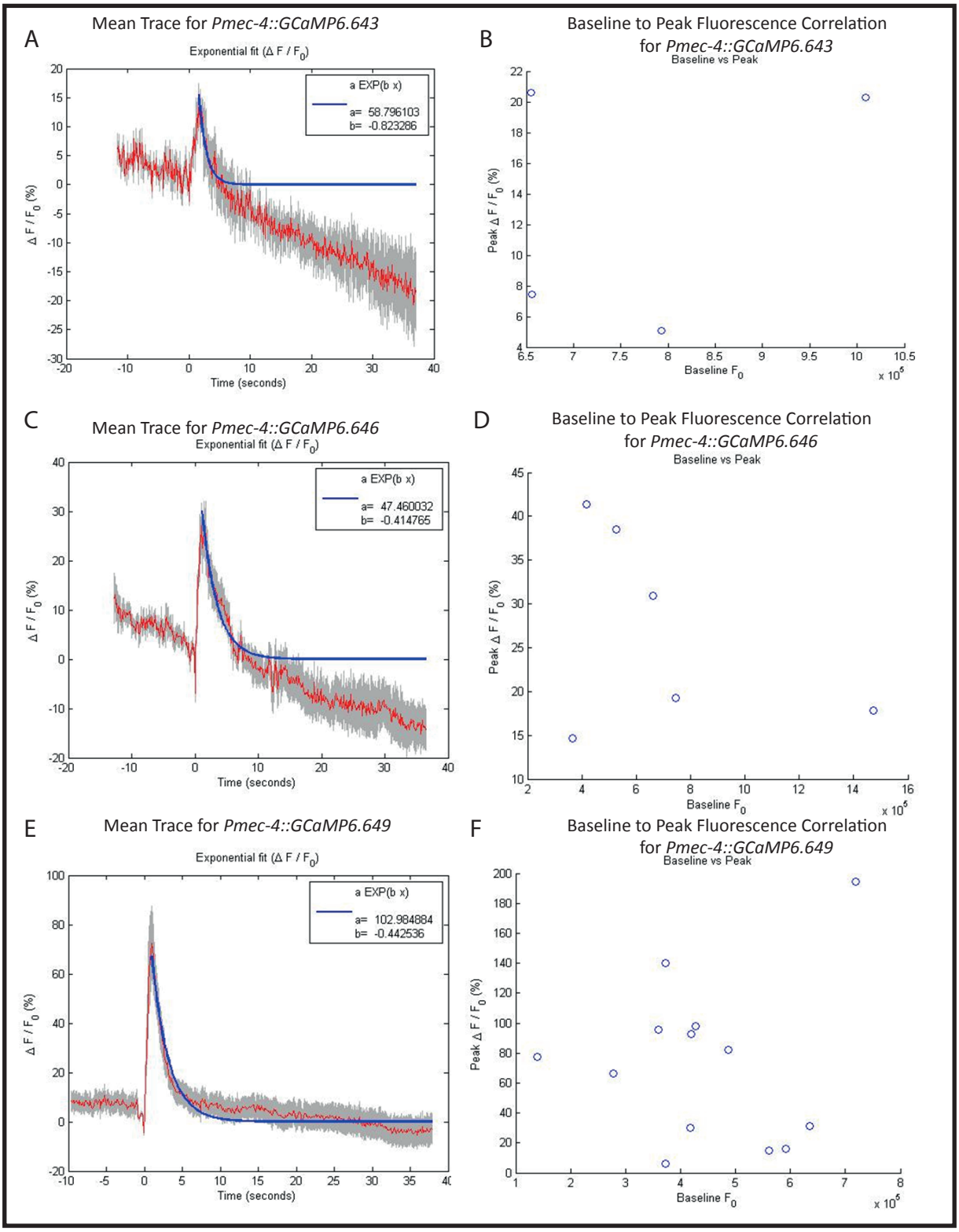

Fig.4.8. Figures A To F Show The Calcium Traces and Baseline To Peak Fluorescence Correlation Of Different GCaMP Variants. A: Calcium trace of *Pmec-4::GCaMP6.643*. B: Baseline to peak fluorescence correlation for *Pmec-4::GCaMP6.643*. C: Calcium trace of *Pmec-4::GCaMP6.646*. D: Baseline to peak fluorescence correlation for *Pmec-4::GCaMP6.646* E: Calcium trace of *Pmec-4::GCaMP6.649.* F: Baseline to peak fluorescence correlation for *Pmec-4::GCaMP6.649*. Calcium traces show the change in fluorescence over a set period of time divided by the peak fluorescence.The red line represents the mean of all traces, the grey shaded area shows the range of all traces. Dissociation rate is measured using the best fit exponential degradation shown with the blue line. Traces start at -10s as, for best analysis, the motion onset was set as the start ofthe trace. Motion onset is the time at which the stimulus was initiated, the stimulus lasted 1s.

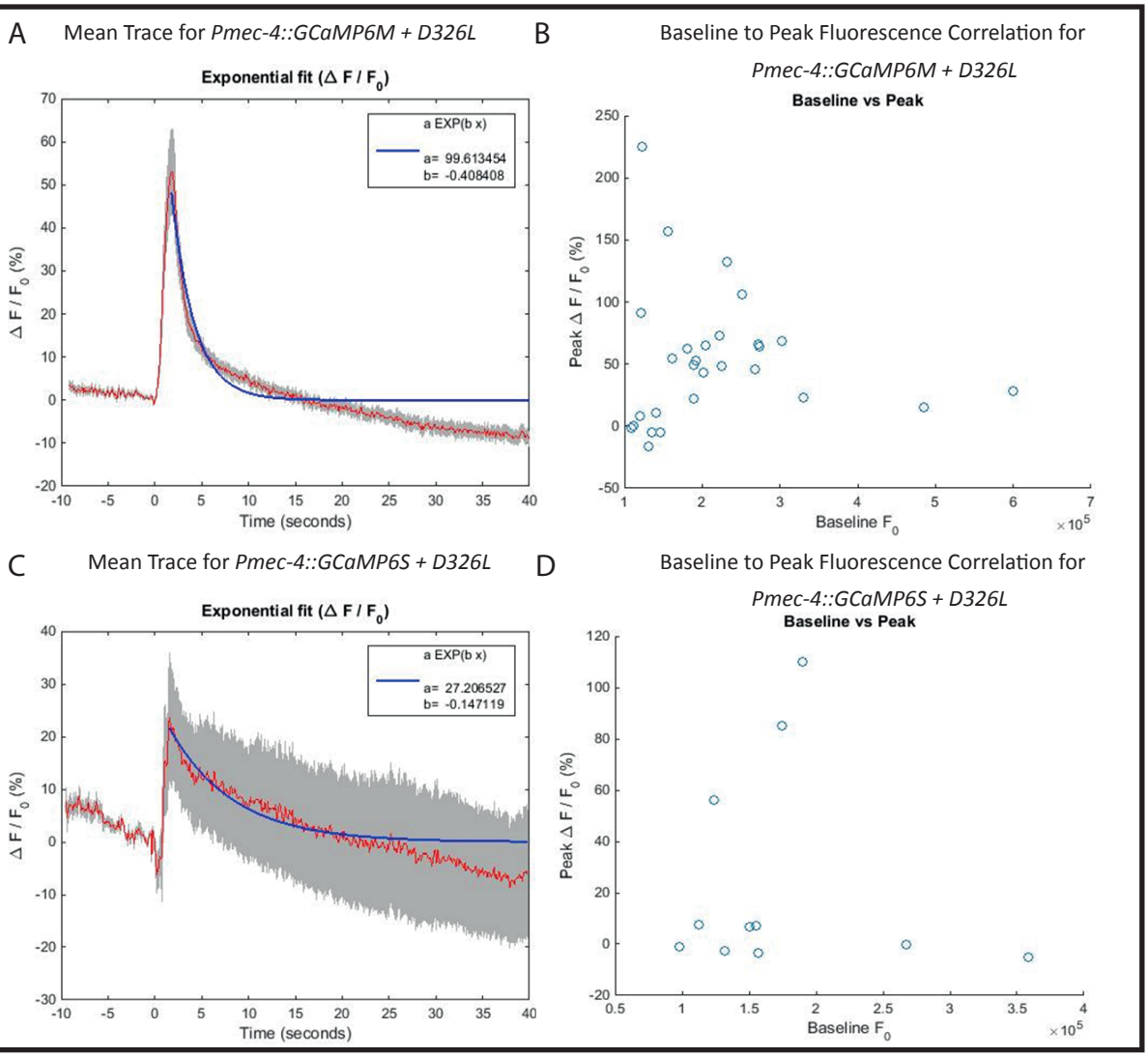

Fig.4.9. Graphs Showing Calcium Traces and Baseline To Peak Fluorescence Correlations For GCaMP6 Variants With Additional Point Mutations. A: Calcium trace for GCaMP6M + D326L B: Baseline to peak fluorescence correlation for GCaMP6M + D326L. C: Calcium trace for GCaMP6S + D326L. D: Baseline to peak fluorescence correlation for GCaMP6S + D326L. Calcium traces show the change in fluorescence over a set period of time, divided by the peak fluorescence. The red line represents the mean of all traces, the grey shaded area shows the range of all traces. Dissociation rate is measured using the best fir exponential degradation shown with the blue line. Traces start at -10s as, for best analysis, the motion onset was set as the start of the trace. Motion onset is the time at which the stimulus was initiate, the stimulus lasted for 1s.

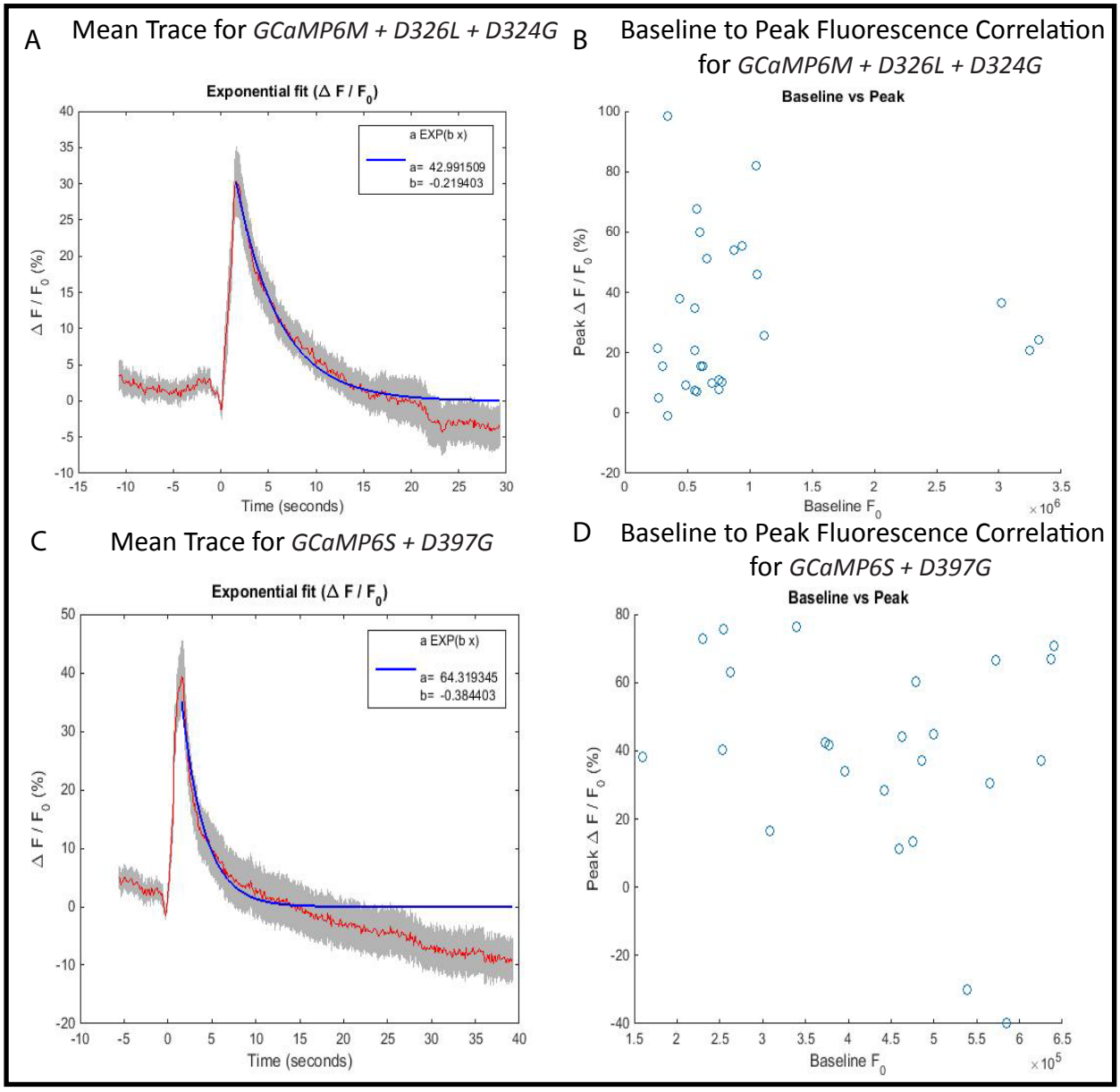

Fig.4.10: The Average Traces and Peak to Baseline Fluorescence Correlation of GCaMP6S and M With Low Affinity Inducing Point Mutations. A: Calcium trace for *GCaMP6M + D326L + D324G*. B: Baseline to peak fluorescence correlation for *GCaMP6M + D326L + D324G.* C: Calcium trace for *GCaMP6S + D397G*. D: Baseline to peak fluorescence correlation for *GCaMP6S + D397G*. Calcium traces show the change in fluorescence over a set period of time, divided by the peak fluorescence. The red line represents the mean of all traces, the grey shaded area shows the range of all traces. Dissociation rate is measured using the best fit exponential degradation shown with the blue line. Traces start at -10s as, for best analysis, the motion onset was set as the start of the trace. Motion onset is the time at which the stimulus was initiate, the stimulus lasted for 1s.

4.3.2 Single Copy GCaMP6 Lines Give Faster Kinetics and Higher Peak Fluorescence

Initially GCaMP6 single copy lines were expressed under *Pmec-4*, as multiple copy array constructs were. The MEC-4 protein is expressed at a low rate in the touch neurons and, although this is sufficient for expression of multiple copy lines, the expression was not strong enough for visualisation of single copy GCaMPs. MEC-7 is a protein that is also expressed in the TRNs but at a much higher rate than MEC-4. For this reason single copy lines were then produced with expression driven by *Pmec-7*. Unfortunately, after much trying, GCaMP6F could not be expressed as a single copy line, for reasons unknown. Both GCaMP6M and GCaMP6S single copy lines were successfully created and imaged as were array lines.

In single copy mutants the baseline fluorescence of both GCaMP6 variants was much less variable, and in most instances was towards the dimmer end of the scale. The exponential decay of both variants was a little improved in the single copy lines, as was peak fluorescence (exp. decay = 87.02 peak fluorescence 240 $\Delta F/F_0$ % GCaMP6M exp. decay 128.81 peak fluorescence 355 $\Delta F/F_0$ % GCaMP6S) (Fig 4.11).

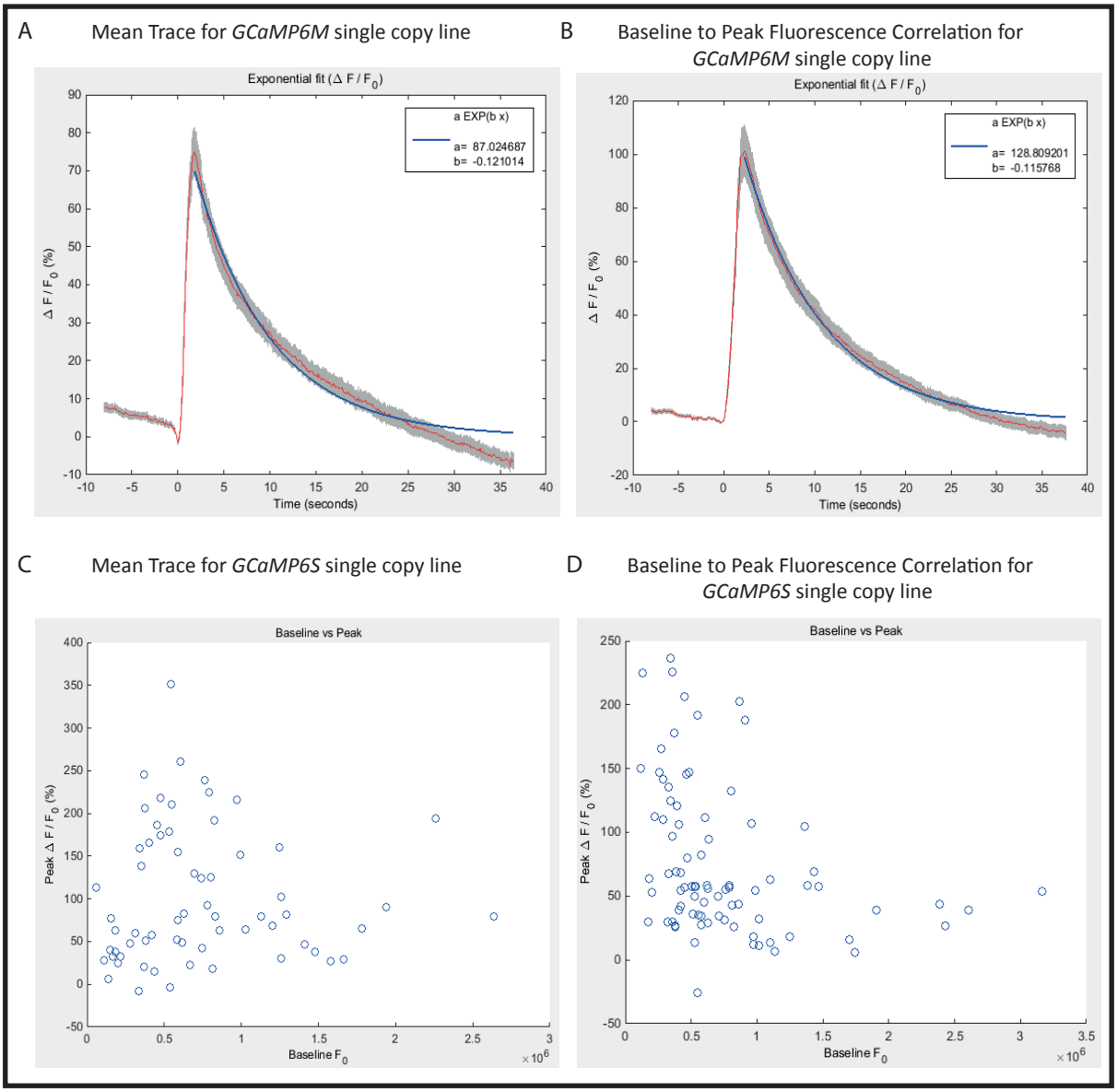

Fig.4.11. Calcium Imaging Results From PLM Expressing Single Copies Of GCaMP6 Varients In Response To Gentle Touch. A to D show the traces and baseline to peak fluorescence correlation of different GCaMP6 variants as single copy, integrated genes in PLM. A: shows the average trace for *GCaMP6M* expressed as a single copy insertion. B: shows the correlation between baseline and peak fluorescence of GCaMP6M expressed as a single copy insertion. C: shows the average trace for GCaMP6S expressed as a single copy insertion. D: shows the correlation between baseline and peak fluorescence of GCaMP6S expressed as a single copy insertion. For mean trace graphs, the red line signifies the mean trace, the grey shaded area shows the reange of all traces and the blue line displays the best fit exponential degradation of the curve. A lower the value of b, the faster the calcium dissociates from the GCaMP and therefore the lower the affinity of that variant for calcium. Traces start at -10s as, for best analysis, the motion onset was set as the start of the trace. Motion onset is the time at which the stimulus was initiate, the stimulus lasted for 1s.

4.3.3 GCaMP6S is not sensitive enough to Detect Changes in Calcium Concentration in Pharyngeal Muscle Cell ER during Excitation.

Calcium ion concentration is maintained at a high level in the ER and highly sensitive, low affinity calcium indicators must be used to detect any Ca+ concentration fluctuations (Grynkiewicz et al. 1985). The highly sensitive, low affinity GCaMP6 variants were expressed in the ER to determine whether they are capable of detecting changes in the calcium ion concentration in this organelle.

For all ER imaging experiments calcium levels were depleted using EGTA before imaging. Varying concentrations of calcium chloride were then perfused over the worm to determine if the GCaMP6M protein was functional in the ER of the pharynx. The results were plotted as average traces of $\Delta F/F_0$ % (Fig. 4.12). These traces show that there is a response in the pharyngeal muscle cell ER in intact worms at calcium chloride concentrations between 5mM and 10mM, where the fluorescence seems to plateau. In *C. elegans* severed heads, where calcium can reach the pharyngeal muscle ER more easily, the optimal GCaMP response is at 10mM calcium chloride. These results initially looked promising, however, following experiments testing the ER calcium levels in non-calcium depleted muscle cell ER, there was no discernible change in GCaMP6M fluorescence. GCaMP6, therefore, does not seem to be sensitive enough to detect the changes in physiological levels of ER calcium before and during calcium transients in excitable cells.

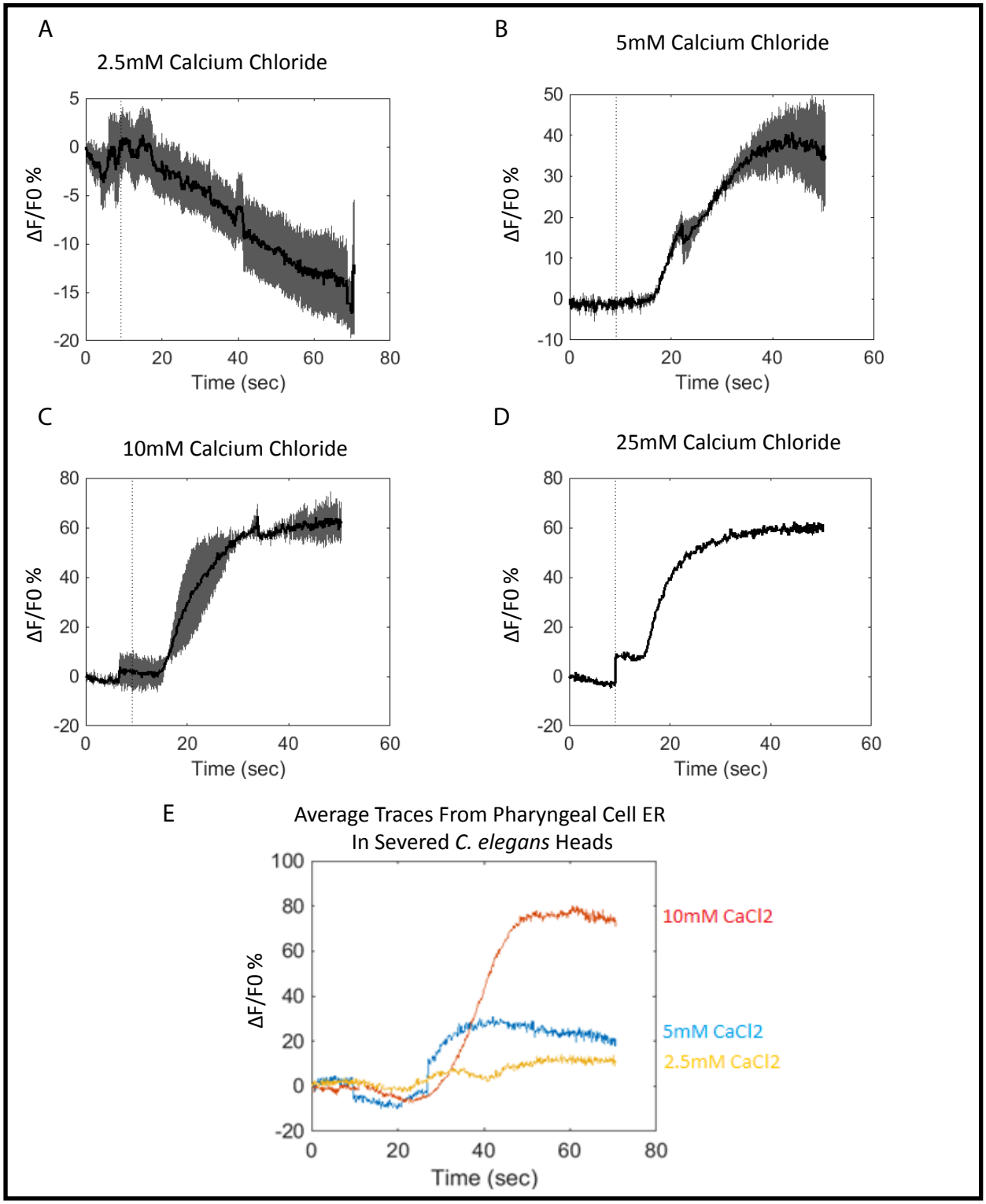

Fig.4.12: The Calcium Responses Of GCaMP6S In The ER Of Pharyngeal Muscle Cells. A: The calcium imaging response in ER to 2.5mM calcium chloride in calcium depleted pharyngeal muscle cells. B: The calcium imaging response in ER to 5mM calcium chloride in calcium depleted pharyngeal muscle cells. C: The calcium imaging response in ER to 10mM calcium chloride in calcium depleted pharyngeal muscle cells. D: The calcium imaging response in ER to 25mM calcium chloride in calcium depleted pharyngeal muscle cells. F: The average traces of GCaMP6S in the ER of pharyngeal muscle cells at differing concentrations of calcium chloride. All traces show the ΔF/F0 %

4.3.4 GCaMP6 Calcium Imaging Can Detect Calcium Transients In Response to Salt in ASK Neurons Expressing *tmc-1*

GCaMP6 variants were co-expressed with *tmc-1* in ASK neurons, a neuron class that does not usually respond to salt. A solution of 0.5M sodium gluconate was perfused over worms and their average traces plotted (Fig. 4.13). Calcium transients were observed in response to salt in ASK neurons. Since these neurons do not usually detect salt it can be concluded that the *tmc-1* expression is conferring the salt response to ASK.

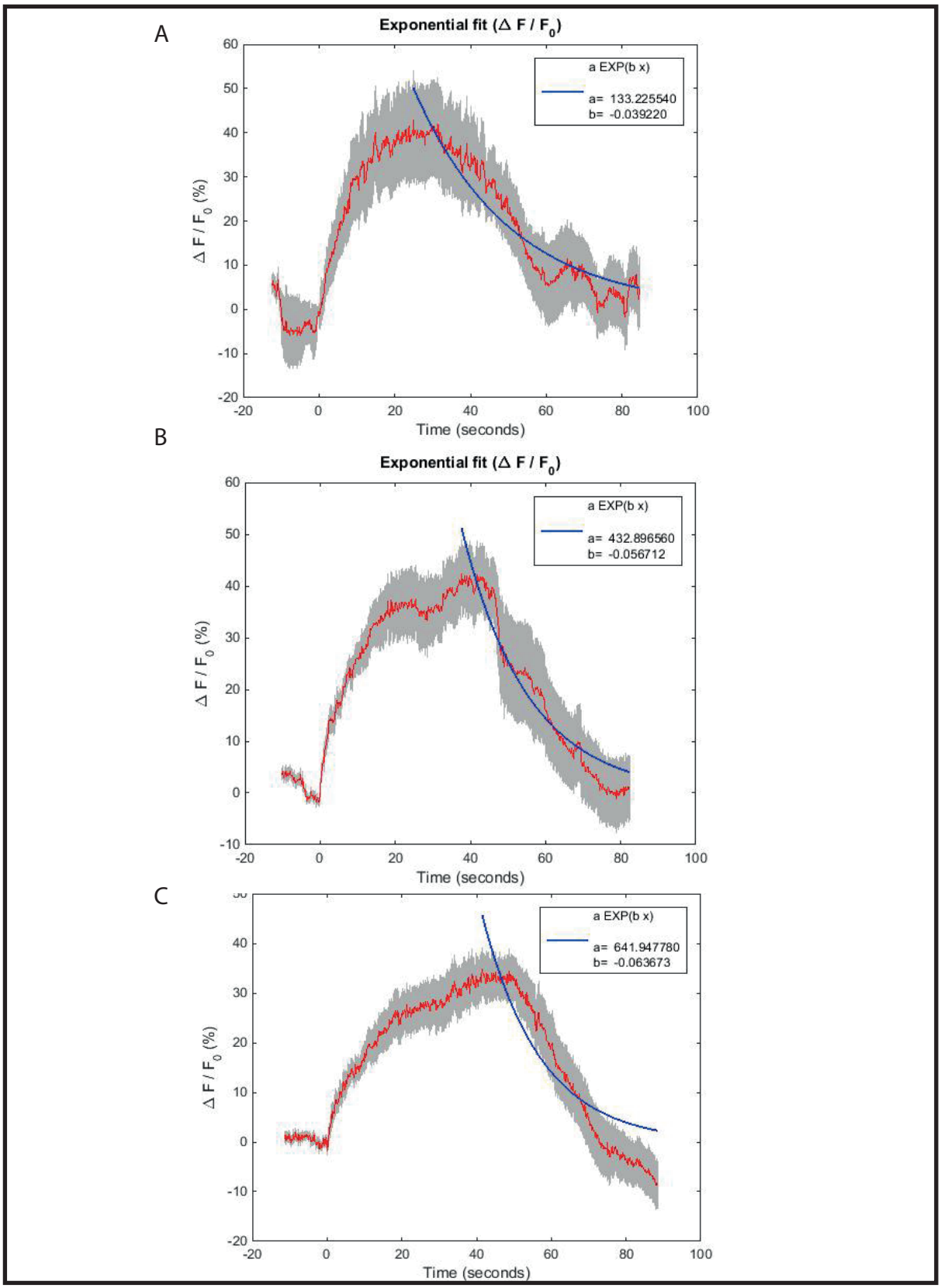

Fig.4.13: Calcium Imaging Responses in ASH expressing *cetmc-1* and GCaMP6 Variants. A: The change in fluorescence of ASH expressing GCaMP6M and *cetmc-1* over a set time-frame divided by the baseline fluorescence. The red line represents the mean of all traces, the grey shaded area shows the range of all traces. Dissociation rate is measured using the best fit exponential degradation shown with the blue line. Traces start at -10s as, for best analysis, the motion onset was set as the start of the trace. Motion onset is the time at which the stimulus was initiated, the stimulus was removed at 50s.B: Is the same but for ASH expressing GCaMP6S and *cetmc-1* C: is the same but for ASH expressing GCaMP6F and *cetmc-1*.

4.4 Discussion

4.4.1 Arrays and Single Copy Lines Are Useful For Different Experiments

The calcium imaging results using GCaMP6 variants as arrays are fairly comparable to the results gained from using single copy lines, each is more suited to separate applications. GCaMP6 arrays, although more variable in baseline fluorescence, do offer a reasonable number of animals with brighter baseline fluorescence than those of single copy lines. This characteristic is useful when doing experiments where there is a chance of movement or interference while imaging. In *C. elegans* imaging from the head neurons can be made difficult by changes in focal plane due to small movements caused by the pumping of the pharynx. It is easier to get accurate fluorescence readings in worms where slight movements are expected if the baseline fluorescence is a little higher than that found in the single copy lines. Perfusion assays are also easier with brighter fluorescence, as the change over from control solution to stimulus solution can cause some disturbance to the image. A brighter neuron can be imaged through this disturbance, while a dim one cannot be as accurately imaged.

Single copy lines are ideal for the comparison of GCaMPs as the number of copies of the gene expressed is standardised. They are also useful for any imaging that will not involve movement, such as imaging from the neurons in the body of a glued worm. The DNA encoding GCaMP is integrated into the genome of the worm, so worms can be selected for imaging without the requirement for a fluorescent microscope. Also the whole population carry GCaMP expression, so there are more worms available for imaging.

It is a shame that GCaMP6F could not be made into a single copy line, as this seemed the most effective when in array form. The variant GCaMP6.649 similarly, could not be introduced as a single copy. It is still unknown as to why these particular variants could not be introduced into the worm's genome via MosSCI. In future, attempts could be made to try to introduce the variants into the genome at a different position. MosSCI allows the option to choose from various introduction sites in the worm's genome. There is a chance that a different introduction site would work where the previous site did not.

4.4.2 GCaMP6 as an Improvement on GCaMP5

There was little improvement on GCaMP5 in the GCaMP6 variants in terms of average dynamic range and kinetics. GCaMP6 variants S, M and F give very variable results in terms of peak fluorescence, unlike GCaMP5, where responses are fairly stable. It is unclear why the mutations in the GCaMP6 variants would cause a greater amount of variability. Figure 4.5 shows the baseline to peak fluorescence correlation for GCaMP5 and GCaMP6M, here the variability in baseline fluorescence for GCaMP5 is comparable to that of GCaMP6M. Therefore the high variability in baseline fluorescence of GCaMP6 variants in array lines is not necessarily the cause of the high variability in their responses. A higher proportion of neurons expressing GCaMP6 did not respond at all to stimuli when compared to GCaMP5 (~40% non-responders for GCaMP6 variants and 29% non-responders for GCaMP5). This could be particularly problematic if using GCaMP6 to image loss of response in a neuron. A large number of worms would have to be imaged to prove a reduction in function when such high rates of wild type worms do not respond. It is also not clear as to why the particular mutations in the GCasMP6 variants would cause the high incidence of non-responders.

There are some differences in activity of GCaMP variants in different neurons, so there may be a chance that GCaMP6 variants are more effective than GCaMP5 in some neurons. Further imaging of

GCaMP6 variants in other neuronal classes would have to be conducted to determine if this is the case.

GCaMP6 variants contain different combinations of new mutations to the GCaMP5G molecule. All the mutations that are altered in the GCaMP6 variants are made in either the GFP molecule or in the calmodulin molecule. There are no extra or missing mutations in the GCaMP6 variants in linkers 1 and 2 in comparison to GCaMP5G. The mutation K78H is found in the GFP molecule, close to the chromophore. This mutation aims to lower the baseline fluorescence of the GCaMP molecule by allowing solvent to reach the GFP chromophore more easily, and thus quenching its fluorescence. This increases the dynamic range of the molecule. K78H is present in GCaMP6M, which does not have baseline fluorescence lower than GCaMP6S and F, suggesting that this mutation is not pivotal in decreasing baseline fluorescence. A317E is found in the CaM domain of GCaMP6F. Alanine is an uncharged amino acid, and glutamic acid a negatively charged amino acid. The shifting of the charge in this case is aimed to increase the affinity for calcium in the bound state, increasing peak fluorescence. GCaMP6F does not have increased mean peak fluorescence in comparison to GCaMP5. However the highest peak response to calcium influx was recorded from GCaMP6F, suggesting that, if the responses were less variable, the mutation may aid in the increase in peak fluorescence.

The mutation K379S is present in the CaM domain of GCaMP6M. A substitution of lysine (positively charged) for serine (uncharged) would also be expected to increase the affinity of CaM in the calcium bound state, again increasing peak fluorescence. Once again this is not the case, suggesting that this mutation is not having the desired effect.

The mutations T318R, S383T and R392G are found in the CaM domains of all three GCaMP6 variants. Each of these mutations is designed to increase the peak fluorescence of the GCaMP molecule in comparison to GCaMP5G. The mean peak fluorescence is higher for GCaMP5G than the GCaMP6 variants these mutations are unlikely to have had the desired effect.

As the mutations added to GCaMP6S and M (D324G, D326L and D397G) were made to decrease the affinity of calmodulin to calcium it may be the case that the low affinity variants are more useful when looking at responses in neurons where the concentration of calcium at resting potential is comparatively high. In this case the GCaMP6s would not be saturated with calcium, while other indicators may be. This allows for high signal to noise traces to be recorded in high Ca+ concentration neurons as the increase in calcium upon activation of the neuron can still be detected.

4.4.3 Future Experiments

There are few applications for which the GCaMP6 variants could be used to further my research into the connection between the DEG/ENaC genes *asic-2* and *acd-5*. Had the mutations added to GCaMP5 resulted in a brighter baseline fluorescence combined with a good signal to noise ratio, the same mutations could have been added to RCaMP in an effort to make it more useful. At present RCaMP1h is not bright enough at baseline to be detected in any *C. elegans* neuron that I have expressed it in. A useable RCaMP variant would be useful in my investigations to determine whether AWC has a synaptic input into ASI. As discussed in section 3.3.6, *acd-5 (ok2657)I* mutant worms have a much reduced response to benzaldehyde in the ASI neurons. The ASIs have not previously been implicated in the detection of benzaldehyde and have not been shown to have synaptic input from the AWCs, a class of neuron that is implicated in benzaldehyde sensation. To determine whether AWC can act presynaptically to ASI, RCaMP could be expressed in ASI and channel rhodopsin in AWC. AWC could then be activated by stimulating channel rhodopsin with blue light, and any response in ASI could be measured by an increase in fluorescence from RCaMP. If a response is observed in ASI it can be

deduced that AWC can act presynaptically to ASI and that the connection between the two is what causes the lack of response to benzaldehyde in the mutant.

4.5 References

Agronskaia, A. V, Tertoolen, L. & Gerritsen, H.C., Fast fluorescence lifetime imaging of calcium in living cells. Available at: https://www.bioee.ee.columbia.edu/courses/upload/Bibliography/agronskaia2004.pdf [Accessed October 12, 2017].

Akerboom, J. et al., 2013. Genetically encoded calcium indicators for multi-color neural activity imaging and combination with optogenetics. *Frontiers in molecular neuroscience*, 6, p.2. Available at: http://www.ncbi.nlm.nih.gov/pubmed/23459413 [Accessed September 6, 2017].

Akerboom, J. et al., 2012. Optimization of a GCaMP Calcium Indicator for Neural Activity Imaging. *Journal of Neuroscience*, 32(40), pp.13819–13840.

Angstadt, J.D. & Stretton, A.O., 1989. Slow active potentials in ventral inhibitory motor neurons of the nematode Ascaris. *Journal of comparative physiology. A, Sensory, neural, and behavioral physiology*, 166(2), pp.165–77. Available at: http://www.ncbi.nlm.nih.gov/pubmed/2607486 [Accessed October 13, 2017].

Bayley, P.M., Findlay, W.A. & Martin, S.R., 1996. Target recognition by calmodulin: Dissecting the kinetics and affinity of interaction using short peptide sequences. *Protein Science*, 5(7), pp.1215–1228. Available at: http://www.ncbi.nlm.nih.gov/pubmed/8819155 [Accessed October 12, 2017].

Chalfie, M. & Sulston, J., 1981. Developmental genetics of the mechanosensory neurons of *Caenorhabditis elegans*. *Developmental biology*, 82(2), pp.358–70. Available at: http://www.ncbi.nlm.nih.gov/pubmed/7227647 [Accessed September 18, 2017].

Chatzigeorgiou, M. et al., 2013. tmc-1 encodes a sodium-sensitive channel required for salt chemosensation in *C. elegans*. *Nature*, 494(7435), pp.95–99. Available at: http://www.ncbi.nlm.nih.gov/pubmed/23364694 [Accessed October 13, 2017].

Chelur, D.S. et al., 2002. The mechanosensory protein MEC-6 is a subunit of the *C. elegans* touch-cell degenerin channel. *Nature*, 420(6916), pp.669–673. Available at: http://www.ncbi.nlm.nih.gov/pubmed/12478294 [Accessed October 24, 2017].

Chen, T.-W. et al., 2013. Ultrasensitive fluorescent proteins for imaging neuronal activity. *Nature*, 499(7458), pp.295–300. Available at: http://www.pubmedcentral.nih.gov/articlerender.fcgi?artid=3777791&tool=pmcentrez&rendertype=abstract.

Davis, R.E. & Stretton, A.O., 1996. The motornervous system of Ascaris: electrophysiology and anatomy of the neurons and their control by neuromodulators. *Parasitology*, 113 Suppl, pp.S97-117. Available at: http://www.ncbi.nlm.nih.gov/pubmed/9051930 [Accessed September 28, 2017].

Du, H. et al., 1996. Extracellular proteins needed for *C. elegans* mechanosensation. *Neuron*, 16(1), pp.183–94. Available at: http://www.ncbi.nlm.nih.gov/pubmed/8562083 [Accessed October 24, 2017].

Frøkjaer-Jensen, C. et al., 2008. Single-copy insertion of transgenes in *Caenorhabditis elegans*. *Nature genetics*, 40(11), pp.1375–83. Available at: http://www.pubmedcentral.nih.gov/articlerender.fcgi?artid=2749959&tool=pmcentrez&rendertype=abstract [Accessed May 11, 2015].

Frøkjær-Jensen, C. et al., 2012. Improved Mos1-mediated transgenesis in *C. elegans*. *Nature Methods*, 9(2), p.117. Available at: http://www.nature.com/nmeth/journal/v9/n2/abs/nmeth.1865.html [Accessed September 18, 2017].

Fukushige, T. et al., 1999. MEC-12, an alpha-tubulin required for touch sensitivity in *C. elegans. Journal of cell science*, 112 (Pt 3), pp.395–403. Available at: http://www.ncbi.nlm.nih.gov/pubmed/9885292 [Accessed September 18, 2017].

Goodman, M.B. et al., 1998. Active currents regulate sensitivity and dynamic range in *C. elegans* neurons. *Neuron*, 20(4), pp.763–72. Available at: http://www.ncbi.nlm.nih.gov/pubmed/9581767 [Accessed October 13, 2017].

Goodman, M.B. et al., 2002. MEC-2 regulates *C. elegans* DEG/ENaC channels needed for mechanosensation. *Nature*, 415(6875), pp.1039–1042.

Grynkiewicz, G., Poenie, M. & Tsien, R.Y., 1985. A new generation of Ca2+ indicators with greatly improved fluorescence properties. *The Journal of biological chemistry*, 260(6), pp.3440–50. Available at: http://www.ncbi.nlm.nih.gov/pubmed/3838314 [Accessed October 24, 2017].

Kaplan, J.M. & Horvitz, H.R., 1993. A dual mechanosensory and chemosensory neuron in *Caenorhabditis elegans. Proceedings of the National Academy of Sciences of the United States of America*, 90(6), pp.2227–31. Available at: http://www.ncbi.nlm.nih.gov/pubmed/8460126 [Accessed October 10, 2017].

Kawashima, Y. et al., 2011. Mechanotransduction in mouse inner ear hair cells requires transmembrane channel-like genes. *The Journal of clinical investigation*, 121(12), pp.4796–809. Available at: http://www.ncbi.nlm.nih.gov/pubmed/22105175 [Accessed October 13, 2017].

Kerr, R. et al., 2000. Optical Imaging of Calcium Neurotechnique Transients in Neurons and Pharyngeal Muscle of *C. elegans* affects the activity of an excitable cell, it is often impor- tant to directly measure its effect on cellular physiology. Unfortunately, the small neurons and hydrostatic skele- ton of *C. elegans* have made physiological studies diffi- cult, especially in live animals. Existing protocols for. *Neuron*, 26, pp.583–594. Available at: http://ac.els-cdn.com/S0896627300811964/1-s2.0-S0896627300811964-main.pdf?_tid=6318fc74-9c8d-11e7-8461-00000aacb35d&acdnat=1505751852_757ddc50e08bbdce8d8ed5fe8ab7905f [Accessed September 18, 2017].

Kurima, K. et al., 2002. Dominant and recessive deafness caused by mutations of a novel gene, TMC1, required for cochlear hair-cell function. *Nature Genetics*, 30(3), pp.277–284. Available at: http://www.nature.com/doifinder/10.1038/ng842 [Accessed October 13, 2017].

Li, W. et al., 2006. A *C. elegans* stretch receptor neuron revealed by a mechanosensitive TRP channel homologue. *Nature*, 440(7084), pp.684–7. Available at: http://www.ncbi.nlm.nih.gov/pubmed/16572173 [Accessed October 11, 2017].

Li, W. et al., 2011. The neural circuits and sensory channels mediating harsh touch sensation in *Caenorhabditis elegans*. *Nature communications*, 2, p.315. Available at: http://www.ncbi.nlm.nih.gov/pubmed/21587232 [Accessed October 24, 2017].

Li, W., Kennedy, S.G. & Ruvkun, G., 2003. *daf-28* encodes a *C. elegans* insulin superfamily member that is regulated by environmental cues and acts in the DAF-2 signaling pathway. *Genes & development*, 17(7), pp.844–58. Available at: http://www.ncbi.nlm.nih.gov/pubmed/12654727 [Accessed October 2, 2017].

Lockery, S.R. & Goodman, M.B., 2009. The quest for action potentials in *C. elegans* neurons hits a

plateau. *Nature Neuroscience*, 12(4), pp.377–378. Available at: http://www.ncbi.nlm.nih.gov/pubmed/19322241 [Accessed October 10, 2017].

Mellem, J.E. et al., 2008. Action potentials contribute to neuronal signaling in *C. elegans*. *Nature neuroscience*, 11(8), pp.865–867.

Miyawaki, A. et al., 1997. Fluorescent indicators for Ca2+based on green fluorescent proteins and calmodulin. *Nature*, 388(6645), pp.882–887. Available at: http://www.nature.com/doifinder/10.1038/42264 [Accessed October 12, 2017].

Nakai, J., Ohkura, M. & Imoto, K., 2001. A high signal-to-noise Ca(2+) probe composed of a single green fluorescent protein. *Nature biotechnology*, 19(2), pp.137–41. Available at: http://www.ncbi.nlm.nih.gov/pubmed/11175727.

Pan, B. et al., 2013. TMC1 and TMC2 are components of the mechanotransduction channel in hair cells of the mammalian inner ear. *Neuron*, 79(3), pp.504–15. Available at: http://www.ncbi.nlm.nih.gov/pubmed/23871232 [Accessed October 13, 2017].

Park, B.J. et al., 2001. Calreticulin, a calcium-binding molecular chaperone, is required for stress response and fertility in *Caenorhabditis elegans*. *Molecular biology of the cell*, 12(9), pp.2835–45. Available at: http://www.ncbi.nlm.nih.gov/pubmed/11553721 [Accessed October 13, 2017].

Savage, C. et al., 1989. *mec-7* is a beta-tubulin gene required for the production of 15-protofilament microtubules in *Caenorhabditis elegans*. *Genes & development*, 3(6), pp.870–81. Available at: http://www.ncbi.nlm.nih.gov/pubmed/2744465 [Accessed September 28, 2017].

Sawin, E.R., Ranganathan, R. & Horvitz, H.R., 2000. *C. elegans* locomotory rate is modulated by the environment through a dopaminergic pathway and by experience through a serotonergic pathway. *Neuron*, 26(3), pp.619–31. Available at: http://www.ncbi.nlm.nih.gov/pubmed/10896158 [Accessed October 10, 2017].

Stevens, F.C., 1983. Calmodulin: an introduction. *Canadian Journal of Biochemistry and Cell Biology*, 61(8), pp.906–910. Available at: http://www.nrcresearchpress.com/doi/10.1139/o83-115 [Accessed October 12, 2017].

Sulston, J., Dew, M. & Brenner, S., 1975. Dopaminergic neurons in the nematode *Caenorhabditis elegans*. *The Journal of Comparative Neurology*, 163(2), pp.215–226. Available at: http://doi.wiley.com/10.1002/cne.901630207 [Accessed October 10, 2017].

Sung-Kyun, K., Xiaoqiang Chen, Juyoung Yoon, Injae Shin. 2011. *Chemical Society Reviews.* 40 (5), pp. 2120-2129.

Suzuki, H. et al., 2003. In Vivo Imaging of *C. elegans* Mechanosensory Neurons Demonstrates a Specific Role for the MEC-4 Channel in the Process of Gentle Touch Sensation. *Neuron*, 39(6), pp.1005–1017. Available at: http://www.sciencedirect.com/science/article/pii/S0896627303005397 [Accessed September 14, 2017].

Tsien, R.Y., 2009. Indicators Based on Fluorescence Resonance Energy Transfer (FRET). *Cold Spring Harbor Protocols*, 2009(7), p.pdb.top57-top57. Available at: http://www.ncbi.nlm.nih.gov/pubmed/20147227 [Accessed October 12, 2017].

Way, J.C. & Chalfie, M., 1989. The *mec-3* gene of *Caenorhabditis elegans* requires its own product for maintained expression and is expressed in three neuronal cell types. *Genes & development*, 3(12A), pp.1823–33. Available at: http://www.ncbi.nlm.nih.gov/pubmed/2576011 [Accessed October 10, 2017].

Zhao, Y. et al., 2011. An expanded palette of genetically encoded Ca^{2+} indicators. *Science (New York, N.Y.)*, 333(6051), pp.1888–91. Available at: http://www.ncbi.nlm.nih.gov/pubmed/21903779 [Accessed September 6, 2017].

Chapter 5: Conclusion

The DEG/ENaC genes *asic-2* and *acd-5* are likely to have some overlapping functions, whether or not they work in the same pathway. Both genes have an effect on lifespan and health-span of the worm, however their effects are opposing. Mutations that remove the entire 2nd transmembrane domain of *acd-5* cause a distinct reduction in the health-span of the worm, with age related paralysis taking place in most individuals by around 9 days, in comparison to around 17 days in N2. The lifespan of *acd-5 (ok2657)I* worms is profoundly reduced to an average of 10 days as opposed to 18 in N2. There are many genes expressed in ASI that have an effect on lifespan, those that cause a reduction in lifespan, if mutated, tend to be involved in the stress-response pathway. This suggests that *acd-5* may be involved in stress response.

Null mutations of *asic-2* cause a distinct increase in health and lifespan, with age related paralysis taking effect on most worms by day 21 and the average lifespan being 22 days. The CRISPR mutant allele *asic-2 (lj112)* has the same effect. As *asic-2* is expressed in the IL2s there is less chance that it is involved in the stress response pathway, as this class of neurons has not been implicated in stress-response. The IL2s do, however, play a role in dauer formation. Many genes that control dauer entry cause an extended lifespan if mutated. Experiments assessing the ability of *asic-2 (ok289)I* to enter dauer phase show interesting results; dauer entry induced by exogenous purified ascarosides is significantly reduced in this mutant. Although this phenotype is not found in *acd-5 (ok2657)I* worms, this mutant shows a defect in entering dauer in the presence of exogenous crude dauer pheromone.

These findings show that tracking of *C. elegans* strains containing mutations in genes of unknown function, and clustering these strains based on micro-motifs is an effective way of establishing functional connections between genes. The method of establishing connections may not be able to detect genes working very closely together, for example genes working in the same complex, or having the same effect in the same pathway. Motif clustering may, also, not be able to detect receptor/ligand integrations, but genes with similarities in mutant phenotypes that are not involved in locomotion can be detected.

It remains to be tested whether or not clustering using pre-determined features can cluster together genes working within the same pathway. An interesting set of experiments would be run to test the functional roles of *delm-2* and *acd-2*, a pair of DEG/ENaCs that cluster strongly using this method of clustering.

The novel GCaMP6 variants do not show any remarkable improvement in their signal to noise ratio, or their kinetics. The low affinity variants of GCaMP6 may have a useful function in neurons where the resting Ca+ concentration is high. This means that they have limited usage in this research project going forward. The neuron classes ASI and IL2 do not have high Ca+ concentrations at resting potential, and both are situated close to the pharynx. This means that the GCaMP6 variants would not be useful in imaging from these neurons as their low affinity properties are not required. Also, GCaMP5 is not the ideal indicator for this research, as its responses are not ratiometric and are therefore susceptible to false positives caused by the movements of the pharynx. Due to the positioning of the neurons the ideal calcium indicator for detecting responses in IL2s and ASIs is Cameleon.

Red-shifted calcium indicators, used in conjunction with channel rhodopsin, would have a useful function in this research going forward, in order to establish the neuronal connectivity of ASI, and therefore the ASIs role in chemosensation of benzaldehyde.

6: Appendix

Table A1: Uncoordinated Mutants

Mutant strain	allele	Locomotory/Morphological phenotype
unc-1	*e1598*	Coiler (Horvitz)
unc-1	*e94*	Coiler (Horvitz)
unc-10	*e102*	Backing increased (Yan hu et al. 2009)
unc-101	*m1*	Coiler (Hodgkin person evidence)
unc-103	*e1597*	Paralysed, egg laying defective (Horvitz)
unc-104	*e1265*	Coiler (Hodgkin person evidence)
unc-105	*ok1432*	Small, body muscle defective (Horvitz)
unc-108	*n501*	Reverse unc (Horvitz)
unc-108	*n777*	Reverse unc (Horvitz)
unc-118	*e2331*	Kinker (Hodgkin)
unc-122	*e2520*	Coiler (Hodgkin)
unc-127	*hs13*	Coiler (Hodgkin)
unc-14	*e57*	Dumpy, egg laying deficient, Paralysed, coiler (Hodgkin)
unc-16	*e109*	Sluggish, Small (Hodgkin), Coiler (trent, Tsung, Horvitz 1983)
unc-17	*e245*	Small, Coiler (Hodgkin)
unc-26	*m2*	Coiler (Jorgensen et al 2000)
unc-29	*e193*	Locomotion variant (Brenner 1974)
unc-3	*e151*	Weak coiler (Hodgkin)
unc-30	*e191*	Sluggish, Shrinker (Hodgkin)
unc-37	*e262*	Coiler (Hodgkin)
unc-4	*e120*	Large (Hodgkin)
unc-4	*gk705*	Locomotion variant (Brenner 1974)
unc-40	*n324*	Locomotion Variant (Brenner 1974)
unc-42	*e270*	Small, Kinker, Egg laying constituitive (Hodgkin)
unc-43	*e755*	Paralysed (Horvitz)
unc-49	*e382*	Short, Sluggish (Koelle etal. 2011), Shrinker (Jorgensen et al. 1999)
unc-55	*e402*	Sluggish, Ventral Coiler (Hodgkin)
unc-69	*e587*	Small, coiler (Hodgkin)
unc-7	*e5*	Backing increased (Lewis and Hodgkin 1977)
unc-75	*e950*	Sluggish, Coiler (Hodgkin)
unc-76	*e911*	Activity level variant (Hodgkin)
unc-77	*e625*	Coiler (Yeh et al. 2008)
unc-79	*e1068*	Fainter (Meneely et al. 1987)
unc-8	*e15*	Coiler (Hodgkin)
unc-8	*n491*	Coiler (Horvitz)
unc-8	*n492*	Coiler (Horvitz)
unc-80	*e1069*	Fainter (Meneely et al. 1987)
unc-86	*e1416*	Behaviour variant (Horvitz 1979)
unc-89	*e1460*	Clear (Hodgkin)
unc-9	*e101*	Forward kinker (Hodgkin)

Part List for a Single Tracking Unit

* All prices are as of 30/03/2009

Part Name	Company	
	Price	Quantity
Camera	**ANMO Electronics Corporation**	
DinoLite Pro AM413T	~ £250.00	1
http://www.anmo.com.tw/db/products-more.asp?id=72		
Motorized stage	**Zaber Technologies**	
T-NA08A50, Linear Actuator, 50mm travel, RS232 plus manual control.	~ £877.5	1
KT-NA08A50, Linear Actuator, 50mm travel, RS232 plus manual control, Kit.	~ £900.00	1
TSB60-M, Translation Stage, 60 mm travel, M6 thread.	~ £266.54	2
* For assembling the system in the US a different power adaptor is need. In this case please add order: SUB-PS15V0410, Power Supply Substitution (subtract one PS15V04, add one PS15V10)	0.00	1
http://www.zaber.com/products/product_detail.php?detail=T-NA08A50 http://www.zaber.com/products/product_detail.php?detail=KT-NA08A50 http://www.zaber.com/products/product_detail.php?detail=TSB60-M http://www.zaber.com/products/product_accessories.php?detail=SUB-PS15V0410		
LED light, lens, holder	**Farnell, Carclo Optics**	
Philips LXHL-FD3C, Lumileds, LXHL-FD3C - LED, Luxeon III Star, Side Emitting	£4.96	1
Carclo 10140 Frosted Wide Lens	£0.68	1
Carclo 10043 Star Board Holder Black	£0.14	1
http://uk.farnell.com/lumileds/lxhl-fd3c/led-luxeon-iii-star-side-emit-red/dp/1109128 (data sheet at http://www.philipslumileds.com/pdfs/DS46.PDF) http://carclo-optics.co.uk/catalog/product_info.php?products_id=40 http://carclo-optics.co.uk/catalog/product_info.php?products_id=48		
LED heat sink	**RS Components Ltd**	
268-111, High power extruded heat sinks designed for use with TO220 devices	£4.33	1
Parts for the rig	**Comar Instruments Ltd**	
50 FQ 50 Fresnel Lens, FL 50mmx64x64mm	£39.00	1
DO 90, Opal diffuser 65x65mm	£7.50	1
203 RM 01, Mounting rod system, 203mm rod	£45.00	1
20 RM 01, Mounting rod system, basic carrier	£51.00	1
30 XT 40, Rack and pinion stage	£132.00	1
427 BR 00, Edge clamp, Holds Fresnel lens, opal diffuser and plate holder	£27.00	2
BR 93, S/S post 300mm x dia 10mm 30cm posts making tripod	£48.00	3
105 BR 10, Cross clamp, 10mm Connect 2 rods holding light, Fresnel lens/diffuser and camera to tripod structure	£11.00	3
BR 94, Cross clamp, 10mm with steel screws Connect rods at top of structure	£12	4

45 BH 10, Post holder, 45mm for 10mm post Holds rod connected to plate holder	£8.00	1
BR 92 252 BR 00, Tube holder, bored out to 33mm dia Holds camera	£31.00	1
16 BR 10, S/S post, 50mm x dia 10mm 5cm poles, 2 for camera and 1 for plate holder	£4.50	3
36 BR 10, S/S Post, 100mm x dia 10mm 10cm poles holding light and Fresnel lens/opal diffuser	£6.00	2
66 BR 10, S/S Post, 150mm x dia 10mm 15cm poles. Connect tripod structure at top	£6.00	2
Custom parts	**In-house mechanical and wood workshops**	
LED Holder, made in house at mechanical workshop		1
Square plastic plate holder 50mm x 55mm, made in house at mechanical workshop		1
Aluminium base, made in house at the mechanical workshop, dimensions 350mm by 350mm, with pads on bottom to dampen vibration and holes to screw stage and mounting rod (worm plate holder)		1
Wooden spacer made in house by carpentry to allow the 5cm post holding the camera to be secured from underneath		1
Wooden square to attach camera and tripod structure, made in house by carpentry		1

Labelled Diagram of the Tracking Unit

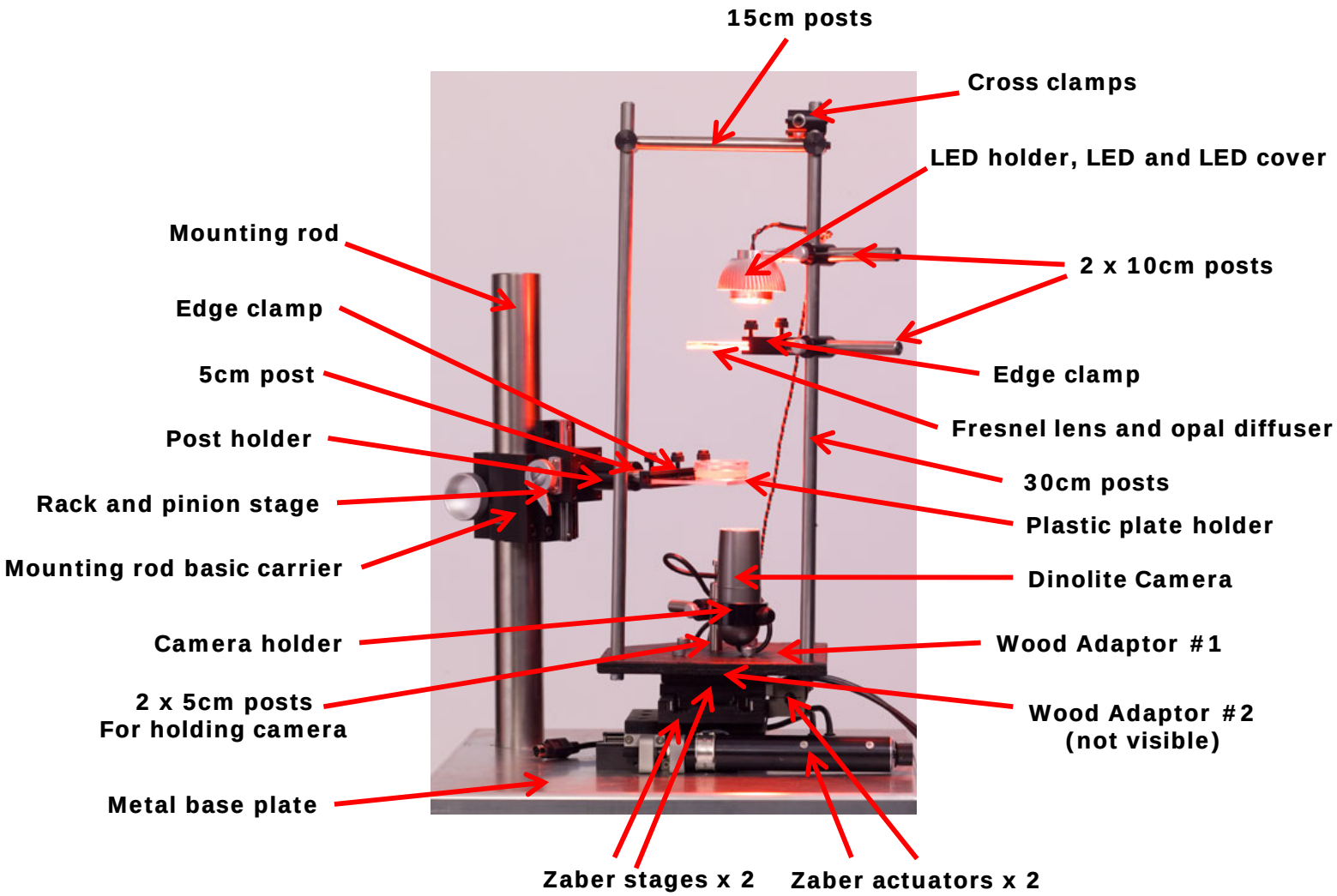

Worm Tracker wood adaptors

Notes:

- Adaptors are all designed to fit Zaber stages. Do not assume they will fit other stage units, please make measurements to be sure
- It would be highly advantageous to have a drill press to make the holes straight, especially if you are making several units at one time
- All measurements are center of holes

Wood Adaptor #1

- Attaches to stage, supports camera and tripod rig structure

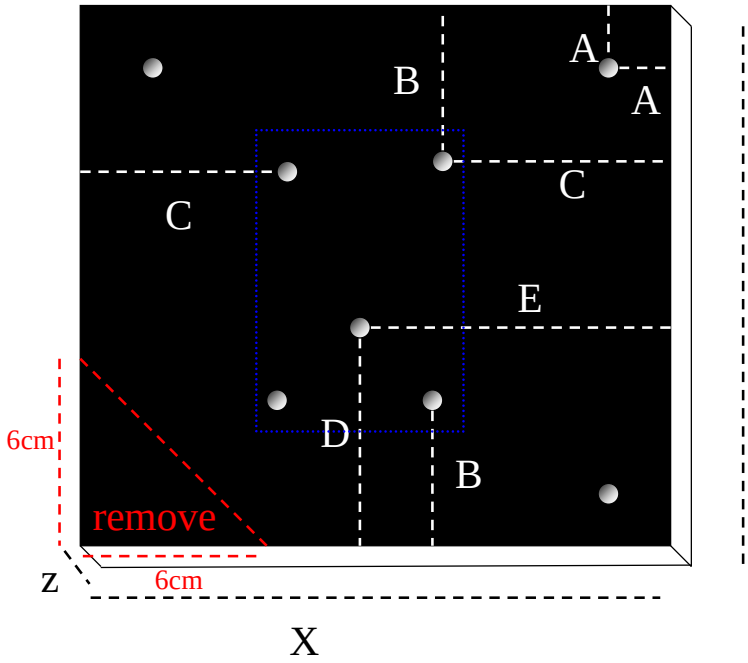

X

A = 1.4cm

B = 4.4cm

C = 5.65cm

D = 6.9cm

E = 8.15cm (center)

X = 16.3cm

Z = 1cm
(as close as you can get with plywood or composite particle/plywood)

= cut so that base does run into pole

= Outline of wood adaptor piece #2
Note: all holes correspond to counterparts in piece #2

= hole large enough for M6 machine screw to fit loosely through (Note: for Zaber stages, scale hole size so that the screws to your stage model fit loosely through.)

- Holes at measurement A are for supporting the 30cm posts making the tripod structure
- Holes at measurements B and C are for screwing the wood adaptor onto the Zaber stage
- Hole at measurements D and E is for holding a 5cm post on which to mount the Dinolite camera

Wood Adaptor #2

- This adaptor is required to allow the 5cm post holding the camera to be secured from underneath

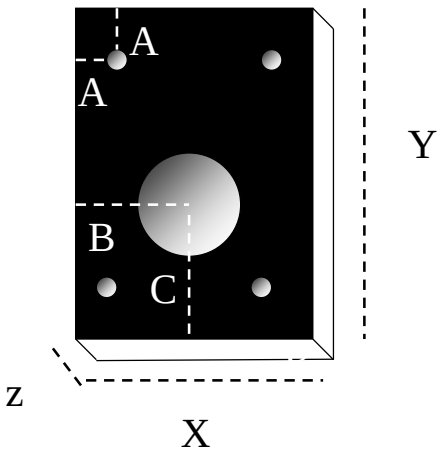

A = 1.25cm

B = 3.75cm (center)

C = 3.75cm

X = 7.5cm

Y = 10cm

Z = <or=0.75cm
(must be high enough to allow for washer and screw head to be recessed within--this is large enough for an M6 machine screw (0.5cm) and a standard 4cm wood washer(0.15cm))

= 4.2cm
(Note: must be larger than the washer used to dampen the stage to camera vibrations -- 4cm)

= hole large enough for M6 machine screw to fit loosely through (Note: for Zaber stages, scale hole size so that the screws to your stage model fit loosely through)

<u>Base Plate Dimensions</u>

- The base plate can be made either of wood or metal
- Needs to be heavy to dampen vibrations
- We suggest adding pads on the bottom to dampen vibrations
- The 3 central holes are for attaching the Zaber stage

- The 5 holes at the edge are for securing the mounting rod (holding worm plates) at variable distances from the stage

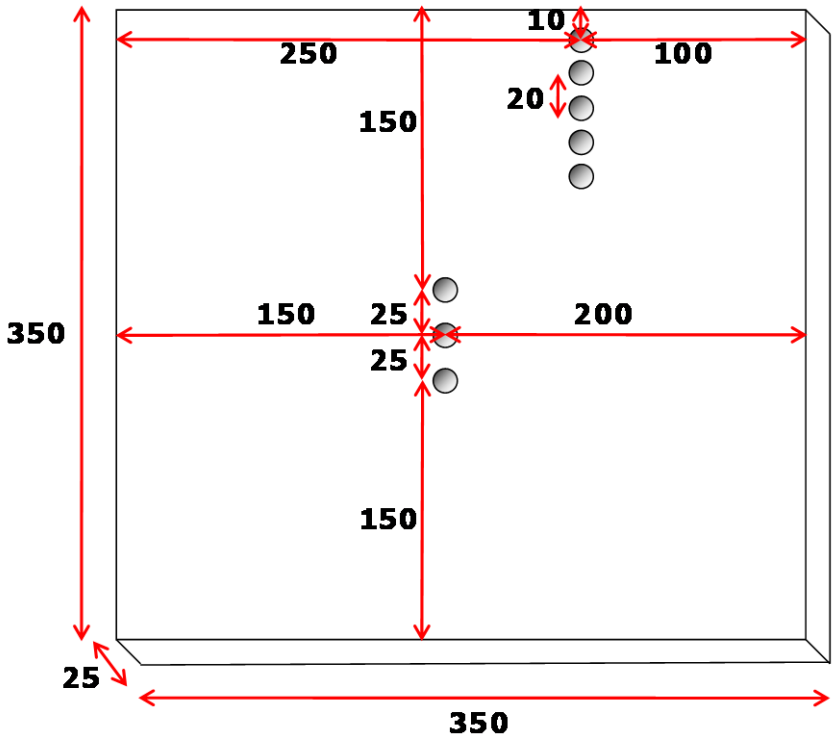

= hole large enough for M6 machine screw to fit loosely through (Note: for Zaber stages, scale hole size so that the screws to your stage model fit loosely through).

All measurements in mm.

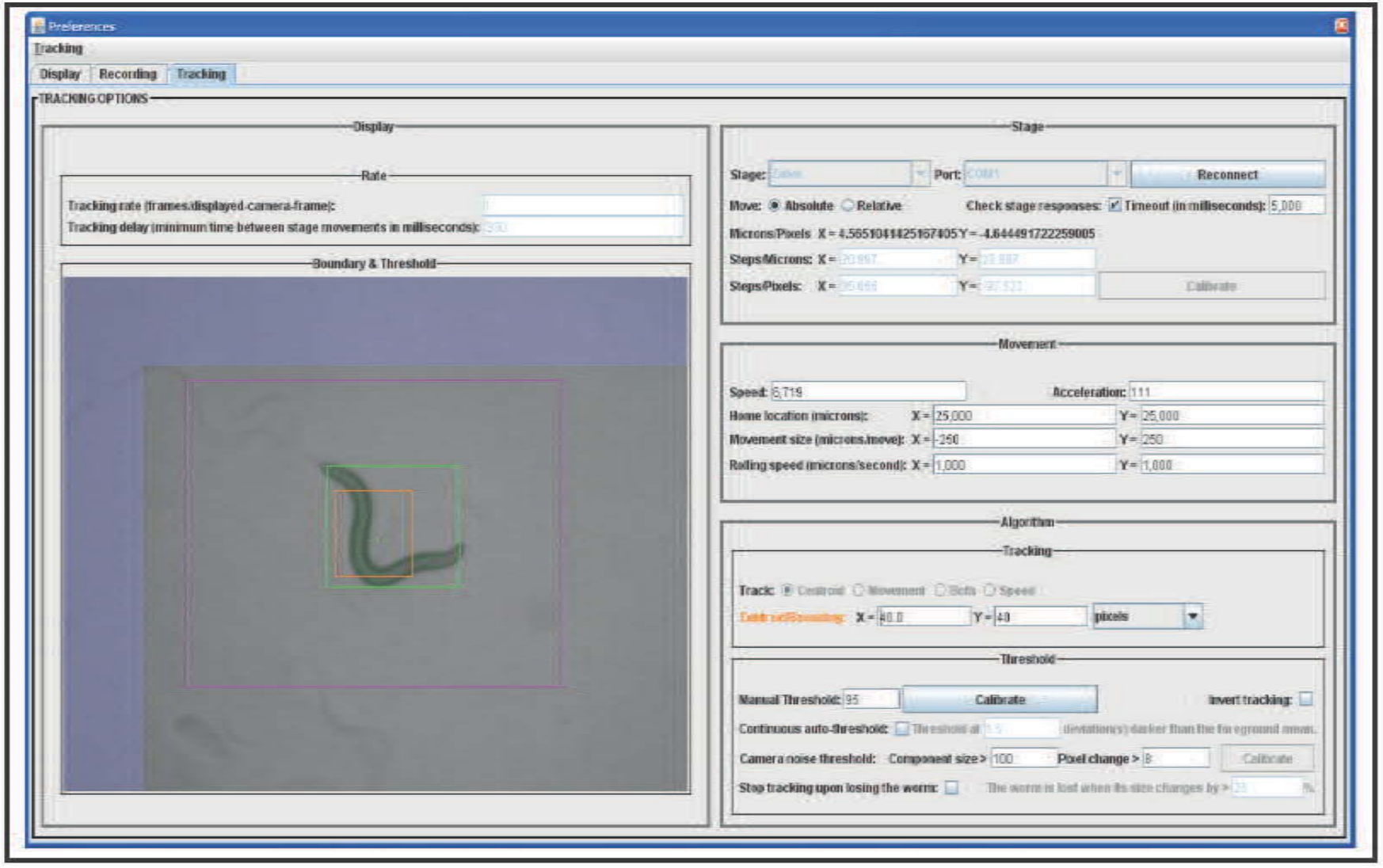

. A screen shot of the parameters set in all high-throughput tracking recordings.

Table A2: Strains Tracked

Column1	Column2	Column3	Column4	Column5
Gene	Allele	Strain	Chromosome	Strain aquired from
		AQ2947		CGC
		CF2027		kenyon or Bargman
		CF2046		kenyon or Bargman
		CB4852		Andre from Kate
		CB4853		Andre from Kate
		CB4856		Andre from Kate
		ED3017		Andre from Kate
		ED3021		Andre from Kate
		ED3049		Andre from Kate
		ED3054		Andre from Kate
		JU258		Andre from Kate
		JU298		Andre from Kate
		JU345		Andre from Kate
		JU393		Andre from Kate
		JU394		Andre from Kate
		JU402		Andre from Kate
		JU438		Andre from Kate
		JU440		Andre from Kate
		LSJ1		Andre from Kate
		MY16		Andre from Kate
npr-1	*g320*	RC301	X	Andre from Kate
acc-4	*ok2371*	RB1832	III	CGC
acr-10	*ok3064*	RB2262	X	CGC
acr-11	*ok1345*	RB1263	I	CGC
acr-14	*ok1155*	RB1132	II	James
acr-15	*ok1214*	RB1172	V	CGC
acr-18	*ok1285*	RB1226	V	CGC
acr-19	*ad1674*	DA1674	I	CGC
acr-2	*ok1887*	RB1559	X	CGC
acr-21	*ok1314*	RB1250	III	CGC
acr-23	*ok2804*	RB2119	V	CGC
acr-3	*ok2049*	RB1659	X	CGC
acr-6	*ok3117*	RB2294	I	CGC
acr-7	*tm863*	FX863	II	CGC
acr-9	*ok933*	VC649	X	CGC
asic-1	*ok415*	RB680	I	CGC
asic-2	*ok289*	RB557	I	Andre
bas-1	*ad446*	MT7988	III	CGC
C04B4.2	*ok1212*	RB1170	X	CGC
C11D2.2	*ok1565*	RB1380	IV	CGC
C18B2.6	*ok2353*	RB1818	X	Andre
C24G7.1	*ok1822*	RB1523	I	CGC

C24G7.4	*ok1237*	RB1192	I	
C38D9.2	*ok1853*	RB1543	V	CGC
C46A5.2	*ok1187*	RB1156	IV	Andre
C52B9.11	*gk596*	VC1340	X	CGC
cat-2	*e1112*	CB1112	II	CGC
cat-4	*e1141*	CB1141	V	schafer lab liquid N2
ced-1	*e1735*	CB3203	I	CGC
ced-6	*n1813*	MT4433	III	CGC
cku-80	*ok861*	RB964	III	CGC
clh-3	*ok763*	VP91	II	Robyn
clh-3	*ok768*	RB905	II	CGC
daf-2	*e1730*			
daf-1	*sa184*	JT184	IV	schafer lab liquid N2
daf-2 (Queelim)	*(e1368)*			
daf-2 (Queelim)	*(e1370)*			
daf-3	*e1376*	CB1376	X	schafer lab liquid N2
daf-4	*e1364*	CB1364	III	schafer lab -80
daf-5	*e1386*	CB1386	II	schafer lab liquid N2
daf-7	*m62*	DR62	III	schafer lab liquid N2
daf-16 (Queelim)	*mu86*			
daf-28 (Queelim)	*tm2308*			
dat-1	*ok157*	RM2702	III	Victoria
del-1	*ok150*	NC279	X	Andre
del-1;unc-8	*ok150;e15lb145*	AQ2937	X;IV	Andre
del-4	*ok1014*	RB1064	I	Andre
dnc-1	*or404*	EU1006	IV	Robyn
dop-1	*vs101*	LX636	X	CGC
dop-1;dop-2	*vs100;vs105*	LX706	V;X	CGC
dop-1;dop-2;dop-3	*vs100;vs105;vs106*	LX734	V;X	CGC
dop-1;dop-3	*vs100;vs106*	LX705	X	CGC
dop-2	*vs105*	LX702	V	CGC
dop-2;dop-3	*vs105;vs106*	LX704	V;X	CGC
dop-3	*vs106*	LX703	X	CGC
dop-4	*tm1392*	FG58	X	CGC
dpy-20	*e1282*	CB1282	IV	CGC
eat-16	*sa609*	JT609	I	schafer lab -80
egg-5	*ok1781*	VC1295	I	CGC
egl-1	*n487*	MT1082	V	CGC
egl-10	*md176*	MT8504	V	schafer lab liquid N2
egl-11	*n587*	MT1217	V	schafer lab liquid N2
egl-12	*n602*	MT1232	V	CGC
egl-13	*n483*	MT1078	X	CGC
egl-14	*n549*	MT1179	X	CGC
egl-15	*n484*	MT1079	X	schafer lab -80
egl-17	*e1313*	CB1313	X	CGC
egl-18	*ok290*	JR2370	IV	CGC

egl-19	*n2368*	MT6129	IV	schafer lab liquid N2
egl-2	*n693*	MT1444	V	CGC
egl-20	*mu39*	CF263	IV	CGC
egl-21	*n476*	KP2018	IV	CGC
egl-21	*n611*	MT1241	IV	schafer lab liquid N2
egl-23	*n601*	MT1231	IV	CGC
egl-24	*n572*	MT1202	III	schafer lab liquid N2
egl-27	*ok151*	KS99	II	CGC
egl-28	*n570*	MT1200	II	CGC
egl-30	*ep271 gain of function*	CE1047	I	Robyn
egl-30;goa-1	*n686;n1134*	AQ916	I	Denise (schafer lab -80)
egl-31	*n472*	MT1067	I	CGC
egl-32	*n155*	MT155	I	schafer lab -80
egl-33	*n151*	MT151	I	schafer lab liquid N2
egl-36	*n728*	MT1540	X	CGC
egl-37	*n742*	MT1542	II	CGC
egl-40	*n606*	MT1236	IV	CGC
egl-42	*n995*	MT2068	II	Robyn
egl-43	*n1079*	MT2246	II	CGC
egl-44	*n1080*	MT2247	II	CGC
egl-46	*n1127*	MT2316	V	CGC
egl-47	*n1081*	MT2248	V	schafer -80
egl-49	*n1107*	MT2293	X	schafer -80
egl-5	*n486*	MT1081	III	schafer lab liquid N2
egl-50	*n1086*	AQ2316	II	Robyn
egl-6	*n592*	MT1222	X	schafer lab liquid N2
egl-7	*n575*	MT1205	III	schafer lab liquid N2
egl-8	*n488*	MT1083	V	schafer lab liquid N2
egl-9	*n586*	MT1216	V	CGC
F14B8.2	*ok3517*	RB2536	X	CGC
F23B2.3	*ok1226*	RB1177	IV	Andre
F54E4.4	*ok2336*	RB1802	X	CGC
flp-1	*yn2*	NY7	IV	CGC
flp-10	*ok2624*	RB1989	IV	CGC
flp-11	*tm2706*	FX2706	X	Victoria
flp-12	*ok2409*	RB1863	X	CGC
flp-13	*tm2427*	FX2427	IV	Victoria
flp-16	*ok3085*	RB2275	II	CGC
flp-17	*ok3587*	RB2575	IV	CGC
flp-18	*db99*	AX1410	X	Victoria
flp-19	*ok2460*	RB1902	X	CGC
flp-20	*ok2964*	RB2188	X	CGC
flp-21	*ok889*	RB982	V	CGC
flp-25	*gk1016*	VC1982	III	Victoria
flp-28	*gk1075*	VC2502	X	CGC
flp-3	*ok3265*	VC2497	X	CGC

flp-33	*gk1038*	VC2423	I	CGC
flp-6	*ok3056*	VC2324	V	Victoria
flp-7	*ok2625*	RB1990	X	CGC
flp-9	*ok2730*	RB2067	IV	CGC
flr-1	*ut11*	JC55	X	Andre
ftn-2	*ok404*	RB668	I	CGC
gar-2	*ok520*	RB756	III	schafer lab liquid N2
gld-1	*op236*	TG34	I	CGC
gly-2	*gk204*	VC335	I	CGC
goa-1	*sa734*	DG1856	I	Robyn
gon-2	*q362*	EJ26	I	Andre
gpa-1	*pk15*	NL332	V	CGC
gpa-10	*pk362*	NL1147	V	CGC
gpa-11	*pk349*	NL787	II	CGC
gpa-12	*pk322*	NL594	X	CGC
gpa-13	*pk1270*	NL2330	V	CGC
gpa-14	*pk347*	AQ495	I	Schafer lab liquid N2
gpa-15	*pk477*	NL797	I	CGC
gpa-16	*ok2349*	RB1816	I	CGC
gpa-17	*ok2334*	RB1800	III	CGC
gpa-2	*pk16*	NL334	V	CGC
gpa-3	*pk35*	NL335	V	CGC
gpa-4	*pk381*	NL790	IV	CGC
gpa-5	*pk376*	NL1137	X	CGC
gpa-6	*pk480*	NL1146	X	Schafer lab liquid N2
gpa-7	*pk610*	NL795	IV	Schafer lab liquid N2
gpa-8	*pk345*	NL1142	V	Schafer lab liquid N2
gpa-9	*pk438*	NL793	V	CGC
gpb-2	*sa603*	JT603	I	CGC
gpc-1	*pk298*	NL792	X	CGC
gsa-1	*ce81*	KG421	I	CGC
hcf-1	*ok559*	RB777	IV	CGC
him-5;spe-41	*e1490;sy693*	PS4330	V;III	Andre
inft-1	*gk386*	VC909	III	CGC
ins-1 (Queelim)	*nr2091*			
ins-2 (Queelim)	*tm4467*			
ins-3 (Queelim)	*tm3608*			
ins-4 (Queelim)	*tm3620*			
ins-5 (Queelim)	*tm2560*			
ins-6 (Queelim)	*tm2416*			
ins-7 (Queelim)	*tm2001*			
ins-8 (Queelim)	*tm4144*			
ins-9 (Queelim)	*tm3618*			
ins-10 (Queelim)	*tm3498*			
ins-11	*tm1053*	FX1053	II	CGC
ins-11 (Queelim)	*tm1053*			

ins-12 (Queelim)	*tm2918*			
ins-13 (Queelim)	*tm4856*			
ins-14 (Queelim)	*tm4886*			
ins-15	*ok3444*	RB2489	II	CGC
ins-15 (Queelim)	*ok3444*			
ins-16	*ok2919*	RB2159	III	CGC
ins-16 (Queelim)	*ok2919*			
ins-17 (Queelim)	*tm0790*			
ins-18	*ok1672*	VC1218	I	CGC
ins-18 (Queelim)	*tm0339*			
ins-19 (Queelim)	*tm5155*			
ins-20 (Queelim)	*tm1947*			
ins-21 (Queelim)	*tm5180*			
ins-22	*ok3616*	RB2594	III	CGC
ins-22 (Queelim)	*ok3616*			
ins-23 (Queelim)	*tm1875*			
ins-25	*ok2773*	RB2098	I	CGC
ins-25 (Queelim)	*ok2773*			
ins-26 (Queelim)	*tm1983*			
ins-27 (Queelim)	*ok2474*			
ins-27	*ok2474*	RB1911	I	CGC
ins-28	*ok2722*	RB2059	I	CGC
ins-28 (Queelim)	*ok2722*			
ins-3	*ok2488*	RB1915	II	CGC
ins-29 (Queelim)	*tm1922*			
ins-30	*ok2343*	RB1809	I	CGC
ins-30 (Queelim)	*ok2343*			
ins-31	*ok3543*	RB2552	II	CGC
ins-31 (Queelim)	*ok3543*			
ins-33 (Queelim)	*tm2988*			
ins-34 (Queelim)	*tm3095*			
ins-35	*ok3297*	RB2412	V	CGC
ins-35 (Queelim)	*ok3297*			
ins-38 (Queelim)	*tm2632*			
ins-4	*ok3534*	RB2544	II	CGC
jnk-1	*gk7*	VC8	IV	CGC
lev-1	*x427*	ZZ427	IV	
lev-8	*x15*	ZZ15	X	James
lig-4	*ok716*	RB873	III	CGC
lin-39	*n709*	MT1514	III	schafer lab liquid N2
lite-1	*kg1180*	ce314	X	Victoria
lon-2	*e678*	CB678	X	CGC
lov-1	*ok522*	RB753	II	Andre
M01A8.2	*gk470*	VC1071	III	CGC
mec-10	*e1515*	CB1515	X	Marios
mec-10	*tm1552*	AQ1413	X	Denise

mec-10	*u20*	AQ2533	X	Marios
mec-12	*e1605*	AQ1031	III	Denise
mec-12	*u76*	AQ1037	III	Denise
mec-14	*u55*	AQ1038	III	Denise
mec-18	*u228*	AQ2649	X	Denise
mec-4	*u253*	AQ908	X	Denise
mec-7	*u448*	AQ1033	X	Denise
mir-124	*n4255*	MT13292	IV	
mod-1	*ok103*	MT9668	V	Victoria
mod-5	*n822*	MT8944	I	Victoria
mtm-9	*ok3523*	RB2541	V	CGC
N2 no wait				
N2 male				
nca-2	*gk5*	VC9	III	CGC
nca-2;nRHO-1	*G14V;gk5*	AQ2934	III;I	Victoria
nca-2;nRHO-1;unc-77	*gk5;G14V;gk9*	AQ2932	III;I;IV	Victoria
nca-2;unc-77	*gk9;gk5*	AQ1441	III;IV	Victoria
nhr-116	*gk728*	VC1565	V	CGC
nhr-95	*gk836*	VC1759	V	CGC
nlp-1	*ok1469*	RB1340	X	CGC
nlp-12	*ok335*	RB607	IV	CGC
nlp-14	*tm1880*	FX1880	X	Schafer lab -80
nlp-15	*ok1512*	VC1063	I	CGC
nlp-17	*ok3461*	RB2498	IV	CGC
nlp-18	*ok1557*	RB1372	II	CGC
nlp-2	*tm1908*	FX1908	X	Schafer lab -80
nlp-20	*ok1591*	RB1396	IV	CGC
nlp-3	*ok2688*	RB2030	X	CGC
nlp-5	*ok1981*	RB1609	II	CGC
nlp-8	*ok1799*	VC1309	I	CGC
npr-1	*ad609*	DA609	X	Victoria
npr-10	*tm1568*	FX1568	X	Victoria
npr-11	*ok594*	RB799	X	Victoria
npr-12	*tm1498*	FX1498	IV	Victoria
npr-13	*tm1504*	AQ2153	V	Victoria
npr-2	*ok419*	AQ2056	IV	Victoria
npr-20	*ok2575*	RB1958	II	CGC
npr-3	*tm1583*	FX1583	IV	Victoria
npr-4	*tm1782*	AX1743	X	Victoria
npr-5	*ok1583*	AX1745	V	Victoria
npr-7	*ok527*	RB761	X	Victoria
npr-8	*tm1553*	FX1553	X	Victoria
npr-9	*tm1652*	IC683	X	CGC
nRHO-1	*G14V*	QT309	I	Victoria
nRHO-1;unc-77	*G14V;gk9*	AQ2933	I;IV	Victoria

nRHO-1;unc-79	*G14V;e1068*	AQ2935	I;III	Victoria
nRHO-1;unc-80	*G14V;e1069*	AQ2936	I;V	Victoria
ocr-1;ocr-2;ocr-4	*ok132;ak47;vs137*	LX982	IV;V	Andre
ocr-2;ocr-4	*ak47;vs137*	LX981	IV	Andre
ocr-3	*ok1559*	RB1374	X	Andre
ocr-4	*tm2173*	FX2173	IV	Andre
ocr-4	*vs137*	LX950	IV	Andre
octr-1	*ok371*	VC224	X	
odr-3	*n2150*	CX2205	V	Schafer lab -80
osm-9	*ky10*	CX10	IV	Andre
osm-9;trpa-1	*ky10;ok999*	AQ1422	IV	Andre
pdl-1	*gk157*	VC282	II	CGC
pdr-1	*gk448*	VC1024	III	CGC
pkc-1	*nj3*	IK130	V	Andre
pkg-1	*n478*	MT1073	IV	schafer lab -80
pmk-1	*km25*	KU25	IV	Andre
pqn-66	*ok1507*	RB1350	II	Andre
rab-3	*y250*	NM210	II	CGC
rgs-6	*vs62*	LX533	X	CGC
ric-19	*ok833*	RB946	I	CGC
rig-6	*gk449*	VC840	II	CGC
sem-4	*ga82*	EW35	I	CGC
ser-1	*ok345*	DA1814	X	Victoria
ser-2	*pk1357*	OH313	X	Victoria
ser-4	*ok512*	AQ866	III	Victoria
ser-5	*tm2654*	AQ2197	I	Victoria
ser-6	*tm2146*	FX2146	IV	Victoria
ser-7	*tm1325*	DA2100	X	Victoria
sma-2	*e502*	CB502	III	Scafer lab
sma-3	*e491*	CB491	III	Scafer lab
snf-1	*ok790*	RB919	I	CGC
snf-10	*hc194*	BA1093	V	CGC
snf-11	*ok156*	RM2710	V	CGC
snf-2	*ok147*	RB641	I	CGC
snf-4	*ok496*	RB738	II	CGC
snf-5	*ok447*	RB687	II	CGC
snf-6	*eg28*	BZ28	III	CGC
snf-7	*ok482*	RB709	III	CGC
snf-8	*ok349*	RB648	IV	CGC
snf-9	*ok957*	RB1030	IV	CGC
sng-1	*ok234*	RB503	X	CGC
srp-8	*ok291*	RB559	V	CGC
sup-9	*n180*	MT180	II	CGC
syg-1	*ok3640*	RB2615	X	CGC
syg-2	*ky671*	CX6391	X	CGC
T14B1.1	*ok1702*	VC1243	X	CGC

T28F2.7	*ok2657*	RB2005	I	Andre
tag-336	*ok1477*	VC975	V	Andre
tbh-1	*n3247*	MT9455	X	CGC
tdc-1	*n3419*	MT13113	II	
tmc-1	*ok1859*	RB1546	X	
tom-1	*ok285*	VC223	I	
tph-1	*mg280*	MT15434	II	Victoria
trp-1	*sy690*	TQ225	III	Andre
trp-2	*gk298*	VC602	III	Andre
trp-2	*sy691*	TQ194	III	Andre
trp-4	*sy695*	TQ296	I	Andre
trpa-1	*ok999*	RB1052	IV	Andre
trpa-2	*tm3085*	FX3085	I	Andre
trpa-2	*ok3189*	RB2351	I	Andre
trpa-2	*tm3092*	FX3092	I	Andre
ttx-1	*p767*	PR767	V	CGC
tyra-2	*tm1846*	FX1846	X	Victoria
tyra-3	*ok325*	VC125	X	Victoria
unc-1	*e1598*	CB1598	X	schafer lab -80
unc-1	*e94*	CB94	X	
unc-10	*md1117*	NM1657	X	
unc-10	*e102*	CB102	X	CGC
unc-101	*m1*	DR1	I	schafer lab -80
unc-103	*e1597*	CB1597	III	schafer lab -80
unc-104	*e1265*	CB1265	II	
unc-105	*ok1432*	RB1316	II	
unc-108	*n501*	MT1093	I	
unc-108	*n777*	MT1656	I	
unc-115	*mn481*	SP1789	X	schafer lab liquid N2
unc-116	*e2310*	FF41	III	CGC
unc-118	*e2331*	CB4371	X	schafer lab -80
unc-122	*e2520*	CB4870	I	schafer lab -80
unc-127	*hs13*	HH27	V	schafer lab -80
unc-14	*e57*	CB57	I	
unc-16	*e109*	CB109	III	
unc-17	*e245*	CB933	IV	schafer lab -80
unc-18	*e81*	CB81	X	CGC
unc-2	*gk366*	VC854	X	CGC
unc-2	*ox106*	EG106	X	schafer lab -80
unc-26	*m2*	DR2	IV	
unc-29	*e193*	CB193	I	
unc-3	*e151*	CB151	X	
unc-30	*e191*	CB845	IV	
unc-31	*e169*	CB169	IV	
unc-32	*e189*	CB189	III	
unc-34	*e566*	CB566	V	schafer lab liquid N2

unc-37	*e262*	CB262	I	schafer lab -80
unc-38	*e264*	CB904	I	schafer lab liquid N2
unc-4	*e120*	CB120	II	schafer lab liquid N2
unc-4	*gk705*	VC1528	II	CGC
unc-40	*n324*	MT324	I	schafer lab -80
unc-42	*e270*	CB270	V	CGC
unc-43	*e755*	CB755	IV	schafer lab liquid N2
unc-44	*e1197*	CB1197	IV	schafer lab -80
unc-49	*e382*	CB382	III	CGC
unc-55	*e402*	CB402	I	
unc-60	*e723*	CB723	V	schafer lab -80
unc-63	*ok1075*	VC731	I	schafer lab -80
unc-69	*e587*	CB587	III	schafer lab -80
unc-7	*e5*	CB5	X	
unc-75	*e950*	CB950	I	schafer lab -80
unc-76	*e911*	DR96	V	CGC
unc-77	*gk9*	VC12	IV	C11D2.6 CGC
unc-77	*e625*	DR1089	IV	CGC
unc-79	*e1068*	CB1068	III	schafer lab -80
unc-8	*e15*	CB15	IV	
unc-8	*e15lb145*	MP145	IV	
unc-8	*n491*	MT1085	IV	
unc-8	*n491n1192*	MT2611	IV	
unc-80	*e1069*	CB1069	V	schafer lab -80
unc-86	*e1416*	CB1416	III	CGC
unc-89	*e1460*	CB1460	I	schafer lab -80
unc-9	*e101*	CB101	X	
unc-98	*st85*	RW85	I	schafer lab -80
unc-98	*su130*	HE130	X	CGC
vab-7	*e1562*	CB1562	III	CGC
W03B1.2	*ok2433*	RB1883	IV	Andre
Y69H2.2	*ok1522*	RB1356	V	CGC
zyg-9	*b244*	DH244	II	CGC
F28A12.1	*ok1508*	RB1351	V	CGC

Table A3: AT2 features

1	'Length'
2	'Forward Length'
3	'Paused Length'
4	'Backward Length'
5	'Head Width'
6	'Forward Head Width'
7	'Paused Head Width'
8	'Backward Head Width'
9	'Midbody Width'
10	'Forward Midbody Width'
11	'Paused Midbody Width'
12	'Backward Midbody Width'
13	'Tail Width'
14	'Forward Tail Width'
15	'Paused Tail Width'
16	'Backward Tail Width'
17	'Area'
18	'Forward Area'
19	'Paused Area'
20	'Backward Area'
21	'Area/Length'
22	'Forward Area/Length'
23	'Paused Area/Length'
24	'Backward Area/Length'
25	'Width/Length'
26	'Forward Width/Length'
27	'Paused Width/Length'
28	'Backward Width/Length'
29	'Head Bend Mean (+/- = D/V Inside)'
30	'Absolute Head Bend Mean (+/- = D/V Inside)'
31	'Positive Head Bend Mean (+/- = D/V Inside)'
32	'Negative Head Bend Mean (+/- = D/V Inside)'
33	'Forward Head Bend Mean (+/- = D/V Inside)'
34	'Absolute Forward Head Bend Mean (+/- = D/V Inside)'
35	'Positive Forward Head Bend Mean (+/- = D/V Inside)'
36	'Negative Forward Head Bend Mean (+/- = D/V Inside)'
37	'Paused Head Bend Mean (+/- = D/V Inside)'
38	'Absolute Paused Head Bend Mean (+/- = D/V Inside)'
39	'Positive Paused Head Bend Mean (+/- = D/V Inside)'
40	'Negative Paused Head Bend Mean (+/- = D/V Inside)'
41	'Backward Head Bend Mean (+/- = D/V Inside)'
42	'Absolute Backward Head Bend Mean (+/- = D/V Inside)'
43	'Positive Backward Head Bend Mean (+/- = D/V Inside)'
44	'Negative Backward Head Bend Mean (+/- = D/V Inside)'

45	'Neck Bend Mean (+/- = D/V Inside)'
46	'Absolute Neck Bend Mean (+/- = D/V Inside)'
47	'Positive Neck Bend Mean (+/- = D/V Inside)'
48	'Negative Neck Bend Mean (+/- = D/V Inside)'
49	'Forward Neck Bend Mean (+/- = D/V Inside)'
50	'Absolute Forward Neck Bend Mean (+/- = D/V Inside)'
51	'Positive Forward Neck Bend Mean (+/- = D/V Inside)'
52	'Negative Forward Neck Bend Mean (+/- = D/V Inside)'
53	'Paused Neck Bend Mean (+/- = D/V Inside)'
54	'Absolute Paused Neck Bend Mean (+/- = D/V Inside)'
55	'Positive Paused Neck Bend Mean (+/- = D/V Inside)'
56	'Negative Paused Neck Bend Mean (+/- = D/V Inside)'
57	'Backward Neck Bend Mean (+/- = D/V Inside)'
58	'Absolute Backward Neck Bend Mean (+/- = D/V Inside)'
59	'Positive Backward Neck Bend Mean (+/- = D/V Inside)'
60	'Negative Backward Neck Bend Mean (+/- = D/V Inside)'
61	'Midbody Bend Mean (+/- = D/V Inside)'
62	'Absolute Midbody Bend Mean (+/- = D/V Inside)'
63	'Positive Midbody Bend Mean (+/- = D/V Inside)'
64	'Negative Midbody Bend Mean (+/- = D/V Inside)'
65	'Forward Midbody Bend Mean (+/- = D/V Inside)'
66	'Absolute Forward Midbody Bend Mean (+/- = D/V Inside)'
67	'Positive Forward Midbody Bend Mean (+/- = D/V Inside)'
68	'Negative Forward Midbody Bend Mean (+/- = D/V Inside)'
69	'Paused Midbody Bend Mean (+/- = D/V Inside)'
70	'Absolute Paused Midbody Bend Mean (+/- = D/V Inside)'
71	'Positive Paused Midbody Bend Mean (+/- = D/V Inside)'
72	'Negative Paused Midbody Bend Mean (+/- = D/V Inside)'
73	'Backward Midbody Bend Mean (+/- = D/V Inside)'
74	'Absolute Backward Midbody Bend Mean (+/- = D/V Inside)'
75	'Positive Backward Midbody Bend Mean (+/- = D/V Inside)'
76	'Negative Backward Midbody Bend Mean (+/- = D/V Inside)'
78	'Hips Bend Mean (+/- = D/V Inside)'
79	'Absolute Hips Bend Mean (+/- = D/V Inside)'
80	'Positive Hips Bend Mean (+/- = D/V Inside)'
81	'Negative Hips Bend Mean (+/- = D/V Inside)'
82	'Forward Hips Bend Mean (+/- = D/V Inside)'
83	'Absolute Forward Hips Bend Mean (+/- = D/V Inside)'
84	'Positive Forward Hips Bend Mean (+/- = D/V Inside)'
85	'Negative Forward Hips Bend Mean (+/- = D/V Inside)'
86	'Paused Hips Bend Mean (+/- = D/V Inside)'
87	'Absolute Paused Hips Bend Mean (+/- = D/V Inside)'
88	'Positive Paused Hips Bend Mean (+/- = D/V Inside)'
89	'Negative Paused Hips Bend Mean (+/- = D/V Inside)'
90	'Backward Hips Bend Mean (+/- = D/V Inside)'
91	'Absolute Backward Hips Bend Mean (+/- = D/V Inside)'

92	'Positive Backward Hips Bend Mean (+/- = D/V Inside)'
93	'Negative Backward Hips Bend Mean (+/- = D/V Inside)'
94	'Tail Bend Mean (+/- = D/V Inside)'
95	'Absolute Tail Bend Mean (+/- = D/V Inside)'
96	'Positive Tail Bend Mean (+/- = D/V Inside)'
97	'Negative Tail Bend Mean (+/- = D/V Inside)'
98	'Forward Tail Bend Mean (+/- = D/V Inside)'
99	'Absolute Forward Tail Bend Mean (+/- = D/V Inside)'
100	'Positive Forward Tail Bend Mean (+/- = D/V Inside)'
101	'Negative Forward Tail Bend Mean (+/- = D/V Inside)'
102	'Paused Tail Bend Mean (+/- = D/V Inside)'
103	'Absolute Paused Tail Bend Mean (+/- = D/V Inside)'
104	'Positive Paused Tail Bend Mean (+/- = D/V Inside)'
105	'Negative Paused Tail Bend Mean (+/- = D/V Inside)'
106	'Backward Tail Bend Mean (+/- = D/V Inside)'
107	'Absolute Backward Tail Bend Mean (+/- = D/V Inside)'
108	'Positive Backward Tail Bend Mean (+/- = D/V Inside)'
109	'Negative Backward Tail Bend Mean (+/- = D/V Inside)'
110	'Head Bend S.D. (+/- = D/V Inside)'
111	'Absolute Head Bend S.D. (+/- = D/V Inside)'
112	'Positive Head Bend S.D. (+/- = D/V Inside)'
113	'Negative Head Bend S.D. (+/- = D/V Inside)'
114	'Forward Head Bend S.D. (+/- = D/V Inside)'
115	'Absolute Forward Head Bend S.D. (+/- = D/V Inside)'
116	'Positive Forward Head Bend S.D. (+/- = D/V Inside)'
117	'Negative Forward Head Bend S.D. (+/- = D/V Inside)'
118	'Paused Head Bend S.D. (+/- = D/V Inside)'
119	'Absolute Paused Head Bend S.D. (+/- = D/V Inside)'
120	'Positive Paused Head Bend S.D. (+/- = D/V Inside)'
121	'Negative Paused Head Bend S.D. (+/- = D/V Inside)'
122	'Backward Head Bend S.D. (+/- = D/V Inside)'
123	'Absolute Backward Head Bend S.D. (+/- = D/V Inside)'
124	'Positive Backward Head Bend S.D. (+/- = D/V Inside)'
125	'Negative Backward Head Bend S.D. (+/- = D/V Inside)'
126	'Neck Bend S.D. (+/- = D/V Inside)'
127	'Absolute Neck Bend S.D. (+/- = D/V Inside)'
128	'Positive Neck Bend S.D. (+/- = D/V Inside)'
129	'Negative Neck Bend S.D. (+/- = D/V Inside)'
130	'Forward Neck Bend S.D. (+/- = D/V Inside)'
131	'Absolute Forward Neck Bend S.D. (+/- = D/V Inside)'
132	'Positive Forward Neck Bend S.D. (+/- = D/V Inside)'
133	'Negative Forward Neck Bend S.D. (+/- = D/V Inside)'
134	'Paused Neck Bend S.D. (+/- = D/V Inside)'
135	'Absolute Paused Neck Bend S.D. (+/- = D/V Inside)'
136	'Positive Paused Neck Bend S.D. (+/- = D/V Inside)'
137	'Negative Paused Neck Bend S.D. (+/- = D/V Inside)'

138	'Backward Neck Bend S.D. (+/- = D/V Inside)'
139	'Absolute Backward Neck Bend S.D. (+/- = D/V Inside)'
140	'Positive Backward Neck Bend S.D. (+/- = D/V Inside)'
141	'Negative Backward Neck Bend S.D. (+/- = D/V Inside)'
142	'Midbody Bend S.D. (+/- = D/V Inside)'
143	'Absolute Midbody Bend S.D. (+/- = D/V Inside)'
144	'Positive Midbody Bend S.D. (+/- = D/V Inside)'
145	'Negative Midbody Bend S.D. (+/- = D/V Inside)'
146	'Forward Midbody Bend S.D. (+/- = D/V Inside)'
147	'Absolute Forward Midbody Bend S.D. (+/- = D/V Inside)'
148	'Positive Forward Midbody Bend S.D. (+/- = D/V Inside)'
149	'Negative Forward Midbody Bend S.D. (+/- = D/V Inside)'
150	'Paused Midbody Bend S.D. (+/- = D/V Inside)'
151	'Absolute Paused Midbody Bend S.D. (+/- = D/V Inside)'
152	'Positive Paused Midbody Bend S.D. (+/- = D/V Inside)'
153	'Negative Paused Midbody Bend S.D. (+/- = D/V Inside)'
154	'Backward Midbody Bend S.D. (+/- = D/V Inside)'
155	'Absolute Backward Midbody Bend S.D. (+/- = D/V Inside)'
156	'Positive Backward Midbody Bend S.D. (+/- = D/V Inside)'
157	'Negative Backward Midbody Bend S.D. (+/- = D/V Inside)'
158	'Hips Bend S.D. (+/- = D/V Inside)'
159	'Absolute Hips Bend S.D. (+/- = D/V Inside)'
160	'Positive Hips Bend S.D. (+/- = D/V Inside)'
161	'Negative Hips Bend S.D. (+/- = D/V Inside)'
162	'Forward Hips Bend S.D. (+/- = D/V Inside)'
163	'Absolute Forward Hips Bend S.D. (+/- = D/V Inside)'
164	'Positive Forward Hips Bend S.D. (+/- = D/V Inside)'
165	'Negative Forward Hips Bend S.D. (+/- = D/V Inside)'
166	'Paused Hips Bend S.D. (+/- = D/V Inside)'
167	'Absolute Paused Hips Bend S.D. (+/- = D/V Inside)'
168	'Positive Paused Hips Bend S.D. (+/- = D/V Inside)'
169	'Negative Paused Hips Bend S.D. (+/- = D/V Inside)'
170	'Backward Hips Bend S.D. (+/- = D/V Inside)'
171	'Absolute Backward Hips Bend S.D. (+/- = D/V Inside)'
172	'Positive Backward Hips Bend S.D. (+/- = D/V Inside)'
173	'Negative Backward Hips Bend S.D. (+/- = D/V Inside)'
174	'Tail Bend S.D. (+/- = D/V Inside)'
175	'Absolute Tail Bend S.D. (+/- = D/V Inside)'
176	'Positive Tail Bend S.D. (+/- = D/V Inside)'
177	'Negative Tail Bend S.D. (+/- = D/V Inside)'
178	'Forward Tail Bend S.D. (+/- = D/V Inside)'
179	'Absolute Forward Tail Bend S.D. (+/- = D/V Inside)'
180	'Positive Forward Tail Bend S.D. (+/- = D/V Inside)'
181	'Negative Forward Tail Bend S.D. (+/- = D/V Inside)'
182	'Paused Tail Bend S.D. (+/- = D/V Inside)'
183	'Absolute Paused Tail Bend S.D. (+/- = D/V Inside)'

184	'Positive Paused Tail Bend S.D. (+/- = D/V Inside)'
185	'Negative Paused Tail Bend S.D. (+/- = D/V Inside)'
186	'Backward Tail Bend S.D. (+/- = D/V Inside)'
187	'Absolute Backward Tail Bend S.D. (+/- = D/V Inside)'
188	'Positive Backward Tail Bend S.D. (+/- = D/V Inside)'
189	'Negative Backward Tail Bend S.D. (+/- = D/V Inside)'
190	'Max Amplitude'
191	'Forward Max Amplitude'
192	'Paused Max Amplitude'
193	'Backward Max Amplitude'
194	'Amplitude Ratio'
195	'Forward Amplitude Ratio'
196	'Paused Amplitude Ratio'
197	'Backward Amplitude Ratio'
198	'Primary Wavelength'
199	'Forward Primary Wavelength'
200	'Paused Primary Wavelength'
201	'Backward Primary Wavelength'
202	'Secondary Wavelength'
203	'Forward Secondary Wavelength'
204	'Paused Secondary Wavelength'
205	'Backward Secondary Wavelength'
206	'Track Length'
207	'Forward Track Length'
208	'Paused Track Length'
209	'Backward Track Length'
210	'Eccentricity'
211	'Forward Eccentricity'
212	'Paused Eccentricity'
213	'Backward Eccentricity'
214	'Bend Count'
215	'Forward Bend Count'
216	'Paused Bend Count'
217	'Backward Bend Count'
218	'Coils Frequency'
219	'Coils Time Ratio'
220	'Coil Time'
221	'Inter Coil Time'
223	'Inter Coil Distance'
224	'Tail-To-Head Orientation'
225	'Absolute Tail-To-Head Orientation'
226	'Positive Tail-To-Head Orientation'
227	'Negative Tail-To-Head Orientation'
228	'Forward Tail-To-Head Orientation'
229	'Absolute Forward Tail-To-Head Orientation'
230	'Positive Forward Tail-To-Head Orientation'

231	'Negative Forward Tail-To-Head Orientation'
232	'Paused Tail-To-Head Orientation'
233	'Absolute Paused Tail-To-Head Orientation'
234	'Positive Paused Tail-To-Head Orientation'
235	'Negative Paused Tail-To-Head Orientation'
236	'Backward Tail-To-Head Orientation'
237	'Absolute Backward Tail-To-Head Orientation'
238	'Positive Backward Tail-To-Head Orientation'
239	'Negative Backward Tail-To-Head Orientation'
240	'Head Orientation'
241	'Absolute Head Orientation'
242	'Positive Head Orientation'
243	'Negative Head Orientation'
244	'Forward Head Orientation'
245	'Absolute Forward Head Orientation'
246	'Positive Forward Head Orientation'
247	'Negative Forward Head Orientation'
248	'Paused Head Orientation'
249	'Absolute Paused Head Orientation'
250	'Positive Paused Head Orientation'
251	'Negative Paused Head Orientation'
252	'Backward Head Orientation'
253	'Absolute Backward Head Orientation'
254	'Positive Backward Head Orientation'
255	'Negative Backward Head Orientation'
256	'Tail Orientation'
257	'Absolute Tail Orientation'
258	'Positive Tail Orientation'
259	'Negative Tail Orientation'
260	'Forward Tail Orientation'
261	'Absolute Forward Tail Orientation'
262	'Positive Forward Tail Orientation'
263	'Negative Forward Tail Orientation'
264	'Paused Tail Orientation'
265	'Absolute Paused Tail Orientation'
266	'Positive Paused Tail Orientation'
267	'Negative Paused Tail Orientation'
268	'Backward Tail Orientation'
269	'Absolute Backward Tail Orientation'
270	'Positive Backward Tail Orientation'
271	'Negative Backward Tail Orientation'
272	'Eigen Projection 1'
273	'Absolute Eigen Projection 1'
274	'Positive Eigen Projection 1'
275	'Negative Eigen Projection 1'
276	'Forward Eigen Projection 1'

277	'Absolute Forward Eigen Projection 1'
278	'Positive Forward Eigen Projection 1'
279	'Negative Forward Eigen Projection 1'
280	'Paused Eigen Projection 1'
281	'Absolute Paused Eigen Projection 1'
282	'Positive Paused Eigen Projection 1'
283	'Negative Paused Eigen Projection 1'
284	'Backward Eigen Projection 1'
285	'Absolute Backward Eigen Projection 1'
286	'Positive Backward Eigen Projection 1'
287	'Negative Backward Eigen Projection 1'
288	'Eigen Projection 2'
289	'Absolute Eigen Projection 2'
290	'Positive Eigen Projection 2'
291	'Negative Eigen Projection 2'
292	'Forward Eigen Projection 2'
293	'Absolute Forward Eigen Projection 2'
294	'Positive Forward Eigen Projection 2'
295	'Negative Forward Eigen Projection 2'
296	'Paused Eigen Projection 2'
297	'Absolute Paused Eigen Projection 2'
298	'Positive Paused Eigen Projection 2'
299	'Negative Paused Eigen Projection 2'
300	'Backward Eigen Projection 2'
301	'Absolute Backward Eigen Projection 2'
302	'Positive Backward Eigen Projection 2'
303	'Negative Backward Eigen Projection 2'
304	'Eigen Projection 3'
305	'Absolute Eigen Projection 3'
306	'Positive Eigen Projection 3'
307	'Negative Eigen Projection 3'
308	'Forward Eigen Projection 3'
309	'Absolute Forward Eigen Projection 3'
310	'Positive Forward Eigen Projection 3'
311	'Negative Forward Eigen Projection 3'
312	'Paused Eigen Projection 3'
313	'Absolute Paused Eigen Projection 3'
314	'Positive Paused Eigen Projection 3'
315	'Negative Paused Eigen Projection 3'
316	'Backward Eigen Projection 3'
317	'Absolute Backward Eigen Projection 3'
318	'Positive Backward Eigen Projection 3'
319	'Negative Backward Eigen Projection 3'
320	'Eigen Projection 4'
321	'Absolute Eigen Projection 4'
322	'Positive Eigen Projection 4'

323	'Negative Eigen Projection 4'
324	'Forward Eigen Projection 4'
325	'Absolute Forward Eigen Projection 4'
326	'Positive Forward Eigen Projection 4'
327	'Negative Forward Eigen Projection 4'
328	'Paused Eigen Projection 4'
329	'Absolute Paused Eigen Projection 4'
330	'Positive Paused Eigen Projection 4'
331	'Negative Paused Eigen Projection 4'
332	'Backward Eigen Projection 4'
333	'Absolute Backward Eigen Projection 4'
334	'Positive Backward Eigen Projection 4'
335	'Negative Backward Eigen Projection 4'
336	'Eigen Projection 5'
337	'Absolute Eigen Projection 5'
338	'Positive Eigen Projection 5'
339	'Negative Eigen Projection 5'
340	'Forward Eigen Projection 5'
341	'Absolute Forward Eigen Projection 5'
342	'Positive Forward Eigen Projection 5'
343	'Negative Forward Eigen Projection 5'
344	'Paused Eigen Projection 5'
345	'Absolute Paused Eigen Projection 5'
346	'Positive Paused Eigen Projection 5'
347	'Negative Paused Eigen Projection 5'
348	'Backward Eigen Projection 5'
349	'Absolute Backward Eigen Projection 5'
350	'Positive Backward Eigen Projection 5'
351	'Negative Backward Eigen Projection 5'
352	'Eigen Projection 6'
353	'Absolute Eigen Projection 6'
354	'Positive Eigen Projection 6'
355	'Negative Eigen Projection 6'
356	'Forward Eigen Projection 6'
357	'Absolute Forward Eigen Projection 6'
358	'Positive Forward Eigen Projection 6'
359	'Negative Forward Eigen Projection 6'
360	'Paused Eigen Projection 6'
361	'Absolute Paused Eigen Projection 6'
362	'Positive Paused Eigen Projection 6'
363	'Negative Paused Eigen Projection 6'
364	'Backward Eigen Projection 6'
365	'Absolute Backward Eigen Projection 6'
366	'Positive Backward Eigen Projection 6'
367	'Negative Backward Eigen Projection 6'
368	'Forward Motion Frequency'

369	'Forward Motion Time Ratio'
370	'Forward Motion Distance Ratio'
371	'Forward Time'
372	'Forward Distance'
373	'Inter Forward Time'
374	'Inter Forward Distance'
375	'Paused Motion Frequency'
376	'Paused Motion Time Ratio'
377	'Paused Motion Distance Ratio'
378	'Paused Time'
379	'Paused Distance'
380	'Inter Paused Time'
381	'Inter Paused Distance'
382	'Backward Motion Frequency'
383	'Backward Motion Time Ratio'
384	'Backward Motion Distance Ratio'
385	'Backward Time'
386	'Backward Distance'
387	'Inter Backward Time'
388	'Inter Backward Distance'
389	'Head Tip Speed (+/- = Forward/Backward)'
390	'Absolute Head Tip Speed (+/- = Forward/Backward)'
391	'Positive Head Tip Speed (+/- = Forward/Backward)'
392	'Negative Head Tip Speed (+/- = Forward/Backward)'
393	'Forward Head Tip Speed (+/- = Forward/Backward)'
394	'Absolute Forward Head Tip Speed (+/- = Forward/Backward)'
395	'Positive Forward Head Tip Speed (+/- = Forward/Backward)'
396	'Negative Forward Head Tip Speed (+/- = Forward/Backward)'
397	'Paused Head Tip Speed (+/- = Forward/Backward)'
398	'Absolute Paused Head Tip Speed (+/- = Forward/Backward)'
399	'Positive Paused Head Tip Speed (+/- = Forward/Backward)'
400	'Negative Paused Head Tip Speed (+/- = Forward/Backward)'
401	'Backward Head Tip Speed (+/- = Forward/Backward)'
402	'Absolute Backward Head Tip Speed (+/- = Forward/Backward)'
403	'Positive Backward Head Tip Speed (+/- = Forward/Backward)'
404	'Negative Backward Head Tip Speed (+/- = Forward/Backward)'
405	'Head Speed (+/- = Forward/Backward)'
406	'Absolute Head Speed (+/- = Forward/Backward)'
407	'Positive Head Speed (+/- = Forward/Backward)'
408	'Negative Head Speed (+/- = Forward/Backward)'
409	'Forward Head Speed (+/- = Forward/Backward)'
410	'Absolute Forward Head Speed (+/- = Forward/Backward)'
411	'Positive Forward Head Speed (+/- = Forward/Backward)'
412	'Negative Forward Head Speed (+/- = Forward/Backward)'
413	'Paused Head Speed (+/- = Forward/Backward)'
414	'Absolute Paused Head Speed (+/- = Forward/Backward)'

415	'Positive Paused Head Speed (+/- = Forward/Backward)'
416	'Negative Paused Head Speed (+/- = Forward/Backward)'
417	'Backward Head Speed (+/- = Forward/Backward)'
418	'Absolute Backward Head Speed (+/- = Forward/Backward)'
419	'Positive Backward Head Speed (+/- = Forward/Backward)'
420	'Negative Backward Head Speed (+/- = Forward/Backward)'
421	'Midbody Speed (+/- = Forward/Backward)'
422	'Absolute Midbody Speed (+/- = Forward/Backward)'
423	'Positive Midbody Speed (+/- = Forward/Backward)'
424	'Negative Midbody Speed (+/- = Forward/Backward)'
425	'Forward Midbody Speed (+/- = Forward/Backward)'
426	'Absolute Forward Midbody Speed (+/- = Forward/Backward)'
427	'Positive Forward Midbody Speed (+/- = Forward/Backward)'
428	'Negative Forward Midbody Speed (+/- = Forward/Backward)'
429	'Paused Midbody Speed (+/- = Forward/Backward)'
430	'Absolute Paused Midbody Speed (+/- = Forward/Backward)'
431	'Positive Paused Midbody Speed (+/- = Forward/Backward)'
432	'Negative Paused Midbody Speed (+/- = Forward/Backward)'
434	'Backward Midbody Speed (+/- = Forward/Backward)'
435	'Absolute Backward Midbody Speed (+/- = Forward/Backward)'
436	'Positive Backward Midbody Speed (+/- = Forward/Backward)'
437	'Negative Backward Midbody Speed (+/- = Forward/Backward)'
438	'Tail Speed (+/- = Forward/Backward)'
439	'Absolute Tail Speed (+/- = Forward/Backward)'
440	'Positive Tail Speed (+/- = Forward/Backward)'
441	'Negative Tail Speed (+/- = Forward/Backward)'
442	'Forward Tail Speed (+/- = Forward/Backward)'
443	'Absolute Forward Tail Speed (+/- = Forward/Backward)'
444	'Positive Forward Tail Speed (+/- = Forward/Backward)'
445	'Negative Forward Tail Speed (+/- = Forward/Backward)'
446	'Paused Tail Speed (+/- = Forward/Backward)'
447	'Absolute Paused Tail Speed (+/- = Forward/Backward)'
448	'Positive Paused Tail Speed (+/- = Forward/Backward)'
449	'Negative Paused Tail Speed (+/- = Forward/Backward)'
450	'Backward Tail Speed (+/- = Forward/Backward)'
451	'Absolute Backward Tail Speed (+/- = Forward/Backward)'
452	'Positive Backward Tail Speed (+/- = Forward/Backward)'
453	'Negative Backward Tail Speed (+/- = Forward/Backward)'
454	'Tail Tip Speed (+/- = Forward/Backward)'
456	'Absolute Tail Tip Speed (+/- = Forward/Backward)'
457	'Positive Tail Tip Speed (+/- = Forward/Backward)'
458	'Negative Tail Tip Speed (+/- = Forward/Backward)'
459	'Forward Tail Tip Speed (+/- = Forward/Backward)'
460	'Absolute Forward Tail Tip Speed (+/- = Forward/Backward)'
461	'Positive Forward Tail Tip Speed (+/- = Forward/Backward)'
462	'Negative Forward Tail Tip Speed (+/- = Forward/Backward)'

463	'Paused Tail Tip Speed (+/- = Forward/Backward)'
464	'Absolute Paused Tail Tip Speed (+/- = Forward/Backward)'
465	'Positive Paused Tail Tip Speed (+/- = Forward/Backward)'
466	'Negative Paused Tail Tip Speed (+/- = Forward/Backward)'
467	'Backward Tail Tip Speed (+/- = Forward/Backward)'
468	'Absolute Backward Tail Tip Speed (+/- = Forward/Backward)'
469	'Positive Backward Tail Tip Speed (+/- = Forward/Backward)'
470	'Negative Backward Tail Tip Speed (+/- = Forward/Backward)'
471	'Head Tip Motion Direction (+/- = Toward D/V)'
472	'Absolute Head Tip Motion Direction (+/- = Toward D/V)'
473	'Positive Head Tip Motion Direction (+/- = Toward D/V)'
474	'Negative Head Tip Motion Direction (+/- = Toward D/V)'
475	'Forward Head Tip Motion Direction (+/- = Toward D/V)'
476	'Absolute Forward Head Tip Motion Direction (+/- = Toward D/V)'
477	'Positive Forward Head Tip Motion Direction (+/- = Toward D/V)'
478	'Negative Forward Head Tip Motion Direction (+/- = Toward D/V)'
479	'Paused Head Tip Motion Direction (+/- = Toward D/V)'
480	'Absolute Paused Head Tip Motion Direction (+/- = Toward D/V)'
481	'Positive Paused Head Tip Motion Direction (+/- = Toward D/V)'
482	'Negative Paused Head Tip Motion Direction (+/- = Toward D/V)'
483	'Backward Head Tip Motion Direction (+/- = Toward D/V)'
484	'Absolute Backward Head Tip Motion Direction (+/- = Toward D/V)'
485	'Positive Backward Head Tip Motion Direction (+/- = Toward D/V)'
486	'Negative Backward Head Tip Motion Direction (+/- = Toward D/V)'
487	'Head Motion Direction (+/- = Toward D/V)'
488	'Absolute Head Motion Direction (+/- = Toward D/V)'
489	'Positive Head Motion Direction (+/- = Toward D/V)'
490	'Negative Head Motion Direction (+/- = Toward D/V)'
491	'Forward Head Motion Direction (+/- = Toward D/V)'
492	'Absolute Forward Head Motion Direction (+/- = Toward D/V)'
493	'Positive Forward Head Motion Direction (+/- = Toward D/V)'
494	'Negative Forward Head Motion Direction (+/- = Toward D/V)'
495	'Paused Head Motion Direction (+/- = Toward D/V)'
496	'Absolute Paused Head Motion Direction (+/- = Toward D/V)'
497	'Positive Paused Head Motion Direction (+/- = Toward D/V)'
498	'Negative Paused Head Motion Direction (+/- = Toward D/V)'
499	'Backward Head Motion Direction (+/- = Toward D/V)'
500	'Absolute Backward Head Motion Direction (+/- = Toward D/V)'
501	'Positive Backward Head Motion Direction (+/- = Toward D/V)'
502	'Negative Backward Head Motion Direction (+/- = Toward D/V)'
503	'Midbody Motion Direction (+/- = Toward D/V)'
504	'Absolute Midbody Motion Direction (+/- = Toward D/V)'
505	'Positive Midbody Motion Direction (+/- = Toward D/V)'
506	'Negative Midbody Motion Direction (+/- = Toward D/V)'
507	'Forward Midbody Motion Direction (+/- = Toward D/V)'
508	'Absolute Forward Midbody Motion Direction (+/- = Toward D/V)'

509	'Positive Forward Midbody Motion Direction (+/- = Toward D/V)'
510	'Negative Forward Midbody Motion Direction (+/- = Toward D/V)'
511	'Paused Midbody Motion Direction (+/- = Toward D/V)'
512	'Absolute Paused Midbody Motion Direction (+/- = Toward D/V)'
513	'Positive Paused Midbody Motion Direction (+/- = Toward D/V)'
514	'Negative Paused Midbody Motion Direction (+/- = Toward D/V)'
515	'Backward Midbody Motion Direction (+/- = Toward D/V)'
516	'Absolute Backward Midbody Motion Direction (+/- = Toward D/V)'
517	'Positive Backward Midbody Motion Direction (+/- = Toward D/V)'
518	'Negative Backward Midbody Motion Direction (+/- = Toward D/V)'
519	'Tail Motion Direction (+/- = Toward D/V)'
520	'Absolute Tail Motion Direction (+/- = Toward D/V)'
521	'Positive Tail Motion Direction (+/- = Toward D/V)'
522	'Negative Tail Motion Direction (+/- = Toward D/V)'
523	'Forward Tail Motion Direction (+/- = Toward D/V)'
524	'Absolute Forward Tail Motion Direction (+/- = Toward D/V)'
525	'Positive Forward Tail Motion Direction (+/- = Toward D/V)'
526	'Negative Forward Tail Motion Direction (+/- = Toward D/V)'
527	'Paused Tail Motion Direction (+/- = Toward D/V)'
528	'Absolute Paused Tail Motion Direction (+/- = Toward D/V)'
529	'Positive Paused Tail Motion Direction (+/- = Toward D/V)'
530	'Negative Paused Tail Motion Direction (+/- = Toward D/V)'
531	'Backward Tail Motion Direction (+/- = Toward D/V)'
532	'Absolute Backward Tail Motion Direction (+/- = Toward D/V)'
534	'Positive Backward Tail Motion Direction (+/- = Toward D/V)'
535	'Negative Backward Tail Motion Direction (+/- = Toward D/V)'
536	'Tail Tip Motion Direction (+/- = Toward D/V)'
537	'Absolute Tail Tip Motion Direction (+/- = Toward D/V)'
538	'Positive Tail Tip Motion Direction (+/- = Toward D/V)'
539	'Negative Tail Tip Motion Direction (+/- = Toward D/V)'
540	'Forward Tail Tip Motion Direction (+/- = Toward D/V)'
541	'Absolute Forward Tail Tip Motion Direction (+/- = Toward D/V)'
542	'Positive Forward Tail Tip Motion Direction (+/- = Toward D/V)'
543	'Negative Forward Tail Tip Motion Direction (+/- = Toward D/V)'
544	'Paused Tail Tip Motion Direction (+/- = Toward D/V)'
545	'Absolute Paused Tail Tip Motion Direction (+/- = Toward D/V)'
546	'Positive Paused Tail Tip Motion Direction (+/- = Toward D/V)'
547	'Negative Paused Tail Tip Motion Direction (+/- = Toward D/V)'
548	'Backward Tail Tip Motion Direction (+/- = Toward D/V)'
549	'Absolute Backward Tail Tip Motion Direction (+/- = Toward D/V)'
550	'Positive Backward Tail Tip Motion Direction (+/- = Toward D/V)'
551	'Negative Backward Tail Tip Motion Direction (+/- = Toward D/V)'
552	'Foraging Amplitude (+/- = Toward D/V)'
553	'Absolute Foraging Amplitude (+/- = Toward D/V)'
554	'Positive Foraging Amplitude (+/- = Toward D/V)'
555	'Negative Foraging Amplitude (+/- = Toward D/V)'

556	'Forward Foraging Amplitude (+/- = Toward D/V)'
557	'Absolute Forward Foraging Amplitude (+/- = Toward D/V)'
558	'Positive Forward Foraging Amplitude (+/- = Toward D/V)'
559	'Negative Forward Foraging Amplitude (+/- = Toward D/V)'
560	'Paused Foraging Amplitude (+/- = Toward D/V)'
561	'Absolute Paused Foraging Amplitude (+/- = Toward D/V)'
562	'Positive Paused Foraging Amplitude (+/- = Toward D/V)'
563	'Negative Paused Foraging Amplitude (+/- = Toward D/V)'
564	'Backward Foraging Amplitude (+/- = Toward D/V)'
565	'Absolute Backward Foraging Amplitude (+/- = Toward D/V)'
566	'Positive Backward Foraging Amplitude (+/- = Toward D/V)'
567	'Negative Backward Foraging Amplitude (+/- = Toward D/V)'
568	'Head Crawling Amplitude (+/- = D/V Inside)'
569	'Absolute Head Crawling Amplitude (+/- = D/V Inside)'
560	'Positive Head Crawling Amplitude (+/- = D/V Inside)'
561	'Negative Head Crawling Amplitude (+/- = D/V Inside)'
562	'Forward Head Crawling Amplitude (+/- = D/V Inside)'
563	'Absolute Forward Head Crawling Amplitude (+/- = D/V Inside)'
564	'Positive Forward Head Crawling Amplitude (+/- = D/V Inside)'
565	'Negative Forward Head Crawling Amplitude (+/- = D/V Inside)'
566	'Paused Head Crawling Amplitude (+/- = D/V Inside)'
567	'Absolute Paused Head Crawling Amplitude (+/- = D/V Inside)'
568	'Positive Paused Head Crawling Amplitude (+/- = D/V Inside)'
569	'Negative Paused Head Crawling Amplitude (+/- = D/V Inside)'
570	'Backward Head Crawling Amplitude (+/- = D/V Inside)'
571	'Absolute Backward Head Crawling Amplitude (+/- = D/V Inside)'
572	'Positive Backward Head Crawling Amplitude (+/- = D/V Inside)'
573	'Negative Backward Head Crawling Amplitude (+/- = D/V Inside)'
574	'Midbody Crawling Amplitude (+/- = D/V Inside)'
575	'Absolute Midbody Crawling Amplitude (+/- = D/V Inside)'
576	'Positive Midbody Crawling Amplitude (+/- = D/V Inside)'
577	'Negative Midbody Crawling Amplitude (+/- = D/V Inside)'
578	'Forward Midbody Crawling Amplitude (+/- = D/V Inside)'
579	'Absolute Forward Midbody Crawling Amplitude (+/- = D/V Inside)'
580	'Positive Forward Midbody Crawling Amplitude (+/- = D/V Inside)'
581	'Negative Forward Midbody Crawling Amplitude (+/- = D/V Inside)'
582	'Paused Midbody Crawling Amplitude (+/- = D/V Inside)'
583	'Absolute Paused Midbody Crawling Amplitude (+/- = D/V Inside)'
584	'Positive Paused Midbody Crawling Amplitude (+/- = D/V Inside)'
585	'Negative Paused Midbody Crawling Amplitude (+/- = D/V Inside)'
586	'Backward Midbody Crawling Amplitude (+/- = D/V Inside)'
587	'Absolute Backward Midbody Crawling Amplitude (+/- = D/V Inside)'
588	'Positive Backward Midbody Crawling Amplitude (+/- = D/V Inside)'
589	'Negative Backward Midbody Crawling Amplitude (+/- = D/V Inside)'
590	'Tail Crawling Amplitude (+/- = D/V Inside)'
591	'Absolute Tail Crawling Amplitude (+/- = D/V Inside)'

592	'Positive Tail Crawling Amplitude (+/- = D/V Inside)'
593	'Negative Tail Crawling Amplitude (+/- = D/V Inside)'
594	'Forward Tail Crawling Amplitude (+/- = D/V Inside)'
595	'Absolute Forward Tail Crawling Amplitude (+/- = D/V Inside)'
596	'Positive Forward Tail Crawling Amplitude (+/- = D/V Inside)'
597	'Negative Forward Tail Crawling Amplitude (+/- = D/V Inside)'
598	'Paused Tail Crawling Amplitude (+/- = D/V Inside)'
599	'Absolute Paused Tail Crawling Amplitude (+/- = D/V Inside)'
600	'Positive Paused Tail Crawling Amplitude (+/- = D/V Inside)'
601	'Negative Paused Tail Crawling Amplitude (+/- = D/V Inside)'
602	'Backward Tail Crawling Amplitude (+/- = D/V Inside)'
603	'Absolute Backward Tail Crawling Amplitude (+/- = D/V Inside)'
604	'Positive Backward Tail Crawling Amplitude (+/- = D/V Inside)'
605	'Negative Backward Tail Crawling Amplitude (+/- = D/V Inside)'
606	'Foraging Speed (+/- = Toward D/V)'
607	'Absolute Foraging Speed (+/- = Toward D/V)'
608	'Positive Foraging Speed (+/- = Toward D/V)'
609	'Negative Foraging Speed (+/- = Toward D/V)'
610	'Forward Foraging Speed (+/- = Toward D/V)'
611	'Absolute Forward Foraging Speed (+/- = Toward D/V)'
612	'Positive Forward Foraging Speed (+/- = Toward D/V)'
613	'Negative Forward Foraging Speed (+/- = Toward D/V)'
614	'Paused Foraging Speed (+/- = Toward D/V)'
615	'Absolute Paused Foraging Speed (+/- = Toward D/V)'
616	'Positive Paused Foraging Speed (+/- = Toward D/V)'
617	'Negative Paused Foraging Speed (+/- = Toward D/V)'
618	'Backward Foraging Speed (+/- = Toward D/V)'
619	'Absolute Backward Foraging Speed (+/- = Toward D/V)'
620	'Positive Backward Foraging Speed (+/- = Toward D/V)'
621	'Negative Backward Foraging Speed (+/- = Toward D/V)'
622	'Head Crawling Frequency (+/- = D/V Inside)'
623	'Absolute Head Crawling Frequency (+/- = D/V Inside)'
624	'Positive Head Crawling Frequency (+/- = D/V Inside)'
625	'Negative Head Crawling Frequency (+/- = D/V Inside)'
626	'Forward Head Crawling Frequency (+/- = D/V Inside)'
627	'Absolute Forward Head Crawling Frequency (+/- = D/V Inside)'
628	'Positive Forward Head Crawling Frequency (+/- = D/V Inside)'
629	'Negative Forward Head Crawling Frequency (+/- = D/V Inside)'
630	'Paused Head Crawling Frequency (+/- = D/V Inside)'
631	'Absolute Paused Head Crawling Frequency (+/- = D/V Inside)'
632	'Positive Paused Head Crawling Frequency (+/- = D/V Inside)'
633	'Negative Paused Head Crawling Frequency (+/- = D/V Inside)'
634	'Backward Head Crawling Frequency (+/- = D/V Inside)'
635	'Absolute Backward Head Crawling Frequency (+/- = D/V Inside)'
636	'Positive Backward Head Crawling Frequency (+/- = D/V Inside)'
637	'Negative Backward Head Crawling Frequency (+/- = D/V Inside)'

638	'Midbody Crawling Frequency (+/- = D/V Inside)'
639	'Absolute Midbody Crawling Frequency (+/- = D/V Inside)'
640	'Positive Midbody Crawling Frequency (+/- = D/V Inside)'
641	'Negative Midbody Crawling Frequency (+/- = D/V Inside)'
642	'Forward Midbody Crawling Frequency (+/- = D/V Inside)'
643	'Absolute Forward Midbody Crawling Frequency (+/- = D/V Inside)'
644	'Positive Forward Midbody Crawling Frequency (+/- = D/V Inside)'
645	'Negative Forward Midbody Crawling Frequency (+/- = D/V Inside)'
646	'Paused Midbody Crawling Frequency (+/- = D/V Inside)'
647	'Absolute Paused Midbody Crawling Frequency (+/- = D/V Inside)'
648	'Positive Paused Midbody Crawling Frequency (+/- = D/V Inside)'
649	'Negative Paused Midbody Crawling Frequency (+/- = D/V Inside)'
650	'Backward Midbody Crawling Frequency (+/- = D/V Inside)'
651	'Absolute Backward Midbody Crawling Frequency (+/- = D/V Inside)'
652	'Positive Backward Midbody Crawling Frequency (+/- = D/V Inside)'
653	'Negative Backward Midbody Crawling Frequency (+/- = D/V Inside)'
654	'Tail Crawling Frequency (+/- = D/V Inside)'
655	'Absolute Tail Crawling Frequency (+/- = D/V Inside)'
656	'Positive Tail Crawling Frequency (+/- = D/V Inside)'
657	'Negative Tail Crawling Frequency (+/- = D/V Inside)'
658	'Forward Tail Crawling Frequency (+/- = D/V Inside)'
659	'Absolute Forward Tail Crawling Frequency (+/- = D/V Inside)'
660	'Positive Forward Tail Crawling Frequency (+/- = D/V Inside)'
661	'Negative Forward Tail Crawling Frequency (+/- = D/V Inside)'
662	'Paused Tail Crawling Frequency (+/- = D/V Inside)'
663	'Absolute Paused Tail Crawling Frequency (+/- = D/V Inside)'
664	'Positive Paused Tail Crawling Frequency (+/- = D/V Inside)'
665	'Negative Paused Tail Crawling Frequency (+/- = D/V Inside)'
666	'Backward Tail Crawling Frequency (+/- = D/V Inside)'
667	'Absolute Backward Tail Crawling Frequency (+/- = D/V Inside)'
668	'Positive Backward Tail Crawling Frequency (+/- = D/V Inside)'
669	'Negative Backward Tail Crawling Frequency (+/- = D/V Inside)'
670	'Omega Turns Frequency'
671	'Omega Turns Time Ratio'
672	'Omega Turn Time (+/- = D/V Inside)'
673	'Absolute Omega Turn Time (+/- = D/V Inside)'
674	'Positive Omega Turn Time (+/- = D/V Inside)'
675	'Negative Omega Turn Time (+/- = D/V Inside)'
676	'Inter Omega Time (+/- = Previous D/V)'
677	'Absolute Inter Omega Time (+/- = Previous D/V)'
678	'Positive Inter Omega Time (+/- = Previous D/V)'
679	'Negative Inter Omega Time (+/- = Previous D/V)'
680	'Inter Omega Distance (+/- = Previous D/V)'
681	'Absolute Inter Omega Distance (+/- = Previous D/V)'
682	'Positive Inter Omega Distance (+/- = Previous D/V)'
683	'Negative Inter Omega Distance (+/- = Previous D/V)'

684	'Upsilon Turns Frequency'
685	'Upsilon Turns Time Ratio'
686	'Upsilon Turn Time (+/- = D/V Inside)'
687	'Absolute Upsilon Turn Time (+/- = D/V Inside)'
688	'Positive Upsilon Turn Time (+/- = D/V Inside)'
689	'Negative Upsilon Turn Time (+/- = D/V Inside)'
690	'Inter Upsilon Time (+/- = Previous D/V)'
691	'Absolute Inter Upsilon Time (+/- = Previous D/V)'
692	'Positive Inter Upsilon Time (+/- = Previous D/V)'
693	'Negative Inter Upsilon Time (+/- = Previous D/V)'
694	'Inter Upsilon Distance (+/- = Previous D/V)'
695	'Absolute Inter Upsilon Distance (+/- = Previous D/V)'
696	'Positive Inter Upsilon Distance (+/- = Previous D/V)'
697	'Negative Inter Upsilon Distance (+/- = Previous D/V)'
698	'Path Range'
699	'Forward Path Range'
700	'Paused Path Range'
701	'Backward Path Range'
702	'Worm Dwelling'
703	'Head Dwelling'
704	'Midbody Dwelling'
705	'Tail Dwelling'
706	'Path Curvature (+/- = D/V Inside)'
707	'Absolute Path Curvature (+/- = D/V Inside)'
708	'Positive Path Curvature (+/- = D/V Inside)'
709	'Negative Path Curvature (+/- = D/V Inside)'
710	'Forward Path Curvature (+/- = D/V Inside)'
711	'Absolute Forward Path Curvature (+/- = D/V Inside)'
712	'Positive Forward Path Curvature (+/- = D/V Inside)'
713	'Negative Forward Path Curvature (+/- = D/V Inside)'
714	'Paused Path Curvature (+/- = D/V Inside)'
715	'Absolute Paused Path Curvature (+/- = D/V Inside)'
716	'Positive Paused Path Curvature (+/- = D/V Inside)'
717	'Negative Paused Path Curvature (+/- = D/V Inside)'
718	'Backward Path Curvature (+/- = D/V Inside)'
719	'Absolute Backward Path Curvature (+/- = D/V Inside)'
720	'Positive Backward Path Curvature (+/- = D/V Inside)'

Clustering

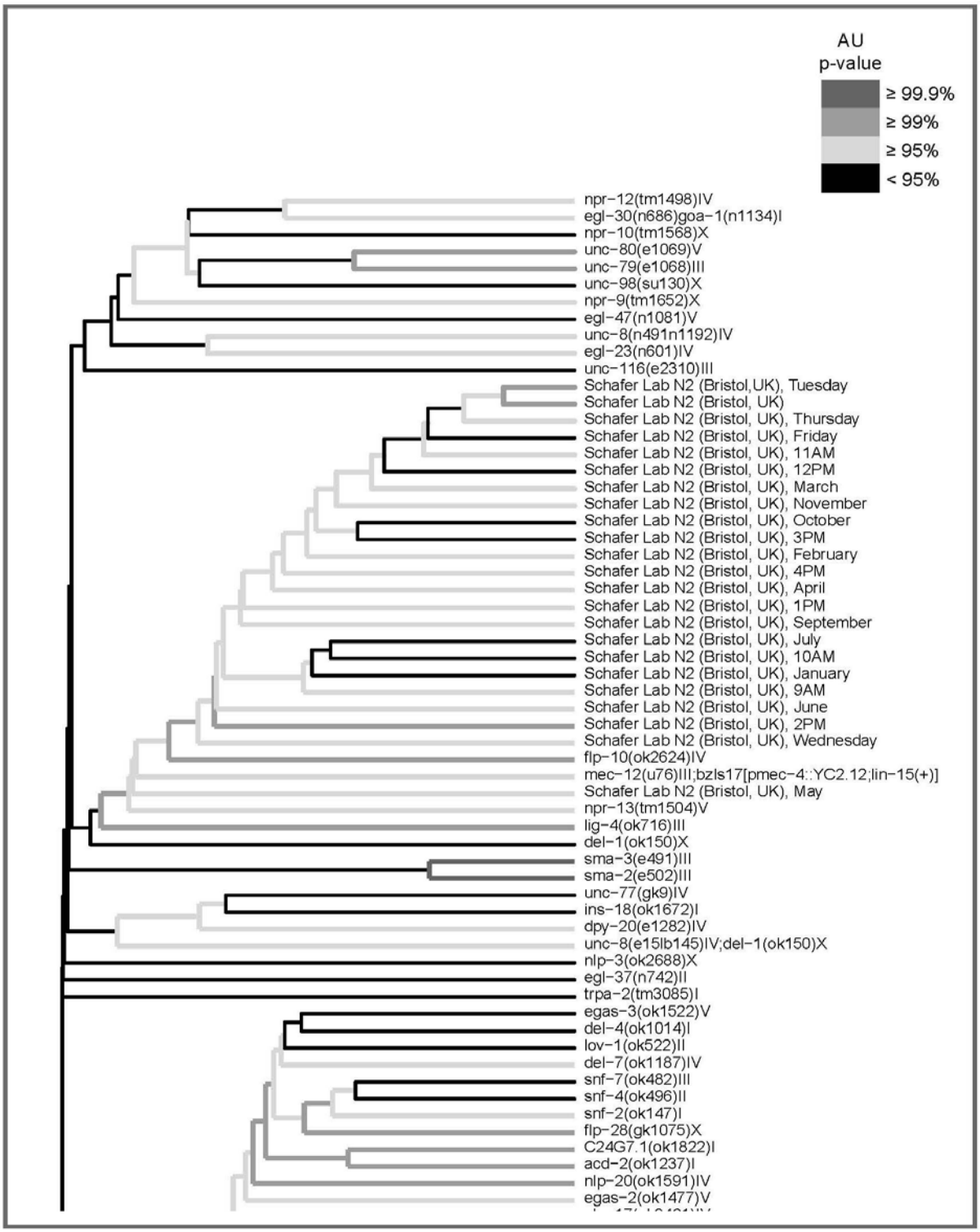
AU
p-value
≥ 99.9%
≥ 99%
≥ 95%
< 95%
npr−12(tm1498)IV
egl−30(n686)goa−1(n1134)I
npr−10(tm1568)X
unc−80(e1069)V
unc−79(e1068)III
unc−98(su130)X
npr−9(tm1652)X
egl−47(n1081)V
unc−8(n491n1192)IV
egl−23(n601)IV
unc−116(e2310)III
Schafer Lab N2 (Bristol,UK), Tuesday
Schafer Lab N2 (Bristol, UK)
Schafer Lab N2 (Bristol, UK), Thursday
Schafer Lab N2 (Bristol, UK), Friday
Schafer Lab N2 (Bristol, UK), 11AM
Schafer Lab N2 (Bristol, UK), 12PM
Schafer Lab N2 (Bristol, UK), March
Schafer Lab N2 (Bristol, UK), November
Schafer Lab N2 (Bristol, UK), October
Schafer Lab N2 (Bristol, UK), 3PM
Schafer Lab N2 (Bristol, UK), February
Schafer Lab N2 (Bristol, UK), 4PM
Schafer Lab N2 (Bristol, UK), April
Schafer Lab N2 (Bristol, UK), 1PM
Schafer Lab N2 (Bristol, UK), September
Schafer Lab N2 (Bristol, UK), July
Schafer Lab N2 (Bristol, UK), 10AM
Schafer Lab N2 (Bristol, UK), January
Schafer Lab N2 (Bristol, UK), 9AM
Schafer Lab N2 (Bristol, UK), June
Schafer Lab N2 (Bristol, UK), 2PM
Schafer Lab N2 (Bristol, UK), Wednesday
flp−10(ok2624)IV
mec−12(u76)III;bzIs17[pmec−4::YC2.12;lin−15(+)]
Schafer Lab N2 (Bristol, UK), May
npr−13(tm1504)V
lig−4(ok716)III
del−1(ok150)X
sma−3(e491)III
sma−2(e502)III
unc−77(gk9)IV
ins−18(ok1672)I
dpy−20(e1282)IV
unc−8(e15lb145)IV;del−1(ok150)X
nlp−3(ok2688)X
egl−37(n742)II
trpa−2(tm3085)I
egas−3(ok1522)V
del−4(ok1014)I
lov−1(ok522)II
del−7(ok1187)IV
snf−7(ok482)III
snf−4(ok496)II
snf−2(ok147)I
flp−28(gk1075)X
C24G7.1(ok1822)I
acd−2(ok1237)I
nlp−20(ok1591)IV
egas−2(ok1477)V

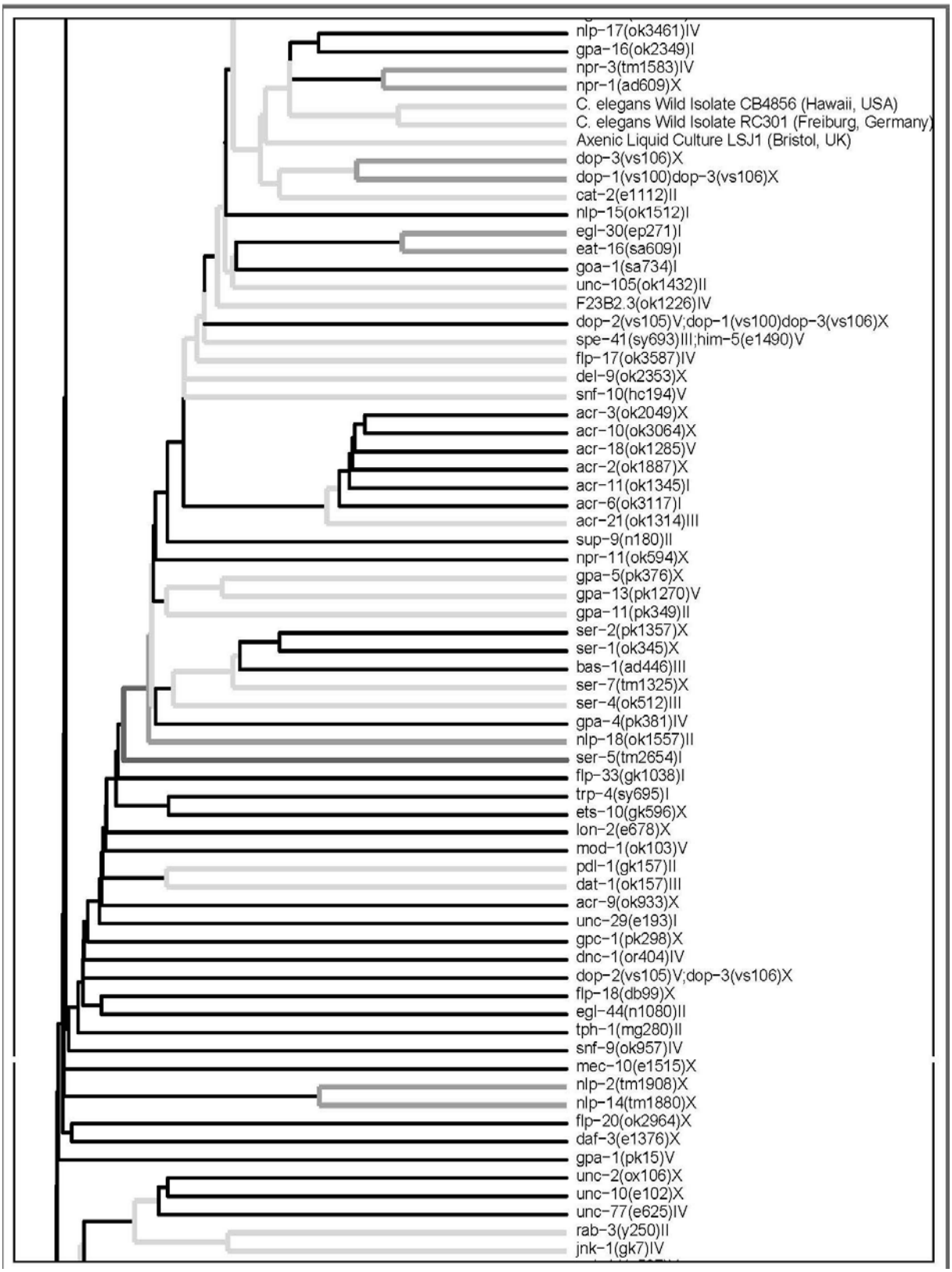
nlp-17(ok3461)IV
gpa-16(ok2349)I
npr-3(tm1583)IV
npr-1(ad609)X
C. elegans Wild Isolate CB4856 (Hawaii, USA)
C. elegans Wild Isolate RC301 (Freiburg, Germany)
Axenic Liquid Culture LSJ1 (Bristol, UK)
dop-3(vs106)X
dop-1(vs100)dop-3(vs106)X
cat-2(e1112)II
nlp-15(ok1512)I
egl-30(ep271)I
eat-16(sa609)I
goa-1(sa734)I
unc-105(ok1432)II
F23B2.3(ok1226)IV
dop-2(vs105)V;dop-1(vs100)dop-3(vs106)X
spe-41(sy693)III;him-5(e1490)V
flp-17(ok3587)IV
del-9(ok2353)X
snf-10(hc194)V
acr-3(ok2049)X
acr-10(ok3064)X
acr-18(ok1285)V
acr-2(ok1887)X
acr-11(ok1345)I
acr-6(ok3117)I
acr-21(ok1314)III
sup-9(n180)II
npr-11(ok594)X
gpa-5(pk376)X
gpa-13(pk1270)V
gpa-11(pk349)II
ser-2(pk1357)X
ser-1(ok345)X
bas-1(ad446)III
ser-7(tm1325)X
ser-4(ok512)III
gpa-4(pk381)IV
nlp-18(ok1557)II
ser-5(tm2654)I
flp-33(gk1038)I
trp-4(sy695)I
ets-10(gk596)X
lon-2(e678)X
mod-1(ok103)V
pdl-1(gk157)II
dat-1(ok157)III
acr-9(ok933)X
unc-29(e193)I
gpc-1(pk298)X
dnc-1(or404)IV
dop-2(vs105)V;dop-3(vs106)X
flp-18(db99)X
egl-44(n1080)II
tph-1(mg280)II
snf-9(ok957)IV
mec-10(e1515)X
nlp-2(tm1908)X
nlp-14(tm1880)X
flp-20(ok2964)X
daf-3(e1376)X
gpa-1(pk15)V
unc-2(ox106)X
unc-10(e102)X
unc-77(e625)IV
rab-3(y250)II
jnk-1(gk7)IV


egl-11(n587)V
mec-14(u55)III;bzIs18[pmec-4::YC2.12;lin-15(+)]
mec-10(tm1552)X;bzIs17[pmec-4::YC2.12;lin-15(+)]
unc-63(ok1075)I
unc-38(e264)I
gpa-7(pk610)IV
gpa-15(pk477)I
unc-115(mn481)X
npr-20(ok2575)II
CGC N2 (Bristol, UK)
unc-2(gk366)X
unc-8(e15)IV
unc-75(e950)I
unc-69(e587)III
unc-40(n324)I
Schafer Lab N2 (Bristol, UK), December
egl-8(n488)V
nlp-12(ok335)IV
egl-2(n693)V
gpa-8(pk345)V
acr-19(ad1674)I
Schafer Lab N2 Male (Bristol, UK)
Schafer Lab N2 (Bristol, UK), August
gpa-14(pk347)I
flp-12(ok2409)X
lin-39(n709)III
egl-36(n728)X
srp-8(ok291)V
hcf-1(ok559)IV
flr-1(ut11)X
egg-5(ok1781)I
egl-27(ok151)II
lev-1(x427)IV
unc-89(st85)I
T14B1.1(ok1702)X
unc-26(m2)IV
pqn-66(ok1507)II
ocr-3(ok1559)X
snf-1(ok790)I
unc-86(e1416)III
egl-10(md176)V
egl-15(n484)X
egl-49(n1107)X
egl-24(n572)III
unc-10(md1117)X
egl-31(n472)I
nlp-8(ok1799)I
ser-6(tm2146)IV
mec-10(u20)X
egl-6(n592)X
nhr-95(gk836)V
snf-11(ok156)V
flp-13(tm2427)IV
unc-4(gk705)II
unc-37(e262)I
unc-4(e120)II
snf-8(ok349)IV
egl-13(n483)X
mod-5(n822)I
daf-5(e1386)II
gar-2(ok520)III
nca-2(gk5)III
flp-3(ok3265)X
ins-30(ok2343)I
ins-11(tm1053)II
mir-124(n4255)IV
ins-16(ok2919)III
ins-28(ok2722)I
ins-25(ok2773)I
ins-3(ok2488)II
ins-4(ok3534)II
unc-34(e566)V
osm-9(ky10)trpa-1(ok999)IV
mec-4(u253)X;bzIs17[pmec-4::YC2.12;lin-15(+)]
gpa-9(pk438)V
ocr-4(vs137)ocr-2(ak47)IV;ocr-1(ok132)V
gly-2(gk204)I
unc-30(e191)IV
unc-122(e2520)I
egl-9(n586)V
mec-12(e1605)III;bzIs17[pmec-4::YC2.12;lin-15(+)]
trp-1(sy690)III
pmk-1(km25)IV
trpa-2(tm3092)I
ocr-4(tm2173)IV

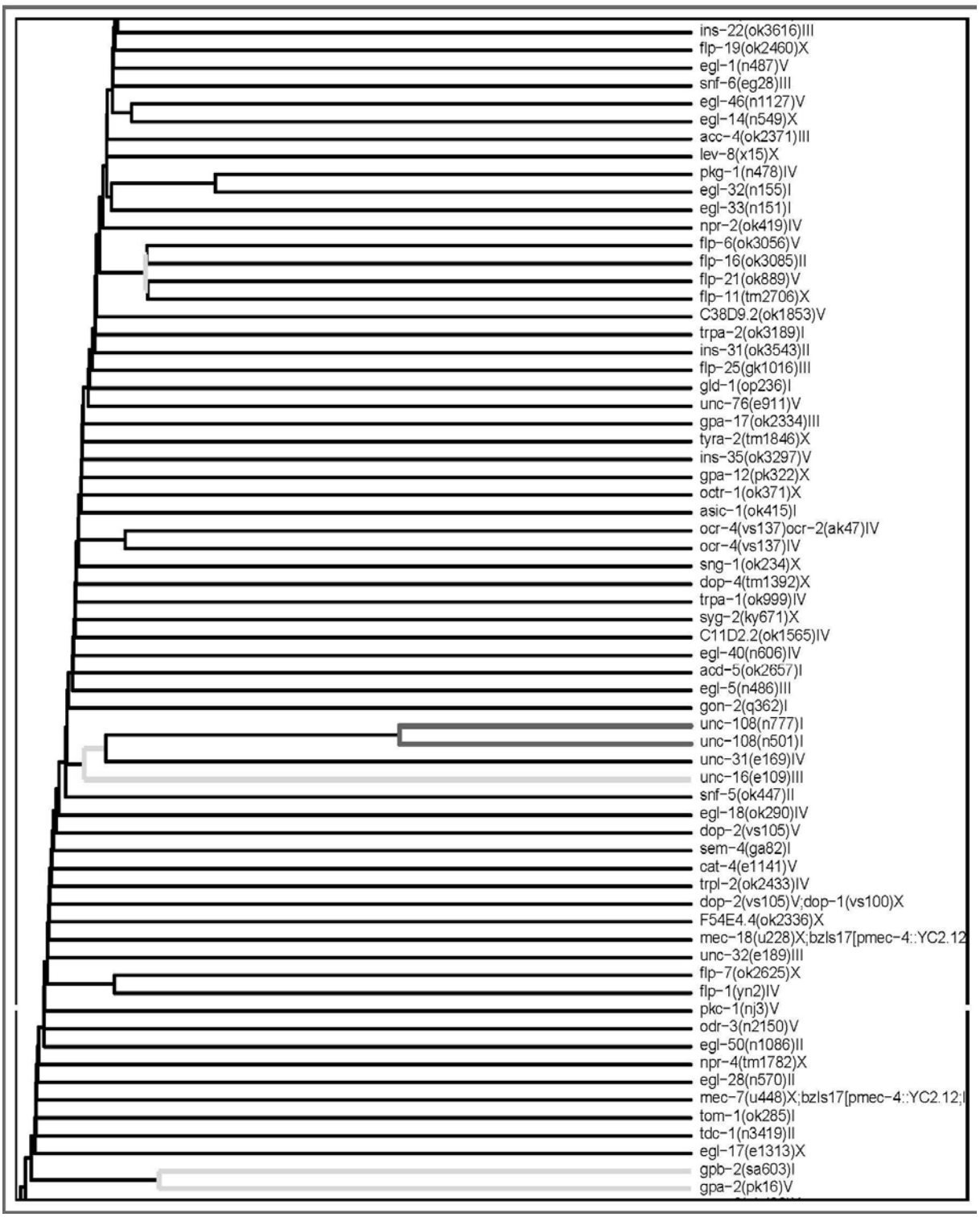
ins-22(ok3616)III
flp-19(ok2460)X
egl-1(n487)V
snf-6(eg28)III
egl-46(n1127)V
egl-14(n549)X
acc-4(ok2371)III
lev-8(x15)X
pkg-1(n478)IV
egl-32(n155)I
egl-33(n151)I
npr-2(ok419)IV
flp-6(ok3056)V
flp-16(ok3085)II
flp-21(ok889)V
flp-11(tm2706)X
C38D9.2(ok1853)V
trpa-2(ok3189)I
ins-31(ok3543)II
flp-25(gk1016)III
gld-1(op236)I
unc-76(e911)V
gpa-17(ok2334)III
tyra-2(tm1846)X
ins-35(ok3297)V
gpa-12(pk322)X
octr-1(ok371)X
asic-1(ok415)I
ocr-4(vs137)ocr-2(ak47)IV
ocr-4(vs137)IV
sng-1(ok234)X
dop-4(tm1392)X
trpa-1(ok999)IV
syg-2(ky671)X
C11D2.2(ok1565)IV
egl-40(n606)IV
acd-5(ok2657)I
egl-5(n486)III
gon-2(q362)I
unc-108(n777)I
unc-108(n501)I
unc-31(e169)IV
unc-16(e109)III
snf-5(ok447)II
egl-18(ok290)IV
dop-2(vs105)V
sem-4(ga82)I
cat-4(e1141)V
trpl-2(ok2433)IV
dop-2(vs105)V;dop-1(vs100)X
F54E4.4(ok2336)X
mec-18(u228)X;bzIs17[pmec-4::YC2.12
unc-32(e189)III
flp-7(ok2625)X
flp-1(yn2)IV
pkc-1(nj3)V
odr-3(n2150)V
egl-50(n1086)II
npr-4(tm1782)X
egl-28(n570)II
mec-7(u448)X;bzIs17[pmec-4::YC2.12;
tom-1(ok285)I
tdc-1(n3419)II
egl-17(e1313)X
gpb-2(sa603)I
gpa-2(pk16)V

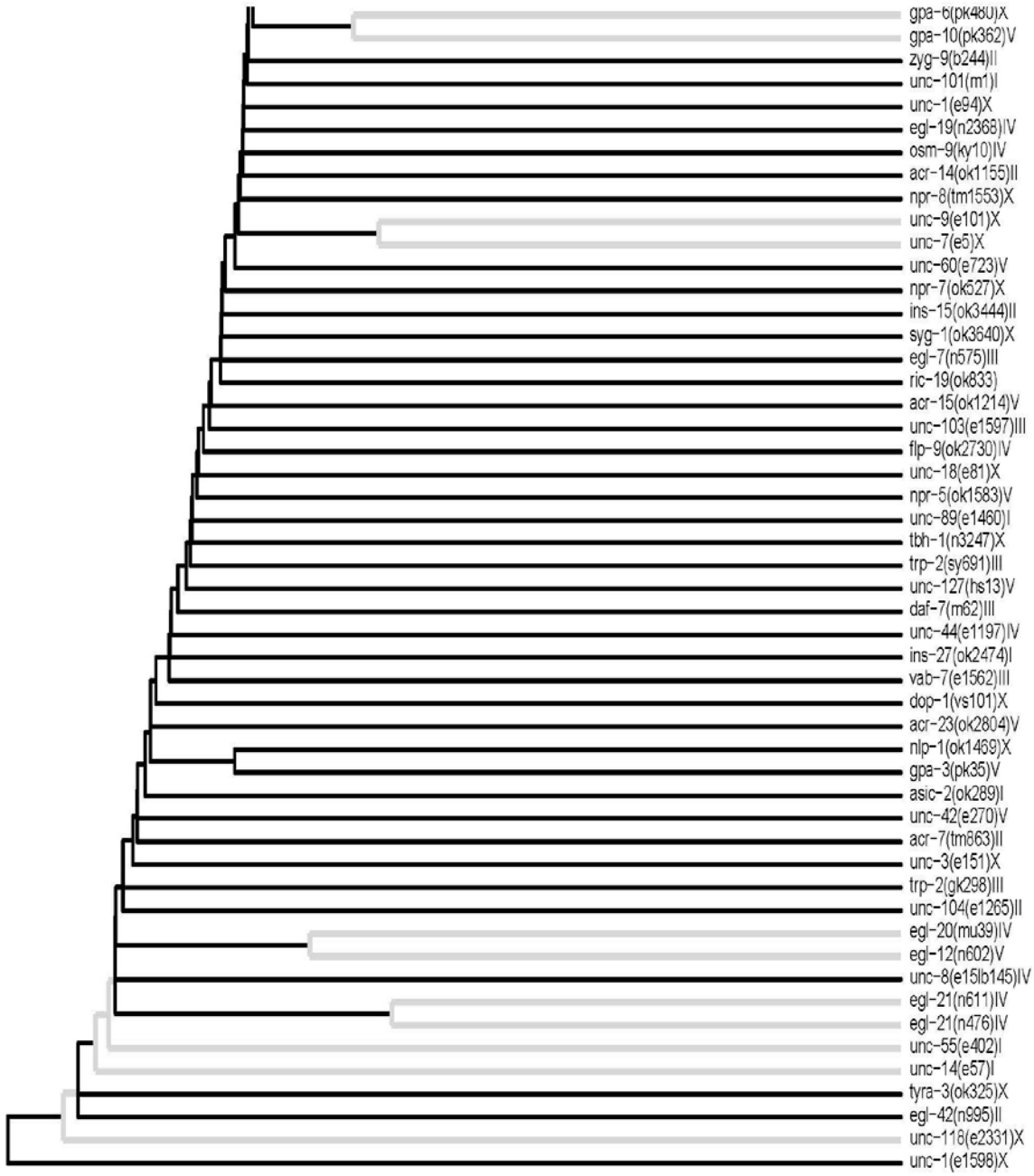

The full clustering is shown for all 330 strains and groups. Hierarchical clustering was performed using uncentered correlation and single linkage. Multiscale resampling was run with 10,000 bootstraps to generate approximately unbiased (AU) p values, measuring the confidence of tree selection for each branch. The horizontal length of each branch is scaled to its correlation value. The horizontal branches are color coded to show the AU of the clusters below them. AU ≥ 99.9% is colored red, AU ≥ 99% orange, AU ≥ 95% yellow, and all else is black. To understand the range of clustering values, the maximum pairwise correlation in the entire clustering was 0.95, between the group of lab-stock N2s and those t racked on Tuesday. In contrast, the minimum was 0.34, found when comparing unc-1(e1598) to all other groups. Similarly, while the top-most branch has an AU of 1 (as is expected for hierarchical clustering), the next greatest AU was 99.98% for the branch connecting the two alleles of unc-108. In contrast, 165 of the 329 branches had an AU of 0%. (Ev Yemini, 2011a)

Primers

Table A4: Genotyping primers

Gene	Forward primer	Reverse primer (in deletion)	Reverse primer (outside of deletion)
asic-2 (ok289)I	CGAGAAACAGGTATCTTTTTGG	CTTCCAATACAAGAGCATCTG	GTAAACTTAATTATATGGACTAG
acd-5 (ok2657)I	GAGTGTAAAAGTCAAGTGTATC	CCGATCCATCCGATCTTTG	GGTATTCCGTACTTCTATGTAC
acd-5 CRISPR PAM 1	ATATTCCGGTACAGCTTCTTGG	GTGAAACAGCAATTCCCTCTG	N/A
acd-5 CRISPR PAM 2	GCATGGACACCAAGATGAAGAAAG	GTTCCGATGTTACTCTGTGCATTG	N/A
acd-5 CRISPR PAM 3	TCGTGTTGAGACCGGGAACC	GTCAGCAGTGAAGTTAGGATGA	N/A
asic-2 CRISPR PAM 1 and 2	AAATTATGGCGGGTCTTAGGCATG	GTTGACAGTGGCAGGATACGAAA	N/A
asic-2 CRISPR PAM 3	ACCTACACACCAACAGTATCTC	GGAACATCTTCAGCCCTGGT	N/A

Table A5: Sequencing primers

GCaMP6 variants	CAAGACTCGTGCCGAAGTTAAG
acd-5 PAM 1	GGGTCAAATTTCTACAGTTTC
acd-5 PAM 2	GAAGCAAGGAAAGCAAGAGACTTGG
acd-5 PAM 3	AGCTAGGCATGAAGATGTACC
asic-2 PAM1 and 2	TAGCAGAGTAGCATCAGTGG
asic-2 PAM3	GCTGCTCTTCAACAAACTCG

Table A6: PCR primers

Product	Forward Primer	Reverse Primer
RCaMP1.035 pDONR221	GGGGACAAGTTTGTACAAAAAAGCAGGCTGCGGCCGCCACCATGGGTTCTCATCATCAT	GGGGACCACTTTGTACAAGAAAGCTGGGTTTACTTCGCTGTCATCATTTGTAC
RCaMP1.034 pDONR221	GGGGACAAGTTTGTACAAAAAAGCAGGCTGGCCGCCACCATGGGTTCTCATC	GGGGACCACTTTGTACAAGAAAGCTGGGTTTACTTCGCTGTCATCATTTGTAC
Pmec-7 pDONR P4-P1r	GGGGACAACTTTGTATAGAAAAGTTGCCGCGGTTTTGGCGC	GGGGACTGCTTTTTTGTACAAACTTGCGATCTCGCGGATG
GCaMP6 pDONR221	GGGGACAAGTTTGTACAAAAAAGCAGGCTCCGTTACGAAACAGACTGATATCG	GGGGACCACTTTGTACAAGAAAGCTGGGTCCTTGAGAGTTTTCGCCCCG
asic-2 cDNA pDONR221	GGGGACAAGTTTGTACAAAAAAGCAGGCTATGCGCGGTGGCGGT	GGGGACCACTTTGTACAAGAAAGCTGGGTTTATTTCTTCTTTTTCTCC
Pasic-2 pDONR P4-P1r	GGGGACAACTTTGTATAGAAAAGT TGGTTGCCGAGTTTCCGTCTAAAGC	GGGGACTGCTTTTTTGTACAAACTTGCAAAACCGCCACCGCGCATCTTGGGC
GCaMP6 ER retention pDONR221	GGGGACAAGTTTGTACAAAAAAGCAGGCTATGAAGTCCCTTTGCCTTCTTGCCATCGTCGCCGTCGTCTCCGCCGAGGGTTCTCATCATCAT	GGGGACCACTTTGTACAAGAAAGCTGGGTTTAGAGCTCGTCGTGTCCCTTCGCTGTCATCATTTG
GCaMP6 pDONR P2R-P3	GGGGACAGCTTTCTTGTACAAAGTGGGGATGGGTTCTCATCATCATCAT	CAACTTTGTATAATAAAGTTGTTACTTCGCTGTCATCATTTGTAC

Pklp-6 pDONR P4-P1r	GGGGACAACTTTGTATAGAAAAGTTGC CTTTTCCACCCTCCAATTT	GGGGACTGCTTTTTTGTACAAACTTGCATT GAAAGGTCGAACCCGAAC
acd-5 gDNA pDONR221	GGGGACAAGTTTGTACAAAAAAGCAGG CTATGCGACGCGTAAGGTGAGTC	GGGGACCACTTTGTACAAGAAAGCTGGGT GAGAGTGTTTGCCACAAACCC
Pdaf-7 pDONR P4-P1r	GGGGACAACTTTGTATAGAAAAGTTGG TGCTACGCATATGTTCATCC	GGGGACTGCTTTTTTGTACAAACTTGGGCT GAACTTCAAGCGGGCTG
Pacd-5 pDONR P4-P1r	GGGGACAACTTTGTATAGAAAAGTTGG TCGCCTCGTTTCCTCTTTCAATTC	GGGGACTGCTTTTTTGTACAAACTTGTGCA AAAAAATTCGATTTTTCTG
daf-7 pDONR221	GGGGACAAGTTTGTACAAAAAAGCAGG CTTACAAAAAAGCAGGCTTGTTCATGGC	GGGGACCACTTTGTACAAGAAAGCTGGGT TGAGCAACCGCATTTCTTGGCG
flp-21 pDONR221	GGGGACAAGTTTGTACAAAAAAGCAGG CTGGCTTGCGGCTGTTCATCTTGC	GGGGACCACTTTGTACAAGAAAGCTGGGT CTCGTCCTCTCCGATTTGGA
Podr-10 pDONR P4-P1r	GGGGACAACTTTGTATAGAAAAGTTGC AGGGAATTGAACCAGTGGGTGC	GGGGACTGCTTTTTTGTACAAACTTGGGA GCTGTAAGGTATCTTAATG
asic-2 RNAi forward transcript pDONR221	GGGGACAAGTTTGTACAAAAAAGCAGG CTCCAATTCAATTAATTTTCAG	GGGGACCACTTTGTACAAGAAAGCTGGGT CTCTTTAACGTGAACGTAC
asic-2 RNAi reverse transcript pDONR221	GGGGACAAGTTTGTACAAAAAAGCAGG CTCTTCAATGATAGGAATATAG	GGGGACCACTTTGTACAAGAAAGCTGGGT GGTTCACCTTTTTTGTGATTACG
acd-5 RNAi forward transcript pDONR221	GGGGACAAGTTTGTACAAAAAAGCAGG CTCTAGCTATCCCACCTCAAATGACTC	GGGGACCACTTTGTACAAGAAAGCTGGGT CCAACTTTTTCGAATTTCAG
acd-5 RNAi reverse transcript pDONR221	GGGGACAAGTTTGTACAAAAAAGCAGG CTCTACTAATTTGCTCACC	GGGGACCACTTTGTACAAGAAAGCTGGGT CCTAATTTAACTAGCTATCC
htmc-1 pDONR P4-P1r	GGGGACAAGTTTGTACAAAAAAGCAGG CTATGTCACCCAAAAAAGTACAAATC	GGGGACCACTTTGTACAAGAAAGCTGGGT TTACTGGCGACCAGCAGCTGCAGC
GCaMP6 low affinity mutation D324G (array)	CCTATTTGACAAGggaGGGG	GTTATTGTCCCATCCCCtccCTTG
GCaMP6 low affinity mutation D397G (array)	CGGTGTGTTTGATAAGggaGGCAATG	GATGTAGCCATTGCCtccCTTATC
GCaMP6 low affinity mutation D326L (array)	CTATTTGACAAGGACGGGctaGGGAC	GGTTGTTATTGTCCCtagCCCG
GCaMP6 low affinity mutation	GTTTGACAAAggaGGAGATGGAACAATC AC	CCATCTCCtccTTTGTCAAACAACGAGAATG CC

D324G (mosSCI)		
GCaMP6 low affinity mutation D397G (mosSCI)	CGATAAAggaGGAAACGGTTATATCAGTGC	GTTTCCtccTTTATCGAAAACTCCAAATG
GCaMP6 low affinity mutation D326L (mosSCI)	GGCATTCTCGTTGTTTGACAAAGATGGActaGGAAC	GTTCCtagTCCATCTTTGTCAAACAACG

Table A7: CRISPR primers

PAM site	Forward Primer	Reverse Primer
acd-5 CRISPR PAM1	GCGCGTCAAGTTGTGTCAAAATGTGCTCCTTCGGGTTTTAGAGCTAGAA	TTCTAGCTCTAAAACCCGAAGGAGCACATTTTGACACAACTTGACGCGC
acd-5 CRISPR PAM2	GCGCGTCAAGTTGTGAACTGCTCTCCGATATCGGGTTTTAGAGCTAGAA	TTCTAGCTCTAAAACCCGATATCGGAGAGCAGTTCACAACTTGACGCGC
acd-5 CRISPR PAM3	GCGCGTCAAGTTGTGCATTTCTGCTCAGTGAAGGGTTTTAGAGCTAGAA	TTCTAGCTCTAAAACCCTTCACTGAGCAGAAATGCACAACTTGACGCGC
asic-2 CRISPR PAM1	GCGCGTCAAGTTGTGACTTGCCCAAGATGCGCGGGTTTTAGAGCTAGAA	TTCTAGCTCTAAAACCCGCGCATCTTGGGCAAGTCACAACTTGACGCGC
asic-2 CRISPR PAM2	GCGCGTCAAGTTGTGTGCCCAAGATGCGCGGTGGGTTTTAGAGCTAGAA	TTCTAGCTCTAAAACCCACCGCGCATCTTGGGCACACAACTTGACGCGC
asic-2 CRISPR PAM3	GCGCGTCAAGTTGTGACGTTATTAATGACTTGGGGTTTTAGAGCTAGAA	TTCTAGCTCTAAAACCCCAAGTCATTAATAACGTCACAACTTGACGCGC

Plasmids

Table A8: Plasmid List

***EP15**

****G= gift, S= Schafer Lab Stock, M= Made by me**

Plasmid Name	Construct	Vector	Origin**
PLG32	*mCherry* Stop	pDONR 221	G, DeBono
pMA122	P*hsp-16.41*:*peel-1*:*tbb-2*UTR	pDEST R4-R3	Q, Ch'ng
pGH8	P*rab-3*:mCherry:*unc-54*UTR	pDEST R4-R3	Q, Ch'ng
pCFJ601	P*eft-3*:Mos1 transposase	pDEST R4-R3	Q, Ch'ng
pCFJ90	P*myo-2*:mCherry:*unc-54*UTR	N/A	Q, Ch'ng
CFJ104	P*myo-3*:mCherry:*unc-54*UTR	pDEST R4-R3	Q, Ch'ng
MOS1	*Pmec-7-RSET-GCaMP3(CEopt)* T302L R303P M378G K379S D380Y T381R S383T R392G-SL2-*TagRFP-unc-54*UTR.*48.629* (*GCaMP6M*)	pGP-CFJ151-SM	G, Kim
MOS2	*Pmec-7-RSET-GCaMP3(CEopt)* K78H T302L R303P D380Y T381R S383T R392G-SL2-*TagRFP-unc-54*UTR.*48.641* (*GCaMP6S*)	pGP-CFJ151-SM	G, Kim
MOS3	*Pmec-7-RSET-GCaMP3(CEopt)* T302L R303P A317E D380Y T381R S383T R392G-SL2-*TagRFP-unc-54*UTR.48.693 (*GCaMP6F*)	pGP-CFJ151-SM	G, Kim
MOS4	*Pmec-4-unc-54*UTR-*GCaMP3*-T302L R303P M378G K379S D380Y T381R S383T R392G.13.629 (*GCaMP6M*)	pGP-L3691	G, Kim
MOS5	*Pmec-4-unc-54*UTR-*GCaMP3*-K78H T302L R303P D380Y T381R S383T R392G.13.641 (*GCaMP6S*)	pGP-L3691	G, Kim
MOS6	*Pmec-4-unc-54*UTR-*GCaMP3*-T302L R303P A317E D380Y T381R S383T R392G.13.693 (*GCaMP6F*)	pGP-L3691	G, Kim
MOS7	*Pmec-4-unc-54*UTR-*GCaMP3*-K78H T302L R303P A317E D380Y T381R S383T R392G.13.649	pGP-L3691	G, Kim
MOS8	*Pmec-4-unc-54*UTR-GCaMP3-K78H T302L R303P A317E K379S D380Y T381R S383T R392G.13.643	pGP-L3691	G, Kim
MOS9	*Pmec-4-unc-54*UTR-GCaMP3-K78H T302L R303P A317E M378G D380Y T381R S383T R392G.13.646	pGP-L3691	G, Kim
MOS10	*Pmec-7-RSET-GCaMP3(CEopt)* T302L R303P D380Y-SL2-*TagRFP-unc-54*UTR.48.29 (*GCaMP5*)	pGP-CFJ151-SM	G, Kim
MOS11	*Pmec-4-unc-54*UTR-*GCaMP3*-T302L R303P D380Y.13.2 (*GCaMP5*)	pGP-L3691	G, Kim
PLG45	*Pmec-7*::*GCaMP6M* D236L::SL2-*tagRFP*	pDEST R4-R3*	M
PLG46	*Pmec-7*::*GCaMP6S* D236L::SL2-*tagRFP*	pDEST R4-R3*	M
PLG76	*acd-5* CDNA	pDONR 221	M
PLG81	*GCaMP6F* ER retention	pDONR 221	M
PLG82	*asic-2* CDNA	pDONR 221	M
PLG92	*GCaMP6M* D326L	pDONR P2R-P3	M
PLG96	*GCaMP6F*	pDONR P2R-P3	M
PLG99	*GCaMP6S* D326L	pDONR P2R-P3	M
PLG100	*GCaMP6S* D324G D397G	pDONR P2R-P3	M
PLG111	*Pacd-5*::*GFP* stop::*unc-54*'UTR	pDEST R4-R3*	M
PLG112	*Pklp-6*	pDONR P4-P1R	M

PLG118	*Pasic-2*::*asic-2* cDNA::SL2-*tagRFP*	pDEST R4-R3*	M
PLG119	*Pklp-6*::*asic-2*:: SL2-*tagRFP*	pDEST R4-R3*	M
PLG120	*Pklp-6*::*acd-5*:: SL2-*tagRFP*	pDEST R4-R3*	M
PLG126	*Pacd-5*::*acd-5*::SL2-*tagRFP*	pDEST R4-R3*	M
PLG127	*GCaMP6M* D324G	pDONR 221	M
PLG128	*GCaMP6M* D326L	pDONR 221	M
PLG129	*GCaMP6S* D324G D397G	pDONR 221	M
PLG130	*Psra-9*::*GCaMP6M*::SL2-*tagRFP*	pDEST R4-R3*	M
PLG136	*GCaMP6F*	pDONR 221	M
PLG137	*GCaMP6S*	pDONR 221	M
PLG140	*Psra-9*::*GCaMP6S*::SL2-*tagRFP*	pDEST R4-R3*	M
PLG141	*Psra-9::GCaMP6F*::SL2-*tagRFP*	pDEST R4-R3*	M
PLG157	*GCaMP6M*	pDONR 221	M
PLG184	*Pdaf-7::acd-5* cDNA::SL2-*tagRFP*	pDEST R4-R3*	M
PLG197	*pdaf-7*	pDONR P4-P1R	M
PLG199	*Pdaf-7::acd-5* cDNA::SL2-*tagRFP*	pDEST R4-R3*	M
PLG200	*asic-2* RNAi forward transcript	pDONR 221	M
PLG201	*asic-2* RNAi reverse transcript	pDONR 221	M
PLG202	*acd-5* RNAi forward transcipt	pDONR 221	M
PLG203	*acd-5* RNAi reverse transcipt	pDONR 221	M
PLG204	*acd-5* gDNA	pDONR 221	M
PLG205	*daf-7*	pDONR 221	M
PLG206	*flp-21*	pDONR 221	M
PLG207	*Podr-10*	pDONR P4-P1R	M
PLG208	*Podr-10*::*YC3.60*::SL2-*tagRFP*	pDEST R4-R3*	M
PLG209	*Pdaf-7*::*daf-7* no stop::*mCherry*	pDEST R4-R3*	M
PLG210	*Pdaf-7::flp-21* no stop::*mCherry*	pDEST R4-R3*	M
PLG211	*Pdaf-7::acd-5* cDNA::SL2-*tagRFP*	PCFJ150	M
PLG212	*Pacd-5::acd-5* gDNA::SL2-*tagRFP*	PCFJ 150	M
PLG213	*Pdaf-7::acd-5* RNAi forward transcript::SL2-*tagRFP*	pDEST R4-R3*	M
PLG214	*Pdaf-7::acd-5* RNAi reverse transcript::SL2-*tagRFP*	pDEST R4-R3*	M
PLG215	*Pacd-5::acd-5* RNAi forward transcript::SL2-*tagRFP*	pDEST R4-R3*	M
PLG216	*Pacd-5::acd-5* RNAi reverse transcript::SL2-*tagRFP*	pDEST R4-R3*	M
PLG217	*Pacd-5::acd-5* gDNA::SL2-*tagRFP*	pDEST R4-R3*	M
PLG218	*Pdaf-7::acd-5* gDNA::SL2-*tagRFP*	pDEST R4-R3*	M
pKA712	*Pdaf-7*:: *daf-28-mCherry*::*unc-54'*UTR	pDEST	G, Ashrafi
	Pdaf-7::GCaMP3	pDEST	G, Lockery
PWRS522	*Psra-9::ceTMC-1*::SL2-*tagRFP*	pDEST R4-R3*	M, Chatzigeorgiou
PWRS516	*Psra-9::mTMC1*::SL2-*tagRFP*	pDEST R4-R3*	M, Chatzigeorgiou

Strains

Table A9 Strains

****G= gift, S= Schafer Lab Stock, M= Made by me**

Strain Name	Plasmid	Array/integrant	Background	Source**
QL74		[*ttTi 5605 II*]	*unc-119 (ed3) III*	Q, Ch'ng
AQ3212	MOS4	*ljEx599* [*Pmec-4::GCaMP6M*::SL2-*tagRFP*; *Pmyo-2::GFP*:: *unc-54* 5'UTR]	N2	M
AQ3213	MOS5	*ljEx600* [*Pmec-4::GCaMP6S*::SL2-*tagRFP*; *Pmyo-2::GFP*::*unc-54* 5'UTR]	N2	M
AQ3214	MOS11	*ljEx601* [*Pmec-4::GCaMP5*::SL2-*tagRFP*; *Pmyo-2::GFP*::*unc-54* 5'UTR]	N2	M
AQ3215	MOS7	*ljIs138* [*Pmec-4::GCaMP6.649*::SL2-*tagRFP*]	QL74	M
AQ3216	MOS5	*ljIs139* [*Pmec-4::GCaMP6S*::SL2-*tagRFP*]	QL74	M
AQ3217	MOS10	*ljIs140* [*Pmec-4::GCaMP5*::SL2-*tagRFP*]	QL74	M
AQ3235	MOS2	*ljSi1* [*Pmec-7::GCaMP6S*::SL2-*tagRFP*]	QL74	M
AQ3236	MOS1	*ljSi2* [*Pmec-7::GCaMP6M*::SL2-*tagRFP*]	QL74	M
AQ3237	MOS6	*ljEx603* [*Pmec-4::GCaMP6F*::SL2-*tagRFP*; *Pmyo-2::RFP*::*unc-54* 5'UTR]	N2	M
AQ3414	PLG105	*ljEx751* [*Pmyo-2::GCaMP6S*+D326L ER retained::SL2-*tagRFP*]	N2	M
AQ3506	PLG130 + PWRS522	*ljEx806* [*Psra-9::GCaMP6M*::SL2-*tagRFP*;*Psra-9::cetmc-1*::SL2-*tagRFP*; *Punc-122::GFP*::*unc-54* 5'UTR]	N2	M
AQ3507	PLG140 + PWRS522	*ljEX807* [*Psra-9::GCaMP6S*::SL2-*tagRFP*;*Psra-9::cetmc-1*::SL2-*tagRFP*; *Punc-122::GFP*::*unc-54* 5'UTR]	N2	M
AQ3508	PLG141 + PWRS522	*ljEX808* [*Psra-9::GCaMP6F*::SL2-*tagRFP;Psra-9::cetmc-1*::SL2-*tagRFP*; *Punc-122::GFP*::*unc-54* 5'UTR]	N2	M
AQ3514	PLG119 1	*ljEx813* [*Pklp-6::asic-2*::SL2-*tagRFP*;*Punc-122::GFP*::*unc-54* 5'UTR] 1	*asic-2 (ok289)I*	M
AQ3515	PLG120 1	*ljEx814* [*Pklp-6::acd-5*::SL2-*tagRFP*; *Punc-122::GFP*::SL2-*tagRFP*] 1	*acd-5 (ok2657)I*	M
AQ3517	PLG219	*ljEx816* [*Pmec-4::GCaMP6M*+D324G::SL2-*tagRFP*; *Punc-122::GFP*::*unc-54* 5'UTR]	N2	M
AQ3518	PLG127	*ljEx817* [*Pmec-4::GCaMP6M*+D324G::SL2-*tagRFP; Punc-122::GFP*::*unc-54* 5'UTR]	N2	M
AQ3519	PLG119 2	*ljEx818* [*Pklp-6::asic-2*::SL2-*tagRFP*;*Punc-122::GFP*::*unc-54* 5'UTR] 2	*asic-2 (ok289)I*	M
AQ3550	PLG101	*ljEx840* [*Pasic-2::mcherry stop*::*unc-54* 5'UTR; *Punc-122::GFP*:: *unc-54* 5'UTR]	N2	M
AQ3552	PLG120 2	*ljEx846*[*Pklp-6::acd-5*::SL2-*tagRFP; Punc-122::GFP*::*unc-54* 5'UTR] 2	*acd-5 (ok2657)I*	M
AQ3554	PLG126	*ljEx848* [*Pacd-5::acd-5*::SL2-*tagRFP*]	*acd-5 (ok2657)I*	M
AQ3623	PLG111	*ljEx887* [*Pacd-5::GFP* stop::*unc-54* 5'UTR] 2	N2	M
AQ3624	PLG101+ PWRS502	*ljEx888* [*Pasic-2::mCherry* stop::*unc-54* 5'UTR;*Pklp-6::YC3.60::unc-54* 5'UTR; P*unc-*	N2	M

		122::GFP unc-54 5'UTR]		
AQ3659	PLG111	*ljEx908*[*Pacd-5::GFP*stop::*unc-54* 5'UTR;*Punc-122::GFP:: unc-54* 5'UTR]	*acd-5 (ok2657)I*	M
AQ3707	PLG80	*ljEx928* [*Pmec-4::GCaMP6S* D326L D397G::SL2RFP;P*unc-122::GFP::unc-54* 5'UTR]	N2	M
AQ3708	PLG166	*ljEx929* [*Pasic-2*::new *GCaMP6M*::SL2-*tagRFP*]	N2	M
AQ3710	PLG147	*ljEx931* [*Pacd-5::GCaMP6F*:: *unc-54* 5'UTR;*Punc-122::GFP::unc-54* 5'UTR]	N2	M
AQ3769	PLG78	*ljEx950* [*Pmec-4::GCaMP6M* D326L::SL2-*tagRFP;Punc-122::GFP::unc-54* 5'UTR]	N2	M
AQ3789	ntEx4	*ntEx4*[*Pdaf-7::YC3.60 ; lin-15*(+)] 1	*acd-5 (ok2657)I*	M
AQ3790	PLG101	*ljEx977* [*Pasic-2::mCherry* stop:: *unc-54* 5'UTR;*Punc-122::GFP::unc-54* 5'UTR]	*acd-5 (ok2657)I*	M
AQ3791	PLG118	*ljEx978* [*Pasic-2::asic-2* cDNA::SL2-*tagRFP;Punc-122::GFP::unc-54* 5'UTR]	*asic-2 (ok289)I*	M
AQ3798	PLG101	*ljEx1047* [*Pasic-2::mCherry* stop:: *unc-54* 5'UTR;*Punc-122::GFP::unc-54* 5'UTR]	*asic-2 (ok289)I*	M
AQ3870	PWRS502	*ljEx889* [*Pklp-6::YC3.60::unc-54* UTR;*Punc-122::GFP:: unc-54* 5'UTR]	*acd-5 (ok2657)I*	M
AQ3872	PLG184	*ljEx1024* [*Pdaf-7::acd-5* cDNA::SL2-*tagRFP;Punc-122::GFP*:: *unc-54* 5'UTR]	*acd-5 (ok2657)I*	M
AQ3878	PLG193	*ljEx1028* [*Pacd-5::acd-5* gDNA up to 5th intron::SL2-*tagRFP*;*Punc-122::GFP::unc-54* 5'UTR]	N2	M
AQ3880	PLG199	*ljEX1030* [*Pdaf-7::acd-5* cDNA::SL2-*tagRFP;Punc-122::GFP:: unc-54* 5'UTR]	N2	M
AQ3881	PLG187	*ljEx1031* [*Pacd-5::acd-5* gDNA up to 1st intron::SL2-*tagRFP*;*Punc-122::GFP*::*unc-54* 5'UTR]	N2	M
AQ3883	PLG188	*ljEx1033* [*Pacd-5::acd-5* gDNA up to 3rd intron::SL2-*tagRFP*]	N2	M
AQ3893	PLG199	*ljEx1042* [*Pdaf-7::acd-5* cDNA::SL2-*tagRFP;Punc-122::GFP:: unc-54* 5'UTR]	*acd-5 (ok2657)I*	M
AQ3894	PLG195	*ljEx1043* [*Pacd-5::acd-5* gDNA up to 3rd intron::SL2-*tagRFP;Punc-122::GFP:: unc-54* 5'UTR]	N2	M
AQ3895	PLG101 + PLG502	*ljEx1045* [*Pasic-2::mCherry* stop::*unc-54* 5'UTR;*Pklp-6::YC3.60::unc-54* 5'UTR; *Punc-122::GFP:: unc-54* 5'UTR]	N2	M
AQ3896	PLG193	ljEx1046 [*Pacd-5::acd-5* gDNA up to 5th intron::SL2-*tagRFP;Punc-122::GFP:: unc-54* 5'UTR]	N2	M
AQ3897	PLG183	*ljEx1044* [*Pdaf-7::acd-5* cDNA::SL2-*tagRFP;Punc-122::GFP:: unc-54* 5'UTR]	N2	M
AQ3974	*acd-5 (lj107)*	N/A	N/A	M
AQ3975	*acd-5 (lj108)*	N/A	N/A	M
AQ3976	*acd-5 (lj109)*	N/A	N/A	M
AQ3977	*acd-5 (lj110)*	N/A	N/A	M
AQ3978	*asic-2 (lj111)*	N/A	N/A	M

AQ3979	*asic-2 (lj112)*	N/A	N/A	M
AQ3980	*asic-2 (lj113)*	N/A	N/A	M
AQ4108	*Pgpa-2::YC3.60*	*ljEx367* [*Pgpa-2::YC3.60;Punc-122::GFP:: unc-54* 5'UTR]	*acd-5 (lj108)*	M
AQ4109	ntEx4 BX2	*ntEx4* [*Pdaf-7::YC3.60 ; lin-15*(+)]	N2	M
AQ4110	PWRS502	*ljEx889* [*Pklp-6::YC3.60*:: *:: unc-54* 5'UTR; *Punc-122::GF*P*:: unc-54* 5'UTR]	*asic-2 (lj112)*	M
AQ4111	PWRS502	*ljEx889* [*Pklp-6::YC3.60*:: *:: unc-54* 5'UTR; *Punc-122::GFP:: unc-54* 5'UTR]	*asic-2 (lj111)*	M
AQ4112	*Pgpa-2::YC3.60*	*ljEx367* [*Pgpa-2::YC3.60;Punc-122::GFP:: unc-54* 5'UTR]	*acd-5 (lj110)*	M
AQ4120	*ntEx4*	*ntEx4*[*Pdaf-7::YC3.60 ; lin-15*(+)]	*acd-5 (lj110)*	M
AQ4121	*ntEx4*	*ntEx4*[*Pdaf-7::YC3.60 ; lin-15*(+)] .	*acd-5 (lj108)*	M
AQ4122	PWRS502	*ljEx889* [*Pklp-6::YC3.60*:: *:: unc-54* 5'UTR; *Punc-122::GF*P*:: unc-54* 5'UTR]	*asic-2 (ok289)I*	M
AQ4123	*PKa712*	*pka712* [*Pdaf-7::daf-28* no stop *mCherry*; *Punc-122::GF*P*:: unc-54* 5'UTR]	*acd-5 (ok2657)I*	M
EU143	*skn-1 (or13)IV*	*Nt1* [*unc-?(n754)let-?*](IV;V)	N/A	GCG
AQ4125	*Pgpa-2::YC3.60*	*ljEx367* [*Pgpa-2::YC3.60;Punc-122::GFP:: unc-54* 5'UTR]	*acd-5 (lj109)*	M
AQ2661	*Pgpa-2::YC3.60*	*ljEx367* [*Pgpa-2::YC3.60;Punc-122::GFP:: unc-54* 5'UTR]	N2	S
XL90	*ntEx4*	*ntEx4 [Pdaf-7::YC3.60 ; lin-15*(+)]	*lin-15(n765ts)*	S, Lockery
	PKa712	*pka712* [*Pdaf-7::daf-28* no stop *mCherry*; *Punc-122::GFP:: unc-54* 5'UTR]	N2	M

Table A10: Features That are Significantly Different from N2 in *acd-5 (ok2657)I* Mutants

Features that are significantly different to N2	P value
'Absolute Backward Eigen Projection 5'	0.007719
'Absolute Backward Foraging Speed (+/- = Toward D/V)'	0.000387
'Absolute Backward Head Bend Mean (+/- = D/V Inside)'	0.003308
'Absolute Backward Head Crawling Frequency (+/- = D/V Inside)'	0.000329
'Absolute Backward Head Motion Direction (+/- = Toward D/V)'	0.001757
'Absolute Backward Head Speed (+/- = Forward/Backward)'	0.020891
'Absolute Backward Head Tip Speed (+/- = Forward/Backward)'	0.001692
'Absolute Backward Hips Bend S.D. (+/- = D/V Inside)'	0.010231
'Absolute Backward Midbody Crawling Frequency (+/- = D/V Inside)'	0.016203
'Absolute Backward Midbody Motion Direction (+/- = Toward D/V)'	0.001007
'Absolute Backward Tail Crawling Amplitude (+/- = D/V Inside)'	0.005977
'Absolute Backward Tail Motion Direction (+/- = Toward D/V)'	0.000139
'Absolute Backward Tail Speed (+/- = Forward/Backward)'	0.004559
'Absolute Backward Tail Tip Motion Direction (+/- = Toward D/V)'	0.022176
'Absolute Backward Tail Tip Speed (+/- = Forward/Backward)'	0.000362
'Absolute Foraging Speed (+/- = Toward D/V)'	0.034373
'Absolute Forward Foraging Speed (+/- = Toward D/V)'	0.000173
'Absolute Forward Head Bend Mean (+/- = D/V Inside)'	0.01208
'Absolute Forward Head Crawling Amplitude (+/- = D/V Inside)'	0.016567
'Absolute Forward Head Crawling Frequency (+/- = D/V Inside)'	0.000523
'Absolute Forward Head Motion Direction (+/- = Toward D/V)'	0.001448
'Absolute Forward Head Speed (+/- = Forward/Backward)'	0.000019
'Absolute Forward Head Tip Motion Direction (+/- = Toward D/V)'	0.002805
'Absolute Forward Head Tip Speed (+/- = Forward/Backward)'	0.000004
'Absolute Forward Hips Bend S.D. (+/- = D/V Inside)'	0.009706
'Absolute Forward Midbody Bend S.D. (+/- = D/V Inside)'	0.028355
'Absolute Forward Midbody Crawling Frequency (+/- = D/V Inside)'	0.011409
'Absolute Forward Midbody Motion Direction (+/- = Toward D/V)'	0.006576
'Absolute Forward Midbody Speed (+/- = Forward/Backward)'	0.000141
'Absolute Forward Tail Crawling Amplitude (+/- = D/V Inside)'	0.000283
'Absolute Forward Tail Speed (+/- = Forward/Backward)'	0.000587
'Absolute Forward Tail Tip Speed (+/- = Forward/Backward)'	0.001262
'Absolute Head Crawling Amplitude (+/- = D/V Inside)'	0.001535
'Absolute Head Crawling Frequency (+/- = D/V Inside)'	0.000218
'Absolute Head Motion Direction (+/- = Toward D/V)'	0.000417
'Absolute Head Speed (+/- = Forward/Backward)'	0.000274
'Absolute Head Tip Motion Direction (+/- = Toward D/V)'	0.00528
'Absolute Head Tip Speed (+/- = Forward/Backward)'	0.00007
'Absolute Hips Bend S.D. (+/- = D/V Inside)'	0.002675
'Absolute Inter Omega Time (+/- = Previous D/V)'	0.000338
'Absolute Inter Upsilon Distance (+/- = Previous D/V)'	0.01892
'Absolute Inter Upsilon Time (+/- = Previous D/V)'	0.008318
'Absolute Midbody Motion Direction (+/- = Toward D/V)'	0.001595

'Absolute Midbody Speed (+/- = Forward/Backward)'	0.000372
'Absolute Neck Bend Mean (+/- = D/V Inside)'	0.023806
'Absolute Neck Bend S.D. (+/- = D/V Inside)'	0.002
'Absolute Omega Turn Time (+/- = D/V Inside)'	0.000281
'Absolute Paused Eigen Projection 5'	0.021227
'Absolute Paused Head Bend Mean (+/- = D/V Inside)'	0.014638
'Absolute Paused Head Crawling Frequency (+/- = D/V Inside)'	0.000781
'Absolute Paused Head Motion Direction (+/- = Toward D/V)'	0.024595
'Absolute Paused Head Speed (+/- = Forward/Backward)'	0.00391
'Absolute Paused Head Tip Speed (+/- = Forward/Backward)'	0.000392
'Absolute Paused Hips Bend S.D. (+/- = D/V Inside)'	0.011797
'Absolute Paused Tail Bend S.D. (+/- = D/V Inside)'	0.026598
'Absolute Paused Tail Crawling Amplitude (+/- = D/V Inside)'	0.00002
'Absolute Paused Tail Crawling Frequency (+/- = D/V Inside)'	0.003942
'Absolute Paused Tail Speed (+/- = Forward/Backward)'	0.029565
'Absolute Paused Tail Tip Speed (+/- = Forward/Backward)'	0.048639
'Absolute Tail Crawling Amplitude (+/- = D/V Inside)'	0.017229
'Absolute Tail Crawling Frequency (+/- = D/V Inside)'	0.037914
'Absolute Tail Motion Direction (+/- = Toward D/V)'	0.000862
'Absolute Tail Speed (+/- = Forward/Backward)'	0.000266
'Absolute Tail Tip Motion Direction (+/- = Toward D/V)'	0.042243
'Absolute Tail Tip Speed (+/- = Forward/Backward)'	0.000247
'Backward Bend Count'	0.010873
'Backward Distance'	0.003811
'Backward Eigen Projection 1'	0.000286
'Backward Foraging Speed (+/- = Toward D/V)'	0.000434
'Backward Head Bend S.D. (+/- = D/V Inside)'	0.042914
'Backward Head Crawling Amplitude (+/- = D/V Inside)'	0.030264
'Backward Head Crawling Frequency (+/- = D/V Inside)'	0.000283
'Backward Head Motion Direction (+/- = Toward D/V)'	0.003137
'Backward Head Speed (+/- = Forward/Backward)'	0.000047
'Backward Head Tip Speed (+/- = Forward/Backward)'	0.000028
'Backward Hips Bend S.D. (+/- = D/V Inside)'	0.005067
'Backward Midbody Bend S.D. (+/- = D/V Inside)'	0.002903
'Backward Midbody Motion Direction (+/- = Toward D/V)'	0.004011
'Backward Midbody Speed (+/- = Forward/Backward)'	0.000055
'Backward Motion Frequency'	0.025529
'Backward Tail Bend Mean (+/- = D/V Inside)'	0.047606
'Backward Tail Crawling Amplitude (+/- = D/V Inside)'	0.004357
'Backward Tail Motion Direction (+/- = Toward D/V)'	0.000165
'Backward Tail Speed (+/- = Forward/Backward)'	0.000066
'Backward Tail Tip Motion Direction (+/- = Toward D/V)'	0.021064
'Backward Tail Tip Speed (+/- = Forward/Backward)'	0.000075
'Backward Time'	0.000719
'Backward Width/Length'	0.005194
'Foraging Amplitude (+/- = Toward D/V)'	0.021232

'Forward Distance'	0.00577
'Forward Eigen Projection 3'	0.011071
'Forward Eigen Projection 5'	0.044349
'Forward Foraging Amplitude (+/- = Toward D/V)'	0.013395
'Forward Foraging Speed (+/- = Toward D/V)'	0.00039
'Forward Head Bend Mean (+/- = D/V Inside)'	0.021886
'Forward Head Crawling Amplitude (+/- = D/V Inside)'	0.000528
'Forward Head Crawling Frequency (+/- = D/V Inside)'	0.00056
'Forward Head Motion Direction (+/- = Toward D/V)'	0.001381
'Forward Head Speed (+/- = Forward/Backward)'	0.000021
'Forward Head Tip Motion Direction (+/- = Toward D/V)'	0.002499
'Forward Head Tip Speed (+/- = Forward/Backward)'	0.000004
'Forward Hips Bend Mean (+/- = D/V Inside)'	0.009295
'Forward Hips Bend S.D. (+/- = D/V Inside)'	0.011291
'Forward Midbody Bend S.D. (+/- = D/V Inside)'	0.00854
'Forward Midbody Crawling Amplitude (+/- = D/V Inside)'	0.039492
'Forward Midbody Crawling Frequency (+/- = D/V Inside)'	0.010284
'Forward Midbody Speed (+/- = Forward/Backward)'	0.000136
'Forward Motion Distance Ratio'	0.003784
'Forward Motion Frequency'	0.003489
'Forward Motion Time Ratio'	0.000273
'Forward Tail Crawling Amplitude (+/- = D/V Inside)'	0.000127
'Forward Tail Crawling Frequency (+/- = D/V Inside)'	0.039971
'Forward Tail Motion Direction (+/- = Toward D/V)'	0.038035
'Forward Tail Speed (+/- = Forward/Backward)'	0.000578
'Forward Tail Tip Speed (+/- = Forward/Backward)'	0.000972
'Forward Time'	0.002881
'Head Crawling Amplitude (+/- = D/V Inside)'	0.00037
'Head Crawling Frequency (+/- = D/V Inside)'	0.000309
'Head Motion Direction (+/- = Toward D/V)'	0.000466
'Head Speed (+/- = Forward/Backward)'	0.000254
'Head Tip Motion Direction (+/- = Toward D/V)'	0.006676
'Head Tip Speed (+/- = Forward/Backward)'	0.000081
'Hips Bend S.D. (+/- = D/V Inside)'	0.003462
'Inter Backward Distance'	0.002761
'Inter Backward Time'	0.019769
'Inter Forward Time'	0.008061
'Inter Omega Distance (+/- = Previous D/V)'	0.002546
'Inter Omega Time (+/- = Previous D/V)'	0.000593
'Inter Upsilon Time (+/- = Previous D/V)'	0.00643
'Max Amplitude'	0.00034
'Midbody Bend S.D. (+/- = D/V Inside)'	0.010011
'Midbody Crawling Amplitude (+/- = D/V Inside)'	0.044095
'Midbody Motion Direction (+/- = Toward D/V)'	0.001414
'Midbody Speed (+/- = Forward/Backward)'	0.000401
'Neck Bend S.D. (+/- = D/V Inside)'	0.001153

'Negative Backward Eigen Projection 6'	0.00446
'Negative Backward Head Bend Mean (+/- = D/V Inside)'	0.000309
'Negative Backward Head Bend S.D. (+/- = D/V Inside)'	0.000851
'Negative Backward Head Crawling Amplitude (+/- = D/V Inside)'	0.036582
'Negative Backward Head Speed (+/- = Forward/Backward)'	0.002826
'Negative Backward Head Tip Speed (+/- = Forward/Backward)'	0.002494
'Negative Backward Midbody Motion Direction (+/- = Toward D/V)'	0.026828
'Negative Backward Midbody Speed (+/- = Forward/Backward)'	0.001729
'Negative Backward Tail Bend Mean (+/- = D/V Inside)'	0.003658
'Negative Backward Tail Motion Direction (+/- = Toward D/V)'	0.010502
'Negative Backward Tail Speed (+/- = Forward/Backward)'	0.001934
'Negative Backward Tail Tip Motion Direction (+/- = Toward D/V)'	0.046504
'Negative Foraging Amplitude (+/- = Toward D/V)'	0.000103
'Negative Forward Midbody Crawling Frequency (+/- = D/V Inside)'	0.049239
'Negative Forward Neck Bend Mean (+/- = D/V Inside)'	0.043112
'Negative Forward Neck Bend S.D. (+/- = D/V Inside)'	0.038509
'Negative Head Bend Mean (+/- = D/V Inside)'	0.000524
'Negative Head Bend S.D. (+/- = D/V Inside)'	0.000332
'Negative Head Crawling Frequency (+/- = D/V Inside)'	0.042268
'Negative Head Motion Direction (+/- = Toward D/V)'	0.012744
'Negative Head Speed (+/- = Forward/Backward)'	0.000046
'Negative Head Tip Motion Direction (+/- = Toward D/V)'	0.026786
'Negative Head Tip Speed (+/- = Forward/Backward)'	0.00001
'Negative Inter Omega Distance (+/- = Previous D/V)'	0.000196
'Negative Inter Omega Time (+/- = Previous D/V)'	0.000576
'Negative Midbody Speed (+/- = Forward/Backward)'	0.00015
'Negative Neck Bend Mean (+/- = D/V Inside)'	0.002965
'Negative Neck Bend S.D. (+/- = D/V Inside)'	0.006273
'Negative Omega Turn Time (+/- = D/V Inside)'	0.001023
'Negative Paused Midbody Speed (+/- = Forward/Backward)'	0.000058
'Negative Paused Neck Bend Mean (+/- = D/V Inside)'	0.000154
'Negative Paused Neck Bend S.D. (+/- = D/V Inside)'	0.001197
'Negative Paused Tail Speed (+/- = Forward/Backward)'	0.000098
'Negative Paused Tail Tip Speed (+/- = Forward/Backward)'	0.000344
'Negative Tail Speed (+/- = Forward/Backward)'	0.00053
'Negative Tail Tip Speed (+/- = Forward/Backward)'	0.001954
'Paused Foraging Amplitude (+/- = Toward D/V)'	0.01689
'Paused Head Crawling Frequency (+/- = D/V Inside)'	0.000179
'Paused Head Motion Direction (+/- = Toward D/V)'	0.018405
'Paused Head Speed (+/- = Forward/Backward)'	0.005312
'Paused Head Tip Speed (+/- = Forward/Backward)'	0.000507
'Paused Hips Bend S.D. (+/- = D/V Inside)'	0.005582
'Paused Midbody Bend S.D. (+/- = D/V Inside)'	0.021381
'Paused Midbody Speed (+/- = Forward/Backward)'	0.047437
'Paused Motion Distance Ratio'	0.000083
'Paused Motion Frequency'	0.000169

'Paused Motion Time Ratio'	0.000028
'Paused Tail Bend S.D. (+/- = D/V Inside)'	0.013014
'Paused Tail Crawling Amplitude (+/- = D/V Inside)'	<0.000001
'Paused Tail Crawling Frequency (+/- = D/V Inside)'	0.000216
'Paused Tail Speed (+/- = Forward/Backward)'	0.01848
'Paused Time'	0.000107
'Positive Backward Eigen Projection 1'	0.008825
'Positive Backward Foraging Speed (+/- = Toward D/V)'	0.001276
'Positive Backward Head Crawling Amplitude (+/- = D/V Inside)'	0.004162
'Positive Backward Head Crawling Frequency (+/- = D/V Inside)'	0.000313
'Positive Backward Head Motion Direction (+/- = Toward D/V)'	0.005492
'Positive Backward Head Orientation'	0.049839
'Positive Backward Head Speed (+/- = Forward/Backward)'	0.000037
'Positive Backward Head Tip Speed (+/- = Forward/Backward)'	0.000023
'Positive Backward Hips Bend S.D. (+/- = D/V Inside)'	0.012763
'Positive Backward Midbody Crawling Amplitude (+/- = D/V Inside)'	0.019816
'Positive Backward Midbody Motion Direction (+/- = Toward D/V)'	0.009202
'Positive Backward Midbody Speed (+/- = Forward/Backward)'	0.000055
'Positive Backward Tail Crawling Amplitude (+/- = D/V Inside)'	0.004148
'Positive Backward Tail Motion Direction (+/- = Toward D/V)'	0.000539
'Positive Backward Tail Speed (+/- = Forward/Backward)'	0.000081
'Positive Backward Tail Tip Motion Direction (+/- = Toward D/V)'	0.023471
'Positive Backward Tail Tip Speed (+/- = Forward/Backward)'	0.000069
'Positive Backward Tail-To-Head Orientation'	0.021869
'Positive Eigen Projection 1'	0.005177
'Positive Eigen Projection 4'	0.010432
'Positive Foraging Amplitude (+/- = Toward D/V)'	0.002983
'Positive Forward Eigen Projection 1'	0.000519
'Positive Forward Foraging Amplitude (+/- = Toward D/V)'	0.00251
'Positive Forward Foraging Speed (+/- = Toward D/V)'	0.001829
'Positive Forward Head Crawling Amplitude (+/- = D/V Inside)'	<0.000001
'Positive Forward Head Crawling Frequency (+/- = D/V Inside)'	0.001806
'Positive Forward Head Motion Direction (+/- = Toward D/V)'	0.00107
'Positive Forward Head Orientation'	0.031943
'Positive Forward Head Speed (+/- = Forward/Backward)'	0.000655
'Positive Forward Head Tip Motion Direction (+/- = Toward D/V)'	0.005221
'Positive Forward Head Tip Speed (+/- = Forward/Backward)'	0.000013
'Positive Forward Midbody Bend S.D. (+/- = D/V Inside)'	0.001729
'Positive Forward Midbody Crawling Amplitude (+/- = D/V Inside)'	0.03515
'Positive Forward Neck Bend Mean (+/- = D/V Inside)'	0.023477
'Positive Forward Neck Bend S.D. (+/- = D/V Inside)'	0.031821
'Positive Forward Tail Crawling Amplitude (+/- = D/V Inside)'	0.000082
'Positive Forward Tail Motion Direction (+/- = Toward D/V)'	0.003779
'Positive Forward Tail Speed (+/- = Forward/Backward)'	0.010218
'Positive Forward Tail-To-Head Orientation'	0.030836
'Positive Head Bend Mean (+/- = D/V Inside)'	0.001692

'Positive Head Crawling Amplitude (+/- = D/V Inside)'	0.000108
'Positive Head Crawling Frequency (+/- = D/V Inside)'	0.00087
'Positive Head Motion Direction (+/- = Toward D/V)'	0.000565
'Positive Head Speed (+/- = Forward/Backward)'	0.000549
'Positive Head Tip Motion Direction (+/- = Toward D/V)'	0.008965
'Positive Head Tip Speed (+/- = Forward/Backward)'	0.000242
'Positive Hips Bend S.D. (+/- = D/V Inside)'	0.020554
'Positive Inter Omega Distance (+/- = Previous D/V)'	0.000145
'Positive Inter Omega Time (+/- = Previous D/V)'	0.00052
'Positive Inter Upsilon Distance (+/- = Previous D/V)'	0.039166
'Positive Inter Upsilon Time (+/- = Previous D/V)'	0.005114
'Positive Midbody Bend S.D. (+/- = D/V Inside)'	0.006539
'Positive Midbody Crawling Amplitude (+/- = D/V Inside)'	0.002373
'Positive Midbody Motion Direction (+/- = Toward D/V)'	0.001323
'Positive Midbody Speed (+/- = Forward/Backward)'	0.001411
'Positive Neck Bend Mean (+/- = D/V Inside)'	0.000527
'Positive Omega Turn Time (+/- = D/V Inside)'	0.000518
'Positive Paused Eigen Projection 1'	0.00384
'Positive Paused Foraging Amplitude (+/- = Toward D/V)'	0.001856
'Positive Paused Head Crawling Frequency (+/- = D/V Inside)'	0.00016
'Positive Paused Head Motion Direction (+/- = Toward D/V)'	0.020439
'Positive Paused Head Speed (+/- = Forward/Backward)'	0.01197
'Positive Paused Head Tip Speed (+/- = Forward/Backward)'	0.000977
'Positive Paused Hips Bend S.D. (+/- = D/V Inside)'	0.024966
'Positive Paused Midbody Bend S.D. (+/- = D/V Inside)'	0.02032
'Positive Paused Midbody Crawling Amplitude (+/- = D/V Inside)'	0.002811
'Positive Paused Midbody Crawling Frequency (+/- = D/V Inside)'	0.045278
'Positive Paused Tail Bend S.D. (+/- = D/V Inside)'	0.017418
'Positive Paused Tail Crawling Amplitude (+/- = D/V Inside)'	<0.000001
'Positive Paused Tail Crawling Frequency (+/- = D/V Inside)'	0.000413
'Positive Paused Tail Speed (+/- = Forward/Backward)'	0.036647
'Positive Paused Tail-To-Head Orientation'	0.005332
'Positive Tail Bend S.D. (+/- = D/V Inside)'	0.046864
'Positive Tail Crawling Amplitude (+/- = D/V Inside)'	0.008084
'Positive Tail Motion Direction (+/- = Toward D/V)'	0.000753
'Positive Tail Speed (+/- = Forward/Backward)'	0.00147
'Positive Tail Tip Motion Direction (+/- = Toward D/V)'	0.026823
'Positive Tail Tip Speed (+/- = Forward/Backward)'	0.001712
'Positive Tail-To-Head Orientation'	0.013076
'Tail Bend S.D. (+/- = D/V Inside)'	0.044782
'Tail Crawling Amplitude (+/- = D/V Inside)'	0.011341
'Tail Motion Direction (+/- = Toward D/V)'	0.000772
'Tail Speed (+/- = Forward/Backward)'	0.000368
'Tail Tip Motion Direction (+/- = Toward D/V)'	0.033076
'Tail Tip Speed (+/- = Forward/Backward)'	0.000374
'Upsilon Turn Time (+/- = D/V Inside)'	0.04536

'Upsilon Turns Frequency'	0.000152

Table A11: Features That are Significantly Different from N2 in *asic-2 (ok289)I* Mutants

Features that are significantly different to N2	P value
'Absolute Backward Eigen Projection 2'	0.003338
'Absolute Backward Foraging Amplitude (+/- = Toward D/V)'	0.009662
'Absolute Backward Hips Bend Mean (+/- = D/V Inside)'	0.045333
'Absolute Backward Tail Bend S.D. (+/- = D/V Inside)'	0.014707
'Absolute Backward Tail Speed (+/- = Forward/Backward)'	0.035902
'Absolute Backward Tail Tip Speed (+/- = Forward/Backward)'	0.028185
'Absolute Eigen Projection 1'	0.000883
'Absolute Eigen Projection 2'	0.00468
'Absolute Forward Head Bend S.D. (+/- = D/V Inside)'	0.006768
'Absolute Forward Hips Bend Mean (+/- = D/V Inside)'	0.009473
'Absolute Forward Neck Bend Mean (+/- = D/V Inside)'	0.037
'Absolute Hips Bend Mean (+/- = D/V Inside)'	0.017769
'Absolute Paused Eigen Projection 1'	0.001625
'Absolute Paused Eigen Projection 2'	0.014267
'Absolute Paused Hips Bend Mean (+/- = D/V Inside)'	0.029243
'Absolute Paused Midbody Bend Mean (+/- = D/V Inside)'	0.014411
'Amplitude Ratio'	0.040977
'Eigen Projection 2'	0.001951
'Forward Head Bend S.D. (+/- = D/V Inside)'	0.001735
'Forward Length'	0.031413
'Length'	0.041848
'Negative Backward Foraging Speed (+/- = Toward D/V)'	0.048001
'Negative Backward Midbody Crawling Amplitude (+/- = D/V Inside)'	0.036637
'Negative Backward Neck Bend Mean (+/- = D/V Inside)'	0.002098
'Negative Backward Neck Bend S.D. (+/- = D/V Inside)'	0.001419
'Negative Eigen Projection 4'	0.044865
'Negative Forward Midbody Bend Mean (+/- = D/V Inside)'	0.022425
'Negative Forward Midbody Bend S.D. (+/- = D/V Inside)'	0.009979
'Negative Forward Tail Bend Mean (+/- = D/V Inside)'	0.018086
'Negative Head Crawling Frequency (+/- = D/V Inside)'	0.00369
'Negative Head Motion Direction (+/- = Toward D/V)'	0.049349
'Negative Head Speed (+/- = Forward/Backward)'	0.010761
'Negative Head Tip Speed (+/- = Forward/Backward)'	0.008129
'Negative Hips Bend Mean (+/- = D/V Inside)'	0.043691
'Negative Midbody Bend Mean (+/- = D/V Inside)'	0.008532
'Negative Midbody Bend S.D. (+/- = D/V Inside)'	0.001447
'Negative Paused Foraging Amplitude (+/- = Toward D/V)'	0.023036
'Negative Paused Hips Bend Mean (+/- = D/V Inside)'	0.002691
'Negative Paused Hips Bend S.D. (+/- = D/V Inside)'	0.007174
'Negative Paused Midbody Bend Mean (+/- = D/V Inside)'	0.029737

'Negative Paused Midbody Bend S.D. (+/- = D/V Inside)'	0.023701
'Negative Paused Tail Bend Mean (+/- = D/V Inside)'	0.006026
'Negative Tail Speed (+/- = Forward/Backward)'	0.032228
'Negative Tail Tip Speed (+/- = Forward/Backward)'	0.038049
'Paused Eigen Projection 3'	0.03652
'Paused Length'	0.02364
'Paused Width/Length'	0.034887
'Positive Backward Eigen Projection 3'	0.001798
'Positive Backward Head Bend Mean (+/- = D/V Inside)'	0.027307
'Positive Forward Eigen Projection 2'	0.008076
'Positive Forward Eigen Projection 3'	0.042664
'Positive Forward Head Bend S.D. (+/- = D/V Inside)'	0.000815
'Positive Midbody Crawling Frequency (+/- = D/V Inside)'	0.037884
'Positive Paused Eigen Projection 6'	0.048577

Nomenclature

All *C. elegans* genes have a sequence name; this is derived from the cosmid, fosmid or YAC clone on which they reside. For instance *C24G7.1* is the first gene found on the cosmid C24G7. Where the gene produces a protein that can be classified as a member of a family, or where the function of the gene has been identified, an approved name is given. These consist of three or four italicized letters a hyphen and an italicised number. For example the gene *unc-1* was the first gene identified in the uncoordinated family, while *mec-4* is the 4th gene to be identified as part of the mechanosensation defective family. Several gene-family names are speculative or are derived from the resultant phenotype of a mutation within the gene. For example, genes defined by sequence similarity are given an approved name relating to the predicted protein product, *nph-4* is named so as it has a sequence similar to that of human NPHP (human kidney disease nephronophthisis gene), while genes in which a mutant is short and fat are of the *dpy*, or dumpy family.

The specific mutation in a strain is denoted in the bracketed allele name that follows the gene name i.e. *unc-8 (e15)IV* . When looking at allele names, the small letter/s indicate the lab in which the strain was isolated (e= (originally) MRC LMB (currently Hodgkin lab, Oxford). Optional additions of 2 letters after the allele number can be used to identify the characteristic of the gene e.g. *ce81gf* where gf stands for gain of function, or *hc17ts* where ts is temperature sensitive (WormBase.org).

Genetic sequence names are expressed in italics, while the proteins they encode are shown in capitals, i.e. *unc-8 (e15)IV* encodes the protein UNC-8.

Buffer and Agar Plate Recipes

M9

6g Na2HPO4.2H2O, 3g KH2PO4, 5g NaCl, make to 1 litre with deionised water, autoclave. Add 1ml MgSO4.

LB

10g Tryptone, 5g Yeast Extract, 10g NaCl, 15g Agar, make to 1 litre with millipure water. Autoclave at 121°C for 15mins at 15psi. Final pH 7.0±0.2 at 25°C.

NGM

3g NaCl, 17g Agar, 2.5g Peptone, 1ml (5mg/ml in ethanol) Cholesterol, make up to 975ml with deionised water. Autoclave. Add separately: 1ml 1M MgSO4 REF.M45, 25ml 1M K2HPO4 pH6.0 REF.54.

Low Peptone Plate

3g NaCl, 20g Difco Agar, 0.13g Bactopeptone, 1ml (5mg/ml in ethanol) Cholesterol, make up to 975ml with deionised water. Autoclave. When at 55°C add 1ml 1M CaCl2, 1ml 1M MgSO4, 25ml 1M K2HPO4 pH6.0.

CTX Agar

10 mM Mops (pH 7.2), 0.25% v/v Tween 20, 15 g/l agar

CTX Buffer

5 mM KH_2PO_4/K_2HPO_4 pH 6, 1 mM $CaCl_2$ and 1 mM $MgSO_4$

Neuronal Buffer

NaCl 80 mM, KCl 5 mM, D-glucose 20 mM, Hepes 10 mM, $MgCl_2$ 5 mM, $CaCl_2$ 1 mM; pH adjusted with NaOH to 7.2 and osmolarity adjusted with sucrose to 320 mOsm

Intracellular Saline

136.5 mM potassium gluconate, 17.5 mM potassium chloride, 9.0 mM sodium chloride, 1.0 mM magnesium chloride, and 10 mM HEPES (pH 7.2)

S-Basal

5.85 g NaCl, 1 g K_2HPO_4, 6 g KH_2PO_4, 1 ml cholesterol (5 mg/ml in ethanol), H_2O to 1 litre. Sterilize by autoclaving.

S-Medium

1 litre S Basal, 10 ml 1 M potassium citrate pH 6, 10 ml trace metals solution, 3 ml 1 M $CaCl_2$, 3 ml 1 M $MgSO_4$. Add components using sterile technique; do not autoclave.

Dauer Formation Assay

General considerations Based on what type of experiment you are doing, you will need to choose: (1) the concentration of the bacteria (generally, 20 μL of either 8 mg/mL or 50 mg/mL OP50 per assay plate) (2) the state of the bacteria (either heat-killed, antibiotic-treated, or live) (3) the type of agar (either noble agar or granulated agar) in the NGM-agar assay plates Because the response to pheromone is antagonized by food, you can make your assay more sensitive by lowering the amount of food (e.g., by using less bacteria, heat-killing the bacteria, using nutrient-poor noble agar). • For a very sensitive assay to test single purified/synthetic pheromones, we use 20 μL 8 mg/ml heat-killed OP50 per assay plate, and we make the NGM-agar (no peptone) with noble agar and leave out the peptone. • For crude pheromone, crude pheromone fractions, or combinations of multiple synthetic pheromone components, we use 20 μL 50 mg/ml heat-killed OP50 per assay plate, and we make the NGM-agar (no peptone) with granulated agar. Making 10X OP50 NOTE: Always make a small-scale 10X bacterial food stock (from a 50 mL culture) for the dauer formation assay since it is less likely to get contaminated than a large-scale bacterial food stock. Do not use 10X stock that is >2 weeks old since the worms will be less responsive to the pheromone in the assay. 1. Start a 5 mL culture in a 50 mL centrifuge tube (with cap loosely taped) at 37 ºC shaker. Inoculate with a single bacterial colony (OP50) from an LB plate (colonies should be 18 h. 4. The next day harvest the bacteria by centrifugation (3500 rpm, 10 min) in two 50 mL falcon tubes. Discard the supernatant. 5. Resuspended in 5 mL S basal to combine the two pellets in one 50 mL tube. • Note: Do NOT use S medium to resuspend. • This 10X OP50 stock can be stored at 4ºC for up to 2 weeks. 6. Calculate the stock concentration by weighing an empty eppendorf tube and then adding 1 mL of 10 X stock to it. 7. Centrifuge the tube at 13K (high) for 1 min, and remove supernatant by sucking out with a 1 mL pipet tip. Centrifuge again at 13K (high) for 1 min, and remove any remaining supernatant with a 200 μL pipet tip. 8. Reweigh the tube with pellet in it. The weight obtained is the 10X stock concentration (usually around 40 mg/mL). Discard pellet. Making 8 mg/mL heat-killed OP50 from 10X stock 1. Put water in the holes in the heating block. Turn on the switch to high, wait for the temperature to reach 95-100 ºC. Make 1 mL of an 8 mg/mL stock by diluting 10X OP50 stock (from step 5 above) with S basal (NOT S medium) in an eppendorf tube. You can make multiple tubes at once if needed. • Note: Use Fisher brand, not VWR brand since it will leak. 2. Before putting tubes in the heating block, refill holes with water if needed (because the water helps transfer heat). Upon adding water, temperature will likely drop. You want the temperature to be 95 ºC (or at least 90 ºC). 3. Heat the bacteria 30 min, vortexing every 5 min for about 10s. • Note: You may need to add a little bit of water to the holes at some point during the 30 min, but don't add too much since it will reduce the temperature of the block. 4. After heat killing the bacteria, put it at room temperature for about half an hour in order for it to cool down and then store it in the 4 ºC fridge. • Note: Use within one month. Egg lay and dauer formation Note: For this assay to be sensitive, the adult worms used in the egg lay must have been fed very well for 2-3 generations (i.e., they should never be allowed to be without food). Day 1: 1. Synchronize your worms by performing an egg lay. That is, move 20 adult worms to a passage plate and allow them to lay eggs for 1-3 hours. 2. Remove the adults, and leave the passage plate on the bench top at room temperature. Day 3: 3. Move a certain number of L4 worms from the passage plate to a new passage plate, and place plate at room temperature. If you want to perform an egg lay on 10 assay plates on Day 4, you will need 5 worms per assay plate. Thus, on Day 3, you should move 50 L4 worms (plus 20 additional L4 worms for further passaging of your worms). By Day 4, these worms will develop into young adults. 4. Make the assay plates as described in the next section, store at 4 °C overnight, and use in the assay the next day (Day 4). Day 4: 5. Pipet 20 μL of heat-killed OP50

onto each plate. Mix the OP50 by inverting the tube and finger-flicking each time you pipet. Spread the droplet of OP50 on the plate (from the size of a dime to the size of a nickel) by rotating the plate on a slight angle. 6. Dry the plates with the top ajar under a laminar flow hood for approximately 15 min. Make sure to remove the plates from the hood as soon as they are dry. 7. Pick 5 young adult worms onto each assay plate. Try to transfer as little live bacteria from the passage plate as possible to the assay plate when moving the worms. • Note: You can also move 20 adults to a new passage plate for an egg lay (and remove them 2-3 h later), if you would like to initiate another synchronized plate of worms to be used in another dauer formation assay 3 d later. 8. Let the worms lay between 60-90 eggs per plate over the course of approximately 2-3 h. At around 2 h, roughly estimate the amount of eggs on each plate. As soon as you see approximately 75 eggs on a given plate, remove the adults. If there are >90 eggs on a plate, you can also remove some eggs with your pick. 9. Once you are done with the egg lay, place all of the plates in an enclosed plastic container. Place a damp paper towel in the container to increase the humidity in the box, and prevent drying of your plates. Place the container in a refrigerated incubator at the desired temperature, typically 25 °C. Day 5-6: 10. Rewet the paper towel in the box each day if it becomes dry. Day 7: 11. Approximately 64-72 h after the completion of the egg lay on Day 4, determine the number of dauers and L4/adults on each plate by examining the worms under a stereomicroscope. Calculate the percent dauer formation by dividing the number of dauers by the total number of dauers plus L4/adults. Do not include data from plates with < 60 worms or > 90 worms. • Note: Mutant worms may take longer than wild-type (N2) worms to develop and thus to form dauers. Making assay plates 1. Autoclave 250 mL of NGM-agar (no peptone). For a sensitive assay, use noble agar instead of granulated agar. • Note: It is recommended to make the NGM-agar and autoclave it for every assay, rather than reusing old NGM-agar. 2. Allow NGM-agar to cool to 65 ºC (so that you can put your hand on the bottle briefly). Add goodies to NGM-agar. • Note: If you are worried that your NGM-agar will cool too quickly before you can make your samples, you can heat the large water bath to 65 ºC and store the NGM-agar there for 1-2 h. 3. To prepare the sample for each assay plate to be made in duplicate, aliquot 207 μL of water into an eppendorf. 4. To each tube, add either 13.2 μL of ethanol (as a negative control), 13.2 μL 500X crude pheromone in ethanol (as a positive control, it will end up being 1X in plate, see notes below), or synthetic ascaroside in ethanol (see notes below for concentration information). Mix by vortexing and then tap-spin briefly. • Note: Samples are dissolved in ethanol because it is relatively non-toxic (unlike methanol). • Note: Make sure that each tube receives the same amount of ethanol as large differences in ethanol concentration can affect the assay result. • Note: Each 3.5 cm assay plate made in step 5 will contain 3 mL of NGM-agar. If the plates are made in duplicate (and 10% extra is made), you should make enough sample in step 4 for 6.6 mL of NGM-agar. For example, if you want the final concentration of pheromone to be 2 μM and your ascaroside stock is 3 mM, the eppendorf tube should contain 207 μL water + 4.4 μL ascaroside (3 mM) + 8.8 μL ethanol = 220 μL sample (calculation: 6.6 mL * 2 μM / 3 mM = 4.4 μL). In step 5, 100 μL of this 220 μL will be put in one assay plate, 100 μL in the duplicate assay plate, and 20 μL (10%) is extra. 5. Aliquot 100 μL of each sample to a 3.5 cm assay plate. 6. Add 3 mL of NGM-agar to the plate using a 5 mL serological pipetfrom step 2, mixing. Let plates cool and congeal for 10 min at room temperature. Store at 4 °C overnight, and use in the assay the next day

General Material and Methods

Molecular Biology

The Invitrogen Gateway® system was used for all cloning.

Concentrations of all plasmid and double stranded DNA samples were determined using a ThermoFisher UV/Vis NanoDrop 2000 micro-volume spectrophotometer.

All plasmid sequences were verified by Source Bioscience using Next Generation sequencing.

Sequencing of lysed worms for verification of CRISPR edits was performed by Eurofins using Next Generation Sequencing.

For antibiotic selection of resistant bacteria concentrations of 100µg/ml was used in ampicillin plates and media, and 50µg/ml was used in kanamycin plates and media.

Injections

For injection, worms were picked as L4 larvae around 16 hours before they were to be injected. Injections were carried out using the method described by (Mello & Fire, 1995).

Dpn-1 removal of plasmid DNA

DpnI recognises 5'-GmeATG-3', since this is a particularly short motif it occurs regularly throughout a DNA sequence. The enzyme will only degrade methylated DNA. PCR products, which have not arisen in an organic source, are not methylated (crystal structure dpni) whereas all bacterial plasmid DNA is methylated. This makes dpnI incredibly useful for ridding PCR products of the original bacterial plasmid.

Genomic DNA

10 day 1 adults were picked to 3 seeded 9cm plates, after 6 days worms were washed off of plates using S-Medium (recipe in appendix) and spun-down using a bench-top microcentrifuge at 2000rpm for 1 minute. The supernatant was pipetted off and replaced with fresh S-Medium. This was repeated twice more. After the final pelleting, a Qiagen blood and tissue culture kit was used to extract the genomic DNA.

Calcium Imaging

Optical recordings were performed essentially as described previously (Kerr R et al., 2000; Kerr RA, 2006) on a Zeiss Axioskop 2 upright compound microscope equipped with a Dual View beam splitter and a Uniblitz Shutter. Fluorescence images were acquired using Andor IQ software. All recordings were performed at 63X magnification under water immersion.

For imaging with cameleon filter-dichroic pairs were excitation, 400–440; excitation dichroic 455; CFP emission, 465–495; emission dichroic 505; YFP emission, 520–550.